Metal nitrosyl and dinitrosyl complexes as small molecule models for NOD and FNOR

A dissertation submitted to the Indian Institute of Technology Guwahati as
Partial fulfillment for the degree of Doctor of Philosophy in Chemistry

Submitted

by

Riya Ghosh

(Roll No. 186122115)

Supervisor

Prof. Biplab Mondal

Department of Chemistry

Indian Institute of Technology Guwahati

Assam, India

August, 2025

Dedicated to My Parents

STATEMENT

I hereby declare that this thesis entitled **“Metal nitrosyl and dinitrosyl complexes as small molecule models for NOD and FNOR”** is the outcome of research work carried out by me under the supervision of Prof. Biplab Mondal in the Department of Chemistry, Indian Institute of Technology Guwahati, India.

In keeping with the general practice of reporting scientific observations, due acknowledgements have been made wherever the work described is based on the findings of other investigators.

Riya Ghosh

August, 2025

Riya Ghosh
IIT Guwahati

भारतीय प्रौद्योगिकी संस्थान गुवाहाटी
INDIAN INSTITUTE OF TECHNOLOGY GUWAHATI
North Guwahati, Assam – 781039, India

Dr. Biplab Mondal
Professor
Department of Chemistry

Phone: + 91-361-258-2317
Fax: + 91-361-258-2349
E-mail: biplab@iitg.ac.in

Certificate

This is to certify that **Ms. Riya Ghosh** has been working under my supervision since March, 2019 as a regular Ph.D. student in the Department of Chemistry, Indian Institute of Technology Guwahati. I am forwarding her thesis entitled **"Metal nitrosyl and dinitrosyl complexes as small molecule models for NOD and FNOR"** being submitted for the Ph.D. degree.

I certify that she has fulfilled all the requirements according to the ordinance of this Institute regarding the investigations embodied in her thesis and this work has not been submitted elsewhere for a degree.

August, 2025 **(Biplab Mondal)**

Acknowledgement

I would like to offer my sincere gratitude to the many extraordinary people who have accompanied me on my half-a-dozen years wonderful PhD journey at IITG; without whom, my journey wouldn't be what it is, and this thesis wouldn't be possible.

First and foremost, my wholehearted acknowledgement is reserved for my supervisor, Prof. Biplab Mondal. I feel fortunate to carry out my PhD work under his supervision. I couldn't imagine a better mentor with constant efforts to bring the best out of his students. I am forever grateful for your constant motivation, guidance, and support and for providing the best possible opportunities. I thank you for always believing in me while providing difficult tasks, which helped me grow and uplift my research grasp. I am forever indebted to my supervisor for transforming my academic perspective and re-inciting an ambition in me. Words are insufficient to express my gratitude towards you. Thank you, Sir!

I would like to extend my gratitude to my doctoral committee members, Prof. Gopal Das sir, Prof. Dipankar Srimani sir, and Dr. Akshai Kumar Alape Seetharam sir for their insightful advice, guidance, and periodic evaluation of my thesis work.

I am thankful to the Department of Chemistry and Central Instruments Facilities (CIF) of Indian Institute of Technology Guwahati for providing the research facilities and instrumental facilities. I also thank all the staff members of Chemistry department, CIF and IITG for their help whenever I was in need. I extend my gratitude to DST-INSPIRE for fellowship and providing all the requirements.

I would like to extend my gratitude to all my teachers/faculties and friends from my academic career, whose direct and indirect support and motivation have guided me to reach this milestone. First and foremost, I wish to thank my father, the late Ram Chandra Ghosh, for your unconditional love, inspiration, guidance, and unwavering support in shaping me into the person I am today. I deeply miss you during these challenging times in my life, but I hold on to the belief that "No matter where I am, Baba! I know *you will always be with me." I would also like to acknowledge Mr. Kalyan Kumar Majumdar, who has been not only a teacher but also a true friend, philosopher, and guide.*

My deepest appreciation cum gratitude go to all the members of CHEL-004, "The NO Chemistry Lab," for creating a friendly work environment and fun-filled moments. I cherish every moment that I spent here with wonderful people around, who made it a "home" away from home. Dr. Rakesh Mazumdar, an inspiring and all-time helpful senior, has been a blessing for me. I have been fortunate *enough to work with Shankhadeep da, Sayani, Bapan da, and Rakesh da, who have created a cooperative lab environment and provided invaluable help and insights, making this journey truly memorable. My heartfelt thanks to my fellow lab mates, Bristi, Mrinmoy, Risha, and Navendu, for always being there and bearing with me through the good and bad times during my wonderful days of Ph.D. I am highly thankful to Sayani for her unending and selfless support when it was utmost required. I will treasure the wonderful time spent with Chandrima ma'am and beloved Gungun. My sincere appreciation goes to everyone, who was part of the lab, whether for a short or long period, during my PhD duration and helped me to create so many beautiful memories.*

I want to express my deepest gratitude to Sujay for inspiring me in my Ph.D. and for introducing me to this platform. My special thanks go to my friends Santanu, Souradeep, Priyam, Surovi, and Subhajit for their constant support and motivation to keep going during the time of downcast. I am thankful to Prasenjit da and Yogesh for their help and for sharing joyful memories during my time at IITG. I was incredibly fortunate to have the support of wonderful friends, including Sanchita, Suparna, Gargi, Subhajit and Pallav for a long time. Finally, I am thankful to Sayani, Santanu, and Shankhadeep da for believing in 'a cup of tea solves everything'.

Finally, I thank my pillar of strength, without whom this endeavour would not have been possible, "my family"; who actuated and accelerated the journey through their countless sacrifice and unconditional love. I am thankful to my maa, Mrs. Sukla Ghosh, who taught me to be independent, courageous, and carefree and supported me in every decision and my baba, who taught me to fly high and dream big; and be positive, patient and strong even during the worst days. I would like to mention my primary source of happiness, 'Gojo & Ghonto'— Video calling with both of you truly acts as a "frustration-killer" for me! I would also like to thank my didi and Arijit da for always motivating me and supporting me in every situation. I wholeheartedly express my sincere regards and respect to other guardians, Tapendra Nath Ghosh and Krishna Ghosh for extending their unwavering strength and support. Last but not least, my beloved, Ayan, Akshay, Subhadip and Promita made this journey very easy for me.

Thank you all for being part of this journey.

Riya Ghosh

Contents

Synopsis

The thesis entitled **"Metal nitrosyl and dinitrosyl complexes as small molecule models for NOD and FNOR"** is divided into five chapters.

Chapter 1: Introduction

Metal Nitrosyls

Nitric oxide (NO) is an essential signalling molecule that is endogenously produced and plays vital role in vasodilation, neurotransmission and immune response *etc.*[1] NO interacts with transition metal ions to form various coordination compounds, highlighting its versatility. The chemistry of NO is not only of great biological and biochemical interest but also emphasizes the importance of its interactions with transition metals, which are significant and noteworthy.[2-3]

Activity of many metalloenzymes such as nitric oxide synthases (NOSs), nitric oxide dioxygenases (NODs), nitric oxide reductases (NORs) and nitrite reductases (NiRs) are associated with the formation of transition metal nitrosyls.[4-6] Therefore, the synthesis and reactivity study of transition metal nitrosyls is an important area of research for chemists and biochemists to understand the mechanism of these enzymatic processes.[7-8] *In-vivo*, NO formation is catalyzes by NO synthases (NOSs) through a series of redox reactions, with degradation of *L*-arginine to *L*-citrulline.[9-10] Heme-iron nitrosyl complex catalyses the transformation of guanosine triphosphate (GTP) into cyclic guanosine monophosphate (cGMP), which results into smooth muscle relaxation and thus vasodilation.[11] cGMP, the second messenger molecule, activates protein kinase G (PKG), regulates cell processes such as vasodilation, immune responses, neurotransmission, apoptosis, reproduction, regulation of gene transcription, mRNA translation, and post-translational modifications of proteins.[12-13]

Reactivity of metal nitrosyls with reactive oxygen species

Nitric oxide (NO) spontaneously reacts with superoxide ions in a diffusion-controlled rate to result in the formation of the peroxynitrite ($ONOO^-$) anion.[14-16] This potent anion causes the nitration of the tyrosine ring in proteins and also leads to the modification of biomolecules, such as lipids and proteins.[17-18]

On the other hand, the concentration/level of NO in mammalian biology is controlled by the nitric oxide dioxygenases (NODs) enzyme. In the NOD, a [Fe^{III}-O_2^-] complex reacts with NO to produce biologically benign nitrate ion (NO_3^-) (Scheme S1).[19-21] This reaction proceeds through the formation of a peroxynitrite intermediate that decomposes into a [Fe^{IV}=O] species and nitrogen dioxide (NO_2) *via* O–O bond cleavage, ultimately forming the NO_3^- anion.

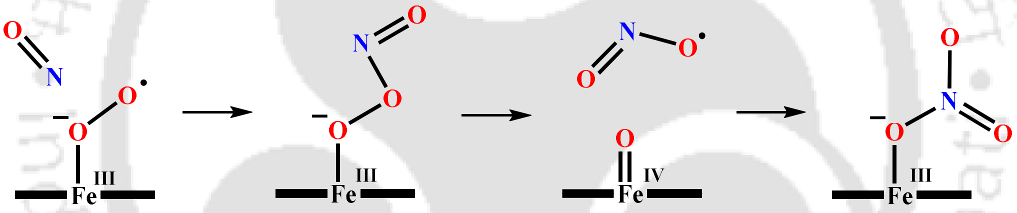

Scheme S1. Proposed mechanism of NOD enzyme.

Peroxynitrite irreversibly oxidizes the Fe(II) centre to Fe(III) in heme-containing proteins like hemoglobin, myoglobin, and cytochrome *c*. It also converts carbohydrates into aldehydes or organic nitrates and nitrites and can oxidize thiols into S-nitrosothiols.[14] Protein tyrosine nitration, a key biomarker for nitrosative stress, significantly affects the protein structure and function, leading to changes in catalytic activity, cytoskeletal organization, and cell signal transduction.[22]

The present thesis originates from our interest in exploring the reactivity of transition metal nitrosyl complexes with reactive oxygen species (ROS). The second chapter describes the reactivity of a non-heme iron-nitrosyl with dioxygen leading to the decomposition of the ligand through NOD-like activity. The third chapter discusses the syntheses of iron nitrosyls having spin-states $\frac{3}{2}$ and $\frac{1}{2}$, respectively. The significant role of spin states in controlling the dioxygen reactivity pathway has been demonstrated. In the fourth chapter, a Cr(II)-nitrosyl has been synthesized with a non-heme ligand framework. The reaction of this nitrosyl with H_2O_2 resulted in the formation of the corresponding Cr(V)-oxo species. Chapter five describes the synthesis and activity of a small molecule model for the flavodiiron nitric oxide reductases (FNORs) enzyme. Conclusion gives an overview and scope of this thesis for further studies.

Chapter 2: Reaction of a non-heme iron-nitrosyl with dioxygen: decomposition of the ligand through NOD-like activity

To explore the activation of NO by a set of non-heme iron complexes, the precursor complex, **2.1** $[Fe^{II}(TPz)(CH_3CN)(H_2O)](ClO_4)_2$ [TPz = *Tris*((3,5-dimethyl-1H-pyrazol-1-yl)methyl)amine] was synthesized and characterized. The complex **2.2**, $[Fe(TPz)(NO)(CH_3CN)](ClO_4)_2$ was prepared by nitrosylation of **2.1** in acetonitrile solution. FT-IR spectroscopy shows a signal at 1790 cm^{-1} assignable to N–O stretching indicating the formation of a $\{Fe(NO)\}^7$ complex {Figure S1(A)}. The X-band EPR spectrum of complex **2.2** displays two sets of signals at g ~ 4.11 and 2.04, respectively, corresponding to the near axial iron(II) nitrosyl with $S = \frac{3}{2}$ spin state.[23]

Single crystal X-ray studies of complex **2.2** revealed that iron centre is coordinated to four nitrogen atoms from the TPz ligand, one nitrosyl, and one acetonitrile moiety forming a distorted octahedral complex {Figure S1(B)}. The N–O and Fe–NO bond distances of complex **2.2** are 1.132(1) Å and 1.732(4) Å, respectively, which are in the range of other reported analogous iron-nitrosyl complexes such as $[(TPz)Fe(NO)(OClO_3)]^+$, $[(TPz)Fe(NO)Cl]^+$ *etc.* This is an example of linear iron-nitrosyl complex with a Fe-N-O bond angle of 174.2°.

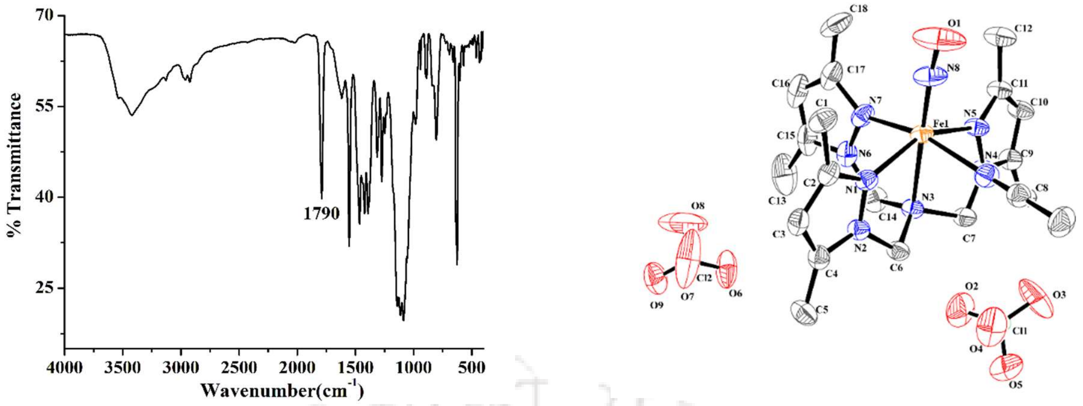

(A) **(B)**

FigureS1. (A) FT-IR spectrum of complex **2.2** in KBr. (B) ORTEP diagram of complex **2.2** (30% thermal ellipsoid plot, H atoms are omitted for clarity).

In acetonitrile solution of complex **2.2**, addition of O_2 gas at room temperature led to an immediate color change of the solution leading to the formation of corresponding nitrate complex **2.3**. This is evident from the presence of nitrate stretching frequency in FT-IR spectroscopy.[24] When the same reaction was carried out at –40 °C and the reaction mixture was kept in freezer for 2 days, it afforded white crystals of modified ligand (**L′**) (Figure S2) and brown precipitate of complex **2.4**, $[Fe^{III}(OH)_3]$.

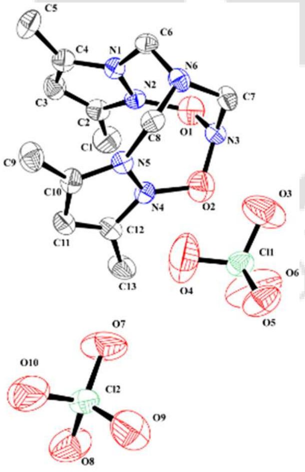

Figure S2. ORTEP diagram of modified ligand (**L′**) (30 % thermal ellipsoid plot, H atoms are omitted for clarity).

In an attempt to interpret the mechanism, the reaction was monitored using FT-IR, UV-visible and X-band EPR spectroscopy. In FT-IR spectroscopic monitoring, the addition of O_2

gas into the degassed acetonitrile solution of complex **2.2** at room temperature, resulted in the disappearance of the N–O stretching frequency at 1799 cm^{-1} (solution phase) with the appearance of a new band at 1835 cm^{-1} {Figure S3(A)}. The 1835 cm^{-1} band can be attributed to the nitrosyl stretching of an $[Fe^{III}(NO)]$ moiety *i.e.,* $\{Fe(NO)\}^6$ complex, which is formed upon oxidation of $[Fe^{II}(NO)]$ by O_2.[25] A ^{15}NO labelling experiment further supports the assignment of this 1835 cm^{-1} peak to the N–O stretch of $\{Fe(NO)\}^6$ intermediate {Figure S3(B)}.

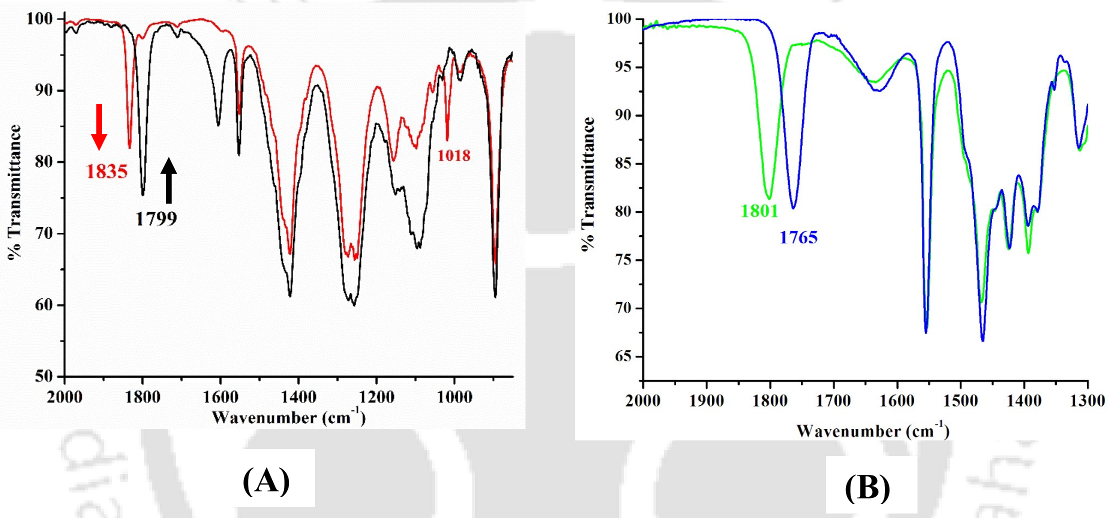

Figure S3. (A) FT-IR spectra of the reaction of complex **2.2** with O_2 in acetonitrile medium. [Complex **2.2** (black), after O_2 addition (red)]. (B) FT-IR spectra of the reaction of ^{15}NO labeled complex **2.2** with O_2 in acetonitrile medium. [Complex **2.2** with ^{15}NO (blue), after O_2 addition (green)].

Upon addition of O_2, iron centre gets oxidized by one electron as evident from FT-IR spectroscopy and O_2 is reduced to O_2^-. It is proposed that the reaction of complex **2.2** with O_2 initially produces the intermediate $\{[(TPz)Fe^{III}(NO)]^{3+}.(O_2^-)\}$ in the reaction cage which subsequently facilitates the formation of the peroxynitrite species, $[(TPz)Fe^{III}(OONO^-)]^{2+}$ (Scheme S2). The peroxynitrite undergoes rapid decomposition yielding an oxo-ferryl species, $[(TPz)Fe^{IV}{=}O]^{2+}$ along with NO_2. These recombine very fast during the warm-up process resulting in the formation of complex **2.3**. However, if the reaction mixture is kept in the freezer for 2 days, it undergoes different reaction leading to the formation of **L′**.

To establish the formation of the peroxynitrite intermediate in the course of the reaction, when 2,4-di-*tert*-butylphenol (2,4-DTBP) was added to the reaction mixture prior to O_2, about 65% of 2,4-di-*tert*-butyl-6-nitrophenol and the complex **2.5** $[(TPz)Fe^{III}(OH)]^{2+}$ were formed. When the reaction was carried out in the presence of TEMPO (TEMPO = 2,2,6,6-*tetra*methylpiperidin-1-yloxyl) the formation of **L′** was not observed. Instead, complex **2.5**, $[(TPz)Fe^{III}(OH)]^{2+}$ and 2,2,6,6-tetramethylpiperidinium nitrate ($tmpH_2^+NO_3^-$) have been isolated from the reaction mixture (Scheme S2).

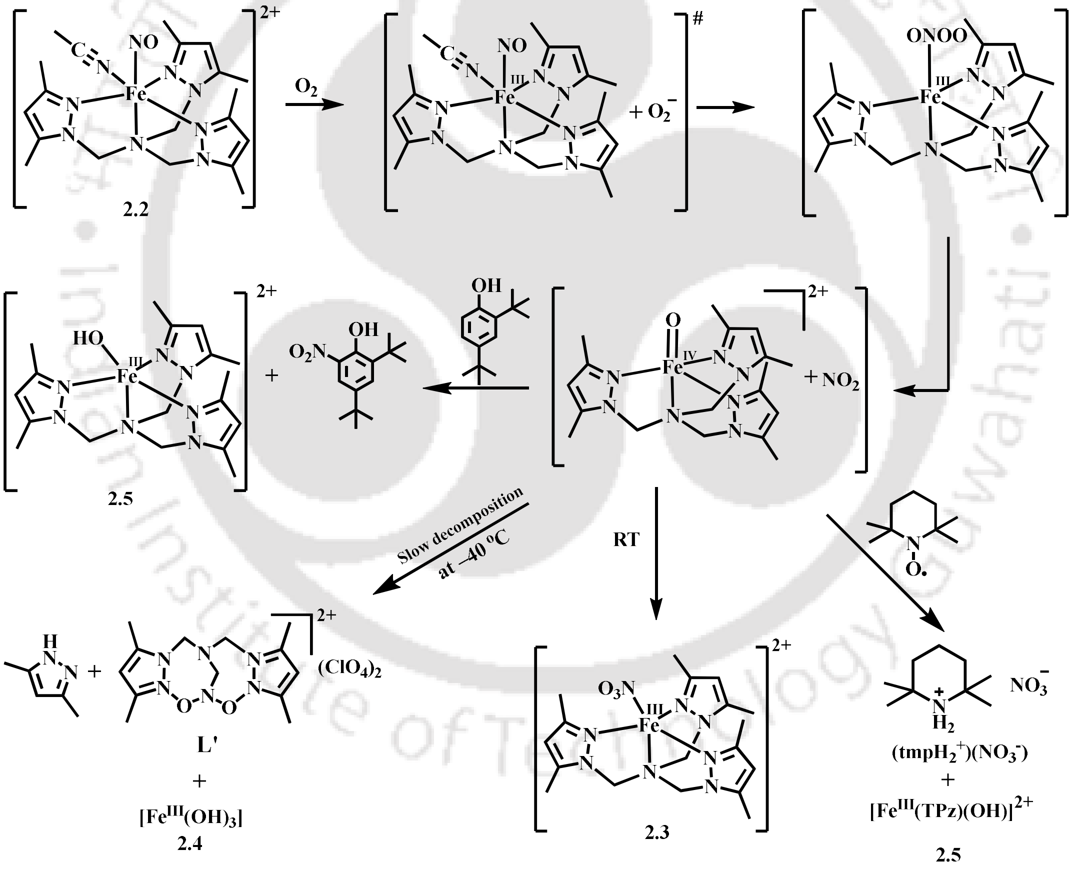

Scheme S2. Overall reaction

In conclusion, the high spin Fe(II)-nitrosyl complex **2.2**, [(TPz)Fe(NO)], having $\{Fe(NO)\}^7$ configuration in acetonitrile solution was found to react with O_2 to result in the ligand modification to **L′** through a presumed peroxynitrite intermediate. In contrast, heme $\{Fe(NO)\}^7$ complexes are known to react with O_2 leading to the formation of the corresponding nitrate (NO_3^-) complexes, but no reports are known where the ligand modification takes place. Although there is no spectroscopic evidence of the formation of the peroxynitrite intermediate, characteristic phenol ring nitration supports the proposition. Additionally, the trapping of NO_2 formed in the reaction also is in agreement with the proposed mechanism. This study, thus, gives an insight into the mechanism of the reaction of metal-nitrosyls with dioxygen leading to the NOD activity.

Chapter 3: Spin state dependent reactivity of iron-nitrosyls with dioxygen

A ferrous precursor complex, $[Fe^{II}(Pz_2Py)(CH_3CN)(H_2O)](ClO_4)_2$, **3.1** was synthesized and characterized by routine spectroscopic method. The structural study of complex **3.1** suggests a distorted octahedral arrangement around the central metal ion featuring four nitrogen atoms from the ligand, one acetonitrile molecule, and one water molecule (Figure S4). The presence of two perchlorate anion confirms the oxidation state of iron is +2.

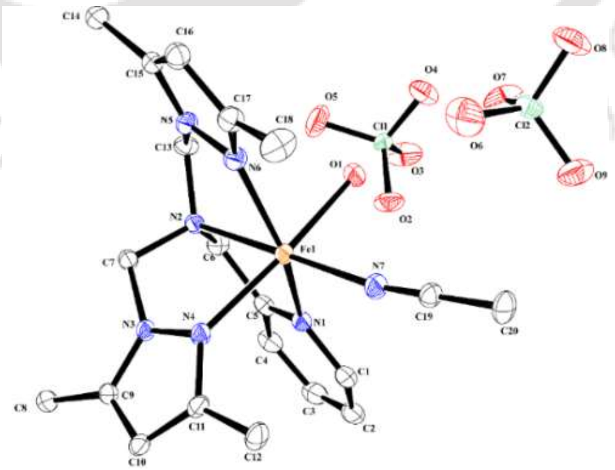

Figure S4: ORTEP diagram of complex **3.1** (30% thermal ellipsoid plot, H atoms are omitted for clarity).

Bubbling of NO into a dry and degassed methanolic solution of complex **3.1** at room temperature produces a green complex, **3.2a**. In contrast, keeping complex **3.1** in acetonitrile under NO atmosphere at –40 °C yields a red complex, **3.2b**. These complexes display distinctly different spectral behaviour in FT-IR, UV-vis and X-band EPR spectroscopy. Complex **3.2a** shows N–O stretching band at 1790 cm^{-1}, while complex **3.2b** shows the N–O stretch at 1711 cm^{-1}. In X-band EPR, the two complexes behave differently. Complex **3.2a** shows a strong signal at g ~ 4.15 and g ~ 2.03, corresponding to spin state $S = \frac{3}{2}$ which can be attributed to Fe(III)-NO^{-}, where a high-spin Fe(III) centre ($S = \frac{5}{2}$) is coordinated to a triplet NO^{-} ligand (S = 1) with the spins being antiferromagnetically coupled {Figure S5(A)}.[28] On the other hand, complex **3.2b** exhibits a signal at g ~ 2.03, corresponding to $S = \frac{1}{2}$ spin state {Figure S5(B)}.[29]

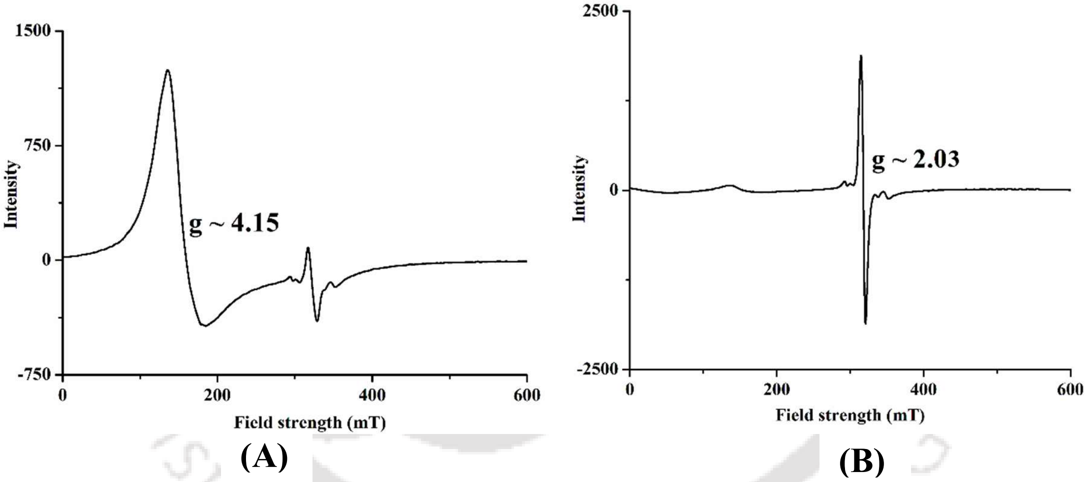

Figure S5. X-band EPR spectra of complex **3.2a** (A) and **3.2b** (B) in acetonitrile at 77 K.

The crystal structure of complex **3.2a** shows that the iron unit is coordinated with four nitrogen atoms from the ligand, one nitrosyl molecule, and one methanol molecule. The N–O bond length is 1.145(9) Å, and the Fe-N-O bond angle is 162.5°, confirming a linear iron nitrosyl complex {Figure S6(A)}. The DFT-optimized structure of complex **3.2b** indicates that the iron unit is coordinated with the ligand, a nitrosyl molecule, and an acetonitrile molecule {Figure S6(B)}.

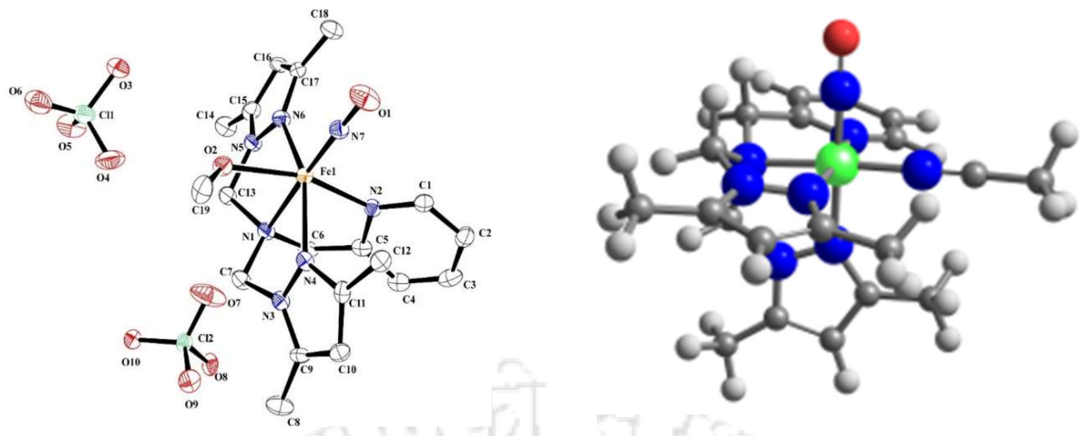

(A) **(B)**

Figure S6. (A) ORTEP diagram of complex **3.2a** (30% thermal ellipsoid plot, H atoms are omitted for clarity). (B) DFT Optimized structure of complex **3.2b.**

Dioxygen reactivity studies

In FT-IR spectral monitoring, the addition of O_2 gas to the acetonitrile solution of complex **3.2a** resulted in a shift of the N–O stretching frequency from 1790 to 1825 cm^{-1}, indicating the formation of $\{Fe(NO)\}^6$ species. The intensity of this 1825 cm^{-1} band decays with time and finally disappears and a new band at 1384 cm^{-1} appears indicating the presence of a nitrate (NO_3^-) group {Figure S7(A)}. In UV-visible spectroscopy, complex **3.2a** exhibited characteristic bands at 635 nm and 310 nm. Upon adding O_2 to a dry and degassed acetonitrile solution of complex **3.2a** at room temperature, the 635 nm band decreases in intensity leading to the formation of the final complex **3.3a** {Figure S7(B)}. This observation is similar to the one observed where the high-spin iron nitrosyl $[Fe(TPz)(NO)]^{2+}$ reacts with O_2 to form the nitrate complex **2.3** through a peroxynitrite intermediate. The phenol ring nitration produces 3,3',5,5'-tetra-*tert*-butyl-(1,1'-biphenyl)-2,2'-diol (~ 65 %), indicating the involvement of a peroxynitrite intermediate during the reaction (Scheme S3).

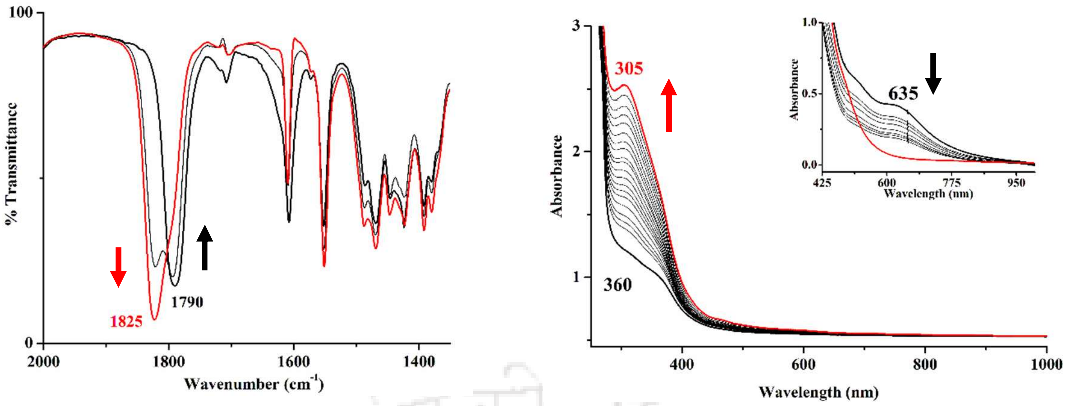

(A) **(B)**

Figure S7. (A) FT-IR spectra of complex **3.2a** before (black) and after addition of O_2 (red). (B) UV-visible spectra of complex **3.2a** in acetonitrile before (black) and after addition of O_2 (red) at room temperature.

The low-spin complex **3.2b** reacts rapidly with O_2. X-band EPR spectroscopy shows a fast decay of the intensity of the signal at g ~ 2.05 leading to an EPR silent intermediate that affords the final Fe(III) complex (Figure S8). It is interesting to note that in the FT-IR spectrum of the final complex, no ν(NO_3^-) or ν(NO_2^-) stretching was present.

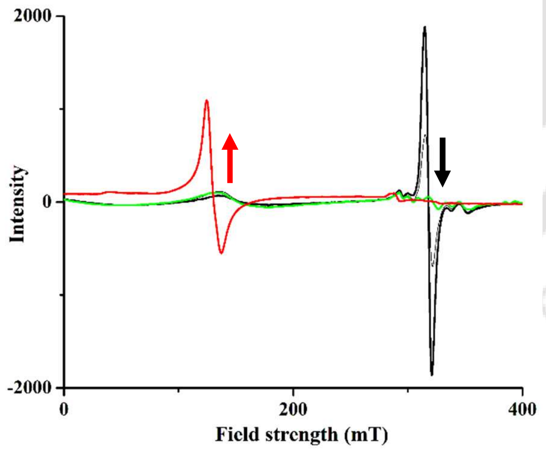

Figure S8. X-band EPR spectra of the reaction of complex **3.2b** (black) and after addition of O_2 (red) towards formation of complex **3.3b** (red, g ~ 4.15) through [Fe^{III}-O_2^-] intermediate (green) in acetonitrile at 77 K.

Gas chromatography-mass spectrometry (GC-MS) reveals that the headspace gas of the reaction mixture contains NO_2. Analysis of the final product suggest that the low-spin complex reacts with O_2 to produce complex **3.3b**, $[Fe^{III}(Pz_2Py)(OH)(CH_3CN)]^{2+}$. This reaction can be described as a simple ligand substitution, where O_2 substitutes the weakly coordinated nitrosyl moiety of the low-spin iron-nitrosyl complex **3.2b** (Scheme S3).

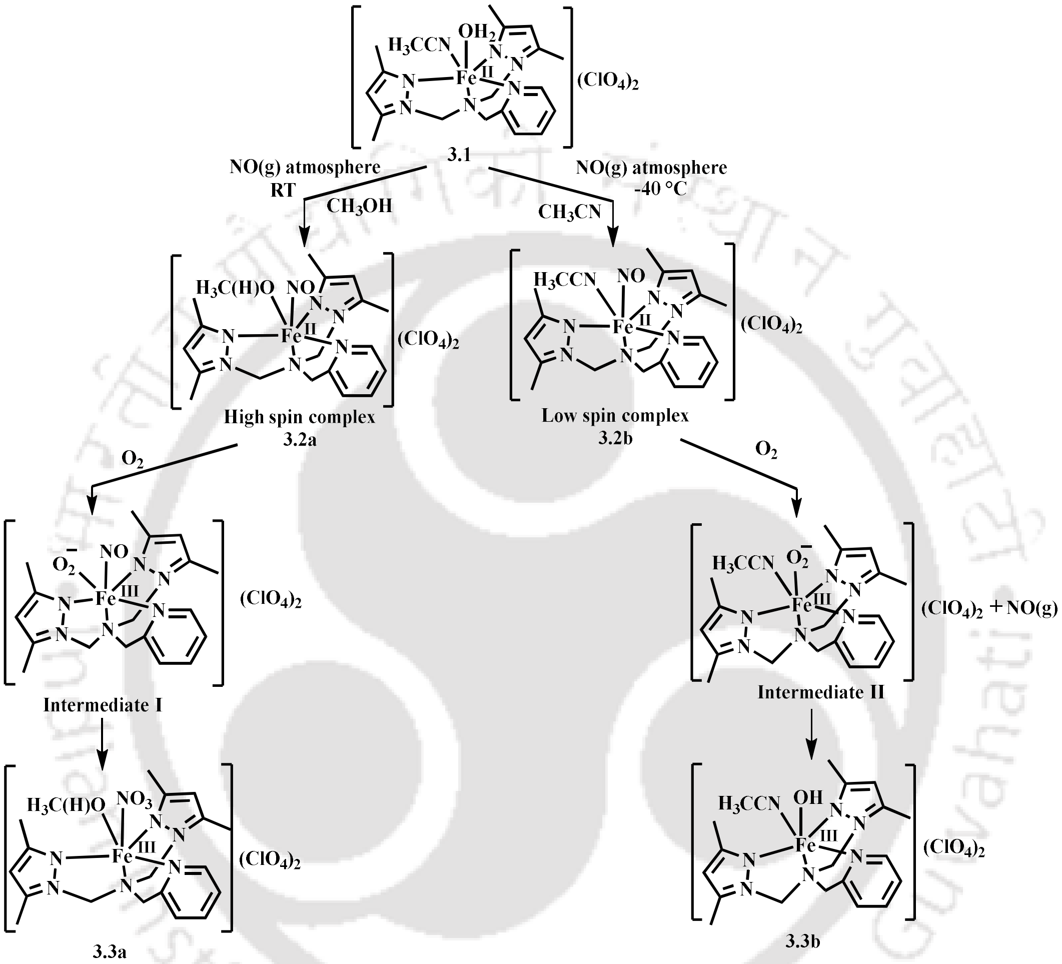

Scheme S3. Overall reaction.

Chapter 4: Reaction of a chromium-nitrosyl complex with H_2O_2: formation of a $[Cr^V{=}O]$ species

To investigate the effect of the metal centre on the oxidation of metal-bound nitrosyls, chromium was chosen. A chromium(II) precursor complex **4.1**, $[Cr^{II}(TPz)Cl_2]$ was synthesized and characterized using both spectroscopic and structural studies. The corresponding nitrosyl complex **4.2**, $[Cr(TPz)(NO)Cl]^+$ was synthesized by bubbling NO gas through a dry and degassed methanol solution of complex **4.1**. Spectroscopic characterization using FT-IR, UV-visible and X-band EPR spectral studies suggest complex **4.2** as a $\{Cr(NO)\}^5$ system. The FT-IR spectrum displays a characteristic nitrosyl stretching frequency at 1709 cm^{-1} for complex **4.2**. Additionally, the X-band EPR shows a strong signal with a g-value at around 2.00. The X-ray crystal structure indicates that complex **4.2** adopts a near linear geometry with a Cr-N-O bond angle of 176° and bond distances of 1.777(6) Å for Cr–N and 0.974(6) Å for N–O, respectively (Figure S9). All of these data are in agreement with previously reported $\{Cr(NO)\}^5$ complexes.[30-31]

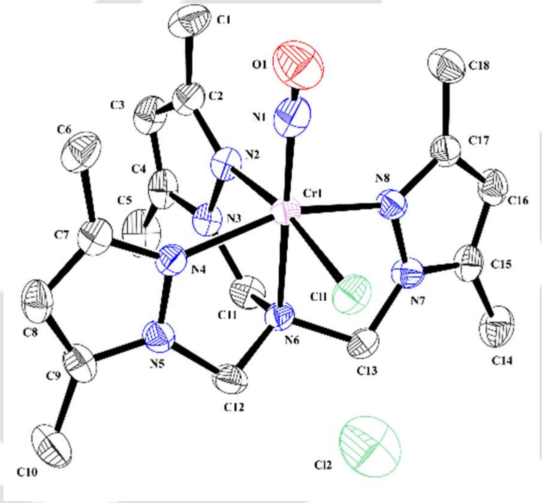

Figure S9. ORTEP diagram of complex **4.2 (**35% thermal ellipsoid plot, H atoms are omitted for clarity).

When complex **4.2** was made to react with H_2O_2 at –40 °C in an acetonitrile medium, the color of the solution changed indicating the formation of the final product, **4.3**. Complex **4.3** was identified as the corresponding nitrate product, $[Cr^{IV}(TPz)(NO_3^-)]^{2+}$.[32] NOD-like activity of complex **4.2** with H_2O_2 was established by its reaction with 2,4-DTBP. The spectral monitoring using UV-visible and EPR spectroscopy suggest that Cr(V)-oxo is formed in the course of the reaction (Figure S10).[33]

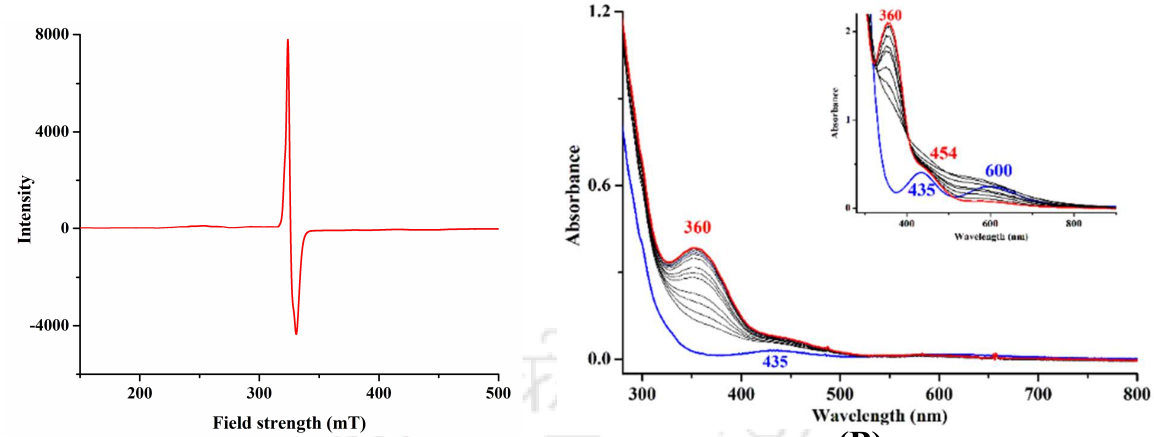

(A) **(B)**

Figure S10. (A) X-band EPR spectrum of intermediate **4a** in acetonitrile at 77 K, formed after the reaction of complex **4.2** with H_2O_2. (B) UV-visible spectral monitoring of the reaction of complex **4.2** (blue) and H_2O_2, intermediate **4a** (red) in acetonitrile at room temperature.

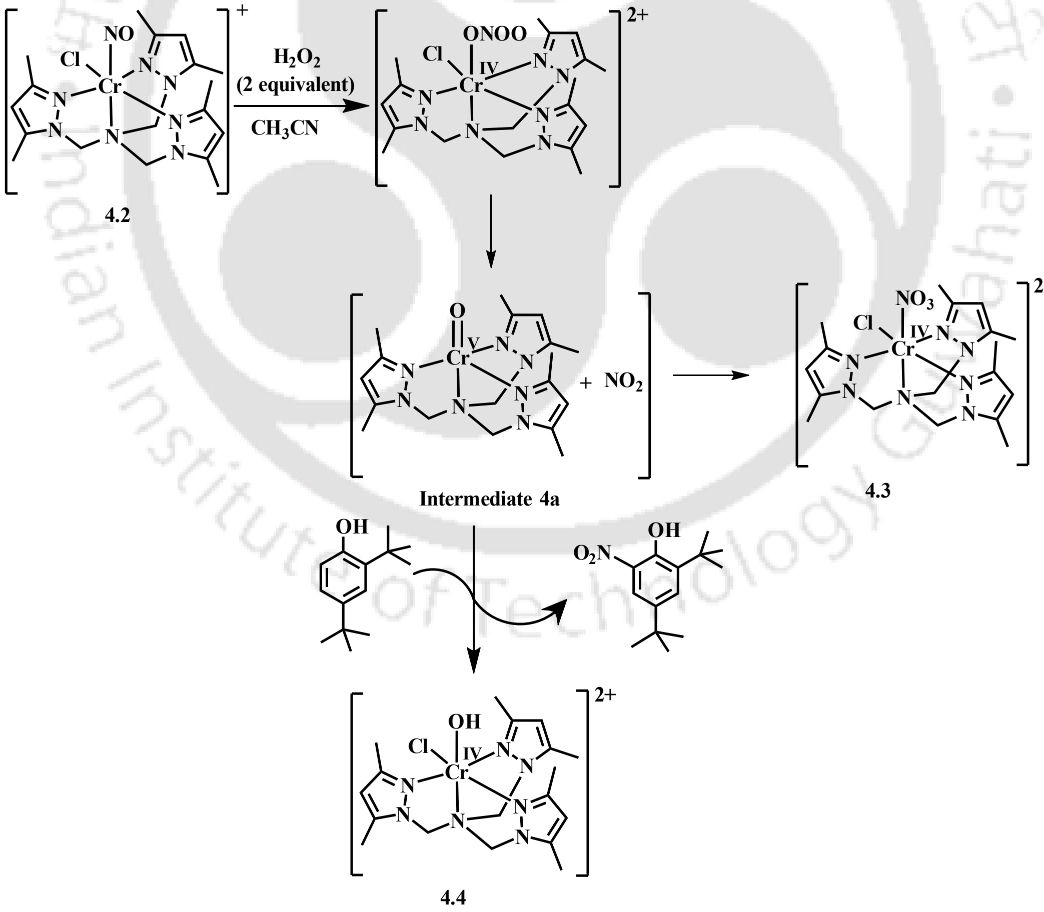

S4. Overall reaction.

In conclusion, a nitrosyl complex of chromium(II), **4.2** in a tripodal ligand framework reacts with H_2O_2 to result in Cr(IV)-nitrate. The reaction proceeds through [Cr^{v}=O] species and NO_2 by the homolytic cleavage of O–O bond of Cr(IV)-peroxynitrite species.

Chapter 5: Nitric oxide reductase activity of a diiron-dinitrosyl complex through the formation of $\{Fe(NO)_2\}^9$ intermediate

In the bacterial denitrification process, nitrate (NO_3^-) is reduced to dinitrogen (N_2), with a critical step involving the conversion of nitric oxide (NO) to nitrous oxide (N_2O) through the action of nitric oxide reductases (NORs) enzymes.[34-35] Amongst them, flavodiiron nitric oxide reductase (FNORs), featuring two non-heme iron centres, also facilitates this reduction effectively.[36] Several mechanistic pathways for FNOR's reduction of NO to N_2O have been proposed, including semi-reduced and super-reduced pathways, direct coupling with diferrous dinitrosyl intermediates, and the hyponitrite pathway.[37]

A precursor complex **5.1**, [$Fe^{II}(Pz_2Py)Cl_2$] has been synthesized and characterized using structural and spectroscopic methods. To obtain the diiron-dinitrosyl complex, an equimolar amount of $FeCl_3$ was added to the methanol solution of complex **5.1** followed by bubbling NO(g). The diiron-dinitrosyl complex **5.2** was isolated as solid and characterized both structurally and spectroscopically. The X-ray crystal structure of **5.2** reveals that one of the iron center is octahedrally coordinated and another one is tetrahedrally coordinated, resulting in an unsymmetrical non-heme diiron-dinitrosyl complex {Figure S11(A)}. Complex **5.2** includes a cationic part, $[Fe(Pz_2Py)(NO)Cl]^+$, with a distorted octahedral iron site coordinated to the ligand Pz_2Py, one NO group, and one chlorine atom. Its anionic part, $[FeCl_3(NO)]^-$, has a tetrahedral iron centre bonded to three chlorine atoms and one NO group.[38]

Complex **5.2** shows two nitrosyl stretching frequencies at 1790 and 1831 cm^{-1}, respectively, as expected for a diiron dinitrosyl complex.[39] Complex **5.2** shows two sets of axial EPR signals with g ~ 4.85 and 2.05 in acetonitrile at 77 K, characteristic of $\{Fe(NO)\}^7$ systems with $S = \frac{3}{2}$ ground state.[40]

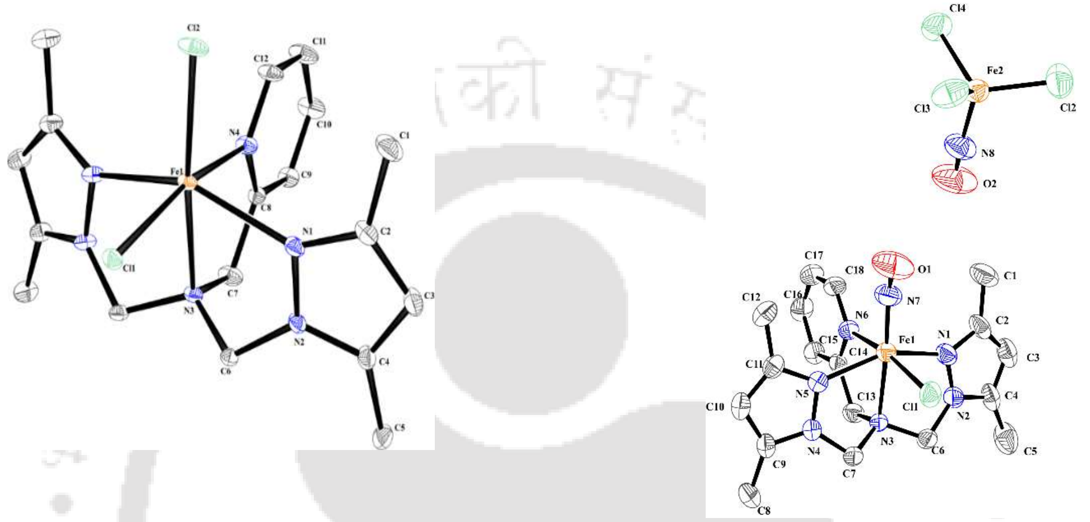

(A) **(B)**

Figure S11. ORTEP diagram of complex **5.1** (A) and **5.2** (B) (30% thermal ellipsoid plot, H-atoms are omitted for clarity).

In acetonitrile solution, complex **5.2** spontaneously decomposes to the corresponding μ-oxo-diferric complex **5.3**, $[(Pz_2Py)ClFe^{III}\text{-}O\text{-}Fe^{III}Cl_3]$, with simultaneous release of nitrous oxide (N_2O). The decomposition product, complex **5.3** was isolated and characterized as a μ-oxo bridged diferric complex and the ORTEP diagram is shown in figure S12(A). The decomposition process was monitored using UV-visible and X-band EPR spectroscopy.

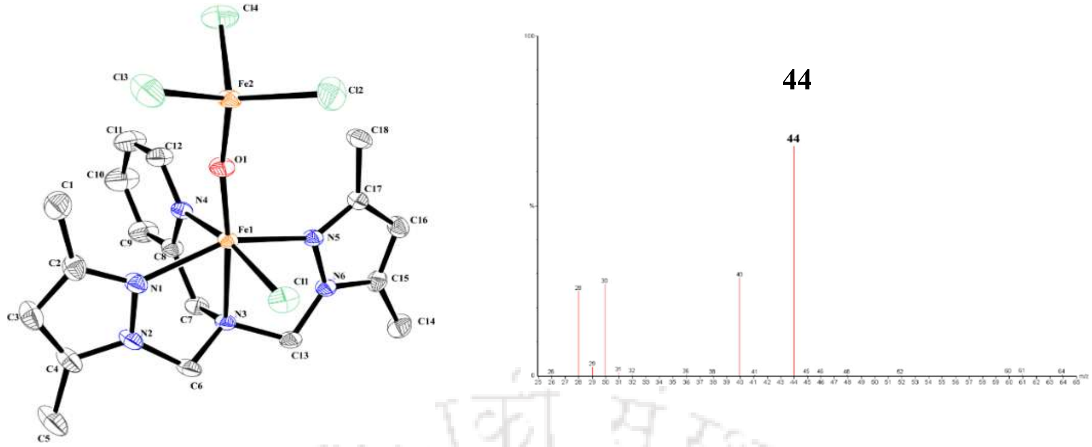

(A) **(B)**

Figure S12. (A) ORTEP diagram of complex **5.3** (30% thermal ellipsoid plot, H-atoms are removed for clarity). (B) GC-mass spectrum of the headspace gas of the acetonitrile solution of complex **5.3**.

Furthermore, complex **5.2** displays two distinct nitrosyl stretching frequencies at 1785 and 1830 cm^{-1} in KBr pellet, respectively, upon dissolution in acetonitrile, these frequencies shift to 1790 and 1704 cm^{-1} {Figure S13(A)}. These frequencies are attributed to the formation of the $\{Fe(NO)_2\}^9$ intermediate (Scheme S5), consistent with the ranges reported for earlier $\{Fe(NO)_2\}^9$ complexes of 1670-1790 cm^{-1}.[41] The compound $[(Pz_2Py)Fe(NO)_2Cl]$ exhibits significant instability and decomposes rapidly decposes to N_2O and $[(Pz_2Py)ClFe^{III}\text{-}O\text{-}Fe^{III}Cl_3]$.

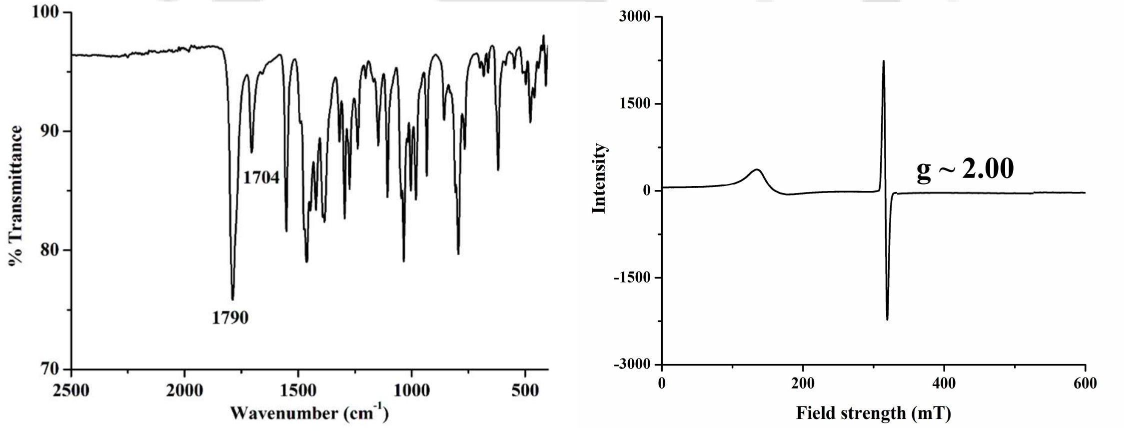

(A) **(B)**

Figure S13. (A) FT-IR spectrum of complex **5.2** after immidiately dissolving in acetonitrile medium. **(B)** X-band EPR spectrum of complex **5.2** immediately after dissolving in acetonitrile.

N_2O formation in nitric oxide reduction (NOR) is proposed to involve the super-reduced species $\{Fe(NO)_2\}^9$. In this intermediate, the *cis* configuration of the NO groups brings them into close proximity, facilitating the formation of an N–N bond and leading to a transient hyponitrite intermediate. This intermediate then cleaves into N_2O and a μ-oxo metal complex, highlighting the intricate dynamics of chemical transformations.

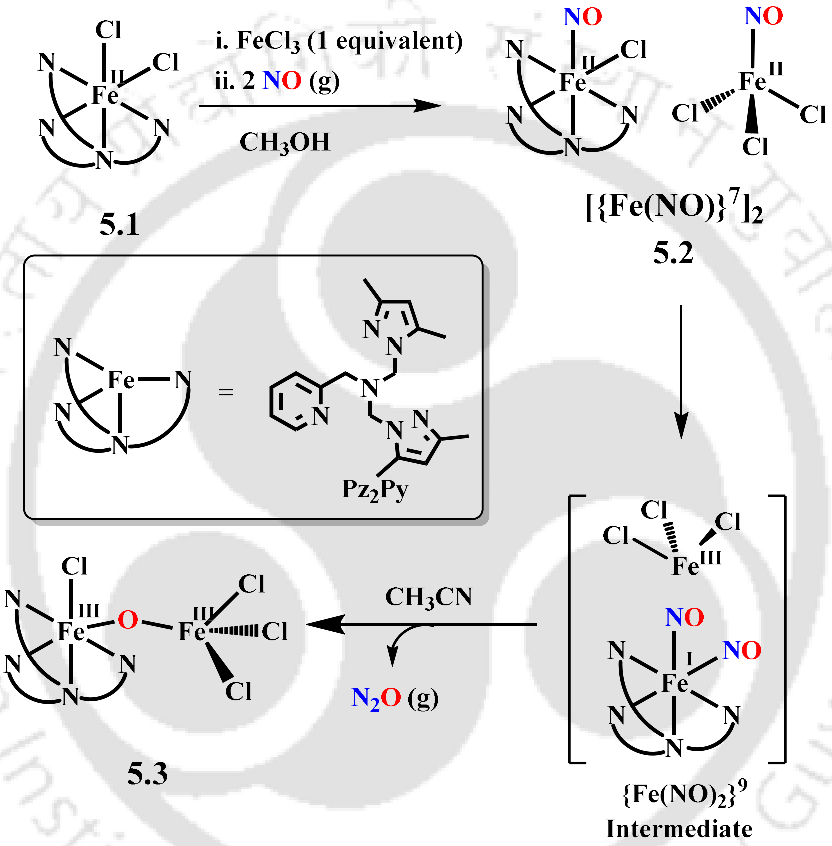

Scheme S5. Overall reaction.

References

1. *Nitric oxide: Biology and pathobiology*; Ignarro L. J., Academic Press, San Diego, **2000**.
2. Harland, J. B.; Manickas, E. C.; Hunt, A. P.; Lehnert, N. *Comprehensive Coordination Chemistry III*, **2021**, 806 – 874.

3. Richter-Addo, G. B.; Legzdins, P. *Metal Nitrosyls*; Oxford University Press: Oxford, UK, **1992**.
4. Gardner, P. R.; Gardner, A. M.; Martin, L. A.; Salzman, A. L. *Proc. Natl. Acad. Sci. U.S.A.* **1995**, *18*, 10378 – 10383.
5. Watmough, N. J.; Field, S. J.; Hughes, R. J. L.; Richardson, D. J. *Biochem. Soc. Trans.* **2009**, *37*, 392 – 399.
6. Besson, S.; Almeida, M. G.; Silveira, C. M. *Coord. Chem. Rev.* **2022**, *464*, 214560.
7. Lee, D.-H.; Mondal, B.; Karlin, K. D. *Nitrogen Monoxide and Nitrous Oxide Binding and Reduction. In Activation of Small Molecules;* Tolman, W. B. Ed. WILEY-VCH Verlag GmbH: Weinheim, **2006**, 43 – 79.
8. Fujisawa, K.; Tateda, A.; Miyashita, Y.; Okamoto, K.-i.; Paulat, F.; Praneeth, V. K. K.; Merkle, A.; Lehnert, N. *J. Am. Chem. Soc.* **2008**, *130*, 1205 – 1213.
9. Wu, G.; Morris, S. M., *Jr. Biochem J.* **1998**, *336*, 1 – 17.
10. Moncada, S.; Higgs, A. *N. Engl. J. Med.* **1993**, *329*, 2002 – 2012.
11. Lucas, K. A.; Pitari, G. M.; Kazerounian, S.; Ruiz-Stewart, I.; Park, J.; Schulz, S.; Chepenik, K. P.; Waldman, S.A. *Pharmacol. Rev.* **2000**, *52*, 375 – 414.
12. (a) Fang, F. C. *Nitric Oxide and Infection*; Ed.; Kluwer Academic/ Plenum Publishers: New York, **1999**; (b) O'Dell, T. J.; Hawkins, R. D.; Kandel, E. R.; Arancio, O. *Proc. Natl. Acad. Sci. USA* **1991**, *88*, 11285 – 11289.
13. (a) Munzel, T.; Feil, R.; Mulsch, A. S.; Lohmann, M.; Hofmann, F.; Walter, U. *Circulation,* **2003**, *108*, 2172 – 2183; (b) Denninger, J. W.; Marletta, M. A. *Biochim. Biophys. Acta* **1999**, *1411*, 334 – 350; (c) Liaudet, L.; Soriano, F. G.; Szabo, C. *Crit. Care Med.* **2000**, *28*, N37 – N52; (d) Thomas, D. D.; Ridnour, L. A.; Isenberg, J. S.; Flores-Santana, W.; Switzer, C. H.; Donzelli, S.; Hussain, P.; Vecoli, C.; Paolocci, N.;

Ambs, S.; Colton, C. A.; Harris, C. C.; Roberts, D. D.; Wink, D. A. *Free Radical Biol. Med.* **2008**, *45*, 18 – 31; (e) Marletta, M. A. *Biochemistry* **2021**, *60*, 3491 – 3496.

14. Radi, R. *Chem. Res. Toxicol*. **1998**, *11*, 720 – 721.
15. Szabo, C.; Ischiropoulos, H.; Radi, R. *Nat. Rev. Drug. Discov*. **2007**, *6*, 662 – 680.
16. (a) Beal, M. F. *Free Radic. Biol. Med*. **2002**, *32*, 797 – 803. (b) Radi, R.; Cassina, A.; Hodara, R.; Quijano, C.; Castro, L. *Free Radic. Biol. Med*. **2002**, *33*, 1451 – 1464.
17. Beckman, J. S.; Ischiropoulos, H.; Zhu, L.; Woerd, M.; Smith, C.; Chen, J.; Harriso, J.; Martin, J. C.; Tsai, M. *Arch. Biochem. Biophys*. **1992**, *298*, 438 – 445.
18. Beckmann, J. S.; Ye, Y. Z.; Anderson, P. G.; Chen, J.; Accavitti, M. A.; Tarpey, M. M.; White, C. R. *J. Biol. Chem*. **1994**, *375*, 81 – 88.
19. Balagopalakrishna, C.; Abugo, O. O.; Horsky, J.; Manoharan, P. T.; Nagababu, E.; Rifkind, J. M. *Biochemistry* **1998**, *37*, 13194 – 13202.
20. Singha, A.; Das, P. K.; Dey, A. *Inorg. Chem*. **2019**, *58*, 10704 – 10715.
21. Yan, J. J.; Kroll, T.; Baker, M. L.; Wilson, S. A.; Decréau, R.; Lundberg, M.; Sokaras, D.; Glatzel, P.; Hedman, B.; Hodgson, K. O.; Solomon, E. I. *Proc. Natl. Acad. Sci. U. S. A*. **2019**, *116*, 2854 – 2859.
22. Schopfer, F. J.; Baker, P. R.; Freeman, B. A. *Trends Biochem. Sci.* **2003**, *28*, 646 – 654.
23. Ray, M.; Golombek, A. P.; Hendrich, M. P.; Yap, G. P.; Liable-Sands, L. M.; Rheingold, A. L.; Borovik, A. S. *Inorg. Chem.* **1999**, *38*, 3110 – 3115.
24. Mondal, B.; Saha, S.; Borah, D.; Mazumdar, R.; Mondal, B. *Inorg. Chem.* **2019**, *58*, 1234 – 1240.
25. Jones, R. D.; Summerville, D. A.; Basolo, F. *Chem. Rev*. **1979**, *79*, 139 – 179.
26. Suzuki, M.; Ishiguro, T.; Kozuka, M.; Nakamoto, K. *Inorg. Chem.* **1981**, *20*, 1993 – 1996.
27. Sugimoto, H.; Sawyer, D. T. *J. Am. Chem. Soc.* **1985**, *107*, 5712 – 5716.

28. Speelman, A. L.; White, C. J.; Zhang, B.; Alp, E. E.; Zhao, J.; Hu, M.; Krebs C.; Penner-Hahn, J.; Lehnert, N. *J. Am. Chem. Soc.* **2018**, *140*, 11341 – 11359.
29. Patra, A. K.; Rose, M. J.; Olmstead, M. M.; Mascharak, P. K. *J. Am. Chem. Soc*. **2004**, *126*, 4780 – 4781.
30. Das, S.; Ray, S.; Devi, T.; Ghosh, S.; Harmalkar, S. S.; Dhuri, S. N.; Mondal, P.; Kumar, P. *Chem. Sci*. **2022**, *13*, 1706 – 1714.
31. Keerthi, A.; Das, S.; Bhardwaj, P.; Sk, M. P.; Kumar, P. *Dalton Trans.* **2023**, *52*, 16492 – 16499.
32. Eljack, N. D.; Sulfab, Y. *Polyhedron,* **2012**, *44*, 28 – 33.
33. Hong, Y. H.; Jang, Y.; Ezhov, R.; Seo, M. S.; Lee, Y. M.; Pandey, B.; Hong, S.; Pushkar, Y.; Fukuzumi, S.; Nam, W. *ACS Catal.* **2021**, *11*, 288 – 2901.
34. Wasser, I. M.; de Vries, S.; Moënne-Loccoz, P.; Schröder, I.; Karlin, K. D. *Chem. Rev.* **2002**, *102*, 1201 – 1234.
35. Hendriks, J.; Oubrie, A.; Castresana, J.; Urbani, A.; Gemeinhardt, S.; Saraste, M. *Biochim. Biophys. Acta Bioenerg.* **2000**, *1459*, 266 – 273.
36. Hayashi, T.; Caranto, J. D.; Wampler, D. A.; Kurtz Jr, D. M.; Moënne-Loccoz, P. *Biochemistry* **2010**, *49*, 7040 – 7049.
37. Khatua, S.; Majumdar, A. *J. Inorg. Biochem.* **2015**, *142*, 145 – 153.
38. In-lam, A.; Wolf, M.; Wilfer, C.; Schaniel, D.; Woike, T.; Klüfers, P. *Chem. Eur. J.* **2019**, *25*, 1304 – 1325.
39. Feig, A. L.; Bautista, M. T.; Lippard, S. J. *Inorg. Chem.* **1996**, *35*, 6892 – 6898.
40. Caranto, J. D.; Weitz, A.; Giri, N.; Hendrich, M. P.; Kurtz, D. M. *Biochemistry* **2014**, *53*, 5631 – 5637.
41. Lehnert, N.; Kim, E.; Dong, H. T.; Harland, J. B.; Hunt, A. P.; Manickas, E. C.; Oakley, K. M.; Pham, J.; Reed, G. C.; Alfaro, V. S. *Chem. Rev.* **2021**, *121*, 14682 – 14905.

Chapter 1

Introduction

1.1 General aspects of transition metal nitrosyl

Transition metal nitrosyls are coordination compounds where nitric oxide (NO) binds to the metal center as a ligand and it has been recognized since the early development of coordination and organometallic chemistry. NO has become a subject of interest in biological research due to its important roles in regulating blood pressure, facilitating neuronal communication, inducing cytotoxic effects *etc.*[1-4] Its interaction with metal ions is of the most considerable interest, as metal ions can mediate many of these aforementioned biological processes.[5] Furthermore, the binding of NO to metalloproteins has a rich and well-documented history, largely because NO has been employed as a 'surrogate' in investigating O_2 binding to hemes, (*i.e.,* iron porphyrins). NO, being a 'non-innocent' ligand, can exist in different oxidation states (*e.g.,* $NO^{\bullet}$, NO^{+}, NO^{-}) in transition metal nitrosyls.[6-7] In addition, the bond between NO and transition metals is oftentimes very covalent, making it impossible to determine the electronic distribution in the M-N-O unit without performing detailed spectroscopic and theoretical studies. For this reason, transition metal nitrosyl complexes are abbreviated according to Enemark-Feltham notation as $\{M(NO)_x\}^n$ [where the index x indicates the number of coordinated NO ligands to metal, and the exponent n counts the number of valence electrons, which is the sum of metal (d) and NO (π^*) electrons].[8]

1.2 Bonding of NO with transition metal ions

The molecular orbital (MO) diagram of NO reveals a $^2\Pi$ ground state with a bond order of 2.5, resulting in a bond length of 1.154 Å, which falls between nitrogen (N_2) at 1.06 Å and oxygen (O_2) at 1.18 Å.[9-10] NO displays a stretching frequency of 1875 cm^{-1}.[11] The highest occupied molecular orbital (HOMO) of NO exhibits exclusively nitrogen character. As a result, it tends to bind to metal centers through the nitrogen atom. It can form a bond by either losing one electron to form the nitrosonium cation (NO^+) or gaining one electron to form the nitroxyl anion (NO^-).

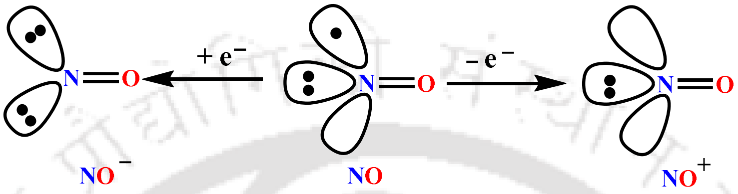

Figure 1.1: Lewis-representation of NO, NO^+ and NO^-.

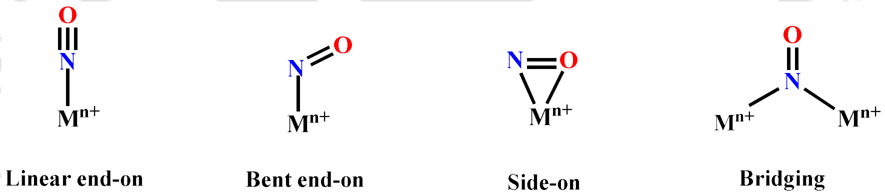

Figure 1.2: Schematic presentation of binding mode of NO to metal centers.

The nitrosonium cation (NO^+) is isoelectronic with carbon monoxide (CO) and possesses a lone pair of electrons in a *sp* hybrid orbital, which predicts a linear M-N-O structure. In contrast, the nitroxide anion (NO^-), isoelectronic with dioxygen (O_2), features nitrogen in an sp^2 hybridization, resulting in a bond angle of approximately 120°.[12] Based on the literature, the binding modes of NO to metal ions can be of three types: (i) end-on (linear and bent), (ii) side-on, and (iii) bridging.[13]

1.3 Reactivity of metal nitrosyls with reactive oxygen species

Reactive oxygen species (ROS), such as superoxide (O_2^-) and peroxide (O_2^{2-}), play a crucial role in biological systems and can also cause cellular damage and cytotoxicity.[14]

Superoxide dismutase (SOD) plays the key role to convert O_2^- into hydrogen peroxide (H_2O_2) and oxygen (O_2). However, during certain conditions, such as sepsis, inflammation, excitotoxicity, there can be high levels of O_2^- and NO inside cells. Then NO can outcompete SOD, causing O_2^- and NO to react in a diffusion control rate and produce peroxynitrite ($ONOO^-$).[15] Alternatively, another reactive oxygen species such as H_2O_2, can generate peroxynitrite through the reaction with nitrite (NO_2^-) in the presence of the peroxidase enzyme.[16-17]

This potent and fleeting oxidant peroxynitrite with a half-life of around 10 ms, (ONOO/ONOOH, pKa, 6.8) once produced *in vivo*, can react directly with various biomolecules, causing one-electron or two-electron oxidation.[18-19] It modifies heme-containing proteins such as hemoglobin, myoglobin, and cytochrome *c* by oxidizing heme unit from ferrous to ferric form.[20-22] Additionally, it inactivates inducible nitric oxide synthase (iNOS) through oxidative modification of its heme group.[23] It can convert carbohydrates into aldehydes or oxidize them to organic nitrates or nitrites. Protein tyrosine nitration is an essential biomarker for detecting peroxynitrite activity in biological systems.[17,24] Tyrosine nitration influences protein structure and function, leading to the formation of antigenic epitopes, changes in enzyme catalytic activity, alterations in cytoskeletal organization, and disruptions in cell signal transduction.[25] Consequently, it is recognized as a critical factor in peroxynitrite-mediated cytotoxicity, essential for understanding cellular damage and potential therapies.

Another important function of the peroxynitrite anion is linked to the nitric oxide dioxygenases (NODs) enzyme.[26] The active site structure of NODs enzyme consists of flavohemoglobins that is basically an iron heme unit in $[Fe^{III}\text{-}(O_2^-)]$ form.[27] This $[Fe^{III}\text{-}(O_2^-)]$ intermediate species reacts with NO to produce nitrate (NO_3^-). The proposed mechanistic pathway involves a $[Fe^{III}\text{-}(ONOO)^-]$ intermediate, which readily decomposes to $[Fe^{IV}{=}O]$ and nitrogen dioxide (NO_2) (Scheme 1.1).[28] The reaction mechanism of NOD is elusive since none of the intermediates are well characterized owing to their highly unstable nature in biological systems.

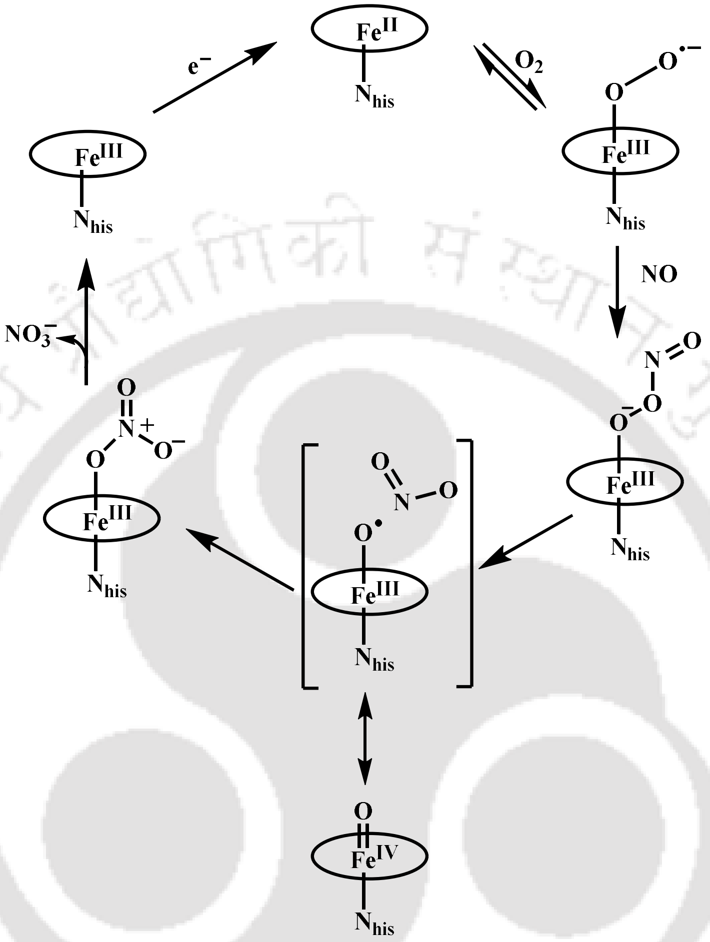

Scheme 1.1

The study of metal peroxynitrite chemistry is essential for advancing our understanding of NOD enzyme mechanisms and their stability. Despite numerous investigations into their formation and decomposition pathways, definitive spectroscopic evidence remains elusive.

Two main approaches for synthesizing metal-peroxynitrite complexes include (i) the reaction of a metal-nitrosyl complexes with O_2 and reactive oxygen species like O_2^- and O_2^{2-}; and (ii) the reaction of a metal-superoxo or peroxo complexes with NO.

1.3.1 Synthesis of transition metal-peroxynitrite complexes to bio-mimic NOD enzyme

Basolo and coworkers proposed the formation of a cobalt-peroxynitrite intermediate in the reaction of a cobalt nitrosyl complex with molecular oxygen, producing the corresponding nitrite (NO_2^-) product.[29] This is the first instance of a metal-peroxynitrite intermediate being linked to such a reaction (Scheme 1.2).

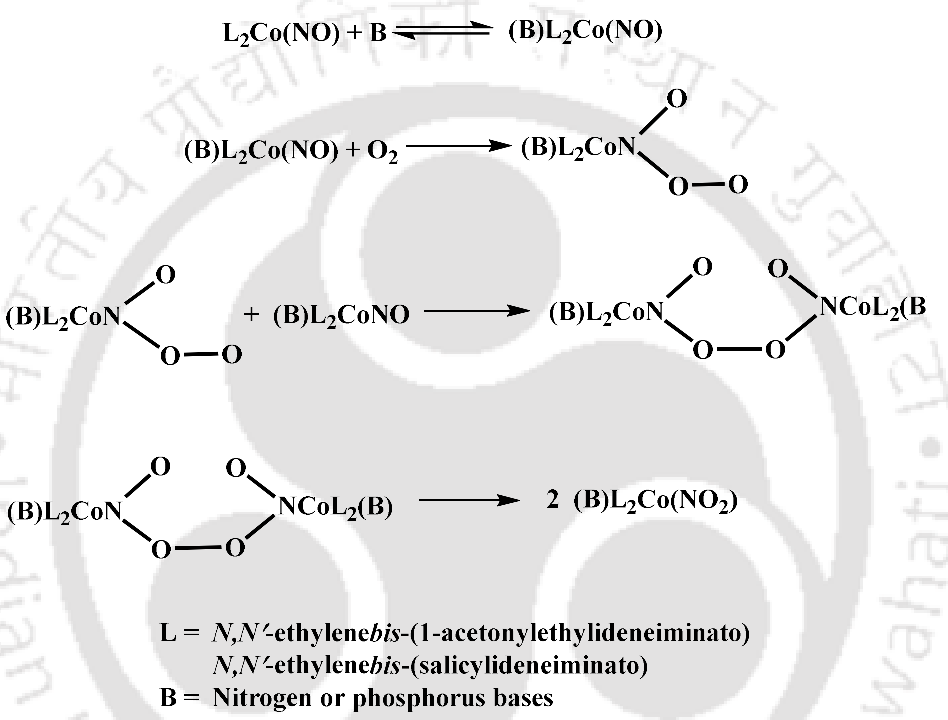

Scheme 1.2

Later on, the formation of peroxynitrite ion has been proposed in a number of examples involving reactions of metal-superoxo complexes and NO or metal-nitrosyls with O_2. For example, a mixed valent dicopper system, $[Cu^{I,II}_2(UN\text{-}O^-)]^{2+}$, [UN-O⁻ = 2-(*bis*(2-(pyridin-2-yl)ethyl)amino)-6-((*bis*(2-(pyridin-2-yl)ethyl)amino)methyl)phenolate] reacts with NO at –80 ºC in CH_2Cl_2 to produce the corresponding µ-nitrosyl complex $[Cu^{I,II}_2(UN\text{-}O^-)(NO)]^{2+}$. This complex further reacts with O_2 to produce the intermediate $[Cu^{II}_2(UN\text{-}O^-)(O_2^-)(NO)]^{2+}$. Low-temperature infrared (IR) spectral monitoring revealed the formation of the corresponding μ-peroxynitrite intermediate (Scheme 1.3).[30]

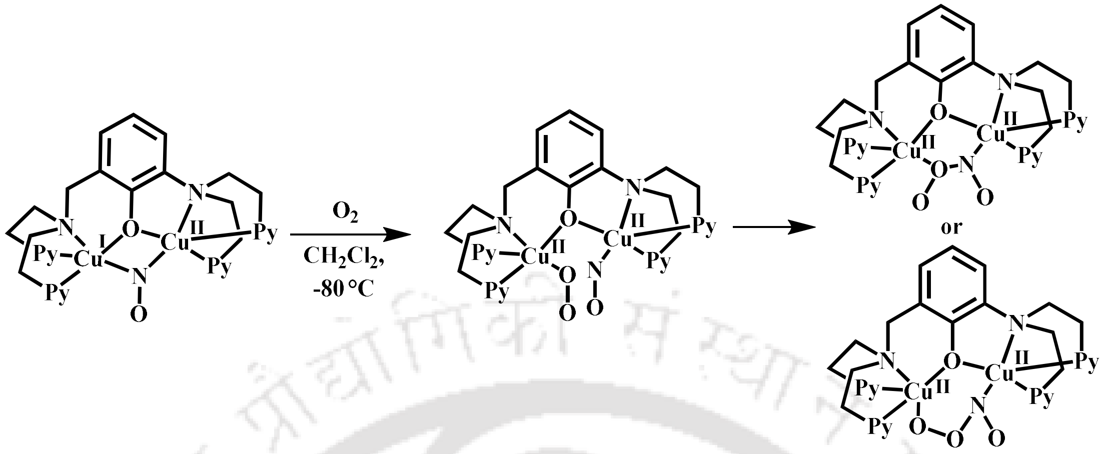

Scheme 1.3

Nam group has reported two cobalt-nitrosyl complexes in *N*-tetramethylatedcyclam, $[Co(12\text{-}TMC)(NO)]^{2+}$ and $[Co(13\text{-}TMC)(NO)]^{2+}$ (12-TMC = 1,4,7,10-tetramethyl-1,4,7,10-tetraazacyclododecane and 13-TMC = 1,4,7,10-tetramethyl-1,4,7,10-tetraazacyclotridecane). These complexes are stable in the presence of molecular oxygen but react with superoxide, forming Co(II)-nitrite complexes and releasing O_2 (Scheme 1.4). It has been proposed that a Co(II)-peroxynitrite intermediate is involved in this reaction.[31]

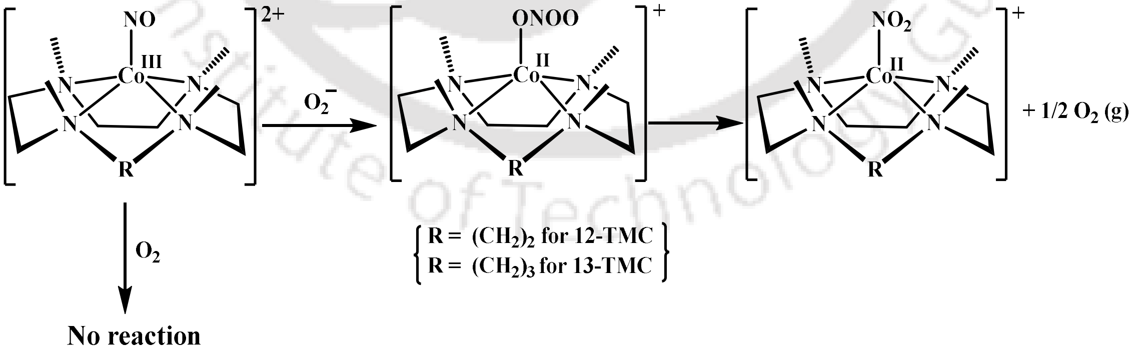

Scheme 1.4

In an alternate study, a cobalt nitrosyl complex $[(14\text{-}TMC)Co(NO)]^{2+}$ (14-TMC = 1,4,7,10-tetraazacyclododecane) dissociates to form a cage molecule, $\{(14\text{-}TMC)Co\cdots NO\}^{2+}$

prior to the reaction with O_2. The cage molecule converts to a cobalt(II)-nitrate complex upon exposure to molecular oxygen, also implicating a cobalt(II)-peroxynitrite intermediate formation (Scheme 1.5).[32]

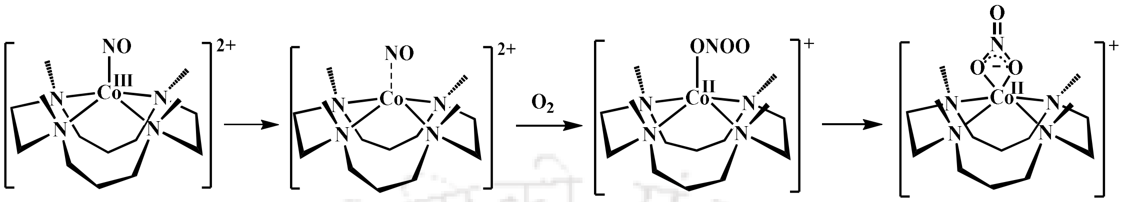

Scheme 1.5

Nitrosyl complexes, $[Co(BPMEN)(NO)]^{2+}$ and $[Cr(BPMEN)(NO)]^{2+}$ [BPMEN = *N, N′*-*bis*(2-pyridylmethyl)-1,2-diaminoethane] upon reaction with the O_2^{2-} anion gives corresponding NO_2^- complexes. The cobalt nitrosyl complex reacts with O_2^- to give $[Co^{II}(BPMEN)(NO_2^-)_2]$ with O_2 as a product *via* a $[Co^{II}(ONOO)]^-$ intermediate. In contrast, the chromium nitrosyl complex generates $[Cr^{III}(BPMEN)(NO_2^-)Cl]^+$ complex and O_2 *via* a transient $[Cr^{III}\text{-}(ONOO)^-]$ intermediate (Scheme 1.6). In these reactions, phenol ring nitration test with 2,4-di-*tert*-butylphenol (2,4-DTBP) were used to establish the involvement of peroxynitrite intermediate.[33]

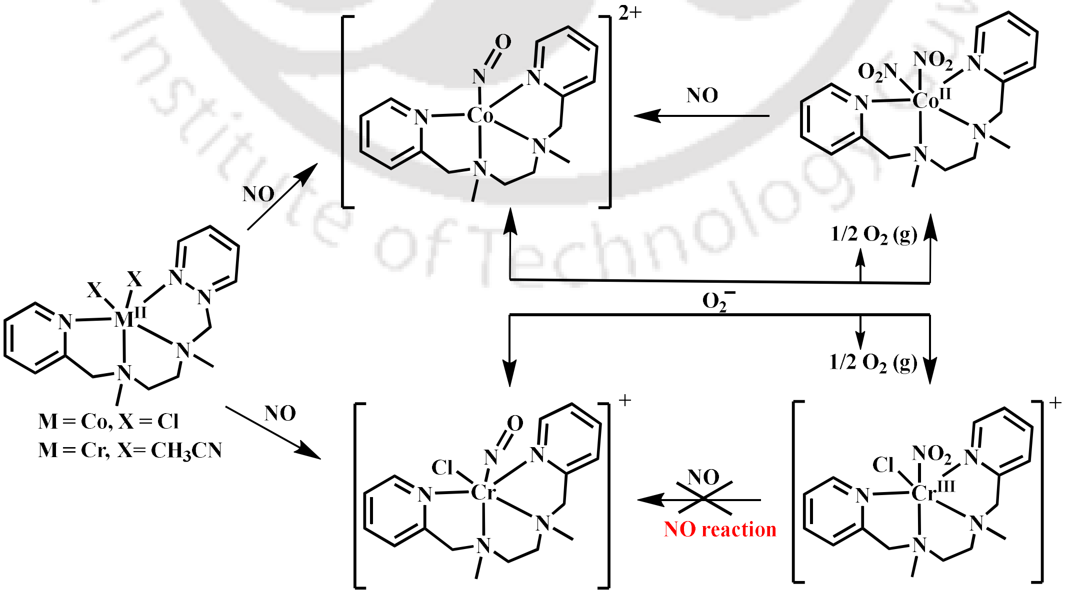

Scheme 1.6

Our research group has been actively studying the metal-peroxynitrite chemistry since long back. A copper-nitrosyl complex [CuL$_1$(NO)](ClO$_4$)$_2$, [L$_1$ = *Bis*(2-ethyl-4-methyl-imidazol-5-yl)methane] was reported which reacts with H_2O_2, resulting in the formation of the corresponding Cu(I)-peroxynitrite intermediate. The formation of peroxynitrite intermediate was confirmed by phenol ring nitration test using 2,4-di-*tert*-butylphenol. Peroxynitrite intermediate readily isomerizes and forms [Cu^{I}L$_1$(NO$_3^-$)], which further converts to [Cu^{II}-NO$_3$] *via* aerial oxidation (Scheme 1.7).[21]

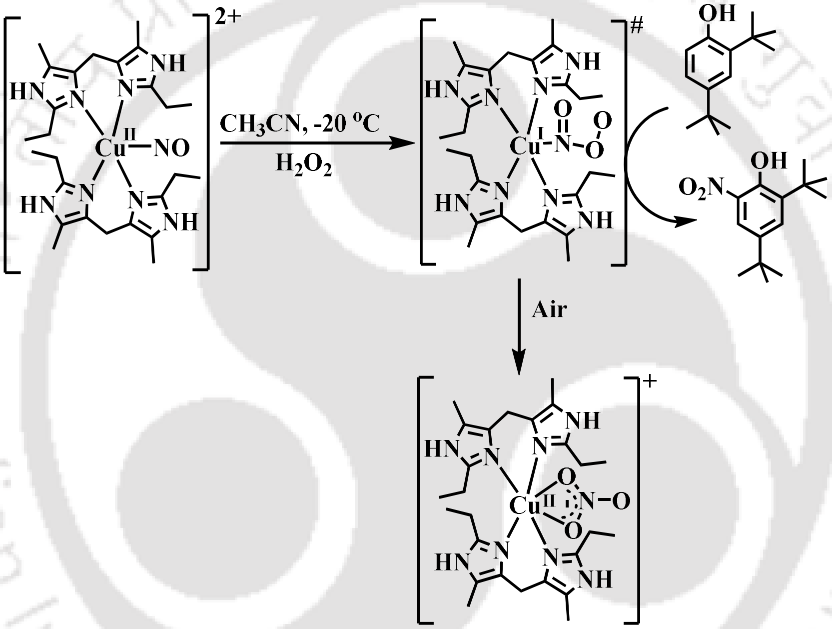

Scheme 1.7

A Cu-nitrosyl complex with histidine-derived ligand, methyl-2-(2-hydroxybenzylamino)-3-(1*H*-imidazol-5-yl)propanoate in the presence of H_2O_2 results in the formation of the corresponding [Cu^I-(ONOO$^-$)] intermediate (Scheme 1.8).[35] This peroxynitrite intermediate was found to induce nitration at the phenol ring present in the ligand framework resembling the tyrosine nitration in biological systems. Further, isolation of NO$_3^-$ as the decomposition product from nitrosyl complex at room temperature also supports the involvement of ONOO$^-$ as an intermediate species.

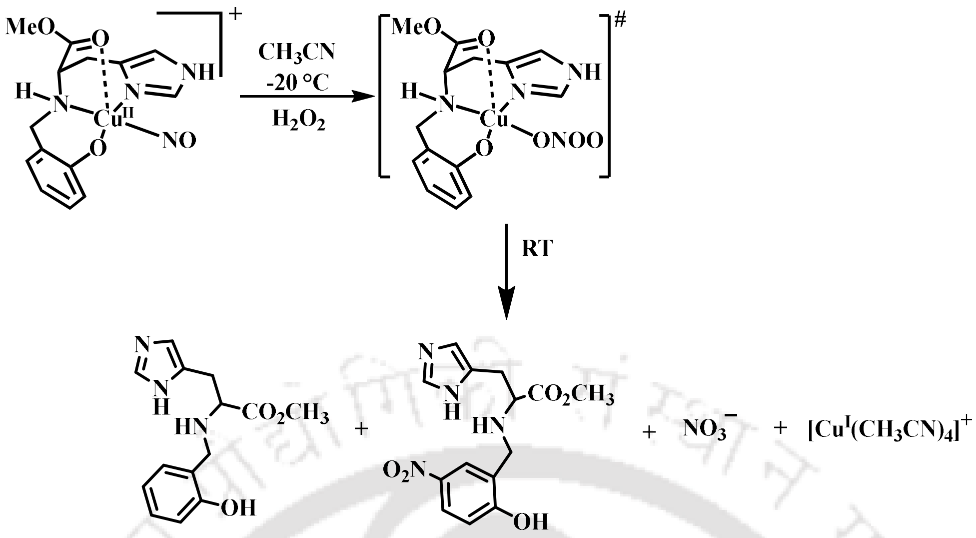

Scheme 1.8

A cobalt-nitrosyl complex, [Co(BPI)(NO)(OAc)], [BPI = *Bis*(pyridylimino)isoindol] having $\{Co(NO)\}^8$ configuration upon reaction with O_2 was reported to yield the nitrite complex, $[Co^{III}(BPI)(NO_2^{-})(OAc)]$ (Scheme 1.9). A six-coordinated intermediate species, $[Co(BPI)(NO)(O_2^{-})(OAc)]$ has been identified from FT-IR spectral monitoring.[36]

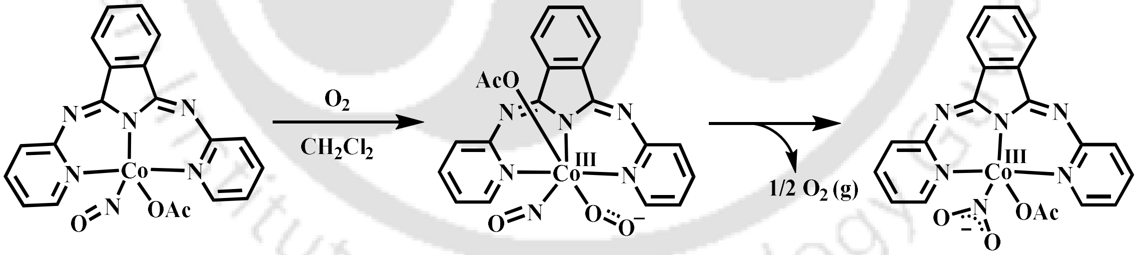

Scheme 1.9

Two cobalt nitrosyl complexes of $\{Co(NO)\}^8$ configurations, $[Co(Cl_4TPP^{2-})(NO)]$ and $[Co(F_8TPP^{2-})(NO)]$, [Cl_4TPP^{2-} = 5,10,15,20-*tetrakis*(4′-chlorophenyl)porphyrinate; F_8TPP^{2-} = 5,10,15,20-*tetrakis*(2,6-difluorophenyl)porphyrinate] react with H_2O_2 to yield corresponding Co(III) complexes, $[Co^{III}(Cl_4TPP^{2-})(NO_2^{-})]$ and $[Co^{III}(F_8TPP^{2-})(NO_3^{-})]$, respectively (Schemes 1.10 and 1.11).[37-38] Both suggest the formation of a $[Co^{III}\text{-}(ONOO)^{-}]$ intermediate, but in the latter case, the involvement of an oxyl radical species, [Co^{III}-$O^{\bullet}$], derived from the homolysis of the O−O bond of the peroxynitrite moiety, has been confirmed through EPR spectroscopy (Scheme 1.11).

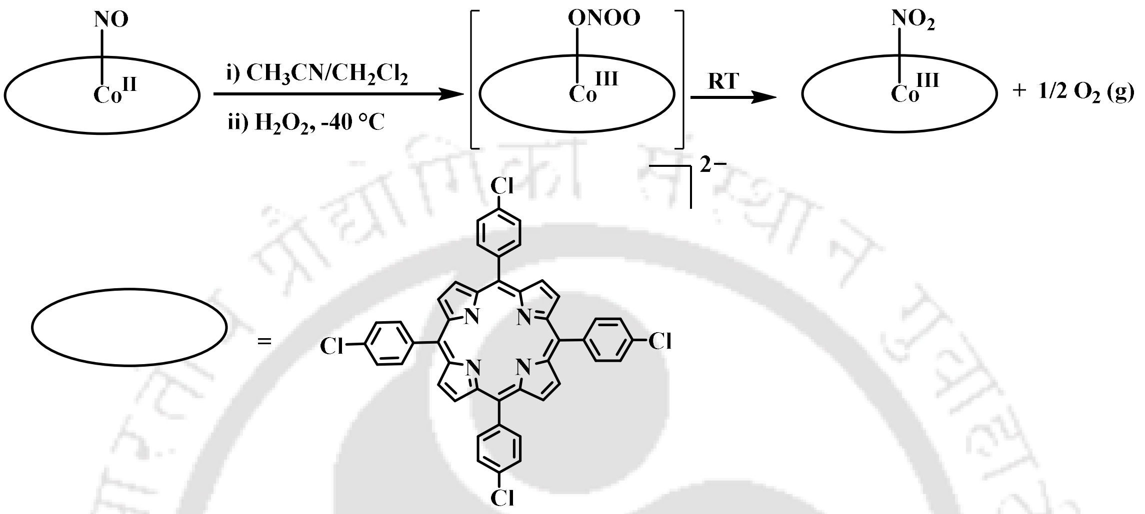

Scheme 1.10

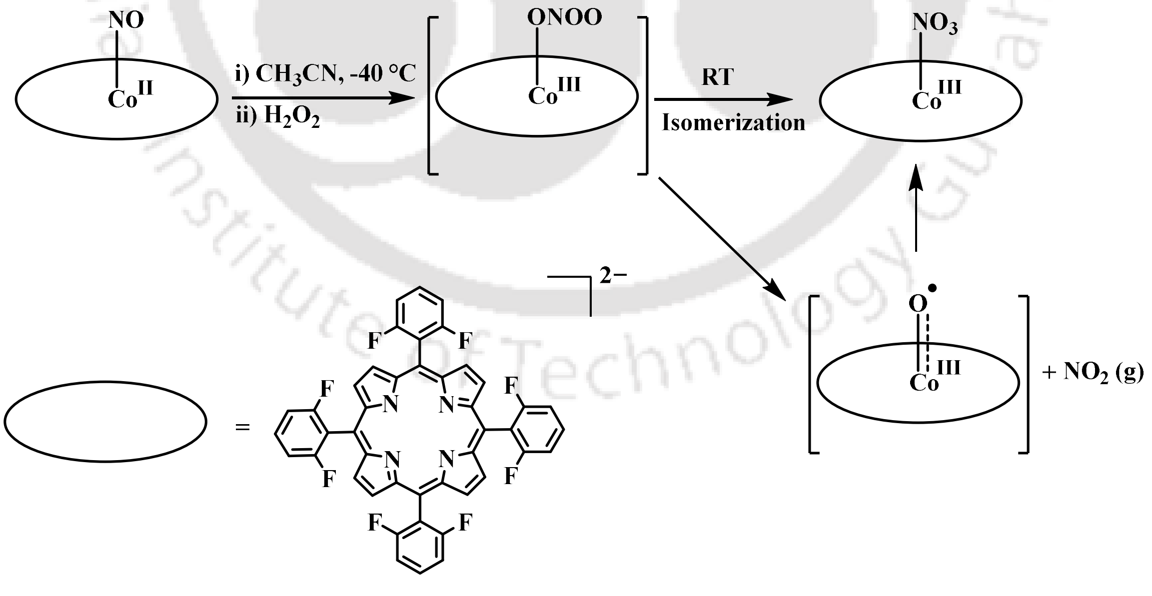

Scheme 1.11

A Co-nitrosyl complex, [Co($F_{20}TPP^{2-}$)(NO)], with more electron deficient ligand framework [$F_{20}TPPH_2$ = 5,10,15,20-*tetrakis*(pentaflurophenyl)porphyrin] has been reported which at –40 °C in dichloromethane medium, upon reaction with O_2^- resulted into [Co^{III}($F_{20}TPP^{2-}$)(NO_2^-)] through a presumed Co(II)-peroxynitrite intermediate (Scheme 1.12). Analyses using UV-visible and X-band EPR spectroscopy and ESI-mass spectrometry confirmed the formation of a transient intermediate, [Co($F_{20}TPP^{2-}$)(NO)(O_2^-)].[39]

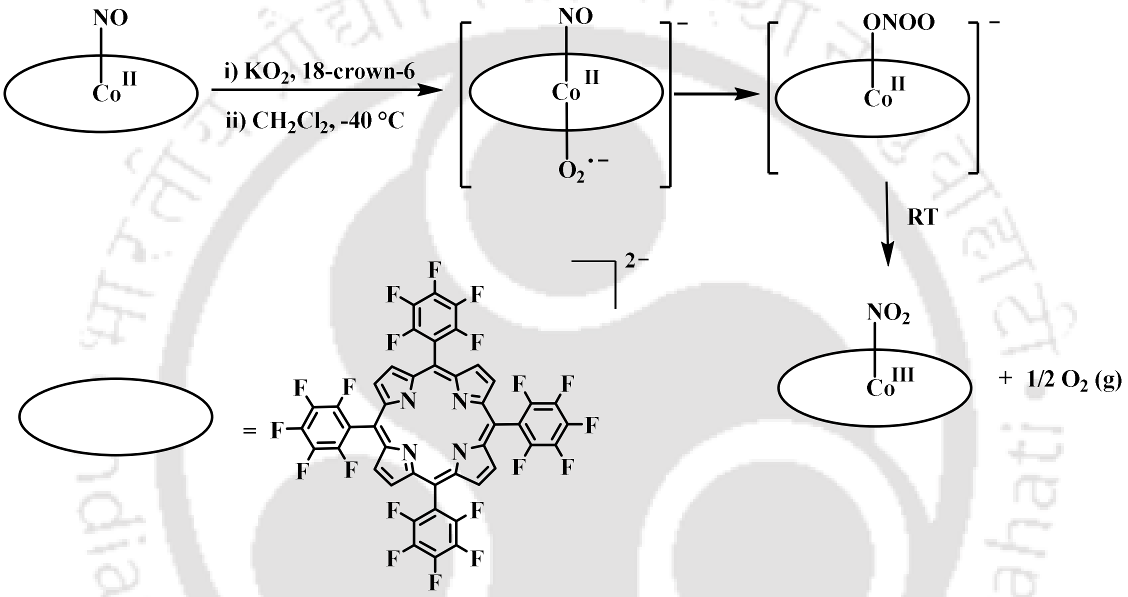

Scheme 1.12

Another nitrosyl complex of Co(II) porphyrinate, [Co($TTMPP^{2-}$)(NO)], [$TTMPPH_2$ = 5,10,15,20-*tetrakis*(3,4,5-trimethoxyphenyl)porphyrin] reacts with H_2O_2 to form a nitrite complex, [Co^{III}($TTMPP^{2-}$)(NO_2^-)]. This reaction is proposed to involve a Co(III)-peroxynitrite intermediate. Spectroscopic studies revealed the formation of a [Co^{IV}=O] species, followed by the generation of a Co(III)-porphyrin radical complex over the course of the reaction (Scheme 1.13).[40]

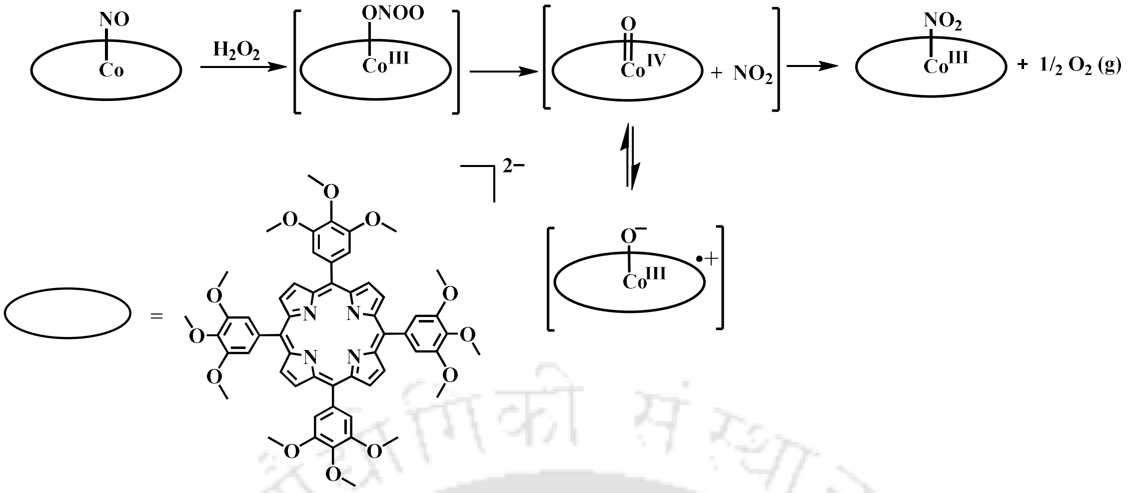

Scheme 1.13

A manganese nitrosyl complex, $[Mn(TMPP^{2-})(NO)]$, [$TMPPH_2$ = 5,10,15,20-*tetrakis*(4-methoxyphenyl)porphyrin has been shown to react with O_2^-, producing $[Mn^{III}\text{-}OH]$ and NO_2, through the formation of peroxynitrite intermediate (Scheme 1.14). Spectroscopic analysis suggests the formation of high-valent $[Mn^{IV}{=}O]$.[41]

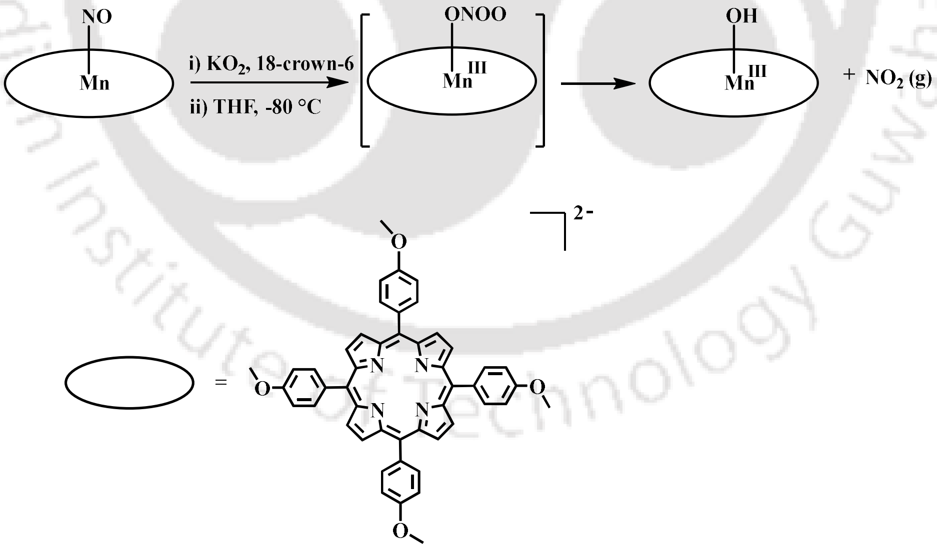

Scheme 1.14

Manganese nitrosyl, $[Mn(F_{20}TPP^{2-})(NO)]$, reacts with O_2^- to yield $[Mn^{III}\text{-}(NO_3)^-]$ presumably through $[Mn^{III}\text{-}(ONOO)^-]$ intermediate (Scheme 1.15).[42] The formation of a high-valent [Mn^{IV}=O] species was observed in UV-visible, X-band EPR spectroscopic and ESI-mass spectrometric analysis.

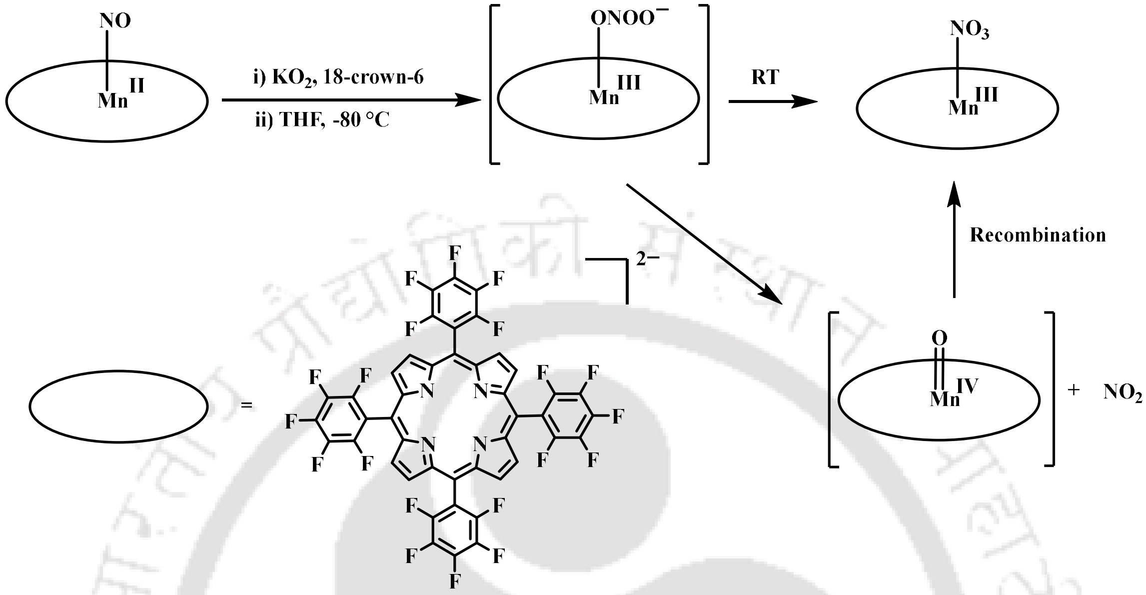

Scheme 1.15

All these results prompted us to study the reactivity of metal nitrosyls with O_2 and reactive oxygen species with an aim to (i) generate the metal peroxynitrite; (ii) identify and characterize the metal-oxo species formed from the decomposition of metal-peroxynitrite species.

1.4 General aspects of metal dinitrosyl

Many first-row transition metals (M = Fe, Co, Ni) can bind with two nitrosyl ligands in their lower oxidation states. Among these, dinitrosyl iron complexes (DNICs) are the most prominent and widely recognized as some of the most abundant nitrosylated species in cellular environments.[43-45] DNICs form through the interaction of NO with iron-sulfur proteins, specifically from the reactions of [2Fe-2S] and [4Fe-4S] clusters with NO.[46-47] Roussin's 'red salt' was the first discovered DNIC complex.[48] Researchers aim to study and biomimic the DNIC complexes to understand the correlation between molecular structures and the chemical reactivity of DNICs. Small molecule models for mononuclear $\{Fe(NO)_2\}^{9/10}$ and dinuclear $[\{Fe(NO)_2\}^{9/10}]_2$ DNICs (Figure 1.3) with biologically relevant S/N/O ligation modes have been synthesized.

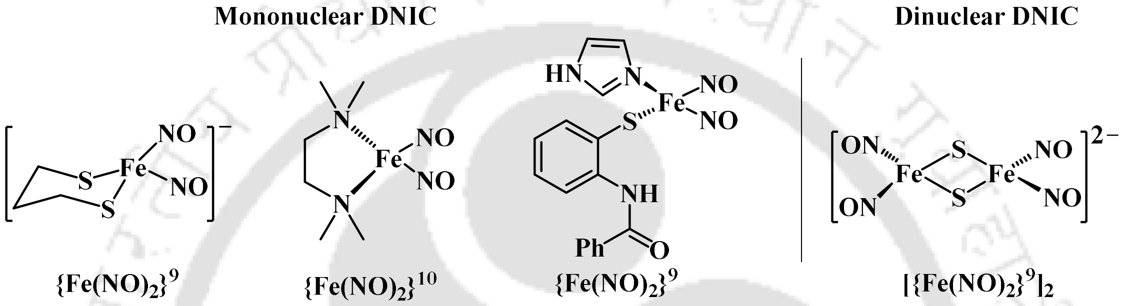

Figure 1.3: Models for small molecule of DNIC.

1.5 Reactivity of DNIC as a model for Flavodiiron nitric oxide reductases (FNORs) enzyme

The active site of the flavodiiron nitric oxide reductases (FNORs) enzyme contains a dinuclear iron unit that protects microbes from nitrosative stress in anaerobic environments by converting harmful NO into the less harmful nitrous oxide (N_2O) (equation 1.1).[49-53]

$$2\,NO + 2\,e^- + 2\,H^+ \longrightarrow 2\,N_2O + H_2O \qquad \text{-------Equation 1.1}$$

The catalytically active form has been characterized as a symmetric, magnetically coupled diferrous-dinitrosyl intermediate of $[\{Fe(NO)\}^7]_2$.[54-55] This $[hs\text{-}\{Fe(NO)\}^7]_2$ intermediate efficiently drives N−N coupling and the release of N_2O. The flavin mononucleotide (FMN) cofactor reduces the $[hs\text{-}\{Fe(NO)\}^7]_2$ intermediate by transferring either one or two electrons, creating highly reactive $[hs\text{-}\{Fe(NO)\}^7]$/ $[hs\text{-}\{Fe(NO)\}^8]$, or [hs-

$\{Fe(NO)^8\}]_2$ intermediates, which are essential for N–N bond formation. Based on detailed analysis, four different mechanisms are proposed, including the semi-reduced (mixed valent), super-reduced, as well as the direct coupling (diferrous dinitrosyl) and hyponitrite pathway (Scheme 1.16).[56] In the semi-reduced mechanism, the $[\{Fe(NO)\}^7]_2$ species is reduced by $FMNH_2$, forming FMNH(•) and the $[\{Fe(NO)\}^7\text{-}\{Fe(NO)\}^8]$ complex, which produces N_2O along with a diferric complex.[57] In the super-reduced pathway, $[\{Fe(NO)\}^7]_2$ is reduced by $FMNH_2$ to generate $[\{Fe(NO)\}^8]_2$ and FMN, which subsequently yields N_2O and a mixed-valent Fe^{II}-Fe^{III}.[58] The diferric dinitrosyl intermediate can undergo N–N coupling in the direct coupling mechanism through the hyponitrite intermediate. N_2O is released alongside the formation of the diferric *bis*-μ-oxo product.[59]

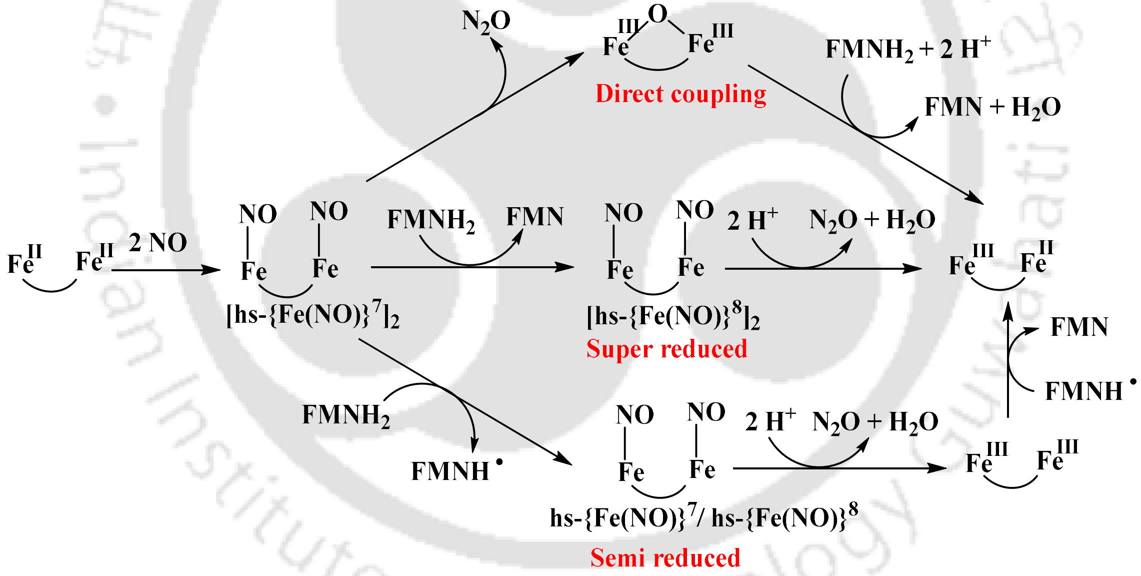

Scheme 1.16

1.5.1 Functional model of FNOR: Direct coupling mechanism

Lehnert's group reported a diferric model complex, $[Fe^{III}_2((Py_2PhO_2)MP)(OPr)_2](OTf)$ $[(Py_2PhO_2)MP$ = 2,6-*bis*{((2-hydroxybenzyl)-(2-pyridylmethyl)amino)methyl}-4-methyl phenol], which effectively mimics the active site structure of FNOR enzyme.[60] This diferric complex reduced to diferrous unit using $CoCp_2$ (Scheme 1.17). Upon reduction, the diferrous complex reacted with NO, demonstrating its capability as the model complex to mimic the direct reduction of NO to N_2O at both room temperature and –80 °C.[57]

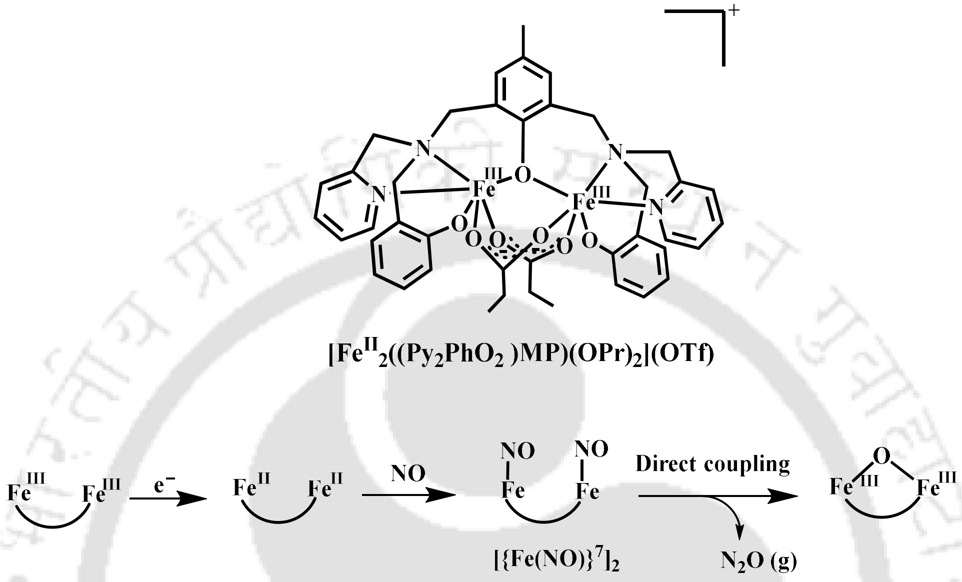

Scheme 1.17

The diiron dinitrosyl complex, $[Fe_2(Et\text{-}HPTB)(O_2CPh)(NO)_2](BF_4)_2$ [Et-HPTB = *N,N,N',N'-tetrakis*(2-(1-ethylbenzimidazolyl))-2-hydroxy-1,3-diaminopropane] was shown to decompose to yield N_2O. It was proposed that coupling of the two nitrosyl ligands generates a transient $N_2O_2^{2-}$ species having an N–N bond (Scheme 1.18).[61]

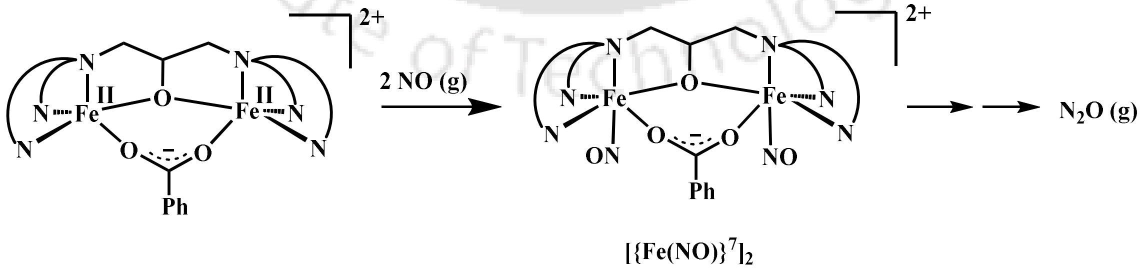

Scheme 1.18

1.5.2 Functional model of FNOR: Semi-reduced mechanism

Lehnert's group has synthesized and characterized a diiron dinitrosyl complex, $[Fe_2(BPMP)(OPr)(NO)_2](X)_2$, [X = BPh_4^-, OTf^-, BF_4^-; H-BPMP = 2,6-*bis*((*bis*(2-pyridylmethyl)amino)methyl)-4-methylphenol] featuring two end-on-coordinated $\{Fe(NO)\}^7$ units. The coplanar *syn/cis* configuration between two NO groups is crucial for N–N coupling and N_2O formation.[62] Chemical reduction with $CoCp_2$ results in intramolecular N−N coupling and quantitative N_2O production (Scheme 1.19).[57] The formation of $[\{Fe(NO)^7\}_2]^{2-}$ intermediate during reductive pathway compellingly supports the "semi-reduced" mechanism of NO reduction by FNORs.

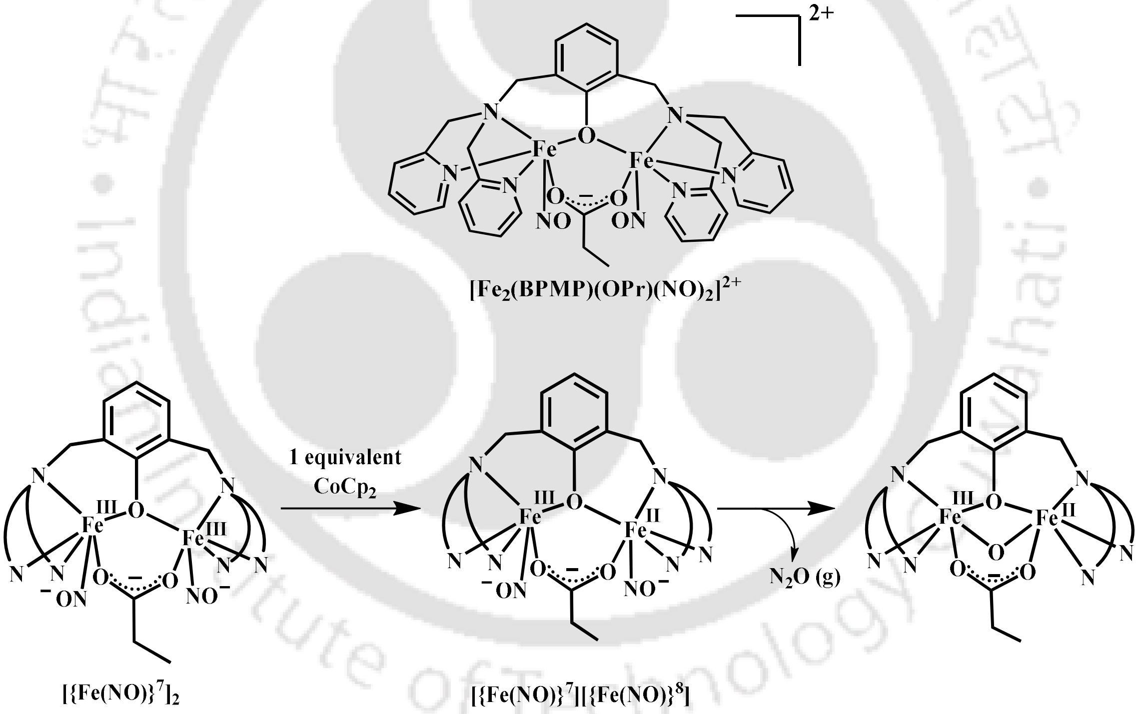

Scheme 1.19

Majumdar's group reported a mononitrosyl diiron complex $[Fe_2(N\text{-}Et\text{-}HPTB)(NO)(DMF)_3](BF_4)_3$ [N-Et-HPTB = anion of *N,N,N',N'-tetrakis*(2-(l-ethylbenzimidazolyl))-2-hydroxy-1,3-diaminopropane; DMF = Dimethylformamide] which upon electrochemical as well as chemical reduction generates N_2O in a near quantitative yield *via* semi-reduction pathway (Scheme 1.20). The mononitrosyl diiron(II) complex produces N_2O through the interaction between two molecules of the reduced product, $[Fe^{II}\{Fe(NO)\}^8]$, which is formed during electrochemical reduction of $[Fe^{II}\{Fe(NO)\}^7]$.[63]

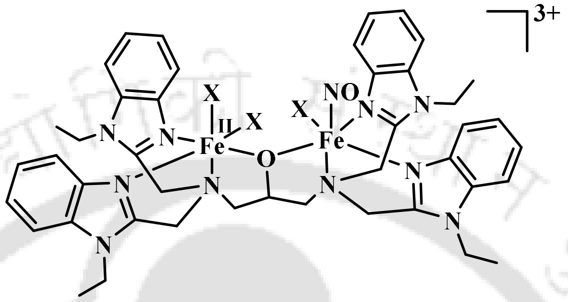

$[Fe_2(N\text{-}Et\text{-}HPTB)(NO)(DMF)_3](BF_4)_3$; X = DMF

$[Fe^{II}\{Fe(NO)\}^7]$

$$[Fe^{II}\{Fe(NO)\}^7] \xrightarrow{e^-} [Fe^{II}\{Fe(NO)\}^8] \longrightarrow \longrightarrow N_2O\ (g)$$

Scheme 1.20

1.5.3 Functional model of FNOR: Super-reduced mechanism

A diiron dinitrosyl complex similar to the previously discussed mononitrosyl complex, $[Fe_2(N\text{-}Et\text{-}HPTB)(DMF)_3(NO)](BF_4)_3$, has been shown to follow a "semi-reduced" pathway for N_2O production. In contrast, the dinitrosyl diiron complex operates through a "super-reduced" pathway. The diiron dinitrosyl complex, $[Fe_2(N\text{-}Et\text{-}HPTB)(NO)_2(DMF)_2](BF_4)_3$, mediates the reduction of NO to N_2O upon chemical and electrochemical reduction at room temperature (Scheme 1.21). NO reduction proceeds through the "super-reduced" mechanism.[64]

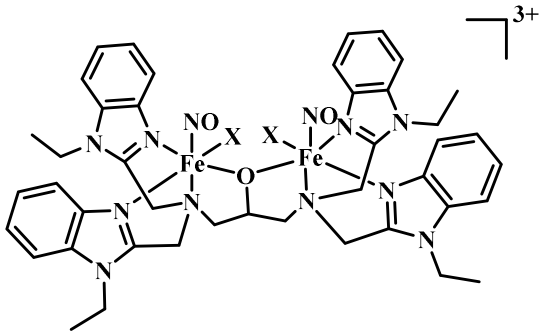

$[Fe_2(N\text{-}Et\text{-}HPTB)(NO)_2(DMF)_2](BF_4)_3$; X = DMF

$$[\{Fe(NO)\}^7]_2 \xrightarrow{e^-} [\{Fe(NO)\}^8]_2 \longrightarrow \longrightarrow N_2O\ (g)$$

Scheme 1.21

1.5.4 Functional model of FNOR: Reactivity of a *trans* diiron dinitrosyl dimer

Meyer and coworkers reported a model system for non-heme diiron active sites of FNORs, which is basically a diiron dinitrosyl adduct $[L\{Fe(NO)\}_2(\mu\text{-}OOCR)](ClO_4)$ [L = 7,7′-(1H-pyrazole-3,5-diyl)*bis*(methylene)*bis*(1,4-dimethyl-1,4,7-triazacyclononane) anion; R = Me, Ph]. This is a rare example of diiron dinitrosyl compounds with *anti*-orientation of the NO ligands, which upon electrochemical reduction of diiron dinitrosyl by one electron produces diiron tetranitrosyl complex, $[L\{Fe(NO)_2\}_2](ClO_4)$ and a diacetato-bridged ferrous complex $[LFe^{II}_2(\mu\text{-}OOCR)_2](ClO_4)$ as final product along with N_2O (Scheme 1.22).[65]

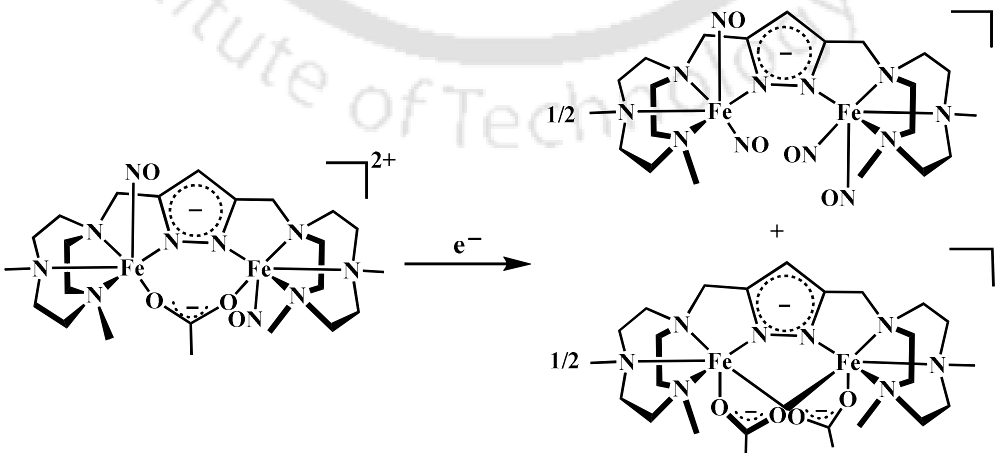

Scheme 1.22

1.6 Scope of the thesis

Nitric oxide (NO) is essential for biological processes, but it must be metabolized efficiently to prevent toxicity. There are two primary pathways for the metabolism of excess NO: oxidative and reductive. The oxidative pathway is predominantly present in mammals, that involves the enzymes, nitric oxide dioxygenases (NODs) which converts NO into harmless nitrate (NO_3^-). The proposed mechanism is well-defined: it begins with the formation of the intermediate complex $[Fe^{III}\text{-}(ONOO)^-]$, which subsequently decomposes into an oxo-ferryl intermediate and nitrogen dioxide (NO_2). However, due to the high instability of these intermediates, explicit spectroscopic characterization has not yet been achieved, making this mechanism somewhat elusive. The reductive pathway of nitric oxide refers to the conversion of NO to other nitrogen species *e.g.,* N_2O, N_2, NH_3 typically under anaerobic or low-oxygen conditions. One of the steps of this reduction process is the NO to N_2O formation with the help of nitric oxide reductase enzyme.

This thesis focuses on the mimicking of enzymatic processes through small molecule models, utilizing first-row transition metal complexes. Both oxidative and reductive pathways were examined, and the intermediates involved were identified and characterized as much as possible. This involves the synthesis of iron and chromium nitrosyls in different tripodal N4 type ligand frameworks. Furthermore, their reactivity toward reactive oxygen species was examined, leading to the formation of metal-peroxynitrite intermediates and their decomposition in pursuit of a well-characterized high-valent metal-oxo species along the mechanistic pathways.

To examine the reductive pathways, a diiron dinitrosyl complex was synthesized and its reactivity was also explored.

In chapters 2, 3, and 4, the oxidative pathway of NO metabolism was studied. Chapter 2 includes an iron-nitrosyl complex of $\{Fe(NO)\}^7$ configuration and its reactivity towards molecular O_2. In chapter 3, iron nitrosyl complexes with two different spin states in the same ligand framework were synthesized and their reactivity towards oxygen was also explored. In chapter 4, moving towards more oxophilic metal, a chromium nitrosyl complex was synthesized, and its reactivity towards reactive oxygen species was studied. In chapter 5, a diiron dinitrosyl complex as a model of FNOR was synthesized and studied.

1.7 References

1. *Nitric Oxide: Biology and Pathobiology*; Ignarro, L. J., Ed.; Academic Press: San Diego, **2000**.
2. Lancaster, Jr. J., Ed.; *Nitric Oxide: Principles and Actions*; Academic Press: San Diego, **1996**.
3. Harland, J. B.; Manickas, E. C.; Hunt, A. P.; Lehnert, N. *Comprehensive Coordination Chemistry III;* Constable, E., Parkin, G., Que, L., Jr., Eds.; Elsevier, **2021**, 806 − 874.
4. Richter-Addo, G. B.; Legzdins, P. *Metal Nitrosyls*; Oxford University Press: Oxford, UK, **1992**.
5. Hayton, T. W.; Legzdins, P.; Sharp, W. B. *Chem. Rev.* **2002**, *102*, 935 − 992.
6. Jørgensen, C. K. *Coord. Chem. Rev.* **1966**, *1*, 164 − 178.
7. Mingos, D. M. P. *J. Organomet.Chem.* **2014**, *751*, 153 − 173.
8. Enemark, J. H.; Feltham, R. D. *Coord. Chem. Rev.* **1974**, *13*, 339 − 406.
9. Greenwood, N. N.; Earnshaw, A. *Chemistry of the elements*; 2nd ed.; Elsevier, **2012**, *412*, pp 445 – 447.
10. Ford, P. C.; Lorkovic, I. M. *Chem. Rev.* **2002**, *102*, 993 − 1017.

11. Laane, J.; Ohlsen, J. R. *Prog. Inorg. Chem.* **2007**, *27*, 465 − 513.
12. Lee, D.-H.; Mondal, B.; Karlin, K. D. *Nitrogen Monoxide and Nitrous Oxide Binding and Reduction. In Activation of Small Molecules: Organometallic and Bioinorganic Perspectives*; Tolman, W. B., Ed.; Wiley-WCH: Weinheim, **2006**, 43 − 79.
13. Fujisawa, K.; Tateda, A.; Miyashita, Y.; Okamoto, K.-i.; Paulat, F.; Praneeth, V. K. K.; Merkle, A.; Lehnert, N. *J. Am. Chem. Soc.* **2008**, *130*, 1205 − 1213.
14. Afzal, S.; Abdul Manap, A. S.; Attiq, A.; Albokhadaim, I.; Kandeel, M.; Alhojaily, S. M. *Front. Pharmacol.* **2023**, *14*, 1 – 22.
15. Gross, S. S.; Wolin, M. S. *Annu. Rev. Physiol.* **1995**, *57*, 737 − 769.
16. Qiao, L.; Lu, Y.; Liu, B.; Girault, H. H. *J. Am. Chem. Soc.* **2011**, *133*, 19823 – 19831.
17. van der Vliet, A.; Eiserich, J. P.; Halliwell, B.; Cross, C. E. *J. Biol. Chem.* **1997**, *272*, 7617 – 7625.
18. Radi, R. *J. Biol. Chem.* **2013**, *288*, 26464 – 26472.
19. Radi, R.; Peluffo, G.; Alvarez, M. N.; Naviliat, M.; Cayota, A. *Free Radic. Biol. Med.* **2001**, *30*, 463 – 488.
20. Boccini, F.; Herold, S. *Biochemistry* **2004**, *43*, 16393 – 16404.
21. Herold, S.; Exner, M.; Boccini, F. *Chem. Res. Toxicol.* **2003,** *16*, 390 – 402.
22. Thomson, L.; Trujillo, M.; Telleri, R.; Radi, R. *Arch. Biochem. Biophys.* **1995**, *319*, 491 – 497.
23. Huhmer, A. F.; Nishida, C. R.; Ortiz de Montellano, P. R.; Schoneich, C. *Chem. Res. Toxicol.* **1997**, *10*, 618 – 626.
24. Bartesaghi, S.; Radi, R. *Redox Biol.* **2018**, *14*, 618 − 625.
25. Schopfer F. J.; Baker, P. R.; Freeman, B. A. *Trends Biochem. Sci.* **2003**, *28*, *646 – 654*.
26. Gardner, P. R. *Scientifica* **2012,** *2012*, 683729.
27. Gardner, P. R.; Gardner, A. M.; Martin, L. A.; Salzman, A. L. *Proc. Natl. Acad. Sci. U.*

S. A. **1998**, *95*, 10378 − 10383.

28. Gardner, P. R. *J. Inorg. Biochem.* **2005**, *99*, 247 − 266.

29. (a) Clarkson, S. G.; Basolo, F. *J. Chem. Soc. Chem. Commun.* **1972**, *11*, 670 − 671. (b) Clarkson, S. G.; Basolo, F. *Inorg. Chem*. **1973**, *12*, 1528 − 1534.

30. Cao, R.; Elrod, L. T.; Lehane, R. L.; Kim, E.; Karlin, K. D. *J. Am. Chem. Soc*. **2016**, *138*, 16148 − 16158.

31. Kumar, P.; Lee, Y. M.; Park, Y. J.; Siegler, M. A.; Karlin, K. D.; Nam, W. *J. Am. Chem. Soc*. **2015**, *137*, 4284 − 4287.

32. Kumar, P.; Lee, Y. M.; Hu, L.; Chen, J.; Park, Y. J.; Yao, J.; Chen, H.; Karlin, K. D.; Nam, W. *J. Am. Chem. Soc*. **2016**, *138*, 7753 – 7762.

33. Akshaya Keerthi, C. S.; Das, S.; Kulbir; Bhardwaj, P.; Sk, Md P.; Kumar, P. *Dalton Trans*. **2023**, *52*, 16492 – 16499.

34. Kalita, A.; Kumar, P.; Mondal, B. *Chem. Commun.* **2012**, *48*, 4636 – 4638.

35. Kalita, A.; Deka, R. C.; Mondal, B. *Inorg. Chem.* **2013**, *52*, 10897 – 10903.

36. Gogoi, K.; Saha, S.; Mondal, B.; Deka, H.; Ghosh, S.; Mondal, B. *Inorg. Chem*. **2017**, *56*, 14438 – 14445.

37. Saha, S.; Gogoi, K.; Mondal, B.; Ghosh, S.; Deka, H.; Mondal, B. *Inorg. Chem*. **2017**, *56*, 7781 – 7787.

38. Mondal, B.; Saha, S.; Borah, D.; Mazumdar, R.; Mondal, B. *Inorg. Chem*. **2019**, *58*, 1234 – 1240.

39. Mazumdar, R.; Mondal, B.; Saha, S.; Samanta, B.; Mondal, B. *J. Inorg. Biochem*. **2022**, *228*, 111698.

40. Samanta, B.; Saha, S.; Ghosh, R.; Maity, S.; Mondal, B. *Chem. Asian J.* **2025**, *20,* e202401082.

41. Mazumdar, R.; Saha, S.; Samanta, B.; Ghosh, R.; Maity, S.; Mondal, B. *Dalton Trans.*

2023, *52*, 7917 – 7925.

42. Mondal, B.; Borah, D.; Mazumdar, R.; Mondal, B. *Inorg. Chem*. **2019**, *58*, 14701 – 14707.
43. Crack, J. C.; Green, J.; Thomson, A. J.; Le Brun, N. E. *Acc. Chem. Res.* **2014**, *47*, 3196 – 3205.
44. Fitzpatrick, J.; Kim, E. *Acc. Chem. Res.* **2015**, *48*, 2453 – 2461.
45. Vanin, A. F. *Nitric Oxide* **2016**, *54*, 15 – 29.
46. Venkateswara, P.; Holm, R. H. *Chem. Rev.* **2004**, *104*, 527 − 560.
47. (a) Tsai, M.-L.; Tsou, C.-C.; Liaw, W.-F. *Acc. Chem. Res.* **2015**, *48*, 1184 − 1193. (b) Tonzetich, Z. J.; Do, L. H.; Lippard, S. J. *J. Am. Chem. Soc.* **2009**, *131*, 7964 − 7965. (c) Foster, M. W.; Cowan, J. A. *J. Am. Chem. Soc.* **1999**, *121*, 4093 − 4100. (d) Tran, C. T.; Skodje, K. M.; Kim, E. *Prog. Inorg. Chem.* **2014**, *59*, 339 − 380. (e) Lewandowska, H.; Kalinowska, M.; Brzoska, K.; Wojciuk, K.; Wojciuk, G.; Kruszewski, M. *Dalton Trans.* **2011**, *40*, 8273 − 8289.
48. Roussin, F. Z. *Ann. Chim. Phys.* **1858**, *52*, 285 − 303.
49. Gardner, A. M.; Helmick, R. A.; Gardner, P. R. *J. Biol. Chem.* **2002**, *277*, 8172 − 8177.
50. Zumft, W. G. *Microbiol. Mol. Biol. Rev.* **1997**, *61*, 533 – 616.
51. Zumft, W. G. *J. Inorg. Biochem.* **2005**, *99*, 194 − 215.
52. Watmough, N. J.; Field, S. J.; Hughes, R. J. L.; Richardson, D. J. *Biochem. Soc. Trans.* **2009**, *37*, 392 – 399.
53. Hendriks, J.; Oubrie, A.; Castresana, J.; Urbani, A.; Gemeinhardt, S.; Saraste, M. *Biochim. Biophys. Acta, Bioenerg.* **2000**, *1459*, 266 − 273.
54. Haskin, C. J.; Ravi, N.; Lynch, J. B.; Münck, E.; Que, L., Jr. *Biochemistry* **1995**, *34*, 11090 – 11098.
55. Lu, S.; Libby, E.; Saleh, L.; Xing, G.; Bollinger, J. M., Jr.; Moënne-Loccoz, P. *J. Biol.*

Inorg. Chem. **2004**, *9*, 818 – 827.

56. Khatua, S.; Majumdar, A. *J. Inorg. Biochem.* **2015**, *142*, 145 − 153.
57. White, C. J.; Speelman, A. L.; Kupper, C.; Demeshko, S.; Meyer, F.; Shanahan, J. P.; Alp, E. E.; Hu, M.; Zhao, J.; Lehnert, N. *J. Am. Chem. Soc.* **2018**, *140*, 2562 – 2574.
58. Kurtz, D. M., Jr. *Dalton Trans.* **2007**, 4115 – 4121.
59. Lu, J.; Bi, B.; Lai, W.; Chen, H. *Angew. Chem., Int. Ed. Engl.* **2019**, *58*, 3795 − 3799.
60. Silaghi-Dumitrescu, R.; Kurtz, D. M., Jr.; Ljungdahl, L. G.; Lanzilotta, W. N. *Biochemistry* **2005**, *44*, 6492 – 6501.
61. Feig, A. L.; Bautista, M. T.; Lippard, S. J. *Inorg. Chem.* **1996**, *35*, 6892 − 6898.
62. Zheng, S.; Berto, T. C.; Dahl, E. W.; Hoffman, M. B.; Speelman, A. L.; Lehnert, N. *J. Am. Chem. Soc*. **2013**, *135*, 4902 − 4905.
63. Jana, M.; Pal, N.; White, C. J.; Kupper, C.; Meyer, F.; Lehnert, N. *J. Am. Chem. Soc.* **2017**, *139*, 14380 – 14383.
64. Jana, M.; White, C. J.; Pal, N.; Demeshko, S.; Cordes, C.; Meyer, F.; Lehnert, N.; Majumdar, A. *J. Am. Chem. Soc.* **2020**, *142*, 6600 – 6616.
65. Kindermann, N.; Schober, A.; Demeshko, S.; Lehnert, N.; Meyer, F. *Inorg. Chem.* **2016**, *55*, 11538 – 11550.

Chapter 2

Reaction of a non-heme iron-nitrosyl with dioxygen: decomposition of the ligand through NOD-like activity

Abstract

A high-spin iron(II) nitrosyl, $[Fe(TPz)(NO)](ClO_4)_2$, **2.2** [TPz = *Tris*((3,5-dimethyl-1H-pyrazol-1-yl)methyl)amine] of $\{Fe(NO)\}^7$ configuration was synthesized and characterized structurally. Dioxygen reactivity of complex **2.2** in acetonitrile solution results in the oxidation of the ligand. Chemical evidence suggest the involvement of a peroxynitrite intermediate in this reaction. Trapping experiment shows the formation of NO_2 during the reaction, which supports the proposition of the involvement of the peroxynitrite intermediate. This study gives an insight into an alternate possibility of the dioxygen reactivity of metal-nitrosyl leading to nitric oxide dioxygenase (NOD) activity.

2.1 Introduction

Nitric oxide (NO), being an important molecule in mammalian biology, has attracted a huge research activity since it's discovery as a signaling molecule.[1-3] The overproduction of NO can be lethal due to the formation of secondary reactive nitrogen species (RNS) such as nitrogen dioxide (NO_2) and peroxynitrite ($OONO^-$).[4,5] The concentration of NO *in vivo* is regulated by the enzyme nitric oxide dioxygenase (NODs). It is known that in NOD activity, the oxy-heme (*i.e.,* iron(III)-superoxo) species of the NOD reacts with NO and forms the biologically benign nitrate (NO_3^-) ion.[6-7] This reaction presumably proceeds through a peroxynitrite intermediate, [Fe^{III}-($OONO^-$)]. It is proposed that an oxo-ferryl, [Fe^{IV}=O] species is formed in the reaction *via* the homolytic cleavage of O–O bond of the [Fe^{III}-($OONO^-$)] intermediate (Scheme 2.1).[6-7]

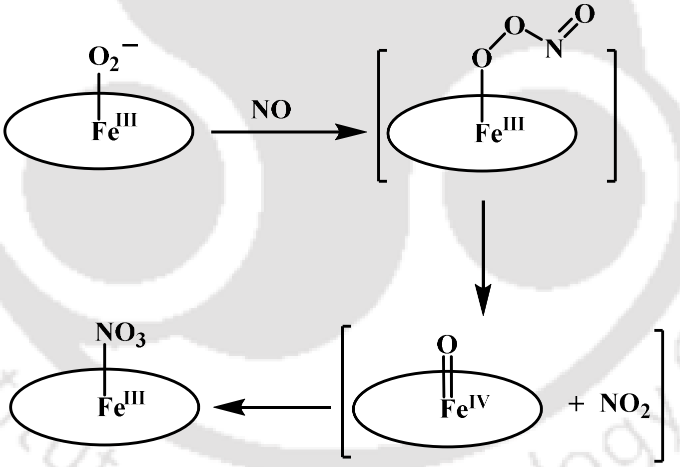

Scheme 2.1

Such an oxo-ferryl species has been evidenced spectroscopically in the reaction of myoglobin with $OONO^-$ ion.[8] Though, in literature, the involvement of a proposed metal-peroxynitrite species was exemplified in the reactions of NO with metal-oxygen adduct or in the reactions of metal-nitrosyls with reactive oxygen species (O_2, O_2^-, O_2^{2-}), the direct evidence is still elusive.[9-16] This is because of the very short life-time of metal-peroxynitrite. In addition, the evidence of formation of high valent metal-oxo species from the homolytic O–O bond cleavage of metal-peroxynitrite intermediate is also in scarce because of very fast recombination of the metal-oxo species with NO_2 in the reaction cage to result in NO_3^-.

Peroxynitrite, being strong oxidizing/nitrating agent, catalyzes the oxidation and/or nitration of various biological substrates like lipid, protein (specifically tyrosine) *etc*. The tyrosine nitration by peroxynitrite is, in fact, used as a marker for NO metabolism in biological systems. In small molecule model studies, the existence of short-lived peroxynitrite intermediate is authenticated using this tyrosine (phenol ring) nitration test. However, in no case having heme group, the nitration of the porphyrin ring has been reported.[12,14-16(c-e)] Similarly, the oxidation/nitration of the ligand framework is also not known in the reaction of non-heme models where a putative peroxynitrite is presumed. As such, no metal nitrosyl is known, which itself undergoes ring/ligand nitration/oxidation in the presence of dioxygen.

This chapter describes the dioxygen reactivity of a non-heme iron-nitrosyl complex, which presumably results in the formation of a metal peroxynitrite intermediate. This has been authenticated by the characteristic ring nitration of externally added phenolic substrate. In the absence of the phenolic substrate, the ligand modification has been observed, which is a rare event in the chemistry of dioxygen reactivity of metal nitrosyl. Trapping experiment suggests the formation of NO_2 in the reaction, which is expected from the decomposition of a metal-peroxynitrite intermediate (Scheme 2.2).

2.2 Results and Discussion

Ligand TPz [TPz = *Tris*((3,5-dimethyl-1H-pyrazol-1-yl)methyl)amine] was synthesized following an earlier report (Appendix I, Figures A1.1-A1.7).[17] The metal complex, $[Fe^{II}(TPz)(CH_3CN)(H_2O)](ClO_4)_2$, **2.1** was prepared by stirring an equimolar mixture of TPz and [Fe^{II}(CH$_3$CN)$_4$(ClO$_4$)$_2$] in dry acetonitrile under Ar atmosphere (Experimental Section). The precursor complex **2.1** was characterized spectroscopically as well as X-ray single crystal structure determination (Appendix I, Figures A1.8-A1.12). Addition of NO gas to the dry and degassed acetonitrile solution of complex **2.1** leads to the formation of green colored complex **2.2,** [Fe(TPz)(NO)(CH$_3$CN)](ClO$_4$)$_2$ (Experimental Section). Complex **2.2**, having {Fe(NO)}^{7} configuration, was isolated as a solid and structurally characterized (Appendix I, Figures A1.13-A1.15). ORTEP diagram of complex **2.2** is shown in figure 2.1. The crystal structure shows that the iron center is coordinated with four N atoms from TPz ligand, one acetonitrile, and one NO group in a distorted octahedral geometry. It would be worth mentioning here that analogous nitrosyl complexes of Fe with the same ligand framework, [Fe(TPz)(NO)(OClO$_3$)]$^+$ and [Fe(TPz)(NO)Cl]$^+$ were reported earlier.[18] In both cases, the iron center was coordinated with a counter anion along with the ligand and NO group.

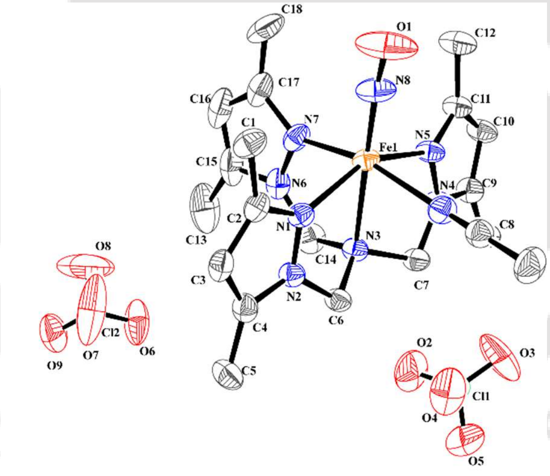

Figure 2.1. ORTEP diagram of complex **2.2** (30% thermal ellipsoid plot, H atoms are omitted for clarity).

In complex **2.2**, the Fe–N$_{NO}$ distance is 1.732(4) Å. The N–O distance and Fe-N-O bond angle are 1.132(1) Å and 174.2°, respectively. The parameters are slightly different from the perchlorate anion coordinated nitrosyl complexes reported earlier (Table 2.1).[18] For instance, in complexes, [Fe(TPz)(NO)(OClO$_3$)]$^+$/[Fe(TPz)(NO)Cl]$^+$ the Fe–N$_{NO}$ distance is 1.767/1.735

Å, N–O distance is 1.103/1.15 Å and Fe-N-O angle is 162.5°/157.1°.[18] In $[Fe(TPA)(NO)(BenzFor)]^+$ [TPA = *Tris*(2-pyridylmethyl)amine, BenzFor = Benzoylformate], the Fe–N_{NO} distance is 1.70 Å, and N–O distance is 1.15 Å and Fe-N-O angle is 162°.[19a] It is evident that the Fe-N-O is more linear in case of complex **2.2** than those reported earlier. The nitrosyl stretching frequency for complex **2.2** appeared at 1790 cm^{-1} (Appendix I, Figure A1.13), which is within the range of reported ones.[18,19]

Table 2.1. List of bond lengths, angles and stretching frequency for reported analogous iron-nitrosyls

Compound	**Fe-N_{NO} length (Å)**	**N-O length (Å)**	**Fe-N-O angle (°)**	**ν(NO) in cm^{-1}**	**Ref**
$[(TPz)Fe(NO)(OClO_3)]^+$	1.767	1.103	162.5	--	18 (b)
$[(TPz)Fe(NO)Cl]^+$	1.735	1.15	157.1	1796	18 (b)
$[Fe(TPA)(NO)(BenzFor)]^+$	1.722	1.152	159.2	1794	19 (a)
[Fe(TPA)(NO)(OTf)](OTf)	1.755	1.144	170	1806	19(b)
$[Fe(TPz)(NO)(CH_3CN)]^{2+}$	1.732	1.132	174.2	1790	This work

The X-band EPR spectrum of complex **2.2** displays two sets of signals at g ~ 4.11 and 2.04 corresponding to the near axial high-spin ($S = \frac{3}{2}$) iron(II) nitrosyl (Appendix I, Figure A1.15).[20] In cases of $[Fe(TPA)(NO)(BenzFor)]^+$ and $[Fe(^6TLA)(NO)(BenzFor)]^+$ [^{6}TLA = *Tris*((6-methyl-2-pyridyl)methyl)amine] these resonances appear at g ~ 4.05, 3.87, 1.99 and g ~ 4.02, 3.93, 1.95, respectively.[19]

Dioxygen reactivity of complex 2.2

In the UV-visible spectrum, complex **2.2** exhibited characteristic absorption bands at 610 nm (ε/$M^{-1}cm^{-1}$, 586), 351 nm (ε/$M^{-1}cm^{-1}$, 4899) and 249 nm (ε/$M^{-1}cm^{-1}$, 20833). Addition of O_2 gas to the degassed acetonitrile solution of complex **2.2** at room temperature resulted in the increase of intensity of 351 nm band with a simultaneous decrease of intensity of 610 nm band with respect to time and resulted in the final product within 5 min (Figure 2.2). The final product was isolated as a solid and characterized spectroscopically as the corresponding nitrate (NO_3^-) complex, **2.3** (Experimental Section and Appendix I, Figures A1.17-A1.20). The 1384 cm^{-1} band in FT-IR spectrum of complex **2.3** suggested the presence of NO_3^- group (Appendix I, Figure A1.17).[21]

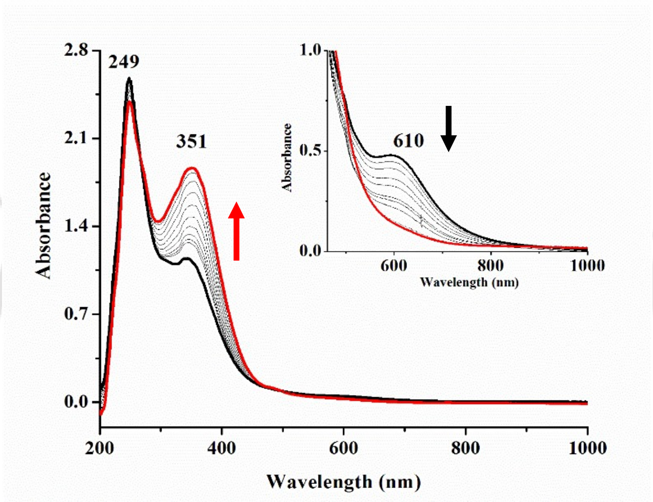

Figure 2.2. UV-visible spectra of the reaction of complex **2.2** (black) with O_2 and formation of complex **2.3** (red) in acetonitrile at room temperature [Inset: complex **2.2** (black), after O_2 addition (red)].

In FT-IR spectroscopic monitoring, addition of O_2 gas into the degassed acetonitrile solution of complex **2.2**, resulted in the disappearance of the NO stretching frequency at 1799 cm^{-1} while a new band simultaneously appeared at 1835 cm^{-1} (Figure 2.3). The intensity of this stretching frequency was found to decay with time and finally disappeared suggesting the formation of an unstable intermediate. Fe(II) complexes in both the heme and non-heme frameworks are known to react with O_2 leading to the formation of corresponding $[Fe^{III}\text{-}(O_2^-)]$ species where the metal center is oxidized by one unit.[7b] In general, metal-superoxide type adducts exhibit $\nu(O_2)$ in the range of 1200-1070 cm^{-1} and metal-peroxo adducts display the O–O stretching in the range of 930-740 cm^{-1}.[22,23] However, no such characteristic stretching was observed in this case except weak stretching at 1018 cm^{-1}. This 1018 cm^{-1} is a bit lower for metal-superoxide and on the higher side for metal-peroxo adducts. In addition, when the reaction was carried out with $^{18}O_2$, the nitrosyl stretching frequency was found to shift to 1835 cm^{-1}, as expected, but no change was observed for the stretching at 1018 cm^{-1} suggesting the non O–O nature of it. On the other hand, in literature, the nitrosyl stretching frequency in $\{Fe(NO)\}^6$ is reported to appear at ~1830 cm^{-1}.[24] Thus, the 1835 cm^{-1} band can be attributed to the nitrosyl stretching of $[Fe^{III}(NO)]$ moiety, which is formed upon reaction of $[Fe^{II}(NO)]$ with O_2. This was further confirmed by the ^{15}NO labelling experiment where the band was found to appear at 1801 cm^{-1} (Appendix I, Figures A1.38-A1.40). It would be worth mentioning here that structurally characterized non-heme $\{Fe(NO)\}^6$ complex, $[Fe(TMG_3tren)(NO)]^{3+}$ [TMG_3tren = 1,1,1-*tris*{2-(N_2-(1,1,3,3-tetramethylguanidino)ethyl}amine] displays nitrosyl stretching at 1879 cm^{-1}.[24b] Spectroscopic and theoretical studies suggest the electronic structure can be best explained by a high-spin Fe(IV) coordinated to a triplet NO^- unit.[24b] Considering the spectral evidence, it is logical to assume that the reaction of complex **2.2** with O_2 results in the formation of $[Fe^{III}(NO)]^{3+}$ and O_2^-, which are present in the reaction cage, but the O_2^- is not coordinated to the metal center (Scheme 2.2).

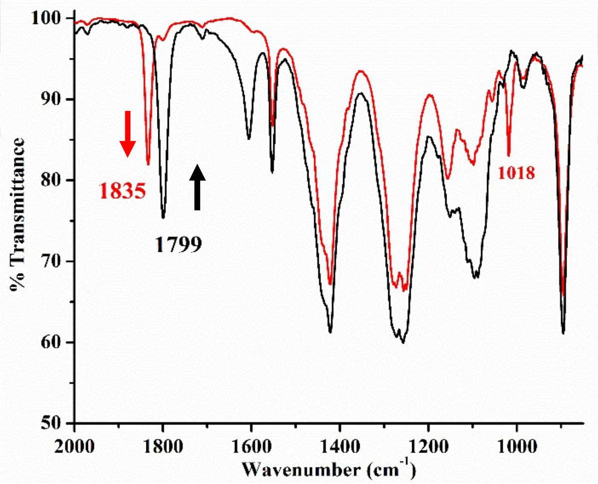

Figure 2.3. FT-IR spectra of the reaction of complex **2.2** with O_2 in acetonitrile [complex **2.2** (black), after O_2 addition (red)].

When the reaction was carried out at –40 °C, the same spectral changes were observed. Upon keeping the reaction mixture in the freezer for 2 days, white crystals of modified ligand (**L′**) and brown precipitate of complex **2.4**, $[Fe^{III}(OH)_3]$, were obtained. They were characterized using various spectroscopic methods (Appendix I, Figures A1.21-A1.28) as well as by single crystal structure determination. The perspective ORTEP view of **L′** is shown in figure 2.4.

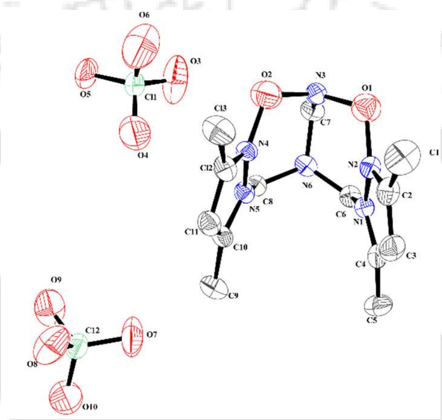

Figure 2.4. ORTEP diagram of modified ligand (**L′**) (30 % thermal ellipsoid plot, H atoms are omitted for clarity).

Interestingly, when the reaction mixture was warmed up to room temperature quickly, $[Fe^{III}(TPz)(NO_3^-)](ClO_4)_2$, complex **2.3** was obtained as a final product.

NO and O_2^- ions are believed to react to result in peroxynitrite ($OONO^-$) intermediate. We propose that the reaction of complex **2.2** with O_2 leads to the initial formation of $\{[Fe^{III}(TPz)(NO)]^{3+}.(O_2^-)\}$ in the reaction cage as an intermediate, which subsequently forms the corresponding peroxynitrite intermediate $[Fe^{III}(TPz)(OONO^-)]^{2+}$ (Scheme 2.2). The peroxynitrite intermediate decomposes leading to the corresponding oxo-ferryl, $[(TPz)Fe^{IV}{=}O]^{2+}$ species and NO_2. They recombine very fast in a quick warm up process and result in complex **2.3**. However, when the reaction mixture was kept in freezer for couple of days, **L′** is formed.

It was reported earlier that the methylene group in a pyrazolyl moiety, in the presence of a radical initiator, results in the corresponding radical.[25] In the present case, the $[(TPz)Fe^{IV}{=}O]^{2+}$ abstracts a H$^\bullet$ from the methylene carbon of the pyrazolyl group and the corresponding radical is formed. This radical then reacts with NO_2 to result in the **L′**. To support this, a few control experiments have been carried out. When 2,4-ditertiarybutylphenol was added in the reaction mixture as external substrate, 2,4-ditertiarybutyl-6-nitrophenol (~ 65 %) was obtained along with $[Fe^{III}(TPz)(OH)]^{2+}$, **2.5** (Appendix I, Figures A1.29-A1.35). This is because, in the presence of an external electron rich phenolic substrate, the oxo-ferryl moiety reacts with the substrate to form phenoxyl radical and $[Fe^{III}(TPz)(OH)]^{2+}$, **2.5**. The phenoxyl radical then combines with NO_2 to afford the nitrophenol product as expected (Scheme 2.2). This experiment, in turn, supports the proposition of the formation of a peroxynitrite intermediate. If the reaction proceeds through the proposed pathway as shown in scheme 2.2, the presence of a substrate that can react with NO_2 is expected to inhibit the formation of **L′**. When the reaction was carried out in the presence of TEMPO (TEMPO = 2,2,6,6-tetramethylpiperidin-1-yloxyl), the formation of **L′** was not observed. Complex **2.5** and 2,2,6,6-tetramethylpiperidin-1-ium nitrate $(tmpH_2^+)(NO_3^-)$ were isolated from the reaction mixture. Spectroscopic characterization and single crystal X-ray structure determination confirm the formulation of $(tmpH_2^+)(NO_3^-)$ (Appendix I, Figures A1.36-A1.37). The ORTEP diagram is shown in figure 2.5.

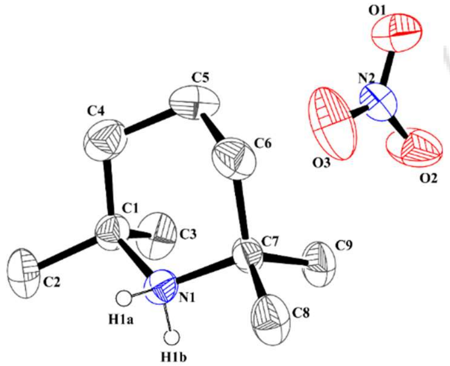

Figure 2.5. ORTEP diagram of $(tmpH_2^+)(NO_3^-)$ (30% thermal ellipsoid plot, H-atoms are omitted for clarity).

Thus, while we do not have any spectroscopic evidence for the formation of peroxynitrite intermediate, based on the control experiments, the formation of a peroxynitrite intermediate in the reaction is presumed.

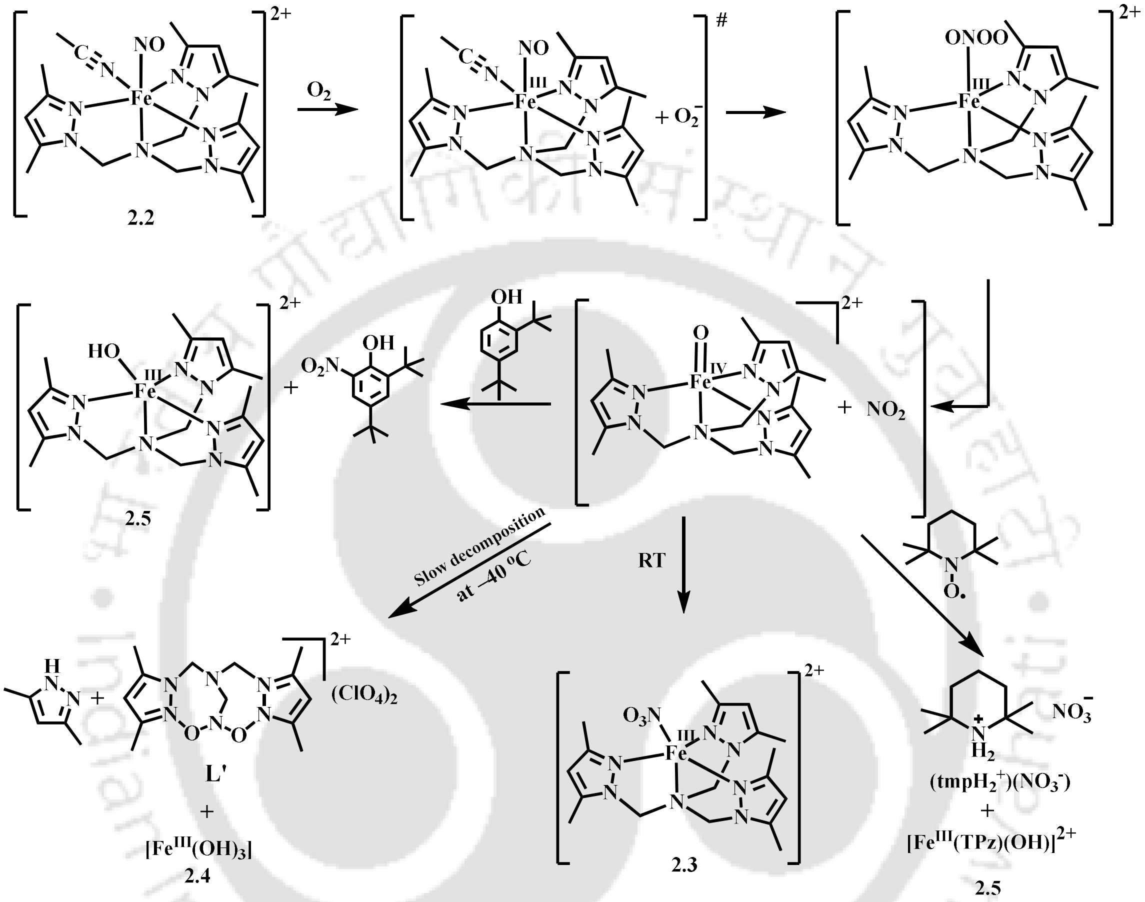

Scheme 2.2. Overall reaction.

2.3 Experimental Section

2.3.1 Materials and methods

All chemicals and solvents were of commercially available quality and used without further purification, unless otherwise mentioned. The anhydrous $[Fe^{II}(CH_3CN)_4(ClO_4)_2]$ was prepared using a previously reported procedure.[26] Acetonitrile was distilled over phosphorus pentoxide under Ar. Diethyl ether was distilled with sodium metal and benzophenone. All the dry solvents were stored over 4 Å molecular sieves under inert condition. Deoxygenation of the solvent and solutions was effected by repeated vacuum/Ar purge cycles or bubbling with Ar for 30 min. All the reactions were performed under inert conditions unless specified. UV-visible spectra were recorded on an Agilent Technologies Cary 8454 UV-visible spectrophotometer by preparing a known concentration of the samples in acetonitrile solution at room temperature (25 °C) using a quartz cuvette of 1 cm path length. FT-IR spectra of the samples were taken on a PerkinElmer spectrophotometer at room temperature with samples prepared either as KBr pellets by grinding the sample with KBr (IR-grade) or in acetonitrile solution in a KBr cell. ^{1}H and ^{13}C NMR spectra were collected in 400 MHz Bruker AVANCE 400 or 500 MHz Bruker AVANCE NEO 500 FT-NMR spectrometer. Chemical shifts were reported as δ (ppm) values relative to an internal standard (tetramethylsilane) or the residual solvent peaks. The X-band Electron Paramagnetic resonance (EPR) spectra were recorded on a JEOL JES-FA200 ESR spectrometer, at 77 K with microwave power, 0.998 mW; microwave frequency, 9.14 GHz. High-resolution Mass spectra were measured in HPLC grade acetonitrile solution by Ultra-High-Performance Liquid Chromatography Quadruple Time of Flight High-resolution Mass Spectrometer (UHPLC-QTOF-HRMS, Agilent G6546A). Mass spectra were measured in HPLC grade acetonitrile and methanol solution.

Single crystals of all complexes suitable for X-ray crystallographic analysis were obtained by layering of diethyl ether into the acetonitrile solution. The intensity data were collected using a Bruker SMART APEX-II CCD diffractometer, equipped with a fine focus 1.75 kW sealed tube MoK$_{\alpha}$ radiation (λ = 0.71073 Å) at 293(3) K, with increasing ω (width of 0.3° per frame) at a scan speed of 3 s/frame. The SMART software was used for data acquisition. Data integration and reduction were undertaken with SAINT and XPREP software.[27] Multi-scan empirical absorption corrections were employed to the data using the program SADABS.[28] Structures were solved by direct methods using SHELXS-2016 and refined with full-matrix least squares on F^2 using SHELXL-2016/6.[29] Structural illustrations have been drawn with ORTEP-3 for Windows.[30]

2.3.2 Syntheses

Tris((3,5-dimethyl-1H-pyrazol-1-yl)methyl)amine, TPz

The ligand TPz was synthesized following a previously reported procedure.[17] Elemental analyses for $C_{18}H_{27}N_7$, calcd. (%): C, 63.32; H, 7.97; N, 28.71, found (%): C, 63.56; H, 7.81; N, 28.34. FT-IR (in KBr): 2922, 1555, 1461, 1313, 1186, 1103, 1029 and 779 cm^{-1}. ^{1}H NMR ($CDCl_3$, 400 MHz): δ_{ppm}, 5.76 (s, 3H), 4.96 (s, 6H), 2.18 (s, 9H), 1.82 (s, 9H). ^{13}C NMR ($CDCl_3$,100 MHz): δ_{ppm}, 147.6, 140.1, 105.9, 62.4, 13.3, 9.9. ESI-mass (m/Z): calcd.: 341.46; found: 342.24 (M+1), 364.23 $(M+Na)^+$.

$[Fe^{II}(TPz)(CH_3CN)(H_2O)](ClO_4)_2$, 2.1

$[Fe^{II}(CH_3CN)_4(ClO_4)_2]$ (0.210 g, 0.5 mmol) was dissolved in dry and degassed acetonitrile.[26] The solution of the ligand TPz (0.170 g, 0.5 mmol) in acetonitrile medium was also degassed under Ar atmosphere. After that, two solutions were mixed and the color of the solution became pale yellow. The solution was stirred for 30 min under Ar atmosphere. After that the solution was layered with diethyl ether and kept in the fridge. After 1 day, white crystalline precipitate of complex **2.1** was formed. Yield: 0.21 g, ~ 62 %. Elemental analyses for $C_{20}H_{32}N_8O_9Cl_2Fe$, calcd. (%): C, 52.64; H, 7.07; N, 24.55. found (%): C, 52.35; H, 7.28; N, 24.82. FT-IR (in KBr): 1637, 1555, 1464, 1423, 1395, 1313, 1274, 1145, 1117, 1084, 886, 806, 636 and 626 cm^{-1}. UV-visible (in acetonitrile): 836 nm (ε/M^{-1}cm^{-1}, 462) and 328 nm (ε/ M^{-1}cm^{-1}, 4850). ESI-mass (m/Z): calcd.: 198.58 (for $[Fe(TPz)]^{2+}$ unit); found: 198.61. X-band EPR (in acetonitrile): silent at 77 K.

$[Fe(TPz)(NO)(CH_3CN)](ClO_4)_2$, 2.2

Complex **2.1** (0.65 g, 1 mmol) was dissolved in 10 mL dry and degassed acetonitrile. To this solution, NO gas was purged for 3 min until the color changed to dark green. Next day, excess NO gas was removed by applying several cycles of vacuum/Ar purging. Then the solution was layered with diethyl ether and after few days green crystals of complex **2.2** were obtained. Same procedure has been used for the formation of 15-Nitrogen labelled complex **2.2**. Yield: 0.48 g, ~ 73 %. Elemental analysis for $C_{20}H_{30}N_9O_9Cl_2Fe$, calcd. (%): C, 36.00; H, 4.53; N, 18.89. found (%): C, 36.35; H, 4.20; N, 18.09. FT-IR (in KBr): 1790, 1617, 1554, 1465, 1421, 1391, 1313, 1274, 1248, 1140, 1113, 1088, 940, 887, 805 and 626 cm^{-1}. [Solution FT-IR for ν_{NO}, 1799 cm^{-1} and labelled ^{15}N ν_{NO}, 1765 cm^{-1}]. UV-visible (in acetonitrile): 610 nm ($\varepsilon/M^{-1}cm^{-1}$, 586), 351 nm ($\varepsilon/M^{-1}cm^{-1}$, 4899) and 249 nm ($\varepsilon$ /$M^{-1}cm^{-1}$, 20833). X-band EPR (in methanol): g ~ 4.11 and 2.04 at 77 K.

Reaction of complex 2.2 with O_2

Complex **2.2** (0.66 g, 1 mmol) was dissolved in 5 mL of dry and degassed acetonitrile. To this solution, O_2 gas was bubbled for 2 min. After sometime, the color of the solution changes from green to brown. This brown colored solution was immediately precipitated out after being layered with diethyl ether and isolated as a solid of complex $[Fe^{III}(TPz)(NO_3^-)](ClO_4)_2$, **2.3**. Reaction of complex **2.2** with O_2 was monitored by FT-IR, UV-visible and X-band EPR spectroscopy.

Complex 2.3

Yield: 0.49 g, ~ 75 %. FT-IR (in KBr):1632, 1556, 1466, 1422, 1384, 1309, 1252, 1144, 1119, 1087, 833 and 636 cm^{-1}. UV-visible (in acetonitrile): 359 nm ($\varepsilon/M^{-1}cm^{-1}$, 6288) and 910 nm ($\varepsilon/M^{-1}cm^{-1}$, 198). ESI-mass (m/Z) calcd.: 558.104 (for $[Fe^{III}(TPz)(NO_3^-)(ClO_4)]^+$ unit); found: 558.289. X-band EPR (in DMSO): g ~ 5.05 at 77 K.

$Fe^{III}(OH)_3$, 2.4 and modified ligand (L′)

The brown colored solution obtained from the reaction of complex **2.2** (0.66 g, 1 mmol) with O_2 was layered with diethyl ether and kept in the freezer. After that white crystal of modified ligand (**L′**) was obtained along with complex **2.4**.

Complex 2.4

Yield: 0.06 g, ~ 60 %. FT-IR (in KBr): 1633, 1557, 1423,1253, 1144, 1121, 1084, 1028 and 626 cm^{-1}. UV-visible (in acetonitrile): 345 nm ($\varepsilon/M^{-1}cm^{-1}$, 8452) and 910 nm ($\varepsilon/M^{-1}cm^{-1}$, 230). X-band EPR (in DMSO): g ~ 5.04 at 77 K.

Modified ligand (L′)

Yield: 0.32 g, ~ 65 %. FT-IR (in KBr): 1655, 1557, 1456, 1426, 1385, 1368, 1338, 1264, 1252, 1152, 1116, 1083, 1040, 995, 918, 829, 735, 678 and 626 cm^{-1}. ^1H NMR (CD_3CN, 400 MHz,): δ_{ppm}, 5.78 (s, 2H), 5.29 (s, 2H), 4.98 (s, 4H), 2.20 (s, 6H), 1.84 (s, 6H).^{13}C NMR (CD_3CN, 100 MHz): δ_{ppm}, 207.7, 149.1, 110.3, 78.1, 68.2, 31, 12.8.

$[Fe^{III}(TPz)(OH)](ClO_4)_2$, 2.5 and 2,4-di-*tert*-butyl-6-nitrophenol

To the dry and degassed acetonitrile solution of complex **2.2** (0.66 g, 1 mmol), degassed solution of 2,4-di-*tert*-butylphenol (0.51 g, 5 mmol) in acetonitrile was added, followed by the addition of O_2 gas at room temperature. The reaction mixture was washed several times with hexane. 2,4-di-*tert*-butyl-6-nitrophenol was separated by preparative TLC of the hexane solution and complex **2.5** was obtained from the acetonitrile part of the reaction mixture.

Complex 2.5

Yield: 0.45 g, ~ 73 %. FT-IR (in KBr): 1633, 1555, 1465, 1423, 1384, 1260, 1275, 1141, 1120, 1088 and 627 cm^{-1}. UV-visible (in acetonitrile): 915 nm ($\varepsilon/M^{-1}cm^{-1}$, 315) and 320 nm (ε/$M^{-1}cm^{-1}$, 7208). ESI-mass (m/Z): calcd.: 613.075; found: 613.176 (M+1). X-band EPR (in DMSO): g ~ 5.06 at 77 K.

2,4-di-*tert*-butyl-6-nitrophenol

Yield: 0.16 g, ~ 65 %. ^{1}H NMR ($CDCl_3$, 400 MHz): δ_{ppm}, 11.44 (s, 1H), 7.96 (s, 1H), 7.65 (s, 1H), 1.45 (s, 9H), 1.32 (s, 9H). ^{13}C NMR ($CDCl_3$, 100 MHz,): δ_{ppm}, 153, 142, 139.9, 133.7, 132.5, 118.9, 35.7, 34.5, 31.1, 29.4. ESI-mass (m/Z): calcd.: 251.15; found: 250.23 (M-1).

Reaction of complex 2.2 with O_2 and 2,2,6,6-*tetra*methylpiperidin-1-yloxyl (TEMPO):

Complex **2.2** (0.66 g, 1 mmol) and TEMPO (0.8 g, 5 mmol) were dissolved in 10 mL dry and degassed acetonitrile solution followed by addition of O_2. After completion the reaction mixture was extracted with hexane solution. The hexane part contains 2,2,6,6-tetramethylpiperidin-1-ium nitrate ($tmpH_2^+$)(NO_3^-) and unreacted TEMPO whereas the acetonitrile part contains complex **2.5**.

2,2,6,6-tetramethylpiperidin-1-ium nitrate ($tmpH_2^+$)(NO_3^-)

Yield: 0.76 g, ~ 60 %.^{1}H NMR ($CDCl_3$, 500 MHz): δ_{ppm}, 1.74 (s, 6H), 1.48 (s, 12H). ^{13}C NMR ($CDCl_3$, 125 MHz): δ_{ppm}, 56.8, 35.0, 27.5, 16.3.

Reaction of complex 2.2 with $AgClO_4$

Complex **2.2** (0.33 g, 0.5 mmol) was dissolved in 3 mL dry and degassed acetonitrile solution. The solution FT-IR spectrum of complex **2.2** was taken. $AgClO_4$ (0.153 g, 0.75 mmol) was dissolved in 0.01 mL dry and degassed acetonitrile solution. After the immediate addition of $AgClO_4$ solution, FT-IR spectrum (solution phase) were taken. In solution FT-IR spectra, the band at 1799 cm^{-1} shifted to 1835 cm^{-1}, which confirms the oxidation of complex **2.2** to the corresponding $\{Fe(NO)\}^6$ complex.

2.4 Conclusion

Thus, the high spin Fe(II)-nitrosyl, [Fe(TPz)(NO)], having $\{Fe(NO)\}^7$ configuration in acetonitrile solution, was found to react with O_2 to result in the ligand modification to **L′** through a presumed peroxynitrite intermediate. In contrast, heme $\{Fe(NO)\}^7$ complexes are known to react with O_2, leading to the formation of corresponding nitrate (NO_3^-) complexes; but no reports are known where the ligand modification takes place. Though, there is no spectroscopic evidence of formation of the peroxynitrite intermediate, the characteristic phenol ring nitration supports the proposition. Additionally, the trapping of NO_2 formed in the reaction is also in agreement with the proposed mechanism. This study, thus, gives an insight into the mechanism of the reaction of metal-nitrosyls with dioxygen leading to the NOD activity.

2.5 References

1. Ignarro, L. J. *Nitric Oxide: Biology and Pathobiology*; Academic Press: San Diego, **2000**.
2. (a) Moncada, S.; Palmer, R. M.; Higgs, E. A. *Pharmacol. Rev.* **1991,** *43*, 109 – 142; (b) Butler, A. R.; Williams, D. L. H. *Chem. Soc. Rev.* **1993**, *22*, 233 – 241; (c) *Methods in nitric oxide research,* Feelisch, M.; Stamler, J. S. Eds.; John Wiley and Sons; Chichester, England, **1996**; (d) Jia, L.; Bonaventura, C.; Bonaventura, J.; Stamler, J. S. *Nature,* **1996**, *380*, 221 – 226; (e) Gladwin, M. T.; Lancaster, J. R.; Freeman, B. A.; Schechter, A. N. *Nat. Med.* **2003**, *9*, 496 – 500.

3. (a) Marletta, M. A.; Yoon, P. S.; Iyengar, R.; Leaf, C. D.; Wishnok, J. S. *Biochemistry* **1988**, *27*, 8706 – 8711; (b) Averill, B. A. *Chem. Rev.* **1996**, *96*, 2951 – 2964.
4. (a) Radi, R. *Proc. Natl. Acad. Sci. U. S. A.* **2004**, *101*, 4003 – 4008; (b) Qiao, L.; Lu, Y.; Liu, B.; Girault, H. H. *J. Am. Chem. Soc.* **2011**, *133*, 19823 – 19831; (c) Tran, N. G.; Kalyvas, H.; Skodje, K. M.; Hayashi, T.; Moënne-Loccoz, P.; Callan, P. E.; Shearer, J.; Kirschenbaum, L. J.; Kim, E. *J. Am. Chem. Soc.* **2011**, *133*, 1184 – 1187.
5. (a) Goldstein, S.; Lind, J.; Merenyi, G. **2005**, *105*, 2457 – 2470; (b) Pacher, P.; Beckman, J. S.; Liaudet, L. *Physiol. Rev.* **2007**, *87*, 315 – 424; (c) Speelman, A. L.; Lehnert, N. *Acc. Chem. Res.* **2014**, *47*, 1106 – 1116.
6. (a) Doyle, M. P.; Hoekstra, J. W. *J. Inorg. Biochem.* **1981**, *14*, 351 – 358; (b) Cooper, C. E.; Torres, J.; Sharpe, M. A.; Wilson, M. T. *FEBS Lett.* **1997**, *414*, 281 – 284.
7. (a) Gardner, P. R.; Gardner, A. M.; Martin, L. A.; Salzman, A. L. *Proc. Natl. Acad. Sci. U.S.A.* **1998**, *95*, 10378 – 10383; (b) Schopfer, M. P.; Mondal, B.; Lee, D.-H.; Sarjeant, A. A. N.; Karlin, K. D. *J. Am. Chem. Soc.* **2009**, *131*, 11304 – 11305; (c) Lehnert, N.; Kim, E.; Dong, H. T.; Harland, J. B.; Hunt, A. P.; Manickas, E. C.; Oakley, K. M.; Pham, J.; Reed, G. C.; Alfaro, V. S. *Chem. Rev.* **2021**, *121*, 14682 – 14905.
8. Su, J.; Groves, J. T. *Inorg. Chem.* **2010**, *49*, 6317 – 6329.
9. Wick, P. K.; Kissner, R.; Koppenol, W. H. *Helv. Chim. Acta* **2000**, *83*, 748 – 754.
10. (a) Roncaroli, F.; Videla, M.; Slep, L. D.; Olabe, J. A. *Coord. Chem. Rev.* **2007**, *251*, 1903 – 1930; (b) Maiti, D.; Lee, D.; Sarjeant, A. A. N.; Pau, M. Y. M.; Gaoutchenova, K.; Sundermeyer, J.; Karlin, K. D. *J. Am. Chem. Soc.* **2008**, *130*, 6700 – 6701.
11. (a) Kurtikyan, T. S.; Ford, P. C. *Chem. Commun.* **2010**, *46*, 8570 – 8572; (b) Kurtikyan, T. S.; Eksuzyan, S. R.; Goodwin, J. A.; Hoyhannisyan, G. S. *Inorg. Chem.* **2013**, *52*, 12046 – 12056.

12. (a) Yokoyama, A.; Han, J. E.; Cho, J.; Kubo, M.; Ogura, T.; Siegler, M. A.; Karlin, K. D.; Nam, W. *J. Am. Chem. Soc.* **2012**, *134,* 15269 – 15272; (b) Yokoyama, A.; Cho, K.-B.; Karlin, K. D.; Nam, W. *J. Am. Chem. Soc.* **2013**, *135*, 14900 – 14903.
13. (a) Clarkson, S. G.; Basolo, F. J. *J. Chem. Soc. Chem. Commun.* **1972**, *119*, 670 – 671. (b) Clarkson, S. G.; Basolo, F. *Inorg. Chem.* **1973**, *12*, 1528 – 1534.
14. Skodje, K. M.; Williard, P. G.; Kim, E. *Dalton Trans.* **2012**, *41*, 7849 – 7851.
15. Park, G. Y.; Deepalatha, S.; Puiu, S. C.; Lee, D.-H.; Mondal, B.; Narducci Sarjeant, A. A.; del Rio, D.; Pau, M. Y. M.; Solomon, E. I.; Karlin, K. D. *J. Biol. Inorg. Chem.* **2009**, *14*, 1301 – 1311.
16. (a) Kalita, A.; Kumar, P.; Mondal, B. *Chem. Commun.* **2012**, *48*, 4636 – 4638; (b) Saha, S.; Ghosh, S.; Gogoi, K.; Deka, H.; Mondal, B.; Mondal, B. *Inorg. Chem.* **2017**, *56*, 10932 – 10938; (c) Mazumdar, R.; Saha, S.; Samanta, B.; Ghosh, R.; Maity, S.; Mondal, B. *Dalton Trans.* **2023**, *52*, 7917 – 7925; (d) Mondal, B.; Borah, D.; Mazumdar, R.; Mondal B. *Inorg. Chem.* **2019**, *58*, 14701 – 14707; (e) Mazumdar, R.; Mondal, B.; Saha, S.; Samanta, B.; Mondal, B. *J. Inorg. Biochem.* **2022**, *228*, 111698.
17. Fujisawa, K.; Chiba, S.; Miyashita, Y.; Okamoto, K. *Eur. J. Inorg. Chem.* **2009**, *48*, 3921 – 3934.
18. (a) Randall, C. R.; Zang, Y.; True, A. E.; Que, L., Jr.; Charnock, J. M.; Garner, C. D.; Fujishima, Y.; Schofield, C. J.; Baldwin, J. E. *Biochemistry* **1993**, *32*, 6664 – 6673; (b) Randall, C. R.; Shu, L.; Chiou, Y.-M.; Hagen, K. S.; Ito, M.; Kitajima, N.; Lachicotte, R. J.; Zang, Y.; Que, L., Jr. *Inorg. Chem.* **1995**, *34*, 1036 – 1039.
19. (a) Chiou, Y.-M.; Que, L., Jr. *Inorg. Chem*. **1995**, *34*, 3270 – 3278; (b) Dong, H. T.; Speelman, A. L.; Kozemchak, C. E.; Sil, D.; Krebs, C.; Lehnert, N. *Angew. Chem., Int. Ed.* **2019**, *58*, 17695 – 17699.

20. Ray, M.; Golombek, A. P.; Hendrich, M. P.; Yap, G. P. A.; Liable-Sands, L. M.; Rheingold, A. L.; Borovik, A. S. *Inorg. Chem.* **1999**, *38*, 3110 – 3115.
21. Mondal, B.; Saha, S.; Borah, D.; Mazumdar, R.; Mondal, B. *Inorg. Chem.* **2019**, *58*, 1234 – 1240.
22. Jones, R. D.; Summerville, D. A.; Basolo, F. *Chem. Rev*. **1979**, *79*, 139 – 179.
23. Suzuki, M.; Ishiguro, T.; Kozuka, M.; Nakamoto, K. *Inorg. Chem.* **1981**, *20*, 1993 – 1996.
24. (a) Ileperuma, O. A.; Feltham, R. D. *Inorg. Chem.* **1977**, *16*, 1876 – 1833; (b) Speelman, A. L.; Zhang, B.; Krebs, C.; Lehnert, N. *Angew. Chem., Int. Ed*. **2016**, *55*, 6685 – 6688.
25. Flammang, R.; Barbieux-Flammang, M.; Van Haverbeke, Y.; Luna, A.; Tortajada, J. *J. Phys. Org. Chem.* **2000**, *13*, 13 – 22.
26. Sugimoto, H.; Sawyer, D. T. *J. Am. Chem. Soc.* **1985**, *107*, 5712 – 5716.
27. SMART, SAINT and XPREP, Siemens Analytical X-ray Instruments Inc., Madison, Wisconsin, USA, **1995**.
28. Sheldrick, G. M. University of Gottingen, Germany, **1999**.
29. Sheldrick, G. M. SHELXS-2016, University of Gottingen, Germany, **2016**.
30. Farrugia, L. J. ORTEP-3 for Windows - a version of ORTEP-III with a Graphical User Interface (GUI). *J. Appl. Crystallogr.* **1997**, *30*, 565.

Chapter 3

Spin state dependent reactivity of iron-nitrosyls with dioxygen

Abstract

Two iron nitrosyls having $\{Fe(NO)\}^7$ configuration but with different spin states have been synthesized in Pz_2Py [Pz_2Py = *Bis*(di(3,5-dimethyl-1H-pyrazolyl)methyl)-(2-pyridylmethyl)amine] ligand and have been characterized spectroscopically. In addition, the high-spin nitrosyl complex, **3.2a** was also studied structurally. FT-IR studies show that the nitrosyl stretching appears at 1790 and 1711 cm^{-1} for high-spin and low-spin analogues, respectively. The dioxygen reactivity of complexes **3.2a** and **3.2b** have been explored. The high-spin complex, **3.2a** was found to react with O_2, leading to the formation of the corresponding nitrate product, **3.3a** through a presumed peroxynitrite intermediate. In contrast, O_2 substitutes the NO group from complex **3.2b**, owing to the weaker Fe–N_{NO} bond, resulting in the formation of $[Fe^{III}(Pz_2Py)(OH)(CH_3CN)](ClO_4)_2$, **3.3b**. The release of NO by O_2, in this case, was evident from the presence of NO_2 in the GC-Mass of the headspace gas from the reaction vessel.

3.1 Introduction

Metal-nitrosyl complexes specially iron-nitrosyls have attracted a considerable research interest for their biological relevance and it is implicated by the huge volume of literature on iron nitrosyls, both in heme and non-heme ligand frameworks.[1-4] Coordination compounds of iron(II) are known to exhibit spin state transition depending upon various factors like nature of the coordinating ligands, temperature, application of pressure or magnetic field, irradiation of light *etc*.[5] The change of spin state is found to be associated with a change of electronic structure of the metal ion and thus, the complex as a whole.[5-6] This results in a considerable change of the physical and chemical properties of the molecule.

Iron(II)-nitrosyls in heme systems having $\{Fe(NO)\}^7$ configuration are more commonly found in low-spin state, whereas the non-heme counterparts can exist both in high-spin or low-spin state.[7-9] For example, five coordinated square pyramidal [Fe(NO)(salen)] [salen = *N,N′*-ethylene*bis*(salicylideneiminato)] was reported long back to exists in high-spin state at 23 °C and it becomes low-spin on decreasing the temperature to –135 °C. Interestingly, the complex in both the spin state has been structurally characterized.[10] There are many such results of spin crossover in cases of iron(II)-nitrosyls. As expected, high-spin $\{Fe(NO)\}^7$ complexes have different electronic structure compared to their low spin analogues. Based on a variety of spectroscopic analyses and theoretical calculations, it has been reported that the high-spin $\{Fe(NO)\}^7$ complexes have an $S = \frac{3}{2}$ ground state, which arises from the antiferromagnetically coupled high-spin iron(III) ($S = \frac{5}{2}$) to a triplet nitroxyl (NO^-) group.[11-15] However, recent theoretical studies on the iron(II)-nitrosyls having $\{Fe(NO)\}^7$ configuration have shown them to exist preferentially in $Fe^{II}–NO^0$ resonance form.[16] Nevertheless, the Fe–N_{NO} distances and N–O stretching frequencies for the complexes are found to be directly related to the effective nuclear charge of the metal center and thus, to the spin state.[17] This, in turn, results in a difference in reactivity of the iron(II)-nitrosyls depending on their spin state.

This chapter describes the synthesis of a $\{Fe(NO)\}^7$ complex in two different spin states, *i.e.,* high-spin and low-spin, depending on the reaction condition and their spectral characterization. The dioxygen reactivity of these two counter parts has been studied with an aim to understand how the spin state of an iron(II)-nitrosyl controls the overall reaction, including the pathway and electron transfer. It is observed that in case of the high-spin complex, the oxidation of the NO group takes place leading to the corresponding nitrate complex. On contrary, in the case of the low-spin analogue, the NO group was found to be substituted by O_2.

3.2 Results and Discussion

The ligand, *Bis*(di(3,5-dimethyl-1H-pyrazolyl)methyl)-(2-pyridylmethyl)amine, Pz_2Py has been synthesized from the reaction of 1-(Hydroxymethyl)-3,5-dimethyl-1-pyrazole and picolylamine following an earlier reported procedure.[18] The isolated ligand was characterized using spectroscopic techniques such as FT-IR, ^1H and ^{13}C NMR, and ESI-Mass spectrometry (Experimental Section and Appendix II, Figures A2.1-A2.6). The precursor complex **3.1**, $[Fe^{II}(Pz_2Py)(CH_3CN)(H_2O)](ClO_4)_2$, was prepared by the reaction of $[Fe(CH_3CN)_4(ClO_4)_2]$ and the ligand Pz_2Py in degassed acetonitrile solution (Experimental Section and Appendix II, Figures A2.7-A2.9). The compound was isolated as solid crystals and spectroscopic as well as structural characterization was carried out to confirm the formulation (Experimental Section). The perspective ORTEP view is shown in figure 3.1. The structural studies reveal that the metal ion, Fe(II) is coordinated by four N atoms from the tripodal ligand along with a water and acetonitrile molecule in a distorted octahedral geometry. The water molecule perhaps came from moisture during the crystallization process or may be from the traces of water present in the solvent.

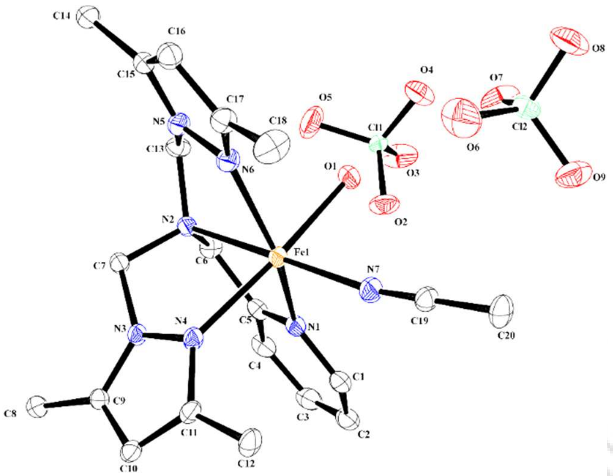

Figure 3.1. ORTEP diagram of complex **3.1** (30% thermal ellipsoid plot, H-atoms are omitted for clarity).

The Fe(II)-nitrosyl complex $[Fe^{II}(Pz_2Py)(CH_3OH)(NO)](ClO_4)_2$, **3.2a**, was prepared by bubbling of NO(g) into the degassed methanol solution of complex **3.1** followed by allowing the reaction mixture to stand for 24 hr under NO pressure at room temperature (Experimental Section). On the other hand, the complex $[Fe^{II}(Pz_2Py)(CH_3CN)(NO)](ClO_4)_2$, **3.2b** was obtained from the similar reaction protocol in acetonitrile solvent and at –40 °C (Experimental Section). The complex **3.2a** was isolated as needle-shaped crystals and subjected to spectroscopic and structural characterization (Experimental Section and Appendix II, Figures A2.10-A2.12). Complex **3.2b** was isolated as a solid, however, even after several attempts, we could not grow X-ray quality crystals for complex **3.2b**. Spectroscopic data confirms that both the nitrosyls are having $\{Fe(NO)\}^7$ configuration.

The figure **3.2** shows the ORTEP view of complex **3.2a**. It suggests that the Fe(II) center is ligated with the ligand Pz_2Py as well as one NO group and MeOH as solvent to fulfill the octahedral coordination though distorted. The crystal data, important bond angles and distances are listed in tables A2.1-A2.3. The Fe–N_{NO} and N–O distances are 1.760(6) and 1.145(9) Å, respectively. It would be worth mentioning that for other reported high-spin iron-nitrosyls having $\{Fe(NO)\}^7$ configuration; for example, $[Fe(TPz)(NO)(CH_3CN)]^{2+}$, $[Fe(TPz)(NO)Cl]^{+}$, $[Fe(TPA)(NO)(OTf)]^{+}$, $[Fe(TPA)(NO)(BenzFor)]^{+}$ [TPz = *Tris*(3,5-dimethyl-1H-pyrazol-1-yl)methyl)amine; TPA = *Tris*(2-pyridylmethyl)amine and BenzFor = Benzoylformate], the Fe–N_{NO}/N–O distances are 1.732/1.132, 1.735/1.150, 1.755/1.144, 1.722/1.152 Å, respectively.[19-22] The measured Fe-N-O angle for complex **3.2a** is 162.5°. Whereas for the analogous reported complexes mentioned above, the Fe-N-O angle falls within the range of 157.1°-174.2°.

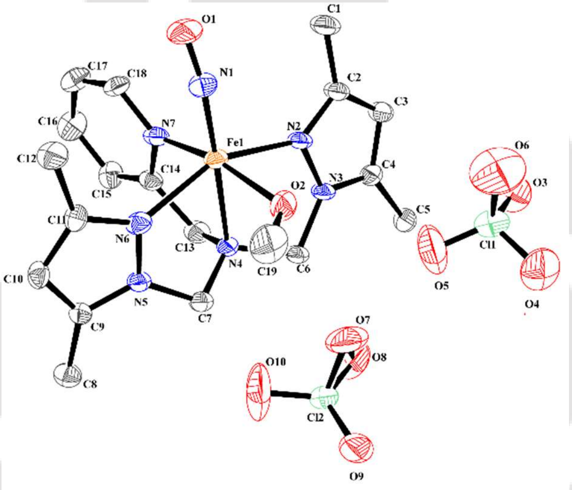

Figure 3.2. ORTEP diagram of complex **3.2a** (30% thermal ellipsoid plot, H-atoms are omitted for clarity).

In FT-IR spectroscopy, the N–O stretching frequency for complexes **3.2a** and **3.2b** appear at 1790 and 1711 cm^{-1} in KBr pellet (Appendix II, Figures A2.10 and A2.23). The stretching frequency is well within the range of the same for earlier reported high-spin iron nitrosyls having $\{Fe(NO)\}^7$ configuration. For instance, $[Fe(TPz)(NO)(CH_3CN)]^{2+}$ shows this stretching at 1790 cm^{-1} (Appendix I, A1.13).[19] Similarly, in cases of $[Fe(TPz)(NO)Cl]^{+}$ and $[Fe(TPA)(NO)(BenzFor)]^{+}$, the NO stretching frequencies appear at 1794 and 1796 cm^{-1}, respectively.[20,22] On the other hand, for complex **3.2b**, the NO stretching is found to appear at 1711 cm^{-1} (Appendix II, Figure A2.23). Such a large difference in stretching frequency of complexes **3.2a** and **3.2b** could be due to the change of oxidation states of the central metal ion. It is known that oxidation state of the central metal ion of metal nitrosyls can shift the NO stretching frequency by 40-100 cm^{-1}.[23] The structural study reveals that in complex **3.2a** the central metal ion, iron is in +2 oxidation state. Since the nitrosyl stretching of complex **3.2b** is approximately 80 cm^{-1} lower than that of complex **3.2a**, iron center has to be in +1 oxidation state, leading to $\{Fe(NO)\}^8$ configuration, if at all this shift has to happen. Now, the earlier reported 6 and 5 coordinated $\{Fe(NO)\}^8$ systems in non-heme ligand framework, in general, show NO stretching in the range of 1588-1618 cm^{-1}.[24-27] Thus, the nitrosyl stretching frequency of **3.2b** apparently suggests that it is not a $\{Fe(NO)\}^8$ system. In addition, the conductance measurement also suggests compound **3.2b** as a 1:2 electrolyte. In contrary, iron nitrosyls with $\{Fe(NO)\}^7$ configuration which show the stretching frequency at around 1690-1710 cm^{-1}, are reported to be low-spin in nature. For example, Lenhert's group reported two iron-nitrosyl complexes, $[Fe(TPA)(NO)(CH_3CN)](BF_4)_2$, where the characteristic N–O stretching band of a hs-$\{Fe(NO)\}^7$ complex with $S = \frac{3}{2}$ appears at 1795 cm^{-1}, the low-spin complex with $S = \frac{1}{2}$ shows at 1701 cm^{-1}.[28] Other illustrative examples in this regard are hs-$\{Fe(NO)\}^7$ and ls-$\{Fe(NO)\}^7$ complexes of [Fe(salen)(NO)], which distinctly demonstrate two different N–O stretching frequencies for the two spin states.[10] Hence, FT-IR spectroscopic studies and conductance measurement suggest both the complexes having different spin states; *i.e.,* complex **3.2a** is high-spin and **3.2b** is low-spin iron nitrosyl, where both of them having $\{Fe(NO)\}^7$ configuration.

Further support of the difference of spin states in complexes **3.2a** and **3.2b** came from X-band EPR studies. Figures 3.3(A) and (B) represent the X-band EPR spectrum displayed by complexes **3.2a** and **3.2b** in frozen acetonitrile solution at 77 K.

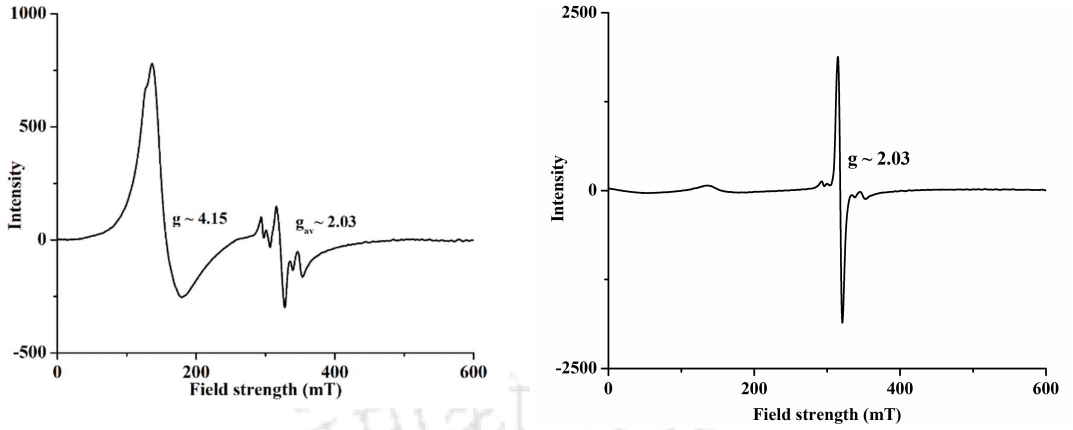

(A) **(B)**

Figure 3.3. X-band EPR spectrum of complexes (A) **3.2a** and (B) **3.2b** in acetonitrile at 77 K.

Complex **3.2a** shows two sets of signals at g ~ 4.15 and 2.03 corresponding to the near axial high-spin (S = $\frac{3}{2}$) ground state resulting from the antiferromagnetic coupling of high-spin Fe(III) to a triplet NO^- in $\{Fe(NO)\}^7$ configuration.[2,12] Similar spectrum was reported earlier in case of high-spin $\{Fe(NO)\}^7$ complex of peralkylguanidine ligand, $[Fe(TMG_2dien)(NO)(OTf)]^+$ [TMG_2dien = 2′,2′-(2,2′-(methylazanediyl)*bis*(ethane-1,2-diyl))*bis*(1,1,3,3-tetramethylguanidine)] with g values at ~ 4 and 2, respectively.[27] In cases of $[Fe(TPA)(NO)(BenzFor)]^+$ and $[Fe(^6TLA)(NO)(BenzFor)]^+$ these resonances appear at g ~ 4.05, 3.87, 1.99 and g ~ 4.02, 3.93, 1.95, respectively [^{6}TLA = *Tris*((6-methyl-2-pyridyl)methyl)amine].[22] Similar complex, $[Fe(TPz)(NO)(CH_3CN)]^{2+}$ in frozen acetonitrile at 77 K was found to show signals at g ~ 4.11 and 2.04 corresponding to the high-spin (S = $\frac{3}{2}$) $\{(Fe(NO)\}^7$.[19] Whereas complex **3.2b**, under similar experimental condition shows sharp signal at g ~ 2.03 characteristic to the $\{Fe(NO)\}^7$ complexes having S = $\frac{1}{2}$ spin state.[2,10,28-30] Thus, physical measurements, FT-IR and X-band spectral studies collectively establish complexes **3.2a** and **3.2b** as high-spin and low-spin iron nitrosyls with $\{Fe(NO)\}^7$ configuration, respectively.

Dioxygen reactivity of high-spin complex, 3.2a

Complex **3.2a** in acetonitrile solution exhibits absorption bands at 635 nm (ε/$M^{-1}cm^{-1}$, 780), 360 nm (ε/$M^{-1}cm^{-1}$, 6810) in UV-visible spectrum (Appendix II, Figure A2.11). When O_2 gas was added through a gas-tight Hamilton syringe to the degassed acetonitrile solution of complex **3.2a** at room temperature, the increase in intensity of the absorption band having λ_{max} at 360 nm band was observed (Figure 3.4). It was associated with a simultaneous decrease of the band intensity of the 635 nm band with respect to time, leading to the stable final product within 5-10 min (Appendix II, Figure A2.14). The final product was isolated as a solid and characterized spectroscopically as the corresponding nitrate complex, **3.3a** (Experimental Section and Appendix II, Figures A2.13-A2.15). It shows a stretching frequency at 1384 cm^{-1} in the FT-IR spectrum, suggesting the presence of a nitrate (NO_3^-) group (Appendix II, Figure A2.13).[31]

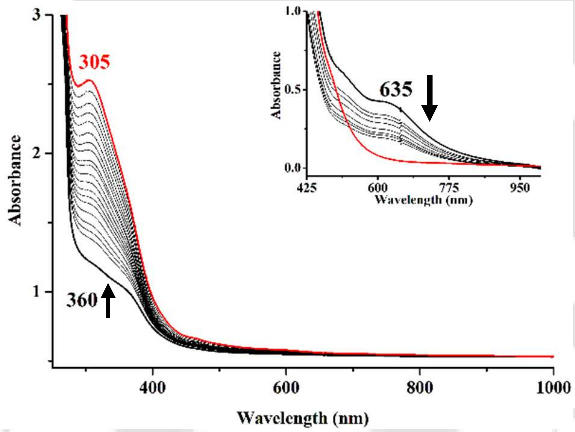

Figure 3.4. UV-visible spectra of the reaction of complex **3.2a** (black) and after the addition of O_2 (red) in acetonitrile at room temperature [Inset: complex **3.2a** (black), after O_2 addition (red) corresponds to the final product].

The reaction of O_2 gas with the degassed acetonitrile solution of complex **3.2a** was monitored using FT-IR spectroscopy. It shows that the NO stretching frequency at 1790 cm^{-1} disappeared upon addition of O_2 into the degassed acetonitrile solution of complex **3.2a** with the simultaneous appearance of a new stretching at 1825 cm^{-1} (Figure 3.5).

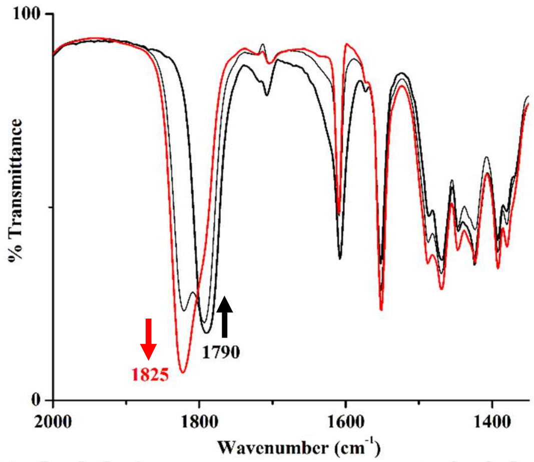

Figure 3.5. FT-IR spectra of the reaction of complex **3.2a** (black) and after addition of O_2 (red) in acetonitrile medium at room temperature.

The intensity of 1825 cm^{-1} stretching frequency decays with time and finally disappears, which suggests that this band is associated with an unstable intermediate. Both heme and non-heme Fe(II) complexes, result in the corresponding [Fe^{III}-(O_2^-)] species in the presence of O_2 with the oxidation of the metal by one unit.[32] Metal-superoxides are reported to exhibit ν(O_2) in the range of 1200-1070 cm^{-1}; whereas, for metal-peroxo species the O–O stretching appears in the range of 930-740 cm^{-1}.[33-34] However, no such characteristic stretching was observed in this case. In addition, Fe(III)-nitrosyls are reported to exhibit nitrosyl stretching frequency at ~ 1830 cm^{-1}.[35-36] Hence, the 1825 cm^{-1} band is assigned to the nitrosyl stretching of $\{Fe(NO)\}^6$ species formed in the reaction of complex **3.2a** with O_2. This was further confirmed by the ^{15}NO labelling experiment, where the band was found to appear at 1805 cm^{-1}. It is to be noted that for the structurally characterized $[Fe(TMG_3tren)(NO)]^{3+}$ complex, [TMG_3tren = 1,1,1-*tris*{2-[*N*^{2}-(1,1,3,3-tetramethylguanidino)]ethyl}amine] nitrosyl stretching frequency appears at 1879 cm^{-1}.[36] Thus, the spectral evidence suggests the formation of $[Fe^{III}(NO)]^{3+}$ in the reaction of complex **3.2a** with O_2. No spectral evidence was observed in support of the formation of O_2^- coordinated to the metal center, perhaps because they are present in the reaction cage, as seen earlier.[19]

The formation of complex **3.3a** in the reaction of complex **3.2a** with O_2 is presumably proceed through a peroxynitrite ($OONO^-$) intermediate as reported earlier. We propose that the reaction of complex **3.2a** with O_2 initially results in the formation of $\{[Fe^{III}(Pz_2Py)(NO)]^{3+}.(O_2^-)\}$ in the reaction cage, which subsequently leads to the corresponding peroxynitrite intermediate $[Fe^{III}(Pz_2Py)(OONO^-)]^{2+}$ (Scheme 3.1). This intermediate, as expected, decomposes leading to the formation of complex **3.3a**. Since the very short lifetime of the peroxynitrite intermediate did not allow its spectral characterization, we sought chemical evidence. When the reaction of complex **3.2a** with O_2 was carried out in the presence of 2,4-di-tertiarybutylphenol, it resulted in ~ 30 % of nitrophenol along with the dimerised product, *bis*phenol (~ 50 %) and complex **3.4a** (Experimental Section and Appendix II, Figures A2.16-A2.22).[37] Phenol nitration/oxidative coupling has been extensively used as evidence to establish the presence of metal-peroxynitrite species.[38] Thus, the dioxygen reactivity of complex **3.2a** proceeds through the peroxynitrite pathway to afford the corresponding nitrate product, complex **3.3a**. This is quite well-established for high-spin iron nitrosyls of $\{Fe(NO)\}^7$ configuration in both the heme and non-heme ligand framework.[19]

Dioxygen reactivity of low-spin complex, 3.2b

When O_2 was added to the degassed acetonitrile solution of complex **3.2b**, no significant visual change was observed in the UV-visible spectrum except an increase in the intensity of band having λ_{max} at 560 nm (Figure 3.6). Isolation and characterization reveal the final compound as the corresponding hydroxide complex, **3.3b** with $[Fe^{III}(Pz_2Py)(OH)](ClO_4)_2$ formulation (Experimental Section and Appendix II, Figures A2.26-A2.29).

The addition of O_2 gas to the degassed acetonitrile solution of complex **3.2b** showed immediate disappearance of the nitrosyl stretching frequency at 1711 cm^{-1} in FT-IR spectroscopic studies, resulting in a spectrum similar to that of the isolated complex **3.3b**. This suggests that the metal center gets oxidised from Fe(II) to Fe(III). The oxidation of the metal center is also evident from the X-band EPR studies (Figure 3.7).

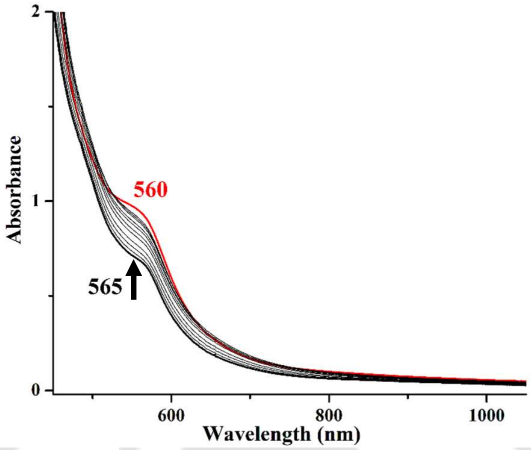

Figure 3.6. UV-visible spectra of the reaction of complex **3.2b** (black) and after addition of O_2 (red) towards the formation of complex **3.3b** in acetonitrile at room temperature.

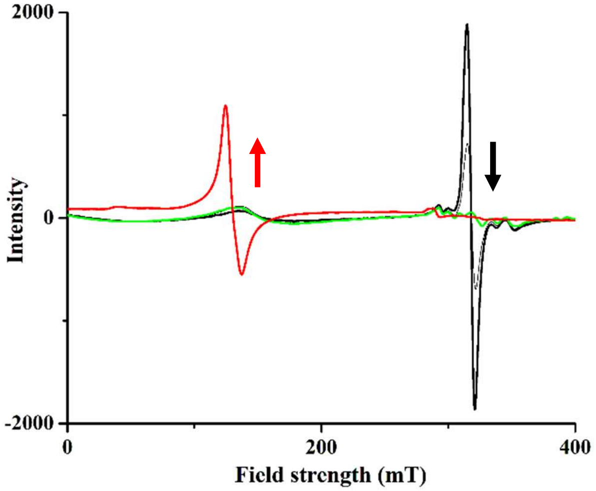

Figure 3.7. X-band EPR spectra of the reaction of complex **3.2b** (black, g ~ 2.03) with O_2 towards the formation of complex **3.3b** (red, g ~ 4.15) through $[Fe^{III}\text{-}(O_2^-)]$ intermediate (green) in acetonitrile solution at 77 K.

It would be noted that the spectrum of complex **3.3b** does not show any stretching which can be assigned to the oxidized product of NO unit such as NO_3^- or NO_2^- *etc*. as observed in the case of complex **3.2a**. In addition, when the head-space gas from the reaction vessel was subjected to GC-Mass analysis, the presence of NO_2 was observed in a near-quantitative amount (~ 55 %) (Experimental Section and Appendix II, Figure A2.30). These observations suggest that the reaction of O_2 with complex **3.2b** leads to the substitution of the NO group by O_2, resulting in the formation of the corresponding $[(Pz_2Py)Fe^{III}(O_2^-)]^{2+}$ moiety (Scheme 3.1). NO group, thus released, reacts with the excess O_2 present in the reaction vessel to form NO_2, which was evident from the GC-Mass studies. Owing to the unstable nature, the Fe(III)-superoxide decomposes very fast to the corresponding hydroxo product, **3.3b**. This has been observed earlier also.[32]

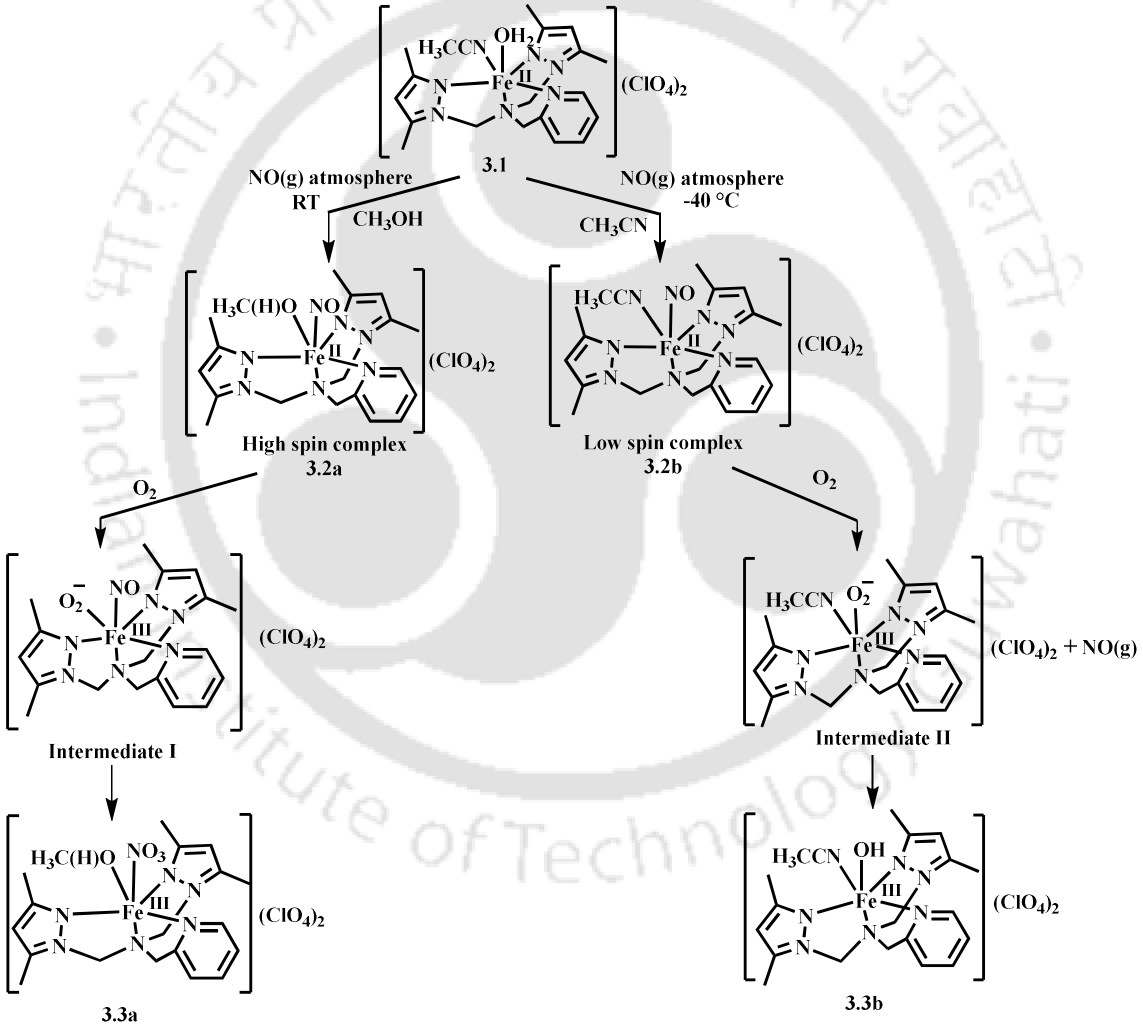

Scheme 3.1. Overall reaction.

Thus, these results suggest the Fe–N_{NO} bond is relatively stronger in case of high-spin complex, **3.2a** compared to that of low-spin one, **3.2b** which is in accordance with the earlier observation that the Fe-N_{NO} bond becomes weaker moving from high-spin to low-spin analogue. For instance, in case of structurally characterized [Fe(NO)(salen)], the Fe–N_{NO} distances for the high- and low-spin complexes are 1.783 and 1.810 Å, respectively.[10]

To get better insight, theoretical calculation has been done. Optimization and calculated FT-IR NO stretching for both the complexes was done using Gaussian 16 suit of program.[39] Optimization was done at M06-2X/def2-TZVP[40-41] and harmonic vibrational frequency calculations were also performed at the same level. All the structures were characterized to be at their local minimum with all real values of the Hessian matrix. All energies were zero-point and thermally corrected. Figure 3.8 shows the energetics (ΔG, kcal/mol) of the formation of **3.3a** and **3.3b**. Complex **3.1** in presence of NO(g) produces a high-spin complex **3.2a** in an exergonic reaction ($\Delta G = -3.4$ kcal/mol). The unscaled NO stretching frequency in complex **3.2a** is found to be 1806 cm^{-1} which is very close to the experimentally observed ν_{NO} of 1792 cm^{-1}. Complex **3.1**, on the other hand, forms a low-spin complex **3.2b** following an exergonic pathway ($\Delta G = -4.6$ kcal/mol). The calculated NO stretching frequency in **3.2b** is found to be 1723 cm^{-1}, very close to the experimentally observed ν_{NO} of 1711 cm^{-1}. Complex **3.2a** then upon reaction with O_2 converts to **3.3a** *via* the corresponding Fe(III) intermediate (**Int-I**) and the process is found to be exergonic. Similarly, complex **3.2b** converts to complex **3.3b** upon reaction with O_2 through the formation of a superoxide bound intermediate [$(Pz_2Py)Fe(O_2^-)$], (**Int-II**). Here also the process is exergonic.

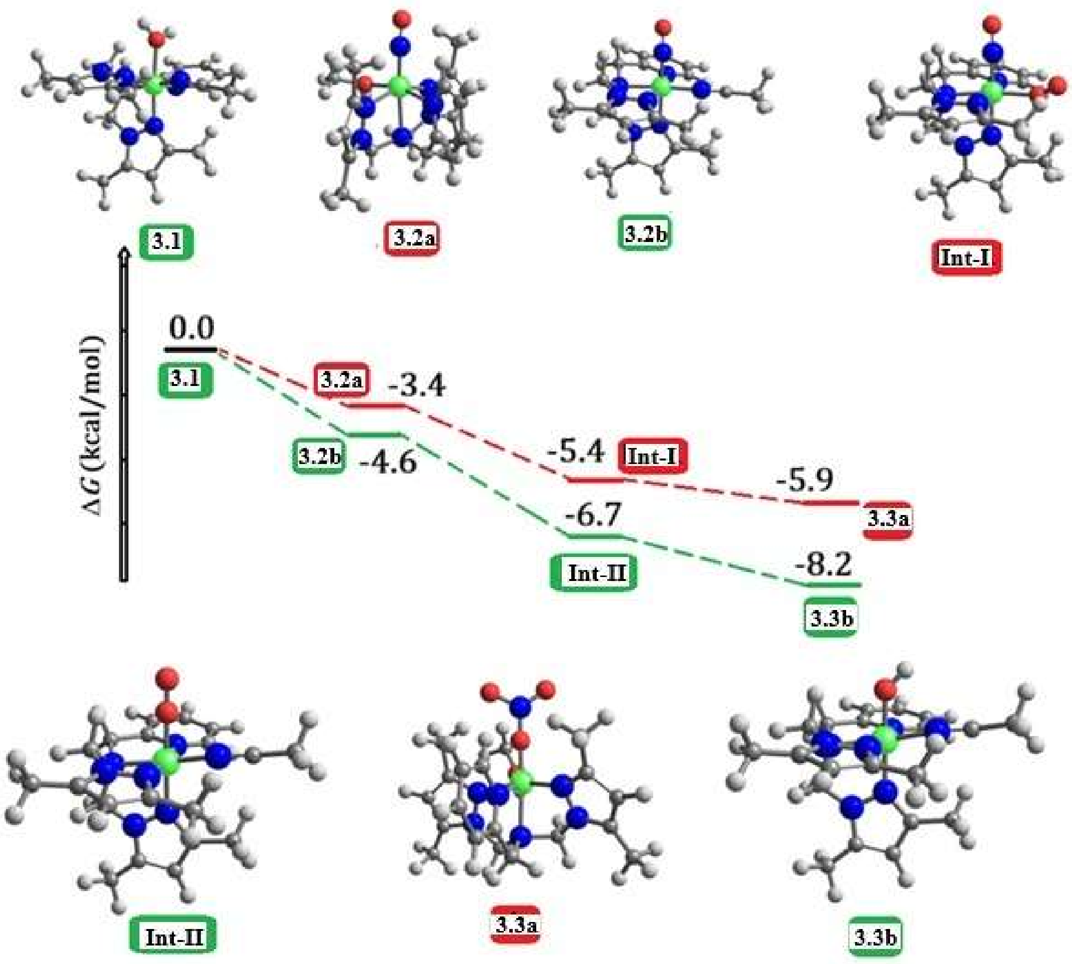

Figure 3.8. Energetics (Δ*G*, kcal/mol) for the formation of complex **3.3a** and **3.3b** from complex **3.1**. Optimized geometries of the molecules are also shown.

3.3 Experimental Section

3.3.1 Materials and methods

All chemicals and solvents were of commercially available quality and used without further purification, unless otherwise mentioned. Acetonitrile was distilled over phosphorus pentoxide under Ar. Diethyl ether was distilled with sodium metal and benzophenone. All the dry solvents were stored over 4Å molecular sieves under inert condition. Deoxygenation of the solvent and solutions was done by repeated vacuum/Ar purge cycles or bubbling with argon for 30 min. All the reactions were performed under inert conditions unless specified. UV-visible spectra were recorded on an Agilent Technologies Cary 8454 UV-visible spectrophotometer by preparing a known concentration of the samples in acetonitrile solution at room temperature (25 °C) using a quartz cuvette of 1 cm width. FT-IR spectra of the samples were taken on a PerkinElmer spectrophotometer at room temperature with samples prepared either as KBr pellets by grinding the sample with KBr (IR-grade) or in dichloromethane solution in a KBr cell. ^{1}H and ^{13}C NMR spectra were collected in 400 MHz Bruker AVANCE 400 or 500 MHz Bruker AVANCE NEO 500 FT-NMR spectrometers. Chemical shifts were reported as δ (ppm) values relative to an internal standard (tetramethylsilane) and the residual solvent peaks. The X-band Electron Paramagnetic Resonance (EPR) spectra were recorded on a JEOL JES-FA200 ESR spectrometer, at 77 K with microwave power, 0.998 mW; microwave frequency, 9.14 GHz. Mass spectra were measured in HPLC grade acetonitrile solution.

Single crystals of all complexes suitable for X-ray crystallographic analysis were obtained by layering of diethyl ether into the acetonitrile solution. The intensity data were collected using a Bruker SMART APEX-II CCD diffractometer, equipped with a fine focus 1.75 kW sealed tube MoK$_\alpha$ radiation ($\lambda = 0.71073$ Å) at 293(3) K, with increasing ω (width of 0.3° per frame) at a scan speed of 3 s/frame. The SMART software was used for data acquisition. Data integration and reduction were undertaken with SAINT and XPREP software.[42] Multi-scan empirical absorption corrections were employed to the data using the program SADABS. Structures were solved by direct methods using SHELXS-2016 and refined with full-matrix least squares on F^2 using SHELXL-2016/6.[43] Structural illustrations have been drawn with ORTEP-3 for Windows.[44]

Computational Details

The formation of complexes **3.3a** and **3.3b** from **3.1** has been studied computationally and all these calculations were performed using Gaussian 16 suite of program.[39] All the molecules were fully optimized at M06-2X/def2-TZVP[40-41] and harmonic vibrational frequency calculations were also performed at the same level. All the structures were characterized to be at their local minimum with all real values of the Hessian matrix. All energies were zero-point and thermally corrected.

3.3.2 Syntheses

1-(Hydroxymethyl)-3, 5-dimethyl-1-pyrazole, S

In a round bottom flask 3,5-dimethyl-1-pyrazole (3.27 g, 34 mmol) was dissolved in 30 mL of 1:2 (V/V) water/ethanol mixture. 37 % solution of formaldehyde (3.0 mL, 39 mmol) in 20 mL water was added to this solution. The reaction mixture was stirred for 2 days at room temperature. It was then extracted with 3 × 25 mL chloroform. Solvent was removed under reduced pressure and a white crystalline residue of 1-(Hydroxymethyl)-3, 5-dimethyl-1-pyrazole was formed. This compound was recrystallized from dichloromethane/toluene (1:3). Yield: 2.57 g, ~ 60%. FT-IR (in KBr): 3146, 1555, 1460, 1395, 1307, 1226, 1068, 1037 and 807 cm^{-1}. ^{1}H NMR ($CDCl_3$, 400 MHz): δ_{ppm} 5.83, 5.40, 2.33, 2.19. ^{13}C NMR (in $CDCl_3$, 100 MHz): δ_{ppm} 148.3, 139.8, 106, 69.9, 12.9, 10.5

***Bis*(di(3,5-dimethyl-1H-pyrazolyl)methyl)-(2-pyridylmethyl)amine], Pz_2Py**

The ligand Pz_2Py was synthesized and purified according to previously reported literature.[18] 2-Picolylamine (0.541 g, 5 mmol) and glacial acetic acid (0.60 g, 10 mmol) to the acetonitrile solution of 1-(Hydroxymethyl)-3, 5-dimethyl-1-pyrazole (1.26 g, 10 mmol) and the reaction mixture was stirred at room temperature for 3 days. After that the solvent was removed by rotary evaporator and it was treated with 10% NaOH solution until pH reaches 4. Solvent extraction was done by CH_2Cl_2 (3 × 25 mL). Organic layer was washed with water and dried with anhydrous Na_2SO_4. Solvent was dried under rotary evaporator and yellow liquid of ligand was obtained. Yield: 1.1 g, ~ 67 %. FT-IR (in KBr): 3400, 2922, 2867, 1590, 1556, 1459, 1434, 1380, 1313, 1246, 1147, 1031, 978, 765, 630 and 402 cm^{-1}. ^1H NMR ($CDCl_3$, 400 MHz): δ_{ppm} 2.02 (s, 6H); 2.18 (s, 6H); 3.87(s, 2H); 4.98 (s, 4H); 5.76 (s, 2H); 7.12-7.14 (m, 1H); 7.16 (d, 1H); 7.57 (m, 1H); 8.47 (d, 1H). ^{13}C NMR ($CDCl_3$, 100 MHz): δ_{ppm} 10.5, 13.3,54.6, 64.9, 105.6, 122,123, 136.3, 139.8, 147.6, 148.6, 158.5.

$[Fe^{II}(Pz_2Py)(CH_3CN)(H_2O)](ClO_4)_2$, 3.1

$[Fe^{II}(CH_3CN)_4(ClO_4)_2]$ (0.42 g, 1 mmol) and the ligand Pz_2Py (0.32 g, 1 mmol) were dissolved in dry and degassed acetonitrile and the color of the solution became red. The solution was stirred for 30 min under Ar atmosphere. After that the solution was layered with diethyl ether and kept into freezer. After 4 days block shaped orange-red crystals of complex **3.1** was formed. Yield: 0.46 g, ~ 73 %. Elemental analyses for $C_{20}H_{29}N_7O_9Cl_2Fe$. Calcd. (%): C, 44.59; H, 5.43; N, 6.58. found (%): C, 44.54; H, 5.47; N, 6.62. FT-IR (in KBr): 3424, 2998, 2283, 1638, 1606, 1555, 1467, 1425, 1392, 1327, 1096, 776 and 626 cm^{-1}. UV-visible (in acetonitrile): 340 nm (ε /M^{-1} cm^{-1}, 6610) and 560 nm (ε /M^{-1} cm^{-1}, 610). X-band EPR (in acetonitrile): Silent at 77 K.

High-spin $[Fe^{II}(Pz_2Py)(CH_3OH)(NO)](ClO_4)_2$, 3.2a

Complex **3.1 (**0.65 g, 1 mmol) was dissolved in dry and degassed 5 mL methanol. This solution was kept under NO(g) atmosphere at room temperature for 1 day until the color changes to dark green. Next day excess NO gas was removed by applying several cycles of vacuum/Ar purged. Then the solution was layered with diethyl ether and after 1 day needle shaped green crystals of complex **3.2a** were obtained. Yield: 0.52 g, ~ 80 %. Elemental analysis for $C_{19}H_{28}N_7O_{10}Cl_2Fe$. Calcd. (%): C, 35.63; H, 4.37; N, 15.24. found (%): C, 34.85; H, 4.04; N, 14.42. FT-IR (in KBr): 1792, 1605, 1551, 1467, 1421, 1392, 1274, 1141, 1089, 941 and 626

cm^{-1}. UV-visible (in acetonitrile): 360 nm (ε /M^{-1} cm^{-1}, 6810) and 635 nm (ε /M^{-1} cm^{-1}, 780). ESI-mass (m/Z): Calcd.: 205.069 (for $[Fe(Pz_2Py)(NO)]^{2+}$ unit); found: 205.338. X-band EPR (in acetonitrile): g ~ 4.15 and 2.03 at 77 K.

Reaction of complex 3.2a with O_2

Complex **3.2a** (0.64 g, 1 mmol) was dissolved in 5 mL of dry and degassed acetonitrile. To this solution O_2 gas was bubbled for 5 min. After 1hr, color of the solution changes from green to brown. This brown colored solution was immediately precipitated out after layered with ether and isolated as solid of complex **3.3a**. Reaction of complex **3.2a** with O_2 was monitored by UV-visible, EPR and solution phase FT-IR spectroscopy.

$[Fe^{II}(Pz_2Py)(CH_3CN)(NO_3)](ClO_4)_2$, 3.3a

Yield: 0.48 g, ~ 72 %. FT-IR (in KBr):1632, 1556, 1466, 1422, 1384, 1309, 1252, 1144, 1119, 1087, 833 and 636 cm^{-1}. UV-visible (in acetonitrile): 305 nm (ε /M^{-1} cm^{-1}, 7195). X-band EPR (in acetonitrile): g ~ 5.19 at 77 K.

Reaction of complex 3.2a with O_2 in presence of 2,4-di-*tert*-butylphenol

To the dry and degasses acetonitrile solution of complex **3.2a** (0.33 g, 0.5 mmol), degassed solution of 2,4 di-*tert*-butyl phenol (0.51 g, 5 mmol) was added followed by addition of O_2 at room temperature. The reaction mixture was washed with hexane by several times. (*bis*phenol) was separated by preparative TLC of the hexane solution and complex **3.4a** was obtained from the acetonitrile part of the reaction mixture.

3,3',5,5'-tetra-*tert*-butyl-(1,1'-biphenyl)-2,2'-diol, *(bis*phenol)

Yield: 0.12 g, ~ 60 %. ^{1}H NMR ($CDCl_3$, 500 MHz): δ_{ppm}: 1.32 (s, 9H); 1.45 (s, 9H); 5.23 (S, 1H); 7.12 (s, 1H); 7.39 (s, 1H). ^{13}C NMR ($CDCl_3$, 125 MHz): δ_{ppm}: 150.0, 143.2, 136.5, 125.5, 125, 122.6, 35.4, 34.7, 31.9, 29.9. ESI-mass (m/Z): Calcd.: 410.32, found: 409.31 (M-1).

$[Fe^{III}(Pz_2Py)(OH)(CH_3OH)](ClO_4)_2$, 3.4a

Yield: 0.18 g, ~ 58 %. Elemental analysis for $C_{19}H_{28}N_7O_{10}Cl_2Fe$. Calcd. (%): C, 36.27; H, 4.62; N, 13.46. found (%) C, 35.85; H, 4.14; N, 14.02. FT-IR (in KBr): 3400, 2945, 1633, 1555, 1465, 1423, 1384, 1260, 1275, 1141, 1120, 1088 and 627 cm^{-1}. UV- visible (in acetonitrile): 345 nm (ε /M^{-1} cm^{-1}, 5240). ESI-mass (m/Z): Calcd.: 496.092 (for $[Fe(Pz_2Py)(OH)(ClO_4)]^+$ unit); found: 496.368. X-band EPR (in acetonitrile): g ~ 5.23 at 77 K.

Low-spin $[Fe^{II}(Pz_2Py)(CH_3CN)(NO)](ClO_4)_2$, 3.2b

The solution of complex **3.1** (0.65 g, 1 mmol) in 5 mL dry and degassed acetonitrile was stored under NO atmosphere for 2 days at –40 °C and color changes to dark red. After that the solution was layered with diethyl ether to precipitate out the complex **3.2b**. Yield: 0.41 g, ~ 63 %. FT-IR (in KBr):1711, 1606, 1553, 1423, 1367, 1089, 940 and 626 cm^{-1}. UV-visible (in acetonitrile): 350 nm (ε /M^{-1} cm^{-1}, 6450) and 565 nm (ε /M^{-1} cm^{-1}, 340). ESI-mass (m/Z): calcd.: 509.092 (for $[Fe(Pz_2Py)(NO)(ClO_4)]^+$unit); found: 508.712. X-band EPR (in acetonitrile): g ~ 2.03 at 77 K.

Reaction of complex 3.2b with O_2

Due to the very unstable nature of the low-spin iron nitrosyl, the O_2 gas was purging through the acetonitrile solution of complex **3.2b** (0.64 g, 1 mmol) at –20 °C, the NO moiety became labile and it immediately gives brown colored complex **3.3b**. Reaction of complex **3.2b** with O_2 was monitored by UV-visible, EPR and solution phase FT-IR spectroscopy.

[Fe^{III}(Pz$_2$Py)(OH)(CH$_3$CN)](ClO$_4$)$_2$, 3.3b

Yield: 0.41 g, ~ 63 %. Elemental analysis for $C_{19}H_{28}N_7O_{10}Cl_2Fe$. Calcd. (%): C, 36.36; H, 4.60; N, 13.32. found (%): C, 35.85; H, 4.14; N, 14.02. FT-IR (in KBr): 3400, 2945, 1605, 1552, 1468, 1442, 1380, 1271, 1275, 1142, 1111, 1088, 940, 768, 636 and 627 cm^{-1}. UV-visible (in acetonitrile): 250 nm (ε /M^{-1} cm^{-1}, 8495) and 345 nm (ε /M^{-1} cm^{-1}, 4960). ESI-mass (m/Z): calcd.: 496.092 (for [Fe(Pz$_2$Py)(OH)(CH$_3$CN)(ClO$_4$)]$^+$ unit); found: 496.368. X-band EPR (in acetonitrile): g ~ 5.21 at 77 K.

3.4 Conclusion

In conclusion, two iron nitrosyls having {Fe(NO)}^{7} configuration but with different spin states have been synthesized in same ligand framework. The different solvent and reaction temperature were found to be key for the formation of the two complexes having different spin states. Both the complexes have been characterized using different spectroscopic studies. In addition, the high-spin nitrosyl complex, **3.2a** was also studied structurally. FT-IR studies display an appreciable difference in nitrosyl stretching frequency for these complexes, as expected. The dioxygen reactivity of complexes **3.2a** and **3.2b** have been explored. The high-spin iron-nitrosyl, **3.2a** reacts with O_2 leading to the formation of the corresponding nitrate product, **3.3a**. This reaction proceeds through the initial oxidation of the iron center leading to the formation of corresponding iron(II)-nitrosyl and superoxide anion. Subsequently, the nitrate analogue is formed *via* the formation of a peroxynitrite intermediate which was confirmed by its characteristic reaction with phenol. In contrary, O_2 substitutes the NO group from complex **3.2b** (low-spin iron-nitrosyl), perhaps because of the weaker Fe–N_{NO} bond, resulting in the formation of [Fe^{III}(Pz$_2$Py)(OH)](ClO$_4$)$_2$, **3.3b**. The release of NO by O_2, in this case was evident from the presence of NO_2 in the GC-Mass of the head space gas from the reaction vessel. Thus, these results depict the difference in reactivity of iron nitrosyls having $\{Fe(NO)\}^7$ configuration towards dioxygen based on their spin state.

3.5 References

1. Ghosh, A.; Enemark, J. H. *J. Inorg. Biochem.* **2025**, *269*, 112897.
2. Lehnert, N.; Kim, E.; Dong, H. T.; Harland, J. B.; Hunt, A. P.; Manickas, E. C.; Oakley, K. M.; Pham, J.; Reed, G. C.; Alfaro, V. S. *Chem. Rev.* **2021**, *121*, 14682 − 14905.
3. Harland, J. B.; Manickas, E. C.; Hunt, A. P.; Lehnert, N. *Comprehensive Coordination Chemistry III,* **2021**, 806 − 874.
4. Richter-Addo, G. B.; Legzdins, P. *Metal Nitrosyls*; Oxford University Press: Oxford, UK, **1992**.
5. Gütlich, P.; Garcia, Y.; Goodwin, H. A. *Chem. Soc. Rev.* **2000**, *29*, 419 – 427.
6. Stepanović, S.; Andjelković, L.; Zlatar, M.; Andjelković, K.; Gruden-Pavlović, M.; Swart, M. *Inorg. Chem.* **2013**, *52*, 13415 – 13423.
7. Berto, T. C.; Speelman, A. L.; Zheng, S.; Lehnert, N. *Coord. Chem. Rev.* **2013**, *257*, 244 – 259.
8. Collman, J. P.; Yang, Y.; Dey, A.; Decréau, R. A.; Ghosh, S.; Ohta, T.; Solomon, E. I. *Proc. Natl. Acad. Sci. U. S. A.* **2008**, *105*, 15660 – 15665.
9. Jiang, Y.; Hayashi, T.; Matsumura, H.; Do, L. H.; Majumdar, A.; Lippard, S. J.; Moënne-Loccoz, P. *J. Am. Chem. Soc.* **2014**, *136*, 12524 – 12527.
10. Haller, K. J.; Johnson, P. L.; Feltham, R. D.; Enemark, J. H.; Ferraro, J. R.; Basile, L. J. *Inorg. Chim. Acta* **1979**, *33*, 119 – 130.
11. Zhang, Y.; Palosky, M. A.; Brown, C. A.; Westre, T. E.; Hedman, B.; Hodgson, K. O.; Solomon, E. I. *J. Am. Chem. Soc.* **1992**, *114*, 9189 – 9191.

12. Brown, C. A.; Palosky, M. A.; Westre, T. E.; Zhang, Y.; Hedman, B.; Hodgson, K. O.; Solomon, E. I. *J. Am. Chem. Soc.***1995**, *117*, 715 – 732.

13. Brown, C. D.; Neidig, M. L.; Neibergall, M. B.; Lipscomb, J. D.; Solomon, E. I. *J. Am. Chem. Soc.* **2007**, *129*, 7427 – 7438.

14. Diebold, A. R.; Brown-Marshall, C. D.; Neidig, M. L.; Brownlee, J. M.; Moran, G. R.; Solomon, E. I. *J. Am. Chem. Soc.* **2011**, *133*, 18148 – 18160.

15. Ye, S.; Price, J. C.; Barr, E. W.; Green, M. T.; Bollinger, J. M., Jr.; Krebs, C.; Neese, F. *J. Am. Chem. Soc.* **2010**, *132*, 4739 – 4751.

16. Phung, Q. M.; Nam, H. N.; Austen, V.; Yanai, T.; Ghosh, A. *Inorg. Chem.* **2025**, *64*, 1702 – 1710.

17. Berto, T. C.; Hoffman, M. B.; Murata, Y.; Landenberger, K. B.; Alp, E. E.; Zhao, J.; Lehnert, N. *J. Am. Chem. Soc.* **2011**, *133*, 16714 – 16717.

18. Massoud, S. S.; Louka, F. R.; Ducharme, G. T.; Fischer, R. C.; Mautner, F. A.; Vančo, J.; Herchel, R.; Dvořák, Z.; Trávníček, Z. *J. Inorg. Biochem.* **2018**, *180*, 39 – 46.

19. Ghosh, R.; Mazumdar, R.; Samanta, B.; Saha, S.; Mondal, B. *Dalton Trans.* **2025**, *54,* 7793 – 7800.

20. Randall, C. R.; Zang, Y.; True, A. E.; Que, L., Jr.; Charnock, J. M.; Garner, C. D.; Fujishima, Y.; Schofield, C. J.; Baldwin, J. E. *Biochemistry* **1993**, *32*, 6664 – 6673.

21. Dong, H. T.; Speelman, A. L.; Kozemchak, C. E.; Sil, D.; Krebs, C.; Lehnert, N. *Angew. Chem., Int. Ed.* **2019**, *58*, 17695 – 17699.

22. Chiou, Y. -M.; Que, L., Jr. *Inorg. Chem.***1995**, *34*, 3270 – 3278.

23. Gogoi, K.; Saha, S.; Mondal, B.; Deka, H.; Ghosh, S.; Mondal, B. *Inorg. Chem.* **2017**, *56,*14438 – 14445.

24. Dey, A.; Confer, A. M.; Vilbert, A. C.; Moënne-Loccoz, P.; Lancaster, K. M.; Goldberg, D. P. *Angew. Chem., Int. Ed.* **2018**, *57*, 13465 – 13469.

25. Confer, A. M.; McQuilken, A. C.; Matsumura, H.; Moënne-Loccoz, P.; Goldberg, D. P. *J. Am. Chem. Soc.* **2017**, *139*, 10621 – 10624.
26. Speelman, A. L.; Lehnert, N. *Angew. Chem., Int. Ed.* **2013**, *52*, 12283 – 12287.
27. Speelman, A. L.; White, C. J.; Zhang, B.; Alp, E. E.; Zhao, J.; Hu, M.; Krebs, C.; Penner-Hahn, J.; Lehnert, N. *J. Am. Chem. Soc.* **2018**, *140*, 11341 – 11359.
28. Dong, H. T.; Speelman, A. L.; Kozemchak, C. E.; Sil, D.; Krebs, C.; Lehnert, N. *Angew. Chem., Int. Ed.* **2019**, *131*, 17859 – 17863.
29. Earnshaw, A.; King, E. A.; Larkworthy, L. F. *J. Chem. Soc. A* **1969**, *0*, 2459 – 2463.
30. Hodges, K. D.; Wollmann, R. G.; Kessel, S. L.; Hendrickson, D. N.; Van Derveer, D. G.; Barefield, E. K. *J. Am. Chem. Soc*. **1979**, *101*, 906 – 917.
31. Mondal, B.; Saha, S.; Borah, D.; Mazumdar, R.; Mondal, B. *Inorg. Chem.* **2019**, *58*, 1234 – 1240.
32. Schopfer, M. P.; Mondal, B.; Lee, D.-H.; Sarjeant, A. A. N.; Karlin, K. D. *J. Am. Chem. Soc.* **2009**, *131*, 11304 – 11305.
33. Jones, R. D.; Summerville, D. A.; Basolo, F. *Chem. Rev.* **1979**, *79*, 139 – 179.
34. Suzuki, M.; Ishiguro, T.; Kozuka, M.; Nakamoto, K. *Inorg. Chem.* **1981**, *20*, 1993 – 1996.
35. Ileperuma, O. A.; Feltham, R. D. *Inorg. Chem.* **1977**, *16*, 1876 – 1883.
36. Speelman, A. L.; Zhang, B.; Krebs, C.; Lehnert, N. *Angew. Chem., Int. Ed.* **2016**, *55*, 6685 – 6688.
37. Mondal, B.; Borah, D.; Mazumdar, R.; Mondal, B. *Inorg. Chem.* **2019**, *58*, 14701 – 14707.
38. (a) Radi, R. *Proc. Natl. Acad. Sci. U. S. A.* **2004**, *101*, 4003 – 4008; (b) Nauser, T.; Koppenol, W. H. *J. Phys. Chem. A* **2002**, *106*, 4084 – 4086; (c) Goldstein, S.; Lind, J.; Merenyi, G. *Chem. Rev.* **2005**, *105*, 2457 – 2470; (d) Tran, N. G.; Kalyvas, H.; Skodje,

K. M.; Hayashi, T.; Moënne-Loccoz, P.; Callan, P. E.; Shearer, J.; Kirschenbaum, L. J.; Kim, E. *J. Am. Chem. Soc.* **2011**, *133*, 1184 – 1187.

39. Frisch, M. J.; Trucks, G. W.; Schlegel, H. B.; Scuseria, G. E.; Robb, M. A.; Cheeseman, J. R.; Scalmani, G.; Barone, V.; Petersson, G. A.; Nakatsuji, H.; Li, X.; Caricato, M.; Marenich, A. V.; Bloino, J.; Janesko, B. G.; Gomperts, R.; Mennucci, B.; Hratchian, H. P.; Ortiz, J. V.; Izmaylov, A. F.; Sonnenberg, J. L.; Williams-Young, D.; Ding, F.; Lipparini, F.; Egidi, F.; Goings, J.; Peng, B.; Petrone, A.; Henderson, T.; Ranasinghe, D.; Zakrzewski, V. G.; Gao, J.; Rega, N.; Zheng, G.; Liang, W.; Hada, M.; Ehara, M.; Toyota, K.; Fukuda, R.; Hasegawa, J.; Ishida, M.; Nakajima, T.; Honda, Y.; Kitao, O.; Nakai, H.; Vreven, T.; Throssell, K.; Montgomery, J. A., Jr.; Peralta, J. E.; Ogliaro, F.; Bearpark, M. J.; Heyd, J. J.; Brothers, E. N.; Kudin, K. N.; Staroverov, V. N.; Keith, T. A.; Kobayashi, R.; Normand, J.; Raghavachari, K.; Rendell, A. P.; Burant, J. C.; Iyengar, S. S.; Tomasi, J.; Cossi, M.; Millam, J. M.; Klene, M.; Adamo, C.; Cammi, R.; Ochterski, J. W.; Martin, R. L.; Morokuma, K.; Farkas, O.; Foresman, J. B.; Fox, D. J. *Gaussian Development Version*, revision I.14+; Gaussian, Inc.: Wallingford, CT, **2018**.
40. Zhao, Y.; Truhlar, D. G. *Theor. Chem. Acc.,* **2008**, *120*, 215 – 241.
41. Weigend, F.; Ahlrichs, R. *Phys. Chem. Chem. Phys.* **2005**, *7*, 3297 – 3305.
42. *SMART, SAINT and XPREP*; Siemens Analytical X-ray Instruments Inc.: Madison, WI, **1995**.
43. Sheldrick, G. M. *SHELXS-2016*; University of Gottingen: Gottingen, Germany, **2016**.
44. Farrugia, L. J. ORTEP-3 for Windows - a version of ORTEP-III with a Graphical User Interface (GUI). *J. Appl. Crystallogr.* **1997**, *30*, 565.

Chapter 4

Reaction of a chromium-nitrosyl complex with H_2O_2: formation of a [Cr^V=O] species

Abstract

A precursor complex of chromium(II), [Cr^{II}(TPz)Cl_2], **4.1** [TPz = *Tris*((3,5-dimethyl-1H-pyrazol-1-yl)methyl)amine] in a tripodal N4 type ligand framework was made to react with nitric oxide (NO) gas to yield corresponding nitrosyl complex, [Cr(TPz)(NO)Cl]Cl, **4.2** having $\{Cr(NO)\}^5$ configuration. Complex **4.2** upon reaction with H_2O_2 yields the nitrate product, **4.3** [Cr^{IV}(TPz)(NO_3^-)Cl]. The reaction is believed to proceed through the formation of a putative Cr(IV)-peroxynitrite intermediate, **4a**. It was supported by the characteristic phenol ring nitration reaction. Spectroscopic studies suggest the involvement of a [Cr^V=O] intermediate in this reaction.

4.1 Introduction

Nitric oxide (NO) is a ubiquitous gaseous molecule having an ability to freely diffuse across the cell membranes.[1] Endogenous NO serves as an important effector and signal transduction molecule in numerous cellular processes involved in physiological states such as vasodilation, immune responses, neurotransmission, apoptosis, regulation of gene transcription, mRNA translation, and post-translational modifications of proteins.[2-7] These physiological functions of NO are modulated at extremely low concentrations ranging from picomolar to nanomolar.[8] On the contrary, higher concentrations of NO promote oxidative stress leading to cytotoxicity. The concentration of NO in biological systems is exceptionally regulated by nitric oxide dioxygenases (NODs) enzymes.[9-12] In this process, an $[Fe^{III}\text{-}(O_2^{-})]$ complex reacts with NO to generate a beneficial nitrate ion (NO_3^{-}).[13-14] This transformation involves with a fleeting intermediate, called peroxynitrite $(ONOO)^{-}$.[11] It is believed that the peroxynitrite intermediate decomposes into an oxo-ferryl species, $[Fe^{IV}{=}O]$, and nitrogen dioxide (NO_2) through the homolytic cleavage of the O−O bond, followed by a recombination that ultimately results in the formation of nitrate (NO_3^{-}).[9-14] The significant instability of the peroxynitrite intermediate renders it challenging to trace or substantiate this proposition with spectroscopic evidence. In almost every instance where the involvement of peroxynitrite intermediate is involved, the well-established phenol ring nitration test is the only reliable method, which is employed as a marker for the intermediate.[15] Though the proposed homolytic cleavage of the O−O bond in peroxynitrite is expected to generate a high-valent metal oxo intermediate, the identification of such intermediates has been limited to just a few examples due to their rapid recombination with NO_2 within the reaction cage, resulting in the formation of the NO_3^{-} ion.[16-19]

Since the initial study by Basolo, several examples have been reported that implicate the involvement of a metal-peroxynitrite intermediate. The reactions involving NO with superoxo and peroxo complexes of iron, cobalt, and chromium reveal the formation of a metal-peroxynitrite intermediate.[20-23] A Cr(IV)-peroxo complex of *N*-tetramethylated cyclam, designated as $[Cr^{IV}(12\text{-}TMC)(O_2^{2-})Cl]^+$, (12-TMC = 1,4,7,10-tetramethyl-1,4,7,10-tetraazacyclododecane) reacts with NO to produce a Cr(III)-nitrate complex, $[Cr^{III}(12\text{-}TMC)(NO_3^-)Cl]^+$.[21] In contrast, the Cr(III)-superoxo analogue, $[Cr^{III}(14\text{-}TMC)(O_2^-)Cl]^+$, (14-TMC = 1,4,7,10-tetramethyl-1,4,7,10-tetraazacyclotridecane) interacts with NO to form a Cr(IV)-oxo complex, $[Cr^{IV}(14\text{-}TMC)(O)Cl]^+$, along with nitrogen dioxide (NO_2). In both instances, the formation of a $[Cr^{III}\text{-}(ONOO)^-]$ intermediate has been proposed.[22]

In addition, the reactions of metal nitrosyl complexes with reactive oxygen species, such as O_2^-, O_2^{2-} are also known to result in the corresponding NO_3^- or NO_2^- through the formation of a peroxynitrite intermediate. For example, a chromium nitrosyl complex, $[Cr(BPMEN)(NO)Cl]^+$ [BPMEN = *N,N′-bis*(2-pyridylmethyl)-1,2-diaminoethane] reacted with O_2^-, generating an oxidized Cr(III)-nitrite complex, $[Cr^{III}(BPMEN)(NO_2^-)Cl]^+$ and O_2 *via* a putative $[Cr^{III}\text{-}(ONOO)^-]^+$ intermediate.[24]

This chapter describes a chromium nitrosyl complex, $[Cr(TPz)Cl(NO)]^+$, **4.2** which in acetonitrile solution at –40 °C upon reaction with H_2O_2 resulted in the corresponding Cr(IV)-peroxynitrite intermediate. This intermediate finally decomposes to the corresponding Cr(IV)-nitrate complex, **4.3**. Chemical evidence using 2,4-di-*tert*-butylphenol (2,4-DTBP) suggests the involvement of a peroxynitrite species in this reaction. Spectroscopic evidence indicates the formation of a $[Cr^V{=}O]$ species in the course of the reaction.

4.2 Results and Discussion

The ligand TPz was prepared following the literature method.[25] Treatment of anhydrous $CrCl_2$ with one equivalent of the ligand TPz in methanol, followed by recrystallization from diethyl ether diffusion, resulted in the initial complex **4.1**, [Cr^{II}(TPz)Cl$_2$] (Experimental Section). Figure 4.1 illustrates the ORTEP diagram of complex **4.1**, as determined by X-ray crystallography. This analysis revealed a tetragonally elongated octahedral geometry around the Cr(II) centre, featuring *cis*-disposed chloride ligands. Selected bond distances and angles, are summarized in the appendix (Appendix III, Tables A3.1-A3.3). The room-temperature magnetic moment of complex **4.1** is calculated to be μ_{eff} ~ 4.76 B.M., confirming its high-spin (S = 2) configuration.[26] Complex **4.1** was also characterized by using other spectroscopic methods such as FT-IR, UV-visible and X-band EPR (Appendix III, Figures A3.1-A3.4).

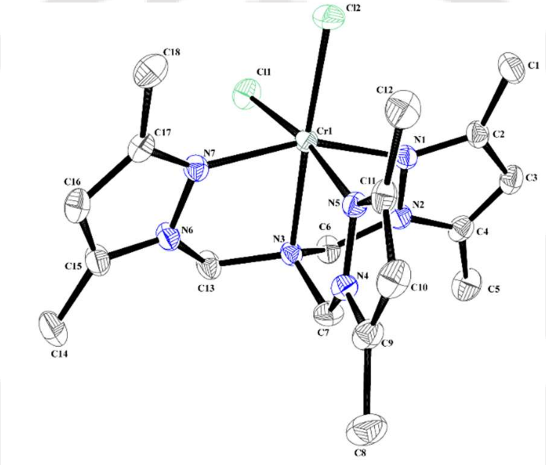

Figure 4.1. ORTEP diagram of complex **4.1** (30% thermal ellipsoid plot, H atoms are omitted for clarity).

Upon addition of NO(g) to the methanol solution of complex **4.1**, a green colored complex **4.2**, [Cr(TPz)Cl(NO)]Cl was obtained. Complex **4.2** was isolated as a solid and characterized using FT-IR, UV-visible and X-band EPR spectroscopic methods, as well as ESI-mass spectrometry (Experimental Section and Appendix III, Figures A3.5-A3.7). The FT-IR spectrum suggests the presence of nitrosyl stretching frequency at 1709 cm^{-1}, affirming the $\{Cr(NO)\}^5$ configuration.[27] The magnetic moments of this $\{Cr(NO)\}^5$ species in the solid-state at room temperature is calculated to be μ_{eff} ~ 1.69 B.M., indicating the presence of one unpaired electron.[28] The X-band EPR spectral analysis of frozen acetonitrile solution of complex **4.2** shows a sharp isotropic signal at g ~ 2.01, as expected.[29-31] Complex **4.2** behaves as a low spin d^5 ($S = \frac{1}{2}$) species and the odd electron is in the $b_2(xy)$ orbital of the MO diagram of the nitrosyl complexes having $\{Cr(NO)\}^5$ configuration.[32] The electronic absorption spectrum of complex **4.2** displays two absorption bands at 435 nm and 600 nm, which can be categorically assigned to the $^2B_2 \rightarrow {}^2B_1$ [*i.e.,* $b_2(xy) \rightarrow b_1(x^2\text{-}y^2)$] and $^2B_2 \rightarrow {}^2E$, [*i.e.,* $e(xz, yz) \rightarrow b_2(xy)$] transitions, respectively (Figure 4.2).[33]

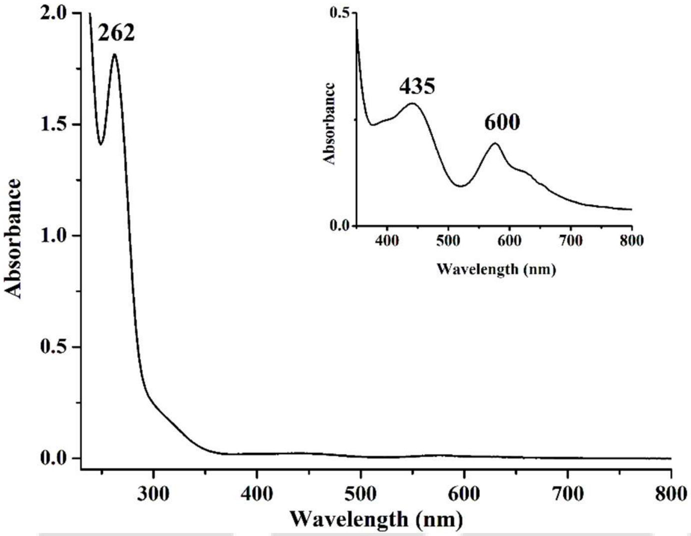

Figure 4.2. UV-visible spectrum of complex **4.2** in acetonitrile at room temperature.

Table 4.1. List of selected Cr-nitrosyls, having $\{Cr(NO)\}^5$ configuration with their respective nitrosyl stretching frequencies (cm^{-1}) and their UV-visible absorption band

Cr-nitrosyl complexes	ν_{NO} (cm^{-1})	Absorption band (λ_{max})	Reference
$[(BPMEN)Cr(NO)Cl]^+$	1690	600	27
$[Cr(Me_2[14]tetraenatoN_4)(NO)]$	1620	653, 450	29 (a)
[Cr(TPP)(NO)]	1700	550, 600, 420	29 (b)
$[Cr(NO)(H_2O)_5]^{2+}$	1733	564, 452	29 (c)

[BPMEN = *N,N′-bis*(2-pyridylmethyl)-1,2-diaminoethane], [TPP = *Tetra*-phenylporphyrin]

Structural characterization was done by growing single crystals of complex **4.2** from methanol solution by a slow diffusion of diethyl ether. The ORTEP diagram of complex **4.2** is shown in figure 4.3 and the matric parameters are listed in the appendix (Appendix III, Tables A3.1-A3.3). The Cr–N and N–O bond distances in complex **4.2** are 1.777(6) and 0.974(6) Å, respectively. The Cr-N-O bond angle is 176°, indicating a linear structure. The crystal structure shows the disorder in the NO ligand, which we could not fixed even after growing the crystals for several times in different sets.[27]

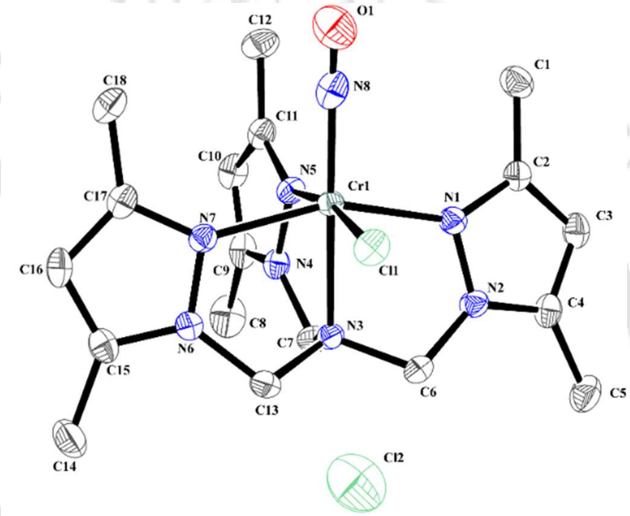

Figure 4.3. ORTEP diagram of complex **4.2** (30% thermal ellipsoid plot, H atoms are omitted for clarity).

Complex **4.2** is stable in open air even after several days. Therefore, the reactivity of complex **4.2** is checked with more reactive oxygen species, H_2O_2. The color of the acetonitrile solution of complex **4.2** changes from green to brown upon addition of 2 equivalent of H_2O_2. Addition of equivalent amount of H_2O_2 to the complex **4.2** was monitored by using FT-IR spectroscopy. The addition of 1 equivalent of H_2O_2 to the acetonitrile solution of complex **4.2** changes its stretching frequency from 1710 to 1770 cm^{-1} (Figure 4.4). It is known that oxidation of metal center changes the stretching frequency ~ 40-100 cm^{-1}.[34] Therefore, it is logical to assume that the one equivalent of H_2O_2 is causing the oxidation of metal center from Cr(II) to Cr(III).

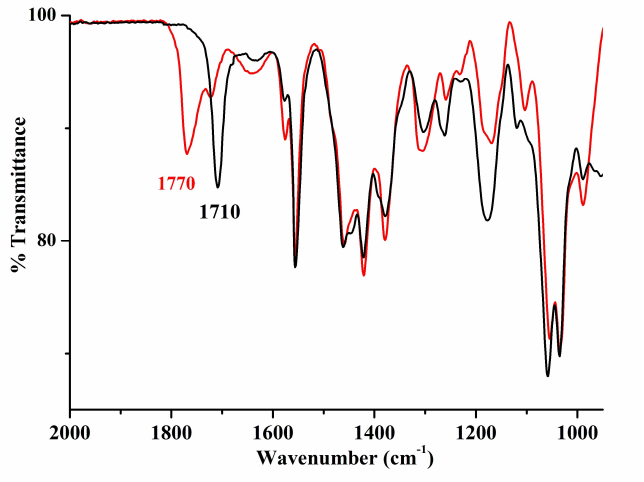

Figure 4.4. FT-IR spectral monitoring of the reaction of complex **4.2** (blue) with 1 equivalent H_2O_2 in acetonitrile medium at room temperature.

Addition of another equivalent of H_2O_2 to this reaction mixture leads to the formation of a new yellowish green colored intermediate, **4a** (Experimental Section), that persists for a day at –20 °C. The greater thermal stability of the intermediate helps to characterize it by using spectroscopic methods and further reactivity studies. In UV-visible spectral monitoring, it shows intense band at 360 nm (ε/M^{-1} cm^{-1}, 3500), which suggests the formation of [Cr^{V}=O] species (Figure 4.5).[35-44]

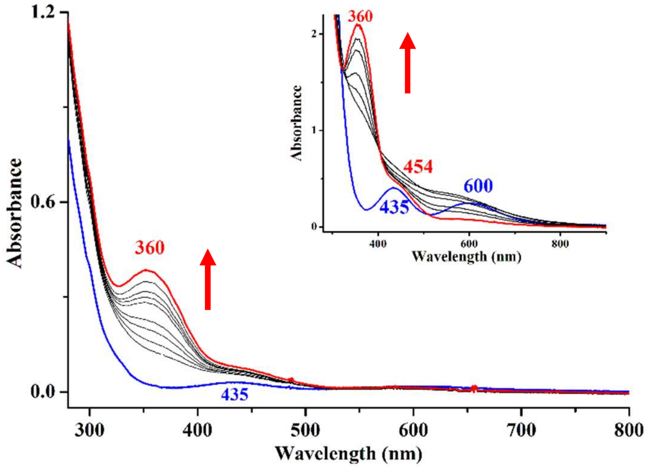

Figure 4.5. UV-visible spectral monitoring of the reaction of complex **4.2** (blue) and H_2O_2, intermediate **4a** (red) in acetonitrile at room temperature.

Similarly, the formation of the intermediate, **4a** was corroborated by X-band EPR spectral monitoring at 77 K, which revealed a sharp signal at g ~ 2.00 with maximum to minimum separation of 6 mT, typical for Cr(V) species ($S = \frac{1}{2}$) (Figure 4.6).[44]

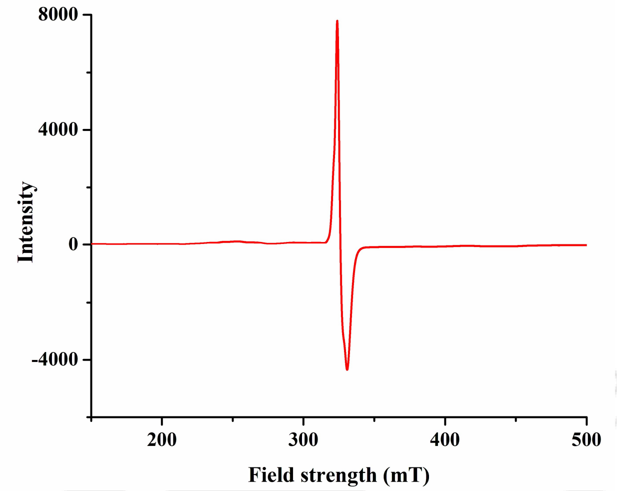

Figure 4.6. X-band EPR spectrum of intermediate **4a** at 77 K, formed after the reaction of complex **4.2** with H_2O_2 in acetonitrile (g ~ 2.00).

When the acetonitrile solution of complex **4.2** are made to react with 2 equivalents of H_2O_2 at –20 °C followed by warm up at room temperature, it yielded a brown colored complex, **4.3**. The complex **4.3** was isolated as a solid and characterized spectroscopically as the corresponding nitrate (NO_3^-) complex (Experimental Section and Appendix III, Figures A3.8-A3.11). The FT-IR spectrum displays a strong band at 1384 cm^{-1}, attributing to the presence of a nitrate (NO_3^-) group. The formation of complex **4.3** suggests the involvement of a putative peroxynitrite intermediate in the course of the reaction. The reaction between NO and O_2^{2-} ions generate a peroxynitrite $(OONO)^-$ intermediate, which subsequently isomerizes to nitrate (NO_3^-), as evidenced by the final decomposition product, complex **4.3**.[45-46] Thus, it is logical to assume that the first equivalent of H_2O_2 oxidizes the Cr(II)-nitrosyl to Cr(III)-nitrosyl and the next equivalent reacts with Cr^{III}-nitrosyl to afford $[Cr^{IV}\text{-}(ONOO)^-]$ intermediate.

While direct spectral evidence for the peroxynitrite intermediate remained elusive due to its instability, we pursued chemical evidence instead. After the addition of 2,4-di-*tert*-

butylphenol to the precooled dry and degassed acetonitrile solution of complex **4.2** prior to the addition of H_2O_2 at –20 °C, 2,4-di-*tert*-butyl-6-nitrophenol was obtained in significant quantity (~ 65 %) along with Cr(IV)-hydroxo product, **4.4** (Scheme 4.1). Both were purified by column chromatography and characterized spectroscopically (Experimental Section and Appendix III, Figures A3.12-A3.18). Formation of 2,4-di-*tert*-butyl-6-nitrophenol unequivocally confirms the involvement of peroxynitrite intermediate.

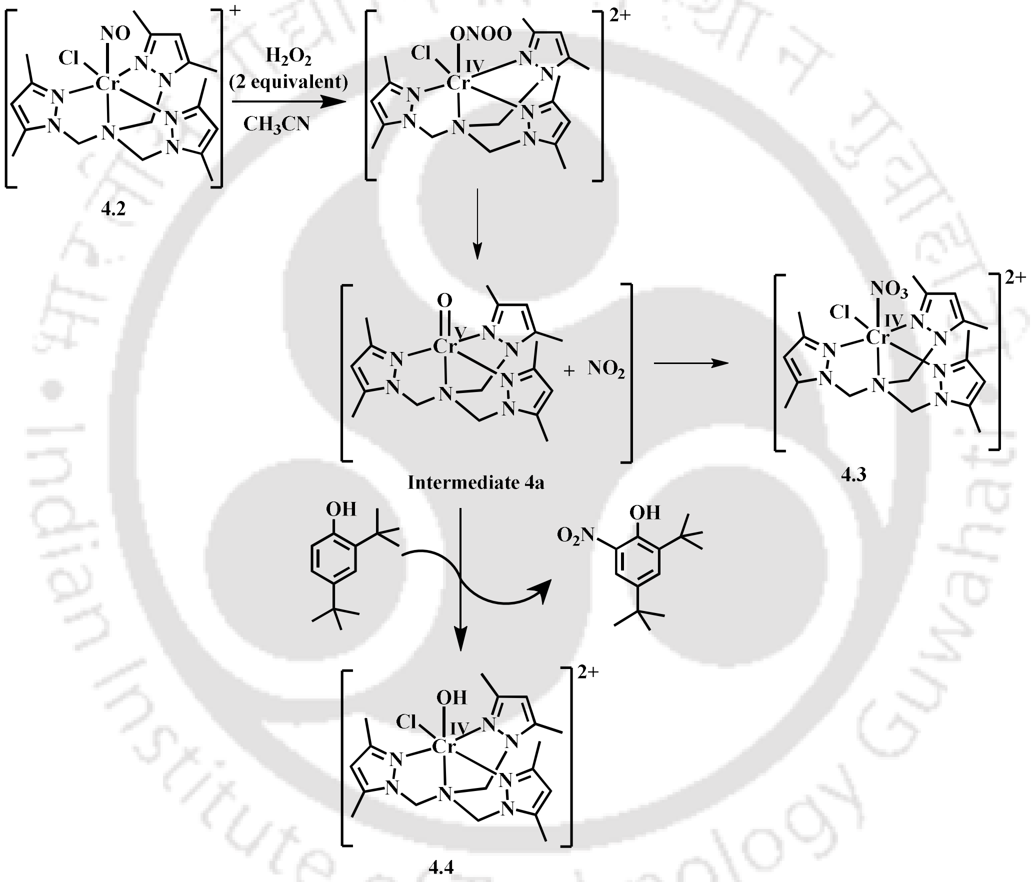

Scheme 4.1. Overall reaction.

The reactivity of the $[Cr^{V}{=}O]$ species was rigorously examined in the context of C–H bond activation. Previous literature has highlighted the ability of $[Cr^{V}{=}O]$ species in the activation of C–H bonds.[44] To test it, fluorene was introduced into the reaction mixture. The subsequent formation of 9-fluorenone along with Cr(IV)-hydroxide species was confirmed by various spectroscopic techniques (Experimental Section and Appendix III, Figures A3.12-A3.15 and Figures A3.19-A3.22). Notably, fluorene cannot be oxidized by H_2O_2 alone to yield 9-fluorenone.[15] This reaction further confirmed that [Cr^{V}=O] is involved in the course of the reaction, which facilitates the C–H bond activation through H atom abstraction mechanism.

The investigation of NOD reactivity in heme-iron complexes suggests that nitration or oxidation mediated by metal-peroxynitrite ions occurs through the formation of an Fe^{IV}-oxo intermediate alongside the release of NO_2. Phenolic substrates rapidly reduce this Fe^{IV}-oxo species to its Fe(III) state, generating a phenoxyl radical that can either combine with NO_2 to form nitrophenol or couple with another phenoxyl radical to create a *bis*phenol product.[45] In the present case, the spectral evidence suggests the formation of Cr^{V}=O species in the reaction of complex **4.2** with H_2O_2. Notably, the Cr(III)-superoxo complex of a tetramethylated cyclam ligand reacts with NO in acetonitrile at –20 °C, leading to the formation of [Cr^{IV}=O] species through O–O bond cleavage of a presumed Cr(IV)-peroxynitrite intermediate.[22] A Co-nitrosyl, [Co(F_8TPP^{2-})(NO)], [F_8TPP^{2-} = 5,10,15,20-*tetrakis*(2,6-difluorophenyl)porphyrinate)] in heme system was found to display NOD reactivity in presence of H_2O_2 through the formation of a transient [Co^{III}-O•] radical.[45] Complexes of Cu, Cr were also reported in the literature to show NOD activity.[47-48] This finding highlights an example of a chromium-nitrosyl complex that shows NOD reactivity in the presence of H_2O_2. The spectral evidence suggests the involvement of a [Cr^{V}=O] intermediate in the NOD reactivity of complex **4.2**.

4.3 Experimental Section

4.3.1 Materials and methods

Unless otherwise stated, all reactions were carried out in an Ar-filled glovebox or using standard Schlenk techniques. Methanol, diethyl ether, and acetonitrile were purified by standard drying procedures and distilled under Ar prior to use. Furthermore, all solvents were stored over activated molecular sieves (4 Å) in the glovebox. Solvents and solutions were subjected to vacuum and Ar purge through a series of cycles to ensure thorough deoxygenation. Anhydrous chromium(II) chloride was purchased from Aldrich and used as received. UV-visible spectra were taken on an Agilent Cary 8454 spectrophotometer. FT-IR spectra were recorded as KBr pellets or with ATR probe using a PerkinElmer spectrophotometer. ^{1}H and ^{13}C NMR studies were done using 400 or 500 MHz Varian FT-NMR spectrophotometers. X-band EPR spectra were recorded on a JES-FA200 EPR spectrophotometer with microwave power, 0.998 mW; microwave frequency, 9.14 GHz; and modulation amplitude, 2. High-resolution Mass spectra were measured in HPLC grade acetonitrile solution by Ultra-High-Performance Liquid Chromatography Quadruple Time of Flight High-resolution Mass Spectrometer (UHPLC-QTOF-HRMS, Agilent G6546A). Mass spectra were measured in HPLC grade acetonitrile, THF and methanol solvent.

Single crystals were grown from dichloromethane-methanol solutions using the slow evaporation technique. The intensity data were collected using a Bruker SMART APEX-IV CCD diffractometer, equipped with a fine focus 1.75 kW sealed tube MoKα radiation (λ = 0.71073 Å), with increasing ω (width of 0.3° per frame) at a scan speed of 3 s/frame. The SMART software was used for data acquisition. Data integration and reduction were undertaken with SAINT and XPREP software.[49] Structures were solved by direct methods using SHELXS-2016 and refined with full-matrix least-squares on F2 using SHELXL-2016/6.[50] Structural illustrations were drawn with ORTEP-3 for Windows.[51]

4.3.2 Syntheses

***Tris*((3,5-dimethyl-1H-pyrazol-1-yl)methyl)amine, TPz**

The ligand was synthesized using procedures described in the literature.[25] All spectral characterization data are already mentioned in chapter 2 (Appendix I, Figures A2.1-A2.8).

[(TPz)Cr^{II}Cl$_2$], 4.1

A mixture of anhydrous CrCl$_2$ (0.122 g, 1 mmol) was dissolved in dry and degassed methanol (3 mL) solution. To this, previously degassed methanolic solution of ligand TPz (0.341 g, 1 mmol) in 2 mL was added and stirred for 3 hr maintaining the inert condition using Ar gas. The color of the solution turned into teal blue. The block shaped crystals of complex **4.1** were obtained by diffusion of diethyl ether into the reaction mixture. Yield: 0.314 g, ~ 70 %. Elemental analyses for $C_{18}H_{35}N_7O_4Cl_2Cr$. Calcd. (%): C, 40.30; H, 6.58; N, 18.28; found (%): C, 40.21; H, 6.55; N, 18.37. FT-IR (using ATR probe): 1627, 1550, 1464, 1416, 1387, 1311, 1268, 1232, 1187, 1121, 1103, 1058, 1029, 897, 806, 785, and 534 cm^{-1}. UV-visible (in acetonitrile): 251 nm (ε/ M^{-1} cm^{-1}, 4100), 445 nm (ε/M^{-1} cm^{-1}, 380) and 623 nm (ε/M^{-1} cm^{-1}, 280). X-band EPR (in acetonitrile): g ~ 2.03 at 77 K. ESI-mass (m/Z): Calcd.: 463.111 (for [Cr^{II}(TPz)(Cl$_2$)] unit); found: 463.115.

[(TPz)CrCl(NO)]Cl, 4.2

Complex **4.1** (0.231 g, 0.05 mmol) was dissolved in 4 mL of dry and degassed methanol. Subsequently, purified NO gas was bubbled through this solution, resulting in the formation of a new complex **4.2**. When the reaction mixture with a layer of 10 mL diethyl ether was allowed to stand for 2 days complex **4.2** was crystallized out. Yield: 0.370 g, ~ 75 %. Elemental analyses for $C_{18}H_{27}N_8Cl_2OCr$. Calcd. (%): C, 43.73; H, 5.51; N, 22.67; found (%): C, 43.78; H, 5.55; N, 22.72. FT-IR (using ATR probe): 2919, 2850, 1709, 1550, 1463, 1420, 1373, 1269, 1125, 1121, 1029, 897, 806, and 563 cm^{-1}. UV-visible (in acetonitrile): 262 nm (ε/M^{-1} cm^{-1}, 3850), 435 nm (ε/M^{-1} cm^{-1}, 260) and 600 nm (ε/M^{-1} cm^{-1}, 130). X-band EPR (in acetonitrile): g ~ 2.01 at 77 K. ESI-mass (m/Z): Calcd.: 458.14 (for [Cr(TPz)(NO)Cl]$^+$ unit), found: 458.125 and 428.142 (for [Cr^{II}(TPz)Cl]$^+$ unit); found: 428.174.

Reaction of complex 4.2 with H_2O_2

Complex **4.2** (0.570 g, 1 mmol) was dissolved in dry and degassed acetonitrile (5 mL) and kept at –20 °C. Precooled 2 mole equivalent of H_2O_2 (37% v/v, 1.4 mL) was added to this solution and stirred for 3 hr. After warm up to room temperature, this mixture was dried using rotary evaporator to obtained complex **4.3** as a solid product.

$[Cr^{IV}(TPz)(NO_3)Cl]Cl_2$, 4.3

Yield: 0.295 g, ~ 60 %. Elemental analyses for $C_{18}H_{27}N_8O_3Cl_3Cr$. Calcd. (%): C, 38.48; H, 4.84; N, 19.95; found (%): C, 38.44; H, 4.88; N, 20.05. FT-IR (using ATR probe): 3300, 2923, 1553, 1418, 1384, 1310, 1251, 1100, 976, 787, 627 and 449 cm^{-1}. UV-visible (in THF): 380 nm ($\varepsilon/M^{-1}\ cm^{-1}$, 480) and 570 nm ($\varepsilon/M^{-1}\ cm^{-1}$, 140). ESI-mass (m/Z): Calcd.: 245.065 (for $[Cr(TPz)(NO_3)Cl]^{2+}$ unit at m/2); found: 245.142. X-band EPR (in methanol): g ~ 2.04 at 77 K.

Reaction of complex 4.2 with H_2O_2 in the presence of 2,4-di-*tert*-butylphenol

Dry and degassed acetonitrile solution (5 mL) of complex **4.2** (0.566 g, 1 mmol) was kept at –20 °C for 2 hr. To this solution, 2 mL of precooled dry and degassed acetonitrile solution containing 2,4-di-*tert*-butylphenol (1.03 g, 5 mmol) followed by precooled 2 mole equivalent H_2O_2 (37% v/v, 1.2 mL) was added. The reaction mixture was allowed to stir for 30 min at –20 °C and warmed up to room temperature. 2,4-di-*tert*-butyl-6-nitrophenol and complex **4.4** were isolated using column chromatography.

2,4-di-*tert*-butyl-6-nitrophenol

Yield: 0.15 g, ~ 60 %. Elemental analyses for $C_{14}H_{21}NO_3$. Calcd. (%): C, 66.91; H, 8.42; N, 5.57; found (%): C, 66.85; H, 8.38; N, 5.68. FT-IR (using ATR probe): 1542, 1481, 1463, 1407, 1363,1315, 1276, 1259, 1238, 1203, 1180, 1139, 1112, 1097, 1022, 923, 887, 865, 852, 819, 806, 773, 748 and 723 cm^{-1}. ^{1}H NMR ($CDCl_3$, 500 MHz): δ_{ppm}, 11.45 (s, 1H), 7.96 (d, 1H), 7.65-7.64 (d, 1H), 1.45 (s, 9H), 1.32 (s, 9H). ^{13}C NMR ($CDCl_3$,125 MHz): δ_{ppm}, 153.2, 142.2, 140.1, 133.9, 132.8, 119.1, 35.9, 34.7, 31.3, 29.6. ESI-mass (m/Z): Calcd.: 251.15, Found: 250.16 (M-1).

[Cr^{IV}(TPz)(OH)Cl]Cl_2, 4.4

Yield: 0.302 g, ~ 55 %. Elemental analyses for $C_{18}H_{28}N_7Cl_3OCr$. Calcd. (%): C, 41.83; H, 5.46; N, 18.97; found (%): C, 41.78; H, 5.44; N, 19.07. FT-IR (using ATR probe): 3300, 2923, 1553, 1418, 1378, 1310, 1251, 1100, 976, 787, 627 and 449 cm^{-1}. UV-visible (in THF): 422 nm (ε/M^{-1} cm^{-1}, 310) and 592 nm (ε/M^{-1} cm^{-1}, 180). ESI-mass (m/Z): Calcd.: 480.113 (for [Cr^{IV}(TPz)Cl_2(OH)]$^+$ unit); found: 480.382. X-band EPR (in THF): g ~ 2.16 at 77 K.

Reaction of complex 4.2 with H_2O_2 in presence of fluorene

Complex **4.2** (0.566 g, 1 mmol) and fluorene (0.33 g, 2 mmol) were dissolved in 5 mL acetonitrile and cooled to −20 °C. Pre-cooled H_2O_2 was then added to it and stirred for 5 hr maintaining the temperature. The reaction mixture was then brought to room temperature and solvent was removed in *vacuo*. The reaction mixture was extracted with hexane (3 × 20 mL) which contained 9-fluorenone along with unreacted fluorene. 9-fluorenone was eluted by hexane in column-chromatography.

9-fluorenone

Yield: 0.027 g, ~ 30 %. FT-IR (ATR): 2917, 2849, 1713, 1610, 1598, 1449, 1297, 1186, 1150, 1097, 917, 812, 784, 732, 669, 649, 506 and 441 cm^{-1}. ^{1}H NMR ($CDCl_3$,500 MHz) δ_{ppm}: 7.67-7.66 (d, 2H), 7.53-7.50 (m, 2H), 7.48-7.47 (m, 2H), 7.31-7.28 (m, 2H). ^{13}C NMR ($CDCl_3$,125 MHz) δ_{ppm}: 193.9, 144.5, 134.7, 134.2, 129.1, 124.3, 120.3. ESI-mass (m/Z): Calcd.: 180.057; found: 181.065 (M+1).

4.4 Conclusion

A chromium-nitrosyl complex, **4.2** of a tripodal tetradentate ligand framework, [TPz = *Tris*((3,5-dimethyl-1H-pyrazol-1-yl)methyl)amine] has been synthesized and characterized using spectroscopic techniques as well as structure determination. Upon reaction with 2 equivalents of H_2O_2 in acetonitrile medium, it gives to the corresponding Cr(IV)-nitrate complex, **4.3**. The reaction is proposed to proceed through a putative $[Cr^{IV}\text{-}(ONOO)^{-}]$ intermediate. UV-visible, X-band EPR spectroscopy confirm the involvement of a $[Cr^{V}{=}O]$ intermediate, resulting from the homolytic cleavage of the O–O bond in the peroxynitrite moiety.

4.5 References

1. *Nitric Oxide: Biology and Pathobiology*; Ignarro, L. J., Ed.; Academic Press: San Diego, **2000**.
2. *Nitric Oxide and Infection*; Fang, F. C., Ed.; Kluwer Academic/ Plenum Publishers: New York, **1999**.
3. Bourassa, J. L.; Ives, E. P.; Marqueling, A. L.; shimanovich, R.; Groves, J. T. *J. Am. Chem. Soc.* **2001**, *123*, 5142 – 5143.
4. Goyal, R. K.; Hirano, I. *N. Engl. J. Med*. **1996**, *334*, 1106 – 1115.
5. Stark, M. E.; Szurszewski, J. H. *Gastroenterology*, **1992**, *103*, 1928 – 1949.
6. Jaffrey, S. R.; Snyder, S. H. *Annu. Rev. Cell. Dev. Biol*. **1995**, *11*, 417 – 440.
7. Bogdan, C. *Nat. Immunol*. **2001**, *2*, 907 – 916.
8. Miller, M. R.; Megson, I. L. *J. Pharmacol.* **2007**, *151*, 305 – 321.
9. Su, J.; Groves, J. T. *Inorg. Chem.* **2010**, *49*, 6317 – 6329.
10. Kurtikyan, T. S.; Eksuzyan, S. R.; Hayrapetyan, V. A.; Martirosyan, G. G.;

Hovhannisyan, G. S.; Goodwin, J. A. *J. Am. Chem. Soc.* **2012**, *134*, 13861 – 13870.

11. Sharma, S. K.; Schaefer, A. W.; Lim, H.; Matsumura, H.; Moënne-Loccoz, P.; Hedman, B.; Hodgson, K. O.; Solomon, E. I.; Karlin, K. D. *J. Am. Chem. Soc.* **2017**, *139*, 17421 – 17430.
12. Herold, S.; Koppenol, W. H. *Coord. Chem. Rev.* **2005**, *249*, 499 – 506.
13. Gardner, P. R.; Gardner, A. M.; Martin, L. A.; Salzman, A. L. *Proc. Natl. Acad. Sci. U. S. A.* **1998**, *95*, 10378 – 10383.
14. Gardner, P. R. *J. Inorg. Biochem.* **2005**, *99*, 247 – 266.
15. Mazumdar, R.; Saha, S.; Samanta, B.; Ghosh, R.; Maity, S.; Mondal, B. *Dalton Trans*. **2023**, *52*, 7917 – 7925.
16. (a) Clarkson, S. G.; Basolo, F. *J. Chem. Soc., Chem. Commun.* **1972**, *11*, 670 – 671; (b) Clarkson, S. G.; Basolo, F. *Inorg. Chem.* **1973**, *12*, 1528 – 1534.
17. (a) Wick, P. K.; Kissner, R.; Koppenol, W. H. *Helv. Chim. Acta* **2000**, *83*, 748 – 754; (b) Wick, P. K.; Kissner, R.; Koppenol, W. H. *Helv. Chim. Acta* **2001**, *84*, 3057 – 3062.
18. Thyagarajan, S.; Incarvito, C.; Rheingold, A. L.; Theopold, K. H. *Inorg. Chim. Acta* **2003**, *345*, 333 – 339.
19. Maiti, D.; Lee, D.-H.; Sarjeant, A. A. N.; Pau, M. Y. M.; Solomon, E. I.; Gaoutchenova, K.; Sundermeyer, J.; Karlin, K. D. *J. Am. Chem. Soc.* **2008**, *130*, 6700 – 6701.
20. (a) Kurtikyan, T. S.; Eksuzyan, S. R.; Hayrapetyan, V. A.; Martirosyan, G. G.; Hovhannisyan, G. S.; Goodwin, J. A. *J. Am. Chem. Soc.* **2012**, *134*, 13861 – 13870; (b) Kurtikyan, T. S.; Eksuzyan, Sh. R.; Goodwin, J. A.; Hovhannisyan, G. S. *Inorg. Chem.* **2013**, *52*, 12046 – 12056.
21. Yokoyama, A.; Han, J. E.; Cho, J.; Kubo, M.; Ogura, T.; Siegler, M. A.; Karlin, K. D.; Nam, W. *J. Am. Chem. Soc.* **2012**, *134*, 15269 – 15272.
22. Yokoyama, A.; Cho, K.-B.; Karlin, K. D.; Nam, W. *J. Am. Chem. Soc.* **2013**, *135*, 14900

– 14903.

23. Saha, S.; Ghosh, S.; Gogoi, K.; Deka, H.; Mondal, B.; Mondal, B. *Inorg. Chem.* **2017**, *56*, 10932 – 10938.
24. Keerthi, A.; Das, S.; Bhardwaj, P.; Sk, M. P.; Kumar, P. *Dalton Trans.* **2023**, *52*, 16492 – 16499.
25. Massoud, S. S.; Louka, F. R.; Ducharme, G. T.; Fischer, R. C.; Mautner, F. A.; Vančo, J.; Herchel, R.; Dvořák, Z.; Trávníček, Z. *J. Inorg. Biochem.* **2018**, *180*, 39 – 46.
26. Robertson, N. J.; Carney, M. J.; Halfen, J. A. *Inorg. Chem.* **2003**, *42*, 6876 – 6885.
27. Das, S.; Kulbir; Ray, S.; Devi, T.; Ghosh, S.; Harmalkar, S. S.; Dhuri, S. N.; Mondal, P.; Kumar, P. *Chem. Sci.* **2022**, *13*, 1706 – 1714.
28. Enemark, J. H.; Feltham, R. D. *Coord. Chem. Rev.* **1974**, *13*, 339 – 406.
29. (a) Wester, D.; Edwards, R. C.; Busch, D. *Inorg. Chem.* **1977**, *16*, 1055 – 1060; (b) Wayland, B. B.; Olson, L. W.; Siddiqui, Z. U. *J. Am. Chem. Soc.***1976**, *98*, 94 – 97; (c) Ardon, M.; Cohen, S. *Inorg. Chem.* **1993**, *32*, 3241 – 3243.
30. Bernal, I.; Harrison, S. E. *J. Chem. Phys.* **1961**, *34*, 102 – 106.
31. Meriwether, L. S.; Robinson, S. D.; Wilkinson, G. *J. Chem. Soc. A*, **1966,** 1488 – 1490.
32. Wayland, B. B.; Olson, L. W.; Siddiqui, Z. U. *J. Am. Chem. Soc.* **1976**, *98*, 94 – 98.
33. Manoharan, P. T.; Ganguli, P. *Chem. Phys. Lett.* **1971**, *11*, 281 – 284.
34. Gogoi, K.; Saha, S.; Mondal, B.; Deka, H.; Ghosh, S.; Mondal, B. *Inorg. Chem.* **2017**, *56*, 14438 – 14445.
35. Siddall, T. L.; Miyaura, N.; Huffman, J. C.; Kochi, J. K. *J. Chem. Soc. Chem. Commun.* **1983**, *21,* 1185 – 1186.
36. Srinivasan, K.; Kochi, J. K. *Inorg. Chem.* **1985**, *24*, 4671 – 4679.
37. Samsel, E. G.; Srinivasan, K.; Kochi, J. K. *J. Am. Chem. Soc.* **1985**, *107*, 7606 – 7617.
38. Garrison, J. M.; Bruice, T. C. *J. Am. Chem. Soc.* **1989**, *111*, 191 – 198.

39. Garrison, J. M.; Ostovic, D.; Bruice, T. C. *J. Am. Chem. Soc.***1989**, *111*, 4960 – 4966.
40. Bakac, A.; Wang, W.-D. *J. Am. Chem. Soc*. **1996**, *118*, 10325 − 10326.
41. Fujii, H.; Yoshimura, T.; Kamada, H. *Inorg. Chem.***1997**, *36*, 1122 – 1127.
42. Meier-Callahan, A. E.; Gray, H. B.; Gross, Z. *Inorg. Chem.* **2000**, *39*, 3605 – 3607.
43. Czernuszewicz, R. S.; Mody, V.; Czader, A.; Gałęzowski, M.; Gryko, D. T. *J. Am. Chem. Soc*. **2009**, *131*, 14214 – 14215.
44. Cho, J.; Woo, J.; Han, J. E.; Kubo, M.; Ogura, T.; Nam, W. *Chem. Sci.* **2011**, *2*, 2057 – 2062.
45. Mondal, B.; Saha, S.; Borah, D.; Mazumdar, R.; Mondal, B. *Inorg. Chem.* **2019**, *58,* 1234 – 1240.
46. Mondal, B.; Borah, D.; Mazumdar, R.; Mondal, B. *Inorg. Chem.* **2019**, *58,* 14701 – 14707.
47. Kalita, A.; Kumar, P.; Mondal, B. *Chem. Commun.* **2012**, *48*, 4636 – 4638.
48. Kalita, A.; Deka, R. C.; Mondal, B. *Inorg. Chem.* **2013**, *52*, 10897 – 10903.
49. SMART, SAINT and XPREP; Siemens Analytical X-ray Instruments Inc.: Madison, WI, **1995**.
50. Sheldrick, G. M. *SHELXS-2016*; University of Gottingen: Gottingen, Germany, **2016**.
51. Farrugia, L. J. ORTEP-3 for Windows - a version of ORTEP-III with a Graphical User Interface (GUI). *J. Appl. Crystallogr.* **1997**, *30*, 565.

Chapter 5

Nitric oxide reductase activity of a diiron-dinitrosyl complex through the formation of $\{Fe(NO)_2\}^9$ intermediate

Abstract

An unsymmetrical non-heme diiron-dinitrosyl complex **5.2**, $[Fe(Pz_2Py)(NO)Cl][FeCl_3(NO)]$, [$Pz_2Py$ = *Bis*(di(3,5-dimethyl-1H-pyrazolyl)methyl)-(2-pyridinyl)-methyl amine] has been synthesized and characterized. In FT-IR study, the nitrosyl stretching frequencies appeared at 1785 and 1830 cm^{-1} in KBr pellet. In acetonitrile solution, complex **5.2** spontaneously decomposes to the corresponding μ-oxo-diferric complex **5.3**, $[(Pz_2Py)ClFe^{III}\text{-}O\text{-}Fe^{III}Cl_3]$, with simultaneous release of nitrous oxide (N_2O). Spectroscopic studies suggest the formation of $[(Pz_2Py)Fe(NO)_2Cl]$ having $\{Fe(NO)_2\}^9$ configuration as intermediate. The close proximity of the NO groups in $\{Fe(NO)_2\}^9$ intermediate promotes the N–N bond formation leading to a transient hyponitrite species, which results in the release of N_2O. The formation of complex **5.3** has been confirmed by its structural characterization.

5.1 Introduction

In the bacterial denitrification process, nitrate (NO_3^-) gets reduced to dinitrogen (N_2). In this sequential event, an essential step is reduction of nitric oxide (NO) to nitrous oxide (N_2O).[1-2] Nitric oxide reductases (NORs) enzymes catalyse this $2e^-$ reduction.[3-6] Its active site consists of a diiron core having a histidine coordinated heme center and a tri-imidazole coordinated non-heme center.[7] N_2O is formed from two equivalent of NO through a two electron and two proton transfer process.[8] Though, there have been a number of enzymatic studies to elucidate the reaction mechanism, the catalytic cycle is still not completely understood. In addition, flavodiiron nitric oxide reductases (FNORs) enzyme, which consists of two non-heme iron centers, reduces NO to N_2O.[9-10] A number of different mechanistic pathways for the reduction of NO to N_2O by FNORs have been proposed, such as mixed valent or semi-reduced, super-reduced, direct coupling pathways involving diferrous-dinitrosyl intermediates and lastly, hyponitrite pathway.[11] Though, some reports suggest the formation of a mononitrosyl intermediate in the catalytic cycle, recently it has been demonstrated that the reduction of NO to N_2O proceeds *via* the successive formation of mononitrosyl, $[Fe^{II}\{Fe(NO)\}^7]$ species and dinitrosyl, $[\{Fe(NO)\}^7]_2$ species.[12] However, dinitrosyl species, $[\{Fe(NO)\}^7]_2$ is found to be involved in the N–N bond formation and thereby reduces NO to N_2O. In this two electron transfer process, the catalytically active diferrous intermediate converts to diferric species.[13] In the mixed valent or semi-reduced mechanism, it has been shown that the diferrous-dinitrosyl intermediate, $[\{Fe(NO)\}^7]_2$ gets reduced by one electron to result in $\{Fe(NO)\}^7$-$\{Fe(NO)\}^8$ which then affords N_2O and a Fe^{II}-Fe^{III} complex.[14] Upon reduction, the mixed valent Fe^{II}-Fe^{III} complex gives back the diferrous species which again takes part in the catalytic process.[14] On the other hand, in super-reduced pathway, the diferrous-dinitrosyl intermediate undergoes two electron reduction to $[\{Fe(NO)\}^8]_2$ species which subsequently results in the formation of N_2O and diferrous complex.[15-16] The direct coupling pathway involves the direct N–N bond formation in the $[\{Fe(NO)\}^7]_2$ species leading to the formation of N_2O and Fe^{III}-O-Fe^{III} complex.[17] In the next step, Fe^{III}-O-Fe^{III} undergoes two electron reduction to form diferrous species. In a detailed spectroscopic study, Kurtz, Jr. and co-workers shown the involvement of a diferrous-dinitrosyl, $[\{Fe(NO)\}^7]_2$, intermediate in the process of generation of N_2O in a deflavinated flavo-diiron protein.[12]

This chapter deals with the spontaneous conversion of an asymmetric diferrous-dinitrosyl complex in acetonitrile to N_2O and the corresponding Fe^{III}-O-Fe^{III} complex. Spectroscopic studies suggest that the reaction proceeds through the conversion of diferrous-dinitrosyl to a Fe(I)-dinitrosyl complex, having $\{Fe(NO)_2\}^9$ configuration. It would be noted that the example of N–N coupling of two NO unit in a monometallic system leading to the formation of N_2O is quite rare as the parallel alignment of the unpaired spins makes the coupling spin-forbidden.[18]

5.2 Results and Discussion

The ligand Pz_2Py was prepared by following the reported literature procedure.[19] Complex **5.1** was synthesized by the reaction of anhydrous iron(II) chloride with the ligand in degassed acetonitrile solution (Experimental Section). The isolated complex **5.1** was characterized using routine spectroscopic techniques (Experimental Section and Appendix IV, Figures A4.1-A4.4). The structure of the complex **5.1** was reported earlier (Appendix IV, Figure A4.5).[20]

In a dry and degassed acetonitrile solution of complex **5.1** and anhydrous $FeCl_3$ (1:1 mole ratio), bubbling of NO gas resulted in the formation of diferrous-dinitrosyl complex **5.2** (Scheme 5.1) (Experimental Section and Appendix IV, Figures A4.6-A4.7).

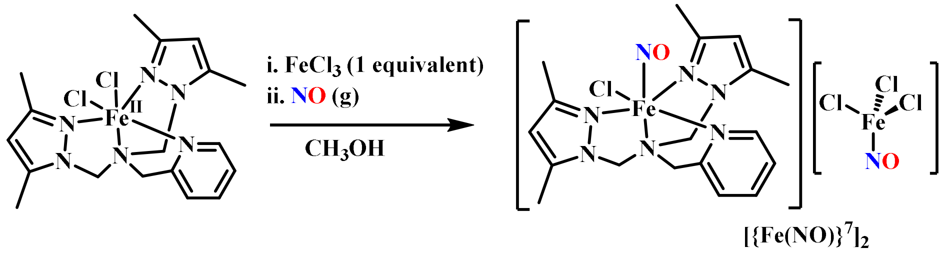

5.1

5.2

Scheme 5.1. Formation of diiron-dinitrosyl complex **5.2**.

It was isolated as solid and structurally characterized (Experimental Section). The ORTEP diagram is shown in figure 5.1 and the matric parameters are listed in appendix (Appendix IV, Tables A4.1-A4.3). The crystal structure reveals the presence of two Fe-nitrosyl units with a formulation of $[(Pz_2Py)Fe(NO)Cl][FeCl_3(NO)]$ and both of them are having $\{Fe(NO)\}^7$ configuration. The Fe–N and N–O bond distances in $[(Pz_2Py)Fe(NO)Cl]^+$ and $[FeCl_3(NO)]^-$ units are 1.737(5), 1.724(6) and 1.143(6), 1.109(6) Å, respectively. These are well within the range for the reported $\{Fe(NO)\}^7$ complexes.[21-26]

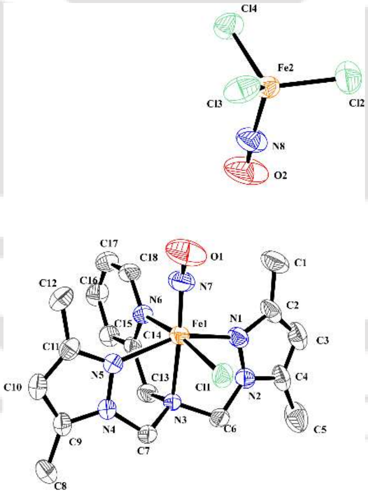

Figure 5.1. ORTEP diagram of complex **5.2** (30% thermal ellipsoid plot, H atoms are omitted for clarity).

In FT-IR spectroscopic studies, complex **5.2** in KBr pellet shows two distinctly different stretching frequencies for NO moieties at 1785 and 1830 cm^{-1}, respectively (Figure 5.2). Separately synthesized and isolated $[(Pz_2Py)Fe(NO)(MeOH)](ClO_4)_2$ and

$[N(CH_3)_4][FeCl_3(NO)]$ show NO stretching frequencies at 1793 and 1818 cm^{-1}, respectively (Experimental Section and Appendix IV, Figures A4.8-A4.9). Hence, it is logical to attribute the 1785 and 1830 cm^{-1} stretching frequency of complex **5.2** to the $[(Pz_2Py)Fe(NO)Cl]^+$ and $[FeCl_3(NO)]^-$ units, respectively.

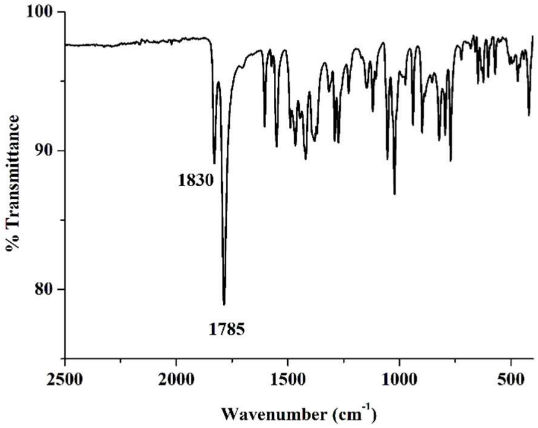

Figure 5.2. FT-IR spectrum of complex **5.2** in KBr.

The individual complexes, $[(Pz_2Py)Fe(NO)(MeOH)](ClO_4)_2$ and $[N(CH_3)_4][FeCl_3(NO)]$ in acetonitrile solution under Ar atmosphere are stable for several days. However, when complex **5.2** was dissolved in dry and degassed acetonitrile, it started decomposing which was monitored using UV-visible (Figure 5.3) and X-band EPR spectroscopy (Appendix IV, Figure A4.12).

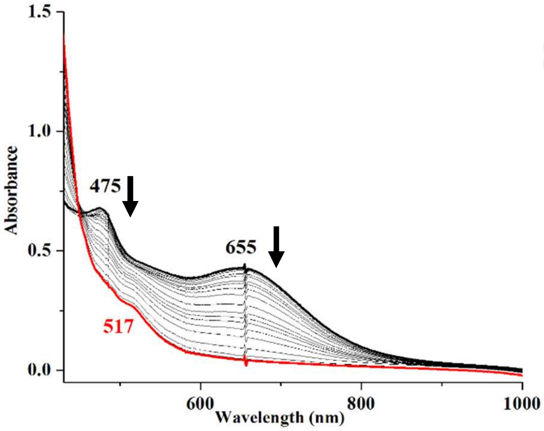

Figure 5.3. UV-visible spectral monitoring of decomposition of complex **5.2** (black) to complex **5.3** (red) in acetonitrile under Ar atmosphere at room temperature.

The decomposition product, complex **5.3** was isolated and characterized as a μ-oxo bridged diferric complex (Experimental Section and Appendix IV, Figures A4.13-A4.15). Single crystal X-ray structure of complex **5.3** was determined and the perspective ORTEP view is shown in figure 5.4. The bond lengths, angles and other parameters are listed in the tables in appendix (Appendix IV, Tables A4.1-A4.3).

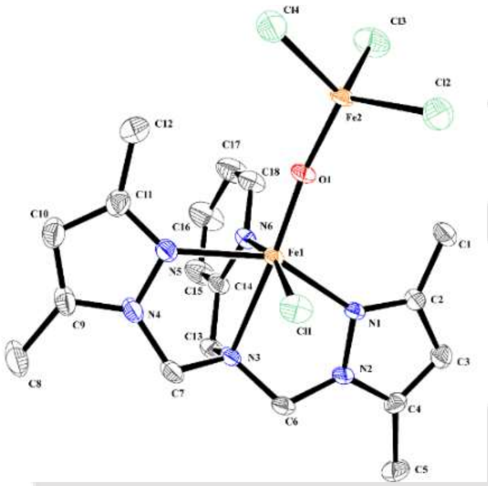

Figure 5.4. ORTEP diagram of complex **5.3** (30% thermal ellipsoid plot, solvent molecules and H atoms are omitted for clarity).

In addition, when the headspace gas was subjected to GC-Mass spectrometry, it shows the presence of N_2O (Appendix IV, Figures A4.16-4.19). Thus, it is logical to assume that complex **5.2** in acetonitrile solution decomposes to yield N_2O and the corresponding μ-oxo diiron complex, **5.3**.

Furthermore, though complex **5.2** displays two distinct nitrosyl stretching frequencies at 1785 and 1830 cm^{-1} in KBr pellet, upon dissolution in acetonitrile, it shows nitrosyl stretching frequencies at 1790 and 1704 cm^{-1} (Appendix IV, Figure A4.20), which gradually diminish. This gradual decrease of the intensity suggests decomposition leading to the formation of complex **5.3** (Appendix IV, Figure A4.21). These two stretching frequencies are attributed to the formation of $\{Fe(NO)_2\}^9$ intermediate (Scheme 5.2). Earlier reported $\{Fe(NO)_2\}^9$ complexes are also found to exhibit nitrosyl stretching in the range of 1670-1790

cm^{-1}.[27] For example, $\{Fe(NO)_2\}^9$ complexes [Na-18-Crown-6-ether][$(NO)_2Fe(C_3H_3N)_2$] the nitrosyl stretching frequencies were observed at 1774 and 1712 cm^{-1} respectively.[28] However, in case of [$(NO)_2Fe(TPA)$], it appeared at 1720 and 1619 cm^{-1}, which was attributed to the better electron donating nature of TPA compound to imidazolate moiety.[29]

Earlier, it has been reported that $[N(CH_3)_4][FeCl_3(NO)]$ acts as a NO^- donor to suitable acceptors.[30] To check this, separately prepared $[N(CH_3)_4][FeCl_3(NO)]$ was treated with $[Fe(dtc)_3]$ (dtc = diethyldithiocarbamate anion). FT-IR and X-band EPR studies suggest the formation of $[Fe(dtc)_2(NO)]$ (Appendix IV, Figures A4.24-A4.25), confirming the NO^- transfer from $[FeCl_3(NO)]^-$ to the acceptor. However, similar experiment with separately prepared $[(Pz_2Py)Fe(MeOH)(NO)]^{2+}$ does not show any such transfer. Hence, it is logical to assume that in acetonitrile solution of complex **5.2**, $[FeCl_3(NO)]^-$ transfers NO^- to $[(Pz_2Py)FeCl(NO)]^+$ unit resulting in the formation of a $\{Fe(NO)_2\}^9$ system, $[(Pz_2Py)FeCl(NO)_2]$ (Scheme 5.2).

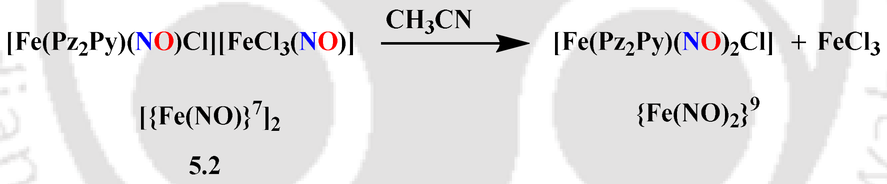

Scheme 5.2. Formation of the $\{Fe(NO)_2\}^9$ intermediate.

The formation of the intermediate having $\{Fe(NO)_2\}^9$ configuration along with $FeCl_3$ in acetonitrile solution was also evidenced from X-band EPR studies (Appendix IV, Figure A4.22). With time, it changes to the EPR spectrum which matches well with that of isolated complex **5.3**. All these evidences suggest that in acetonitrile solution of complex **5.2**, $[FeCl_3(NO)]^-$ moiety transfers NO^- to $[(Pz_2Py)FeCl(NO)]^+$ to form $[(Pz_2Py)FeCl(NO)_2]$, a $\{Fe(NO)_2\}^9$ system and $FeCl_3$. It is proposed that NO^- transfer to $[(Pz_2Py)FeCl(NO)]^+$ is accompanied by the dissociation of one Pz (Pz = pyrazole) from metal center allowing it to maintain the coordination number. Such ligand dissociation was proposed in the formation of N_2O from NO in bacterial cNOR and qNOR.[31]

The [(Pz$_2$Py)FeCl(NO)$_2$] is unstable in nature and decomposes fast to release N_2O with a concomitant formation of [(Pz$_2$Py)ClFe^{III}-O-Fe^{III}Cl$_3$], complex **5.3**. It is to be noted that one of the most probable mechanisms of formation of N_2O in NOR proposes the involvement of the super reduced $\{Fe(NO)_2\}^9$ species. The *cis* configuration of the NO groups in the $\{Fe(NO)_2\}^9$ intermediate brings them to the close proximity to promote N–N bond formation, resulting a transient hyponitrite intermediate.[14] In the next step, the hyponitrite intermediate cleaves down to N_2O and μ-oxo metal complex (Scheme 5.3).

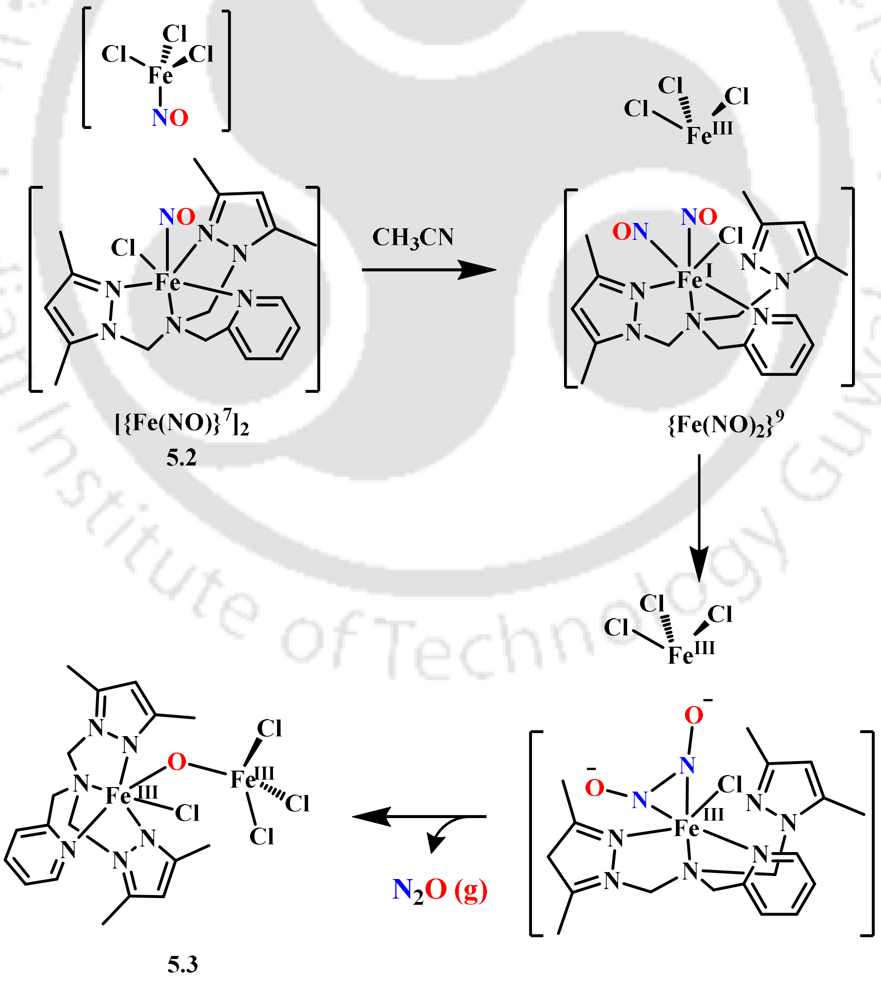

Scheme 5.3. Decomposition pathway of complex **5.2** in acetonitrile.

In biological system, the reduction of $\{Fe(NO)\}^7$ unit takes place by electron transfer from flavo protein. In the present case, one component, $[FeCl_3(NO)]^-$, of the complex **5.2** is transferring NO^- group to the other unit, $[(Pz_2Py)FeCl(NO)]^+$ to form a $\{Fe(NO)_2\}^9$ system leading to the release of N_2O. To the best of our knowledge, this is perhaps the first example showing such a unique behavior.

5.3 Experimental Section

5.3.1 Materials and methods

Preparation and handling of air sensitive materials were done under inert conditions (Ar gas) using standard Schlenk techniques, or in glovebox, equipped with O_2 and moisture concentrations less than 1 ppm. All solvents were dried using standard techniques, freeze-pump-thaw to remove O_2 and stored over activated molecular sieves (4 Å). Deoxygenation of the solvent and solutions were effected by repeated vacuum/Ar purge cycles or bubbling with Ar gas for 30 min. All chemicals and solvents were of commercially available quality and used without further purification, unless otherwise mentioned. Infrared spectra of the samples were obtained using PerkinElmer spectrophotometer at room temperature. Samples were prepared either as KBr pellets by grinding the sample with KBr (IR-grade) or in ATR probe. Solution FT-IR were recorded in KBr cells. UV-visible spectra were recorded on an Agilent Technologies Cary 8454 UV-visible spectrophotometer by preparing a known concentration of the samples at room temperature (25 °C) using a quartz cuvette of 1 cm width. ^1H and ^{13}C NMR spectra were collected in 400 MHz Bruker AVANCE 400 or 500 MHz Bruker AVANCE NEO 500 FT-NMR spectrometers. Chemical shifts were reported as δ (ppm) values relative to an internal standard (tetramethylsilane) or the residual solvent peaks. X-band Electron Paramagnetic Resonance (EPR) spectra were recorded on a JES-FA200 ESR spectrometer. Spectra were taken at 77 K, with 0.998 mW microwave power, 9.14 GHz microwave frequency and 10 G modulation amplitude. High-resolution Mass spectra were measured in HPLC grade acetonitrile solution by Ultra-High-Performance Liquid Chromatography Quadruple Time of Flight High-resolution Mass Spectrometer (UHPLC-QTOF-HRMS, Agilent G6546A). Gas chromatograms were obtained on PerkinElmer Clarus® 590. Mass spectra were measured in HPLC grade acetonitrile and methanol solvent.

Single crystals of all complexes suitable for X-ray crystallographic analysis were obtained from methanol/diethyl ether solution in refrigerator. The intensity data were collected using a Bruker SMART APEX-II CCD diffractometer, equipped with a fine focus 1.75 kW sealed tube MoK$_\alpha$ radiation ($\lambda = 0.71073$ Å) at 293(3) K, with increasing ω (width of 0.3° per frame) at a scan speed of 3 s/frame. The SMART software was used for data acquisition. Data integration and reduction were undertaken with SAINT and XPREP software.[32] Multi-scan empirical absorption corrections were employed to the data using the program SADABS. Structures were solved by direct methods using SHELXS-2019 and refined with full-matrix least squares on F^2 using SHELXL-2019/1.[33-34] Structural illustrations have been drawn with ORTEP-3 for Windows.[35]

5.3.2 Syntheses

[Fe^{II}(Pz$_2$Py)Cl$_2$], 5.1

In the glovebox, anhydrous FeCl$_2$ (0.126 g, 1 mmol) and ligand Pz$_2$Py (0.324 g, 1 mmol) were dissolved in dry and degassed methanol (3 mL) and the reaction mixture was stirred for 2 hr. The color of the solution became yellow. This yellow colored solution was then layered with dry and degassed diethyl ether (7 mL) and after 2 days yellow block type crystal of complex **5.1** was obtained. Yield: 0.29 g, ~ 65 %. All characterized data are matches well with previously reported one.[20] Elemental analyses for $C_{18}H_{24}N_6Cl_2Fe$. Calcd. (%): C, 47.92; H, 5.36; N, 18.63. found (%): C, 47.82; H, 5.34; N, 18.79. FT-IR (using ATR probe): 2962, 1603, 1554, 1465, 1421, 1392, 1261, 1153, 1101, 1021, 895, 801, 771, 627 and 463 cm^{-1}. UV-visible (in acetonitrile): 320 nm (ε/M $^{-1}$ cm^{-1}, 1850) and 385 nm (ε/M^{-1} cm^{-1}, 1500). ESI-mass (m/Z): Calcd.: 415.11 (for [Fe^{II}(Pz$_2$Py)Cl]$^+$ unit); found: 415.07. X-band EPR (in methanol): silent at 77 K.

[Fe^{II}(Pz$_2$Py)Cl(NO)][FeCl$_3$(NO)], 5.2

Complex **5.1** (0.46 g, 1 mmol) was dissolved in dry and degassed methanol (5 mL). After that, 1 mole equivalent of anhydrous FeCl$_3$ (0.16 g,1 mmol) in dry and degassed methanolic solution was added to it. Then, NO gas was bubbled into this solution for 5 min until the color changed to dark green. The reaction mixture was kept overnight in NO atmosphere to result in the green crystals of complex **5.2**. Excess NO gas was removed by applying several cycles of vacuum/Ar purge and the crystals were isolated by filtration using Schlenk frit. Yield: 0.44 g, ~ 70 %. Elemental analyses for $C_{18}H_{24}N_8O_2Cl_5Fe_2$. Calcd. (%): C, 33.89; H, 3.79; N, 17.57. found (%): C, 33.82; H, 3.75; N, 17.72. FT-IR (using ATR probe): 1818, 1785, 1602, 1553, 1465, 1418, 1380, 1274, 1152, 1117, 1053, 1021, 940, 823, 770, 624, 569 and 420 cm^{-1}. UV-visible (in acetonitrile): 360 nm (ε/M^{-1} cm^{-1}, 1660), 475 nm (ε/M^{-1} cm^{-1}, 610) and 655 nm (ε/M^{-1} cm $^{-1}$, 480). X-band EPR (in acetonitrile): g ~ 4.85 and 2.05 at 77 K.

[Fe^{III}(Pz$_2$Py)Cl(μ-O)Fe^{III}Cl$_3$], 5.3

Complex **5.2** (0.637 g, 1 mmol) was dissolved in dry and degassed acetonitrile solution and kept at room temperature. Upon keeping the solution under Ar atmosphere for 3 days, complex **5.3** was precipitated out from the solution as red crystals and was isolated by filtration. Yield: 0.48 g, ~ 80 %. Elemental analyses for $C_{20}H_{27}N_7Cl_4OFe_2$. Calcd. (%): C, 37.83; H, 4.29; N, 15.44. found (%): C, 37.76; H, 4.26; N, 15.52. FT-IR (using ATR probe): 1601, 1550, 1466, 1388, 1275, 1054, 1020, 855, 816, 772, 646, 660 and 470 cm^{-1}. UV-visible (in DMF): 320 nm (ε/M^{-1} cm^{-1}, 2750) and 495 nm (ε/M^{-1} cm^{-1}, 160). X-band EPR (in DMF): g ~ 5.13 at 77 K.

$[Fe(Pz_2Py)(NO)(CH_3OH)](ClO_4)_2$

The equivalent mixture of $[Fe(CH_3CN)_4(ClO_4)_2]$ (0.419 g, 1 mmol) and Pz_2Py (0.326 g, 1 mmol) was dissolved in dry and degassed acetonitrile solution. NO gas was bubbled to this reaction mixture and the color changed to dark green. The green colored solution was layered with diethyl ether to obtain the $[Fe(Pz_2Py)(NO)(CH_3OH)](ClO_4)_2$ complex as green block shaped crystal. Yield: 0.39 g, ~ 60 %. FT-IR (in KBr): 3421, 2926, 1793, 1605, 1551, 1468, 1422, 1392, 1273, 1109, 1089, 896, 818, 626 and 420 cm^{-1}.

$[N(CH_3)_4][FeCl_3(NO)]$

The complex, $[N(CH_3)_4][FeCl_3(NO)]$ was prepared using a previously described procedure with slight modification.[29] In the glovebox, $FeCl_2.4H_2O$ (0.99 g, 0.5 mmol) and tetramethylammonium chloride (0.054 g, 0.5 mmol) was dissolved in deoxygenate methanol to obtain yellow colored solution. After that, NO gas was bubbled through this solution and it was kept for 3 days in refrigerator. The needle shaped green colored crystals of complex of $[N(CH_3)_4][FeCl_3(NO)]$ was obtained. Yield: 0.63 g, ~ 48 %. FT-IR (in KBr): 3396, 1818, 1634, 1482, 1415, 1285 and 948 cm^{-1}.

Determination of yield of N_2O

Different amounts of *N*-hydroxybenzenesulfonamide were taken in four 25 mL round bottom flask and degassed with vacuum/Ar purge. Each flask was then treated with 10 mL 0.1 M NaOH solution under sealed condition. At the end of the reaction 1 mL of headspace gas was subjected to GC. From there, a calibration curve between concentration of *N*-

hydroxybenzenesulfonamide and peak intensity at 2.73 min (corresponding to N_2O) was generated (Appendix IV, Figures A4.16-A4.17).

Complex **5.2** (0.669 g, 0.437 mmol) dissolved in 5 mL dry and degassed acetonitrile was taken in a 25 mL round bottom flask in three different sets. After 1, 4 and 24 hr the headspace gas of three different sets was subjected to GC and it was found that after 24 hr of the reaction the amount of released N_2O was highest. The amount of N_2O was measured from the calibration curve (Appendix IV, Figure A4.18). Yield: ~ 65%.

[Fe(dtc)$_3$] (dtc = Diethyldithiocarbamate anion)

[Fe(dtc)$_3$] was prepared according to previously reported procedure.[37]

Reaction of [N(CH$_3$)$_4$][FeCl$_3$(NO)] with [Fe(dtc)$_3$]

[N(CH$_3$)$_4$][FeCl$_3$(NO)] (0.002 g, 0.001 mmol) and Fe(dtc)$_3$ (0.004 g, 0.001 mmol) was taken in 5 mL round bottom flask then acetonitrile solution (3 mL) was added to it. The reaction mixture was stirred under Ar atmosphere for 30 min. After that, the reaction mixture was subjected to FT-IR and X-band EPR spectroscopic studies. FT-IR (ATR probe): ν(NO), 1683 cm^{-1}. X-band EPR (in acetonitrile): g ~ 2.02 at 77 K.

5.4 Conclusion

In conclusion, an unsymmetrical diiron-dinitrosyl complex, **5.2** has been synthesized and characterized structurally. Although the complex is stable in solid state, in acetonitrile solution it releases N_2O spontaneously with the formation of the corresponding μ-oxo bridged diiron complex **5.3**. GC-Mass analysis suggests a near quantitative conversion of N_2O. Spectroscopic studies indicate the formation of $\{Fe(NO)_2\}^9$ intermediate *via* NO^- transfer from

$[FeCl_3(NO)]^-$ unit to $[(Pz_2Py)FeCl(NO)]^+$ unit. The close proximity of the NO groups in $\{Fe(NO)_2\}^9$ unit promotes the N–N bond formation leading to a transient hyponitrite intermediate. Successively, this intermediate decomposes to release N_2O with a concomitant formation of μ-oxo diferric complex **5.3**.

5.5 References

1. van Spanning, R. J.; Richardson, D. J.; Ferguson, S. J. *In Biology of the Nitrogen Cycle*; Elsevier, **2007**; pp 3 – 20.
2. Wasser, I. M.; de Vries, S.; Moënne-Loccoz, P.; Schröder, I.; Karlin, K. D. *Chem. Rev.* **2002**, *102*, 1201 – 1234.
3. Zumft, W. G. *Microbiol. Mol. Biol. Rev.* **1997**, *61*, 533 – 616.
4. Zumft, W. G. *J. Inorg. Biochem.* **2005**, *99*, 194 – 215.
5. Watmough, N. J.; Field, S. J.; Hughes, R. J. L.; Richardson, D. J. *Biochem. Soc. Trans.* **2009**, *37*, 392 – 399.
6. Hendriks, J.; Oubrie, A.; Castresana, J.; Urbani, A.; Gemeinhardt, S.; Saraste, M. *Biochim. Biophys. Acta, Bioenerg.* **2000**, *1459*, 266 – 273.
7. Collman, J. P.; Yang, Y.; Dey, A.; Decreau, R. A.; Ghosh, S.; Ohta, T.; Solomon, E. I. *Proc. Natl. Acad. Sci. U. S. A.* **2008**, *105*, 15660 – 15665.
8. Weitz, A. C.; Giri, N.; Caranto, J. D.; Kurtz, D. M., Jr.; Bominaar, E. L.; Hendrich, M. P. *J. Am. Chem. Soc.* **2017**, *139*, 12009 – 12019.
9. Silaghi-Dumitrescu, R.; Kurtz, D. M.; Ljungdahl, L. G.; Lanzilotta, W. N. *Biochemistry* **2005**, *44*, 6492 – 6501.
10. Hayashi, T.; Caranto, J. D.; Wampler, D. A.; Kurtz, D. M.; Moënne-Loccoz, P. *Biochemistry* **2010**, *49*, 7040 – 7049.
11. Khatua, S.; Majumdar, A. *J. Inorg. Biochem.* **2015**, *142*, 145 – 153.

12. Caranto, J. D.; Weitz, A.; Hendrich, M. P.; Kurtz, D. M. *J. Am. Chem. Soc.* **2014**, *136*, 7981 – 7992.
13. Jana, M.; White, C. J.; Pal, N.; Demeshko, S.; Meyer, F.; Cordes, C.; Lehnert, N.; Majumdar, A. *J. Am. Chem. Soc.* **2020**, *142*, 6600 – 6616.
14. White, C. J.; Speelman, A. L.; Kupper, C.; Demeshko, S.; Meyer, F.; Shanahan, J. P.; Alp, E. E.; Hu, M.; Zhao, J.; Lehnert, N. *J. Am. Chem. Soc.* **2018**, *140*, 2562 – 2574.
15. Confer, A. M.; McQuilken, A. C.; Matsumura, H.; Moenne-Loccoz, P.; Goldberg, D. P. *J. Am. Chem. Soc.* **2017**, *139*, 10621 – 10624.
16. Jana, M.; Pal, N.; White, C. J.; Kupper, C.; Meyer, F.; Lehnert, N.; Majumdar, A. *J. Am. Chem. Soc.* **2017**, *139*, 14380 – 14383.
17. Dong, H. T.; White, C. J.; Zhang, B.; Krebs, C.; Lehnert, N. *J. Am. Chem. Soc.* **2018**, *140*, 13429 – 13440.
18. (a) Speelman, A. L.; Zhang, B.; Silakov, A.; Skodje, K. M.; Alp, E. E.; Zhao, J.; Hu, M. Y.; Kim, E.; Krebs, C.; Lehnert, N. *Inorg. Chem.* **2016**, *55*, 5485 – 5501; (b) Ye, S.; Neese, F. *J. Am. Chem. Soc.* **2010**, *132*, 3646 – 3647; (c) Bar, A. K.; Heras Ojea, M. J.; Tang, J.; Layfield, R. A. *J. Am. Chem. Soc.* **2020**, *142*, 4104 – 4107.
19. Massoud, S. S.; Louka, F. R.; Ducharme, G. T.; Fischer, R. C.; Mautner, F. A.; Vančo, J.; Herchel, R.; Dvořák, Z.; Trávníček, Z. *J. Inorg. Biochem.* **2018**, *180*, 39 – 46.
20. Xue, F.; Zhao, J.; Hor, T. S. A. *Dalton Trans.* **2011**, *40*, 8935 – 8940.
21. Chiou, Y.-M.; Que, L., Jr. *Inorg. Chem.* **1995**, *34*, 3270 – 3278.
22. Dong, H. T.; Speelman, A. L.; Kozemchak, C. E.; Sil, D.; Krebs, C.; Lehnert, N. *Angew. Chem. Int., Ed.* **2019**, *58*, 17695 – 17699.
23. Dey, A.; Confer, A. M.; Vilbert, A. C.; Moënne-Loccoz, P.; Lancaster, K. M.; Goldberg, D. P. *Angew. Chem. Int., Ed.* **2018**, *57*, 13465 – 13469.

24. Ghosh, R.; Mazumdar, R.; Samanta, B.; Saha, S.; Mondal, B. *Dalton Trans.* **2025**, *54*, 7793 – 7800.
25. Harrop, T. C.; Song, D.; Lippard, S. J. *J. Am. Chem. Soc.* **2006**, *128*, 3528 – 3529.
26. Keilwerth, M.; Hohenberger, J.; Heinemann, F. W.; Sutter, J.; Scheurer, A.; Fang, H.; Bill, E.; Neese, F.; Ye, S.; Meyer, K. *J. Am. Chem. Soc.* **2019**, *141*, 17217 – 17235.
27. Lehnert, N.; Kim, E.; Dong, H. T.; Harland, J. B.; Hunt, A. P.; Manickas, E. C.; Oakley, K. M.; Pham, J.; Reed, G. C.; Alfaro, V. S. *Chem. Rev.* **2021**, *121*, 14682 – 14905.
28. Huang, H.-W.; Tsou, C.-C.; Kuo, T.-S.; Liaw, W.-F. *Inorg. Chem.* **2008**, *47*, 2196 – 2204.
29. Shih, W.-C.; Lu, T.-T.; Yang, L.-B.; Tsai, F.-T.; Chiang, M.-H.; Lee, J.-F.; Chiang, Y.-W.; Liaw, W.-F. *J. Inorg. Biochem.* **2012**, *113*, 83 – 93.
30. In-Iam, A.; Wolf, M.; Wilfer, C.; Schaniel, D.; Woike, T.; Klüfers, P. *Chem. Eur. J.* **2019**, *25*, 1304 – 1325.
31. Shiro, Y. *Biochim. Biophys. Acta Bioenerg.* **2012**, *1817*, 1907 – 1913.
32. SMART and SAINT; Siemens Analytical X-ray Instruments Inc.: Madison, WI, **1995**.
33. Sheldrick, G. M. SADABS: software for Empirical Absorption Correction, University of Gottingen, Institut fur Anorganische Chemieder Universitat, Tammanstrasse 4, D-3400 Gottingen, Germany, **1999**.
34. Sheldrick, G. M. *Acta. Crystallogr. Sect. C Struct. Chem.* **2015**, *71*, 3 – 8.
35. Farrugia, L. J. ORTEP-3 for Windows - a version of ORTEP-III with a Graphical User Interface (GUI), *J. Appl. Crystallogr.* **1997**, *30*, 565.
36. Dvoretzky, I.; Richter, G. H. *J. Org. Chem.* **1950**, *15*, 1285 – 1288.
37. Mazumdar, R.; Saha, S.; Samanta, B.; Mondal, B. *Inorg. Chem.* **2021**, *60*, 18024 – 18030.

Conclusion

This thesis broadly covers our endeavor to comprehend some interesting reactivity of a series of nitrosyl complexes. All these nitrosyl complexes were synthesized using a non-heme ligand framework with first row transition metal ions, iron and chromium. Our findings demonstrate that under NO atmosphere, solvent and temperature significantly affect the spin state of iron(II)-nitrosyl complexes of non-heme ligands. The reactivity of these metal nitrosyls with O_2 and H_2O_2 was explored with an attempt to mimic the mechanism of the nitric oxide dioxygenase (NOD) enzyme, as discussed in chapters 2 to 4. In every instance formation of a putative peroxynitrite intermediate was observed. Tedious efforts to identify and characterize the associated intermediates that form during its formation and decomposition led to some significant findings. For instance, in chapter 2, the formation of Fe(III)-peroxynitrite intermediate was observed, which decomposes to $[Fe^{IV}=O]$ and NO_2, leading to modify the ligand itself. In chapter 3, study of the dioxygen reactivity of two analogous iron-nitrosyls with different spin-states suggest an interesting difference in the reaction pathway. In chapter 4, a $[Cr^{v}=O]$ intermediate was observed in the reaction of chromium nitrosyl complex with H_2O_2. However, despite our best efforts, the characterization of the peroxynitrite itself was not successful because of its highly unstable nature. These findings will significantly enhance our current understanding of NOD chemistry and make a substantial contribution to the field of metalloenzyme chemistry.

On the other hand, in chapter 5, a diiron dinitrosyl complex was synthesized as a model complex of flavodiiron nitric oxide reductase (FNOR). This diiron dinitrosyl complex promotes N–N bond formation leading to transient hyponitrite species to result in the spontaneous release of N_2O. This is reactivity for such complexes definitely needs more investigation in future. The mechanism of the process needs further experimental support with fine tuning of the ligand framework.

Appendix I

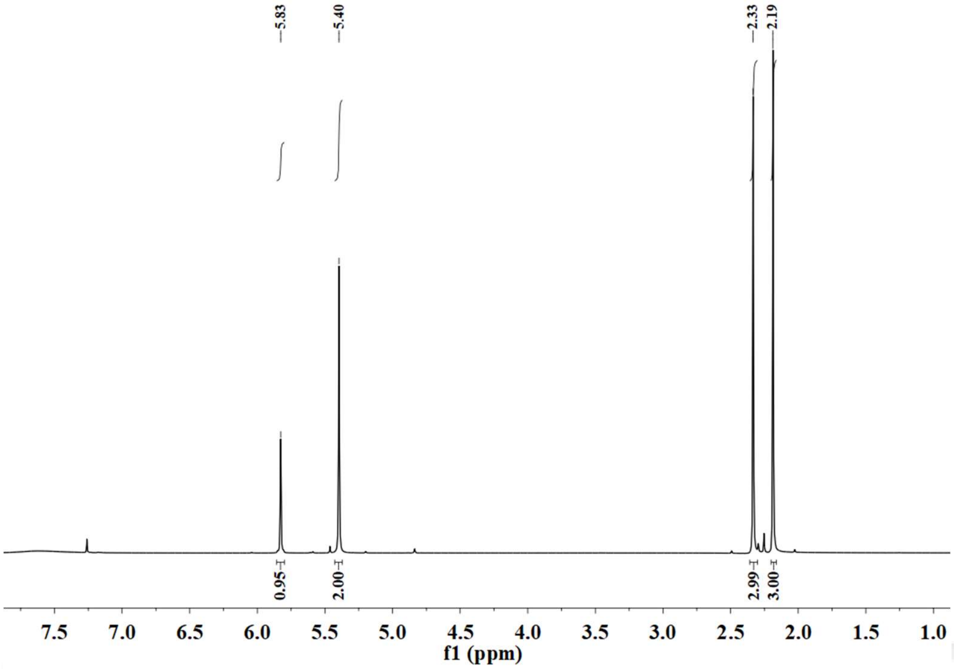

Figure A1.1: ^{1}H NMR spectrum of 1-(hydroxymethyl)-3,5-dimethyl-1-pyrazole in $CDCl_3$.

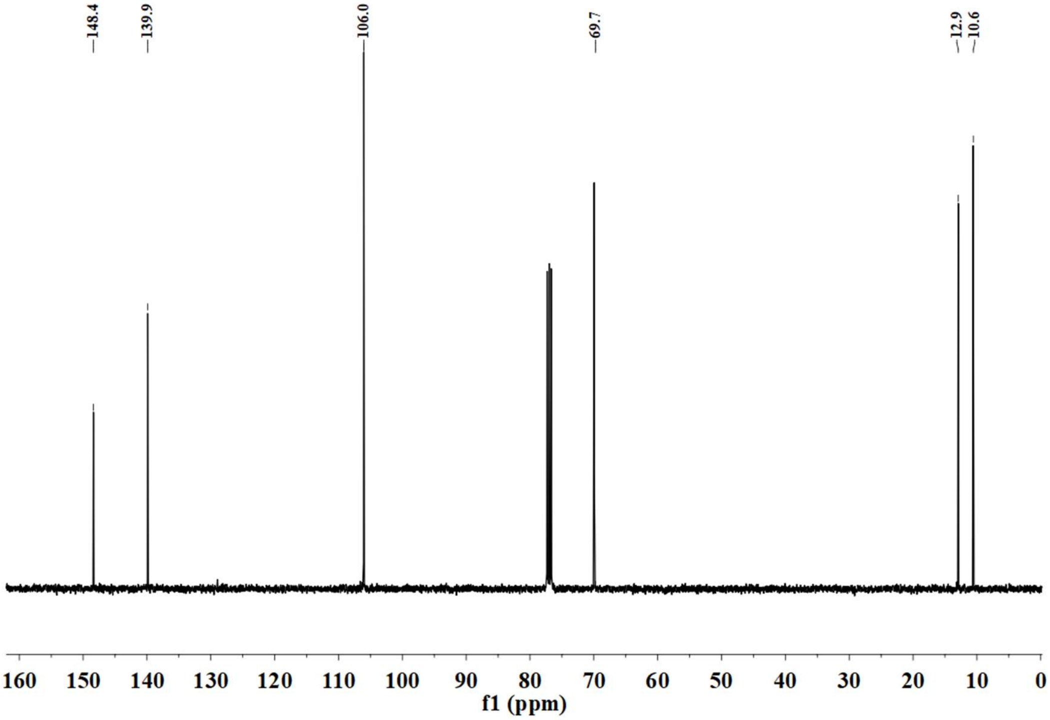

Figure A1.2: ^{13}C NMR spectrum of 1-(hydroxymethyl)-3,5-dimethyl-1-pyrazole in $CDCl_3$.

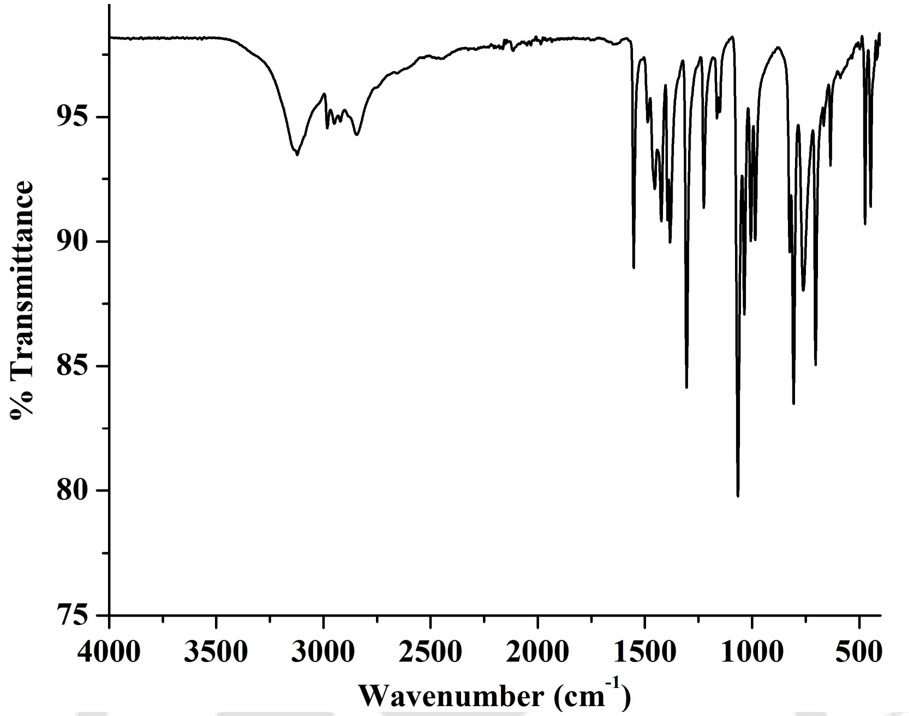

Figure A1.3: FT-IR spectrum of 1-(hydroxymethyl)-3,5-dimethyl-1-pyrazole in KBr.

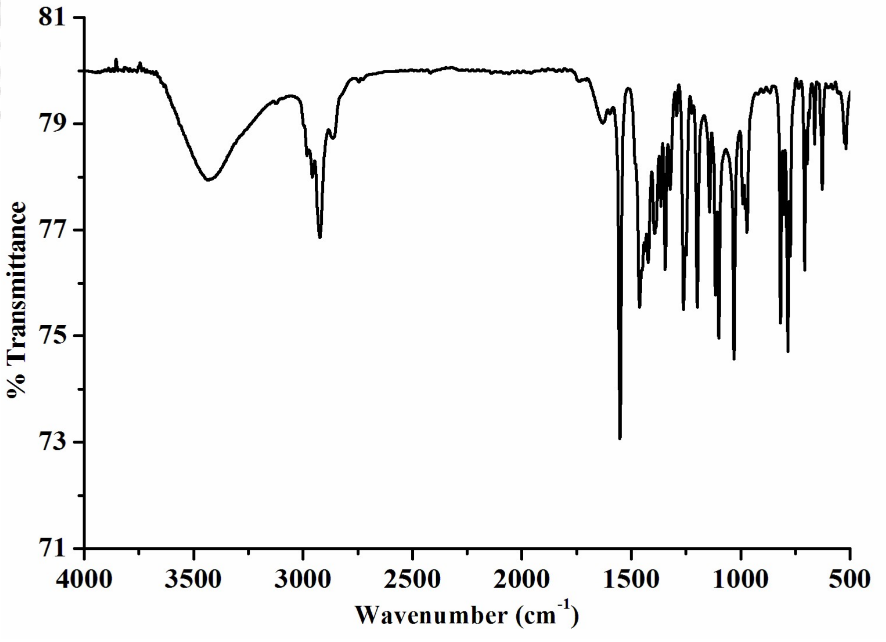

Figure A1.4: FT-IR spectrum of **TPz** in KBr.

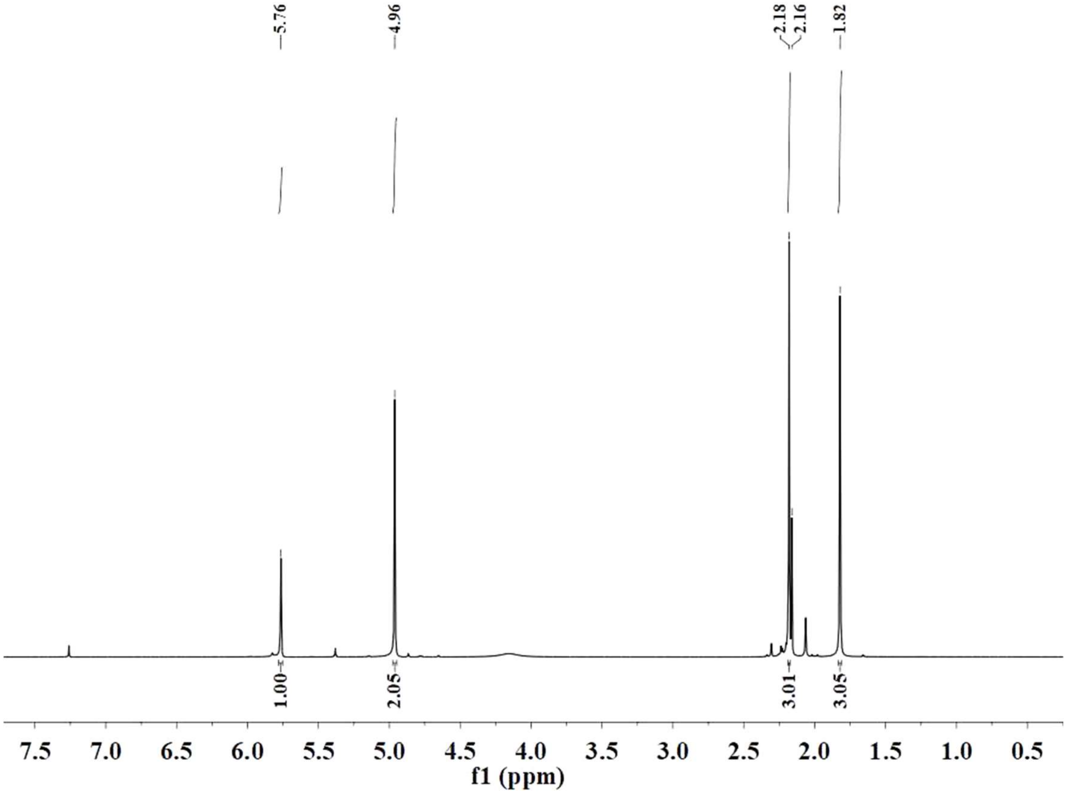

Figure A1.5: ^{1}H NMR spectrum of **TPz** in CDCl$_3$.

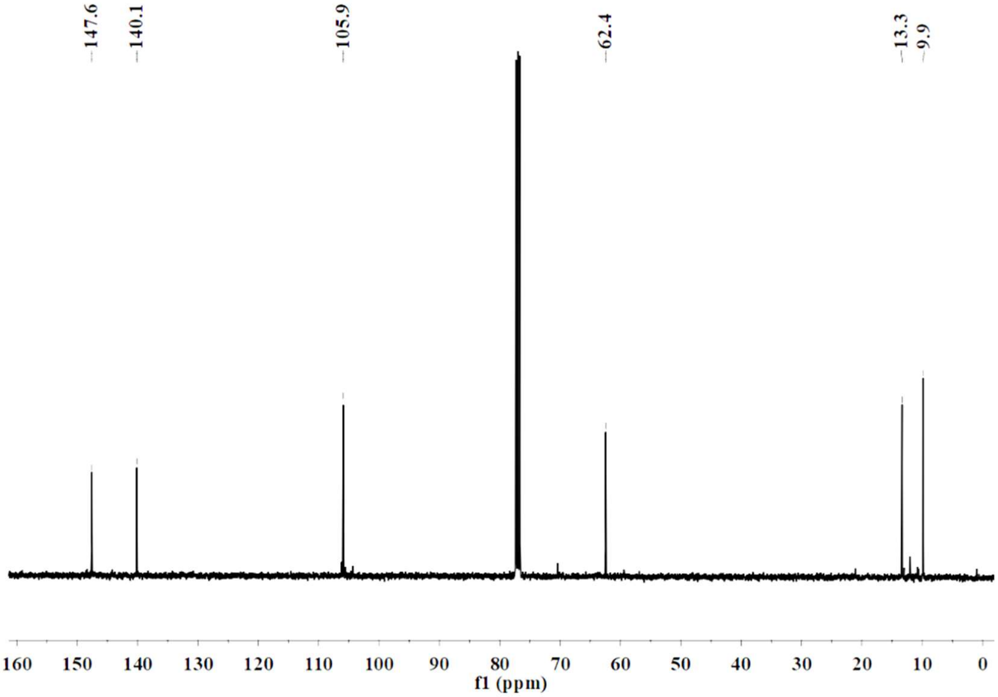

Figure A1.6: ^{13}C NMR spectrum of **TPz** in CDCl$_3$.

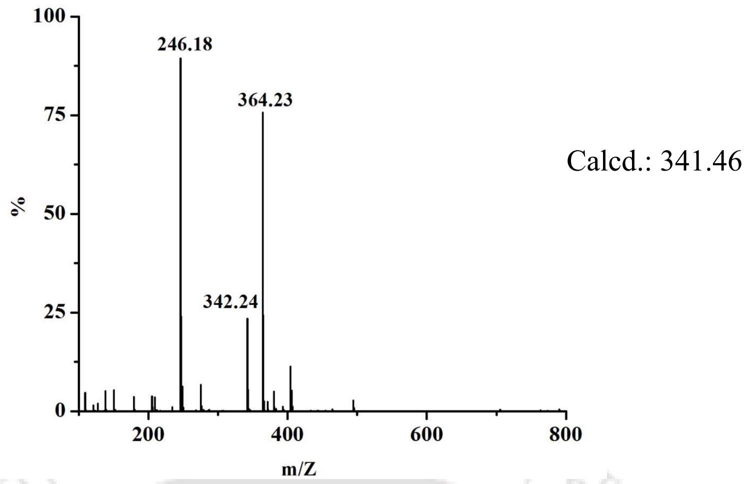

Figure A1.7: ESI-mass spectrum of ligand **TPz** in acetonitrile.

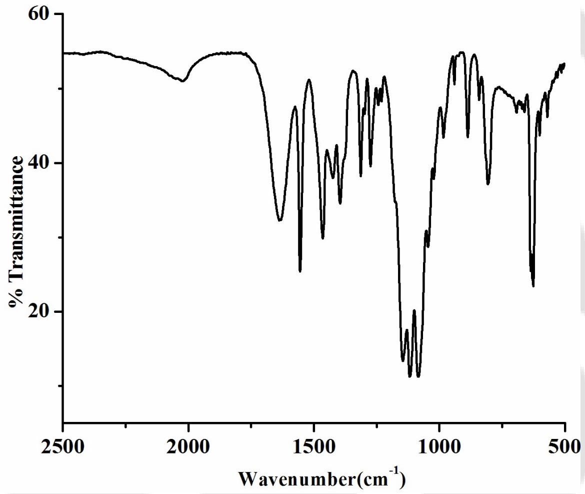

Figure A1.8: FT-IR spectrum of complex **2.1** in KBr.

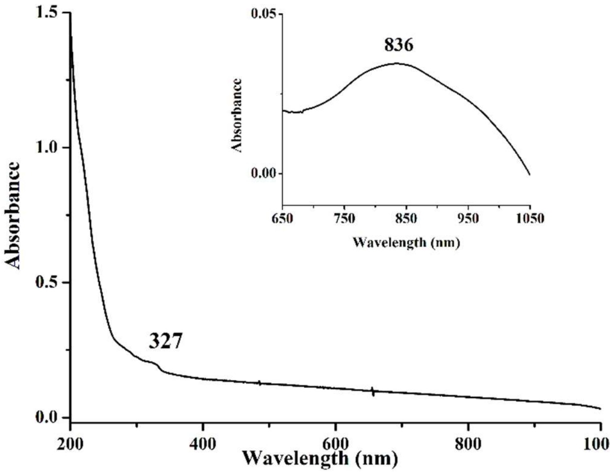

Figure A1.9: UV-visible spectrum of complex **2.1** in acetonitrile at room temperature.

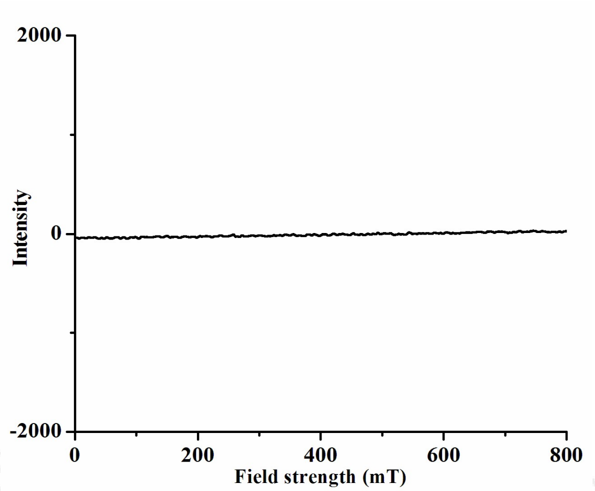

Figure A1.10: X-band EPR spectrum of complex **2.1** in acetonitrile at 77 K.

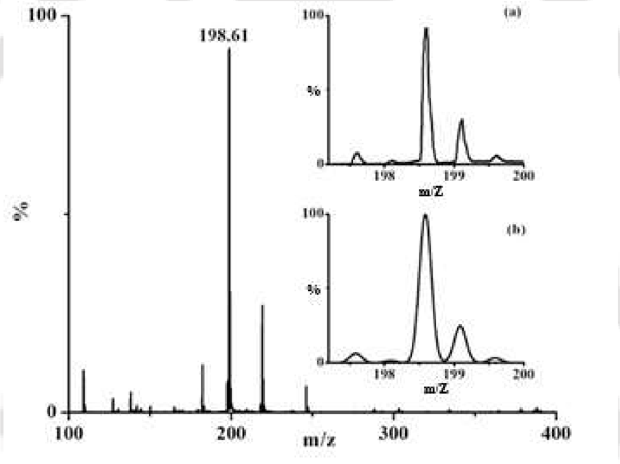

Calcd.: 198.58

Figure A1.11: ESI-mass spectrum of complex **2.1** in acetonitrile [Inset: (a) experimental and (b) simulated isotopic distribution pattern].

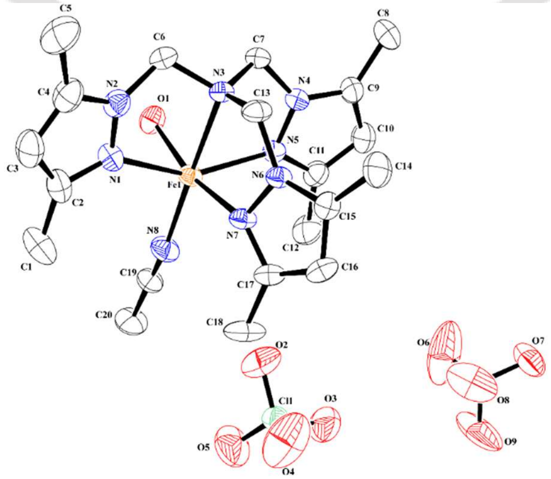

Figure A1.12: ORTEP diagram of complex **2.1** (30% thermal ellipsoid plot, H atoms are omitted for clarity).

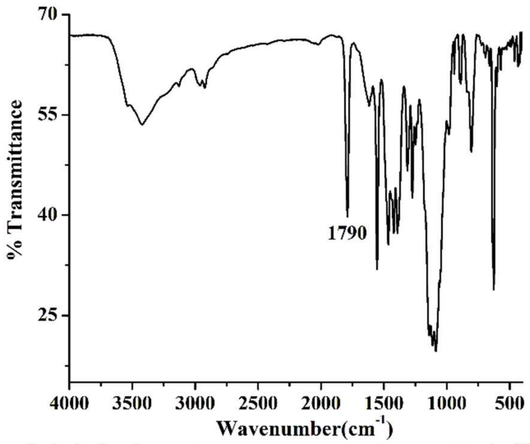

Figure A1.13: FT-IR spectrum of complex **2.2** in KBr pellet.

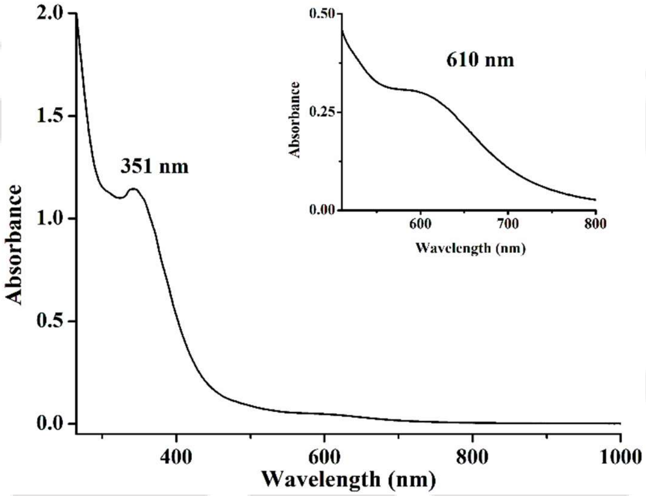

Figure A1.14: UV-visible spectrum of complex **2.2** in acetonitrile at room temperature.

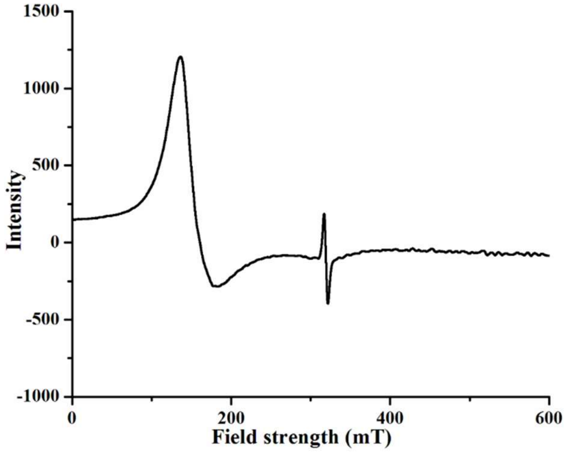

Figure A1.15: X-band EPR spectrum of complex **2.2** in methanol at 77 K (g ~ 4.11, 2.04) [Note: a very small amount impurity (< 0.5%) accounting for the isotropic signal near g ~ 2 in the EPR spectrum].

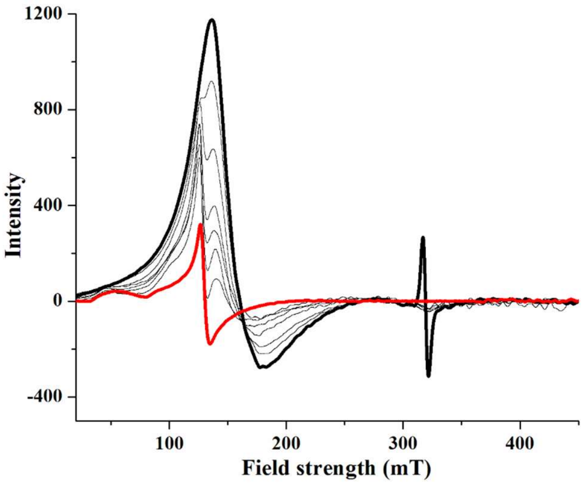

Figure **A1.16:** X-band EPR Spectra of reaction of complex **2.2** with O_2 at 77 K in methanol [Complex **2.2** (black) at g ~ 4.11 and 2.04, after O_2 addition final product (red) at g ~ 5.05].

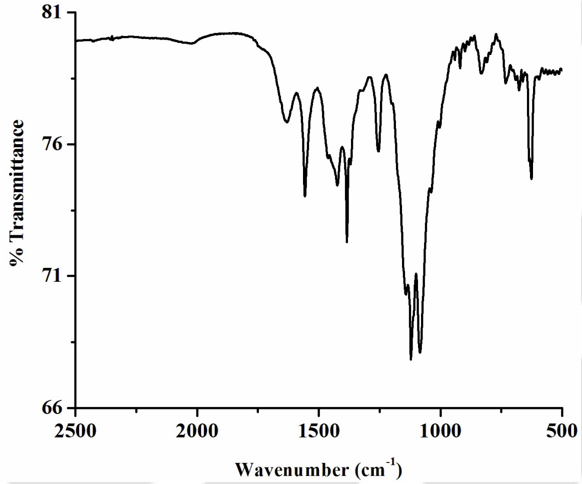

Figure A1.17: FT-IR spectrum of complex **2.3** in KBr.

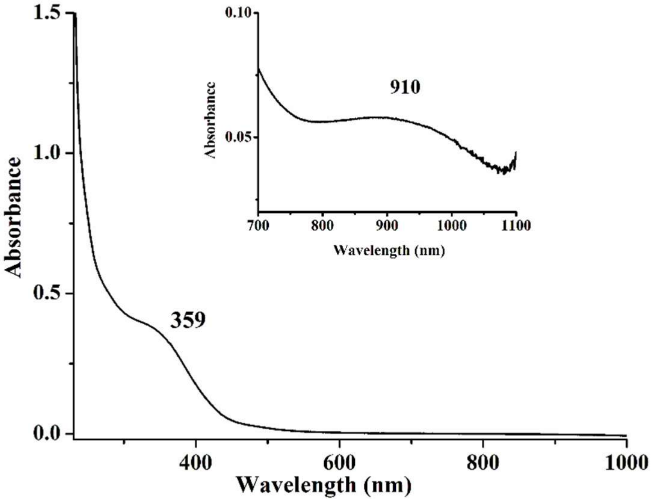

Figure A1.18: UV-visible spectrum of complex **2.3** in DMSO at room temperature.

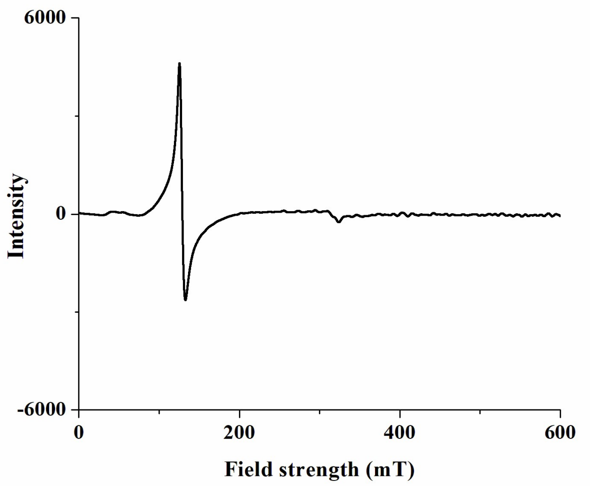

Figure A1.19: X-band EPR spectrum of complex **2.3** in DMSO at 77 K (g ~ 5.05).

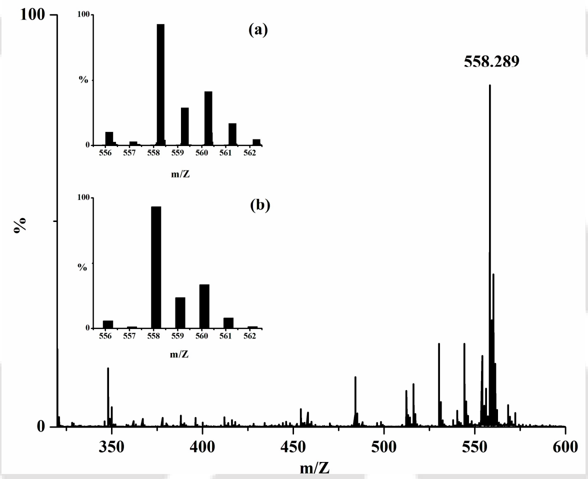

Calcd.: 558.104

Figure A1.20: ESI-mass spectrum of complex **2.3** in acetonitrile [Inset: (a) experimental and (b) simulated isotopic distribution pattern].

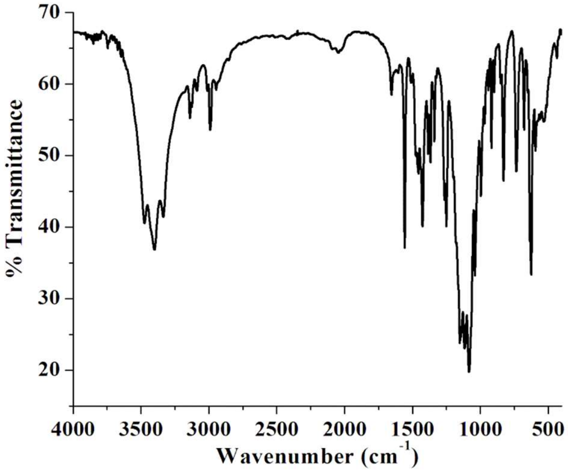

Figure A1.21: FT-IR spectrum of **L′** in KBr.

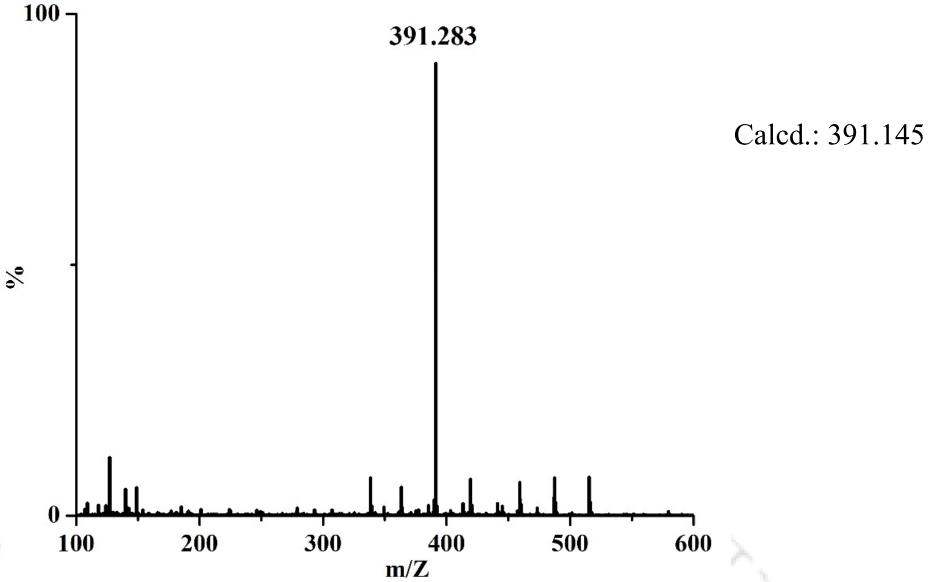

Figure A1.22: ESI-mass spectrum of **L′** in acetonitrile.

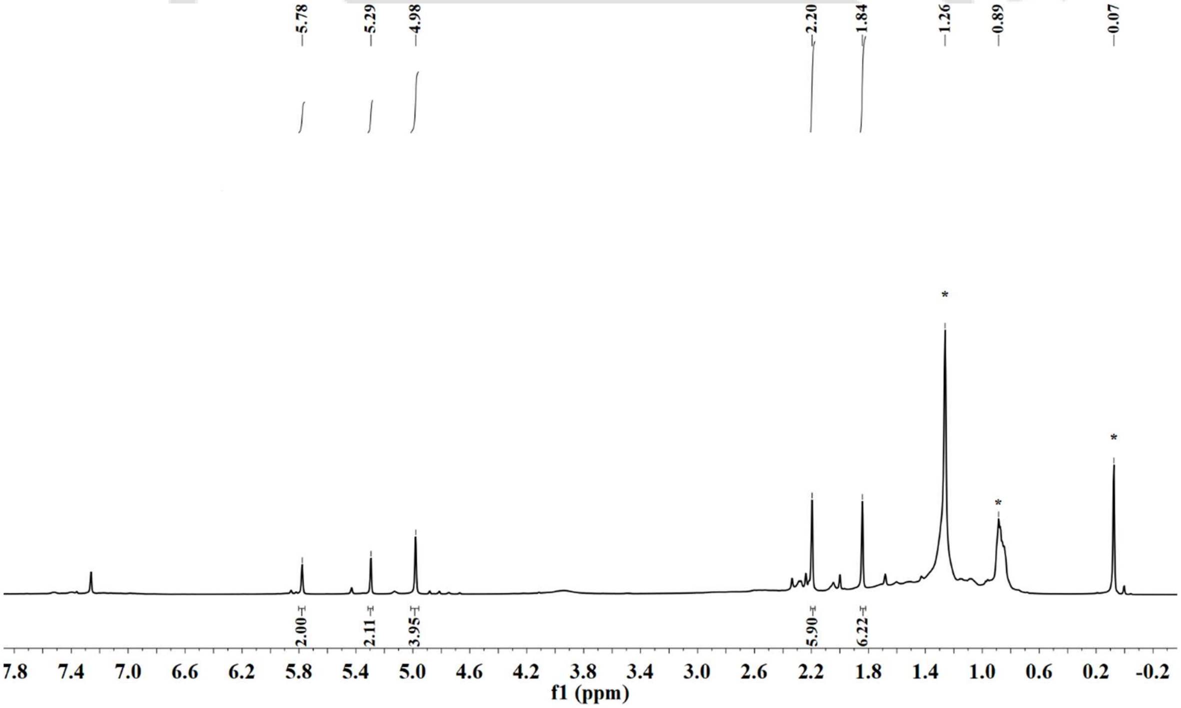

Figure A1.23: ^{1}H NMR spectrum of **L´** in $CDCl_3$ (* for solvent).

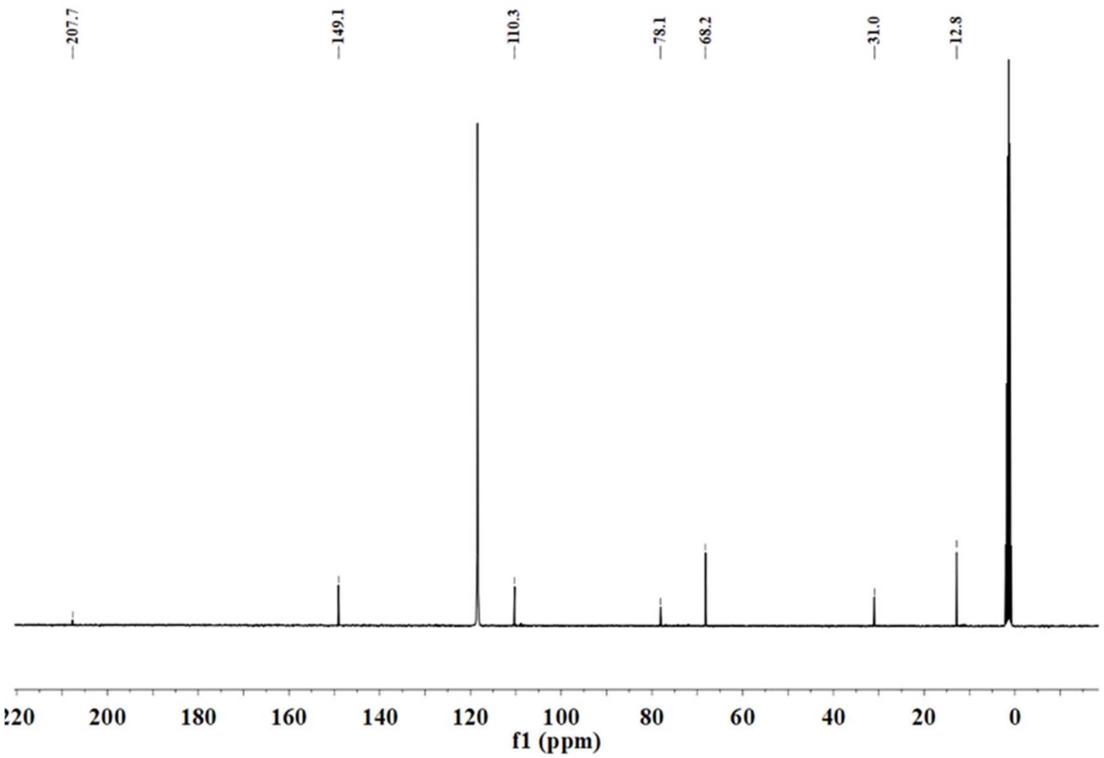

Figure A1.24: ^{13}C NMR spectrum of **L′** in CD_3CN.

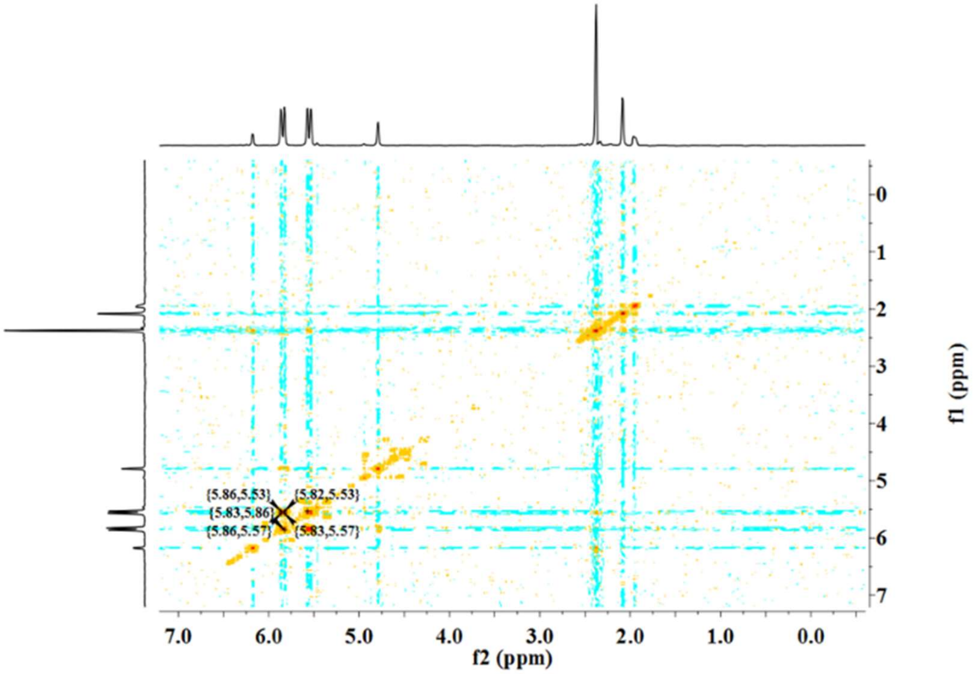

Figure A1.25: COSY NMR spectrum of **L′** in CD_3CN.

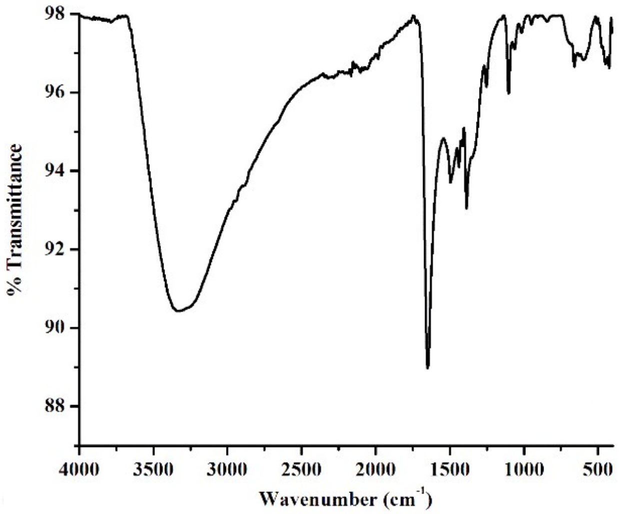

Figure A1.26: FT-IR spectrum of complex **2.4** in ATR.

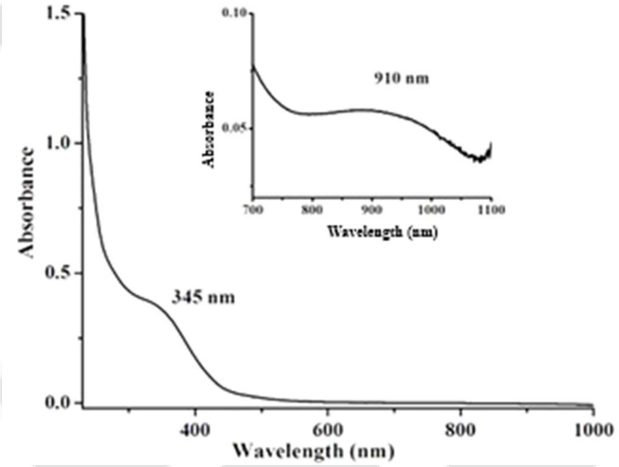

Figure A1.27: UV-visible spectrum of complex **2.4** in DMSO at room temperature.

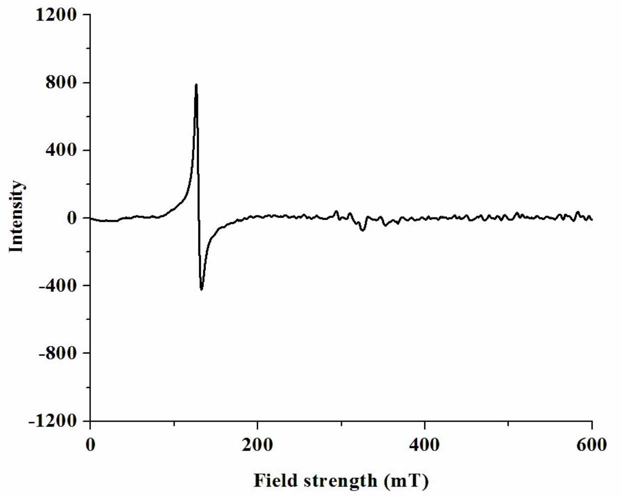

Figure A1.28: X-band EPR spectrum of complex **2.4** in DMSO at 77 K (g ~ 5.04).

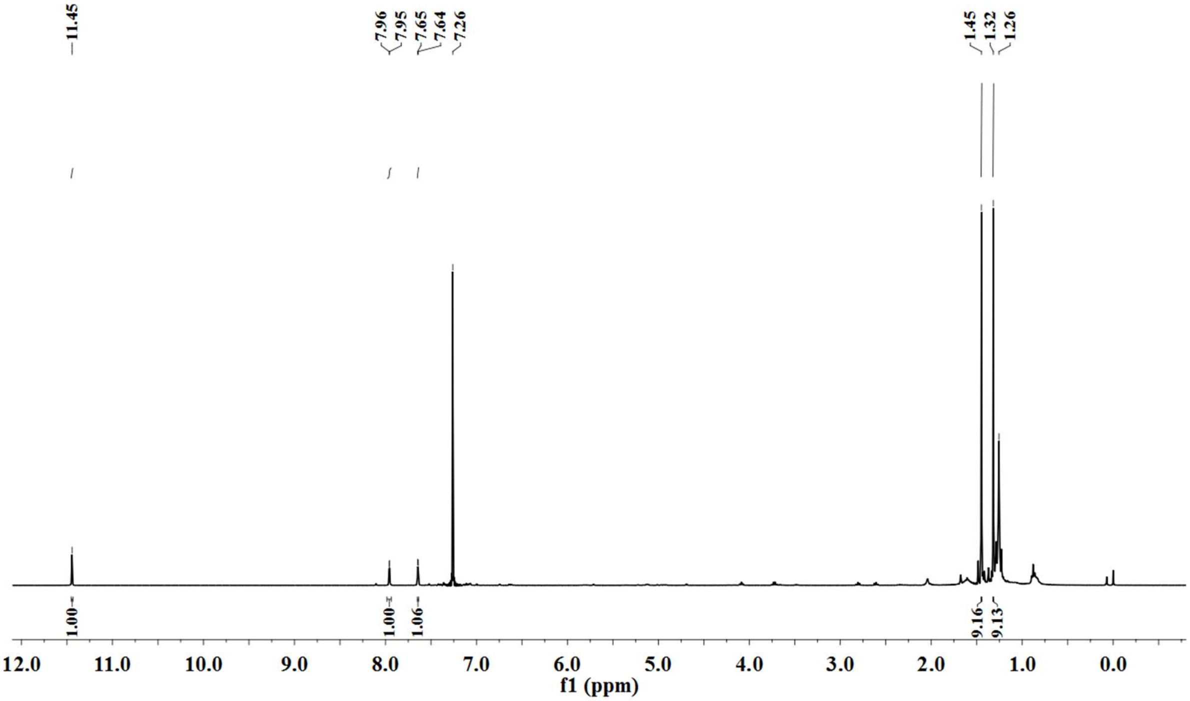

Figure A1.29: ^{1}H NMR spectrum of 2,4-di-*tert*-butyl-6-nitrophenol in $CDCl_3$.

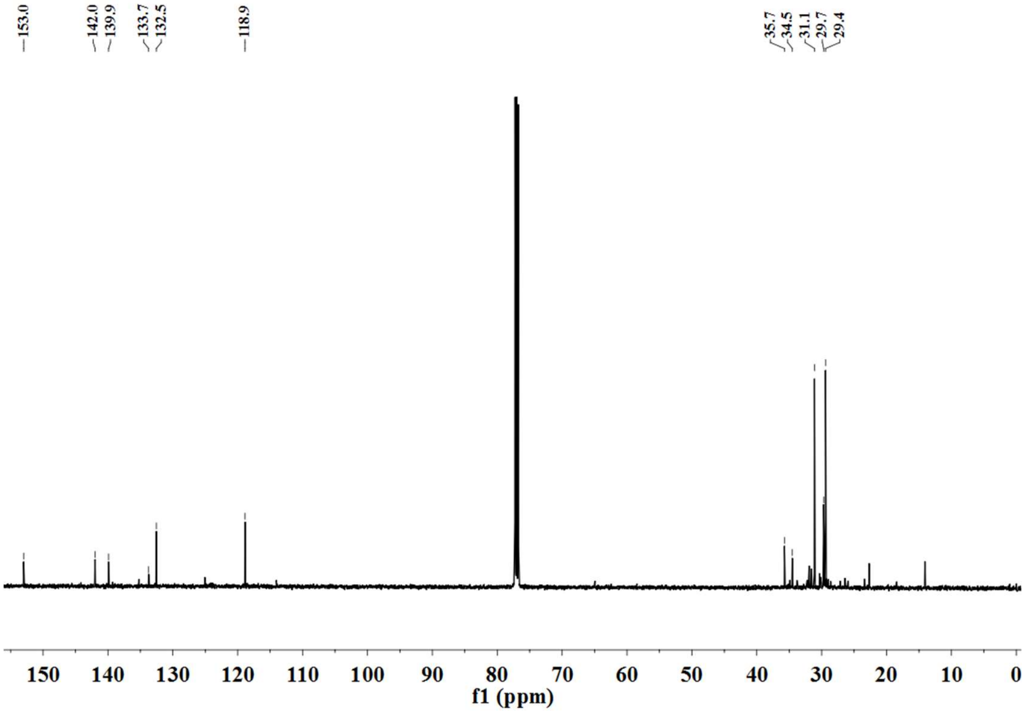

Figure A1.30: ^{13}C NMR spectrum of 2, 4-di-*tert*-butyl-6-nitrophenol in $CDCl_3$.

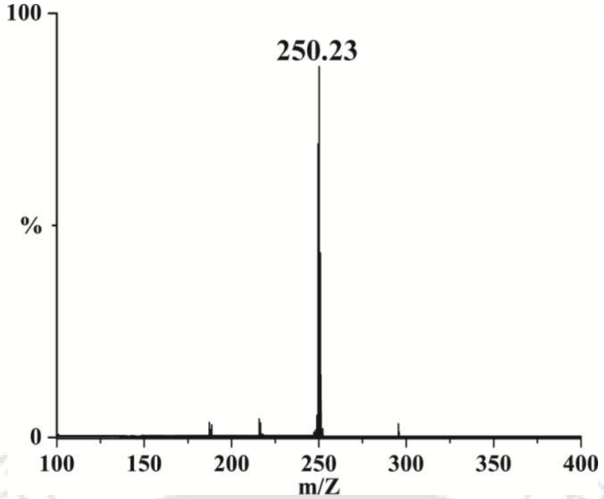

Calcd.: 251.15

Figure A1.31: ESI-mass spectrum of 2, 4-di-*tert*-butyl-6-nitrophenol in methanol.

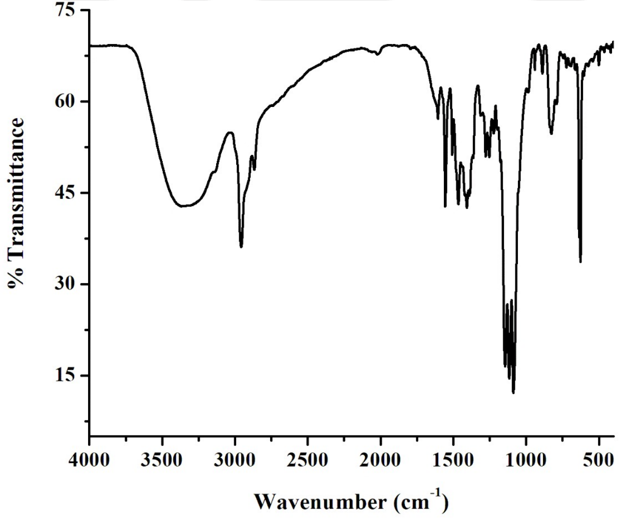

Figure A1.32: FT-IR spectrum of complex **2.5** in KBr.

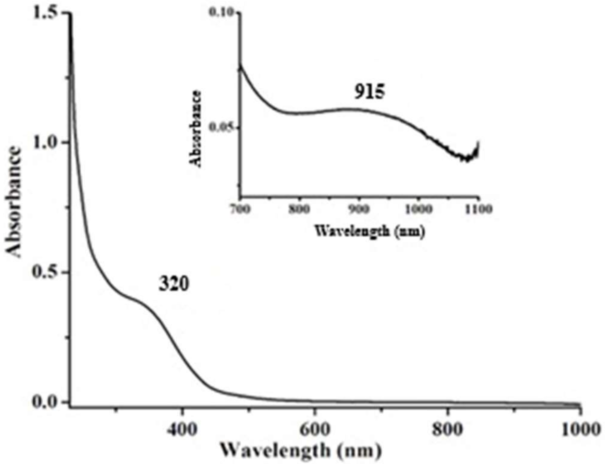

Figure A1.33: UV-visible spectrum of complex **2.5** in DMSO at room temperature.

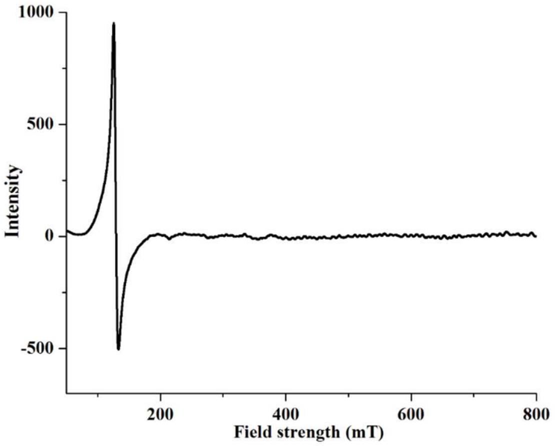

Figure A1.34: X-band EPR spectrum of complex **2.5** in DMSO at 77 K (g ~5.06).

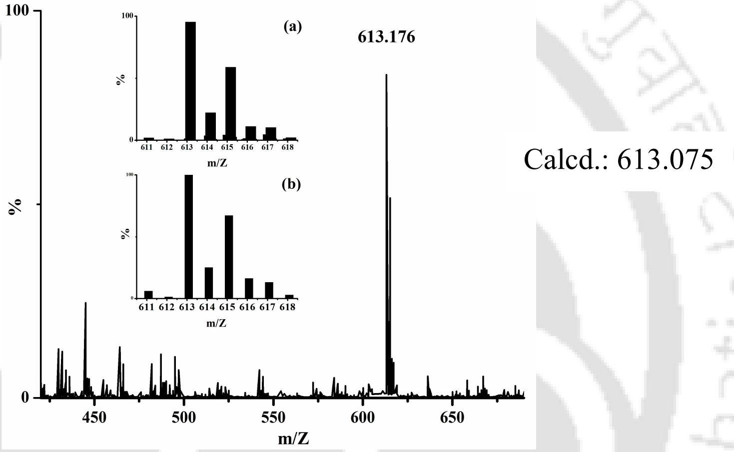

Figure A1.35: ESI-mass spectrum of complex **2.5** in acetonitrile [Inset: (a) experimental and (b) simulated isotopic distribution pattern].

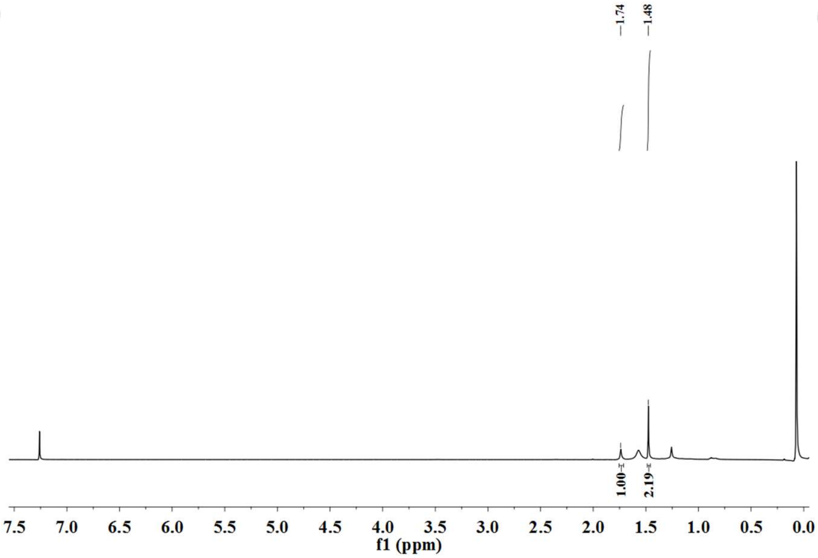

Figure A1.36: ^{1}H NMR spectrum of $(tmpH_2^+)(NO_3^-)$ in $CDCl_3$.

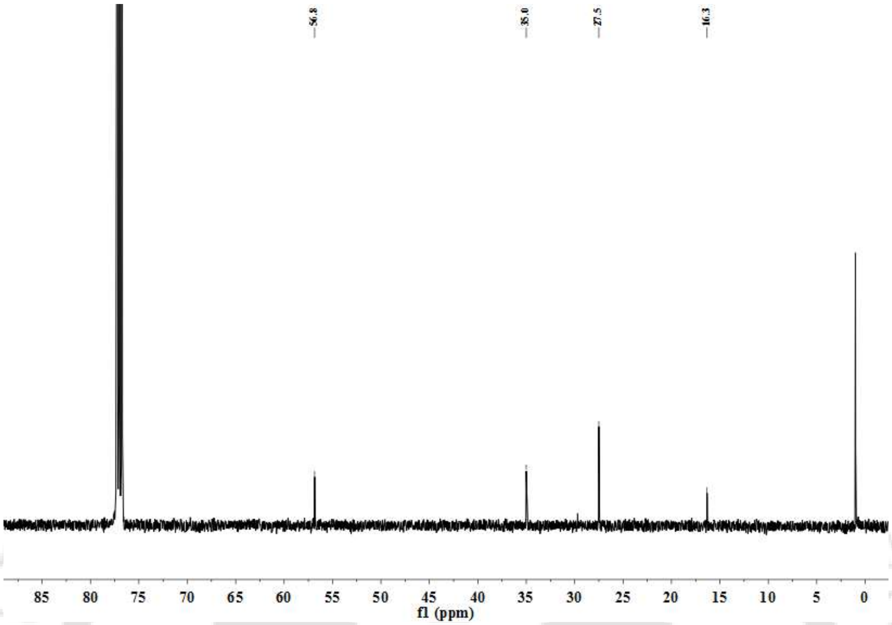

Figure A1.37: ^{13}C NMR spectrum of $(tmpH_2^+)(NO_3^-)$ in $CDCl_3$.

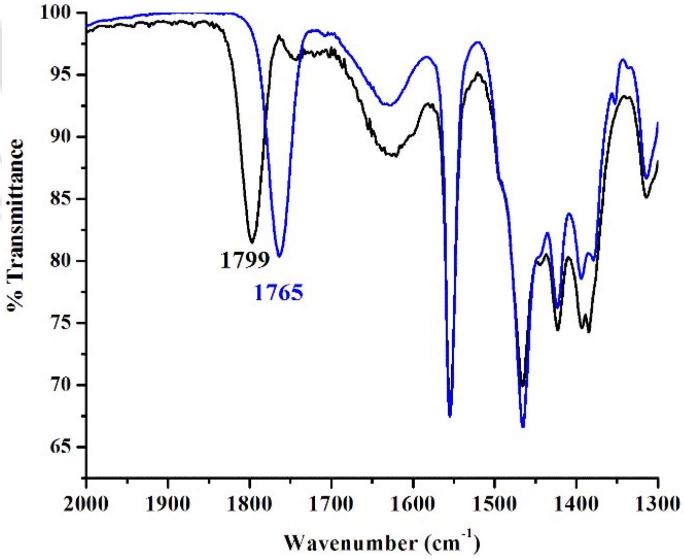

Figure A1.38: FT-IR spectra of reaction of complex **2.1** with natural abundance isotopes NO gas (black) and ^{15}NO gas (blue) in acetonitrile medium at room temperature.

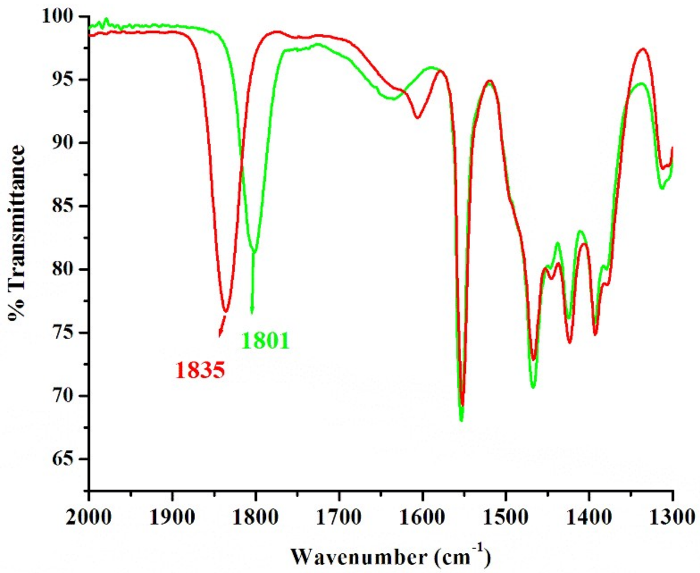

Figure A1.39: FT-IR spectra of O_2 reactivity of complex **2.2** $[Fe^{II}(TPz)(NO)(CH_3CN)]^{2+}$ (red) and ^{15}N labeled complex **2.2** $[Fe^{II}(TPz)(^{15}NO)(CH_3CN)]^{2+}$ (green) in acetonitrile medium at room temperature.

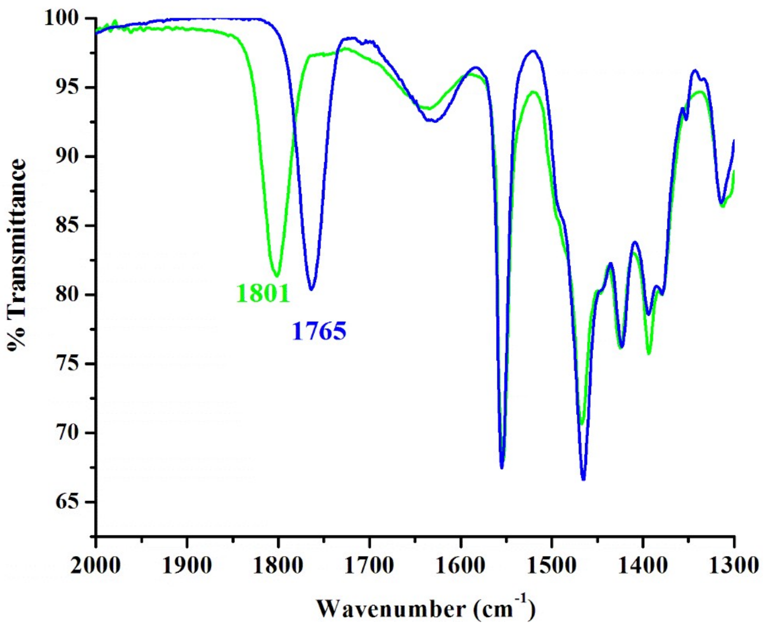

Figure A1.40: FT-IR spectra of the reaction of ^{15}N labeled complex **2.2** with O_2 in acetonitrile medium [^{15}N labeled complex **2.2** (blue), after O_2 addition (green)].

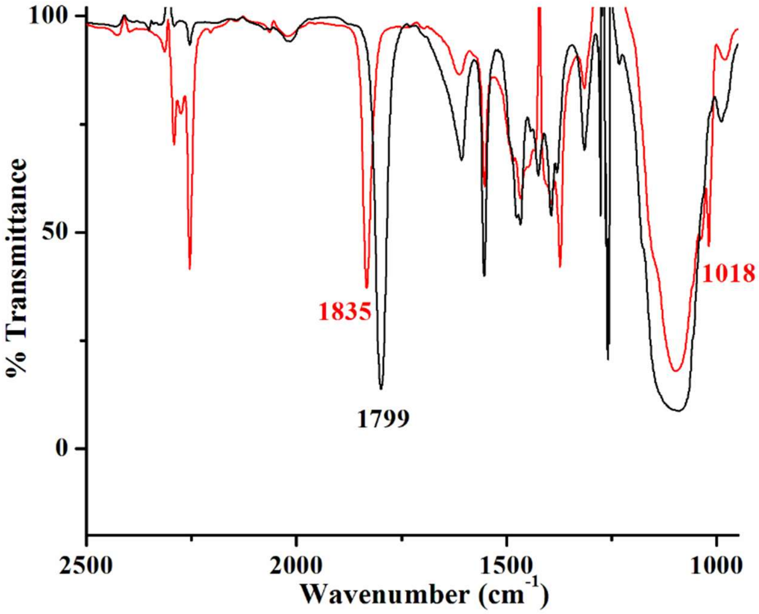

Figure A1.41: FT-IR spectra of the reaction complex **2.2** with $AgClO_4$ in acetonitrile-dichloromethane mixture (1:1 v/v).

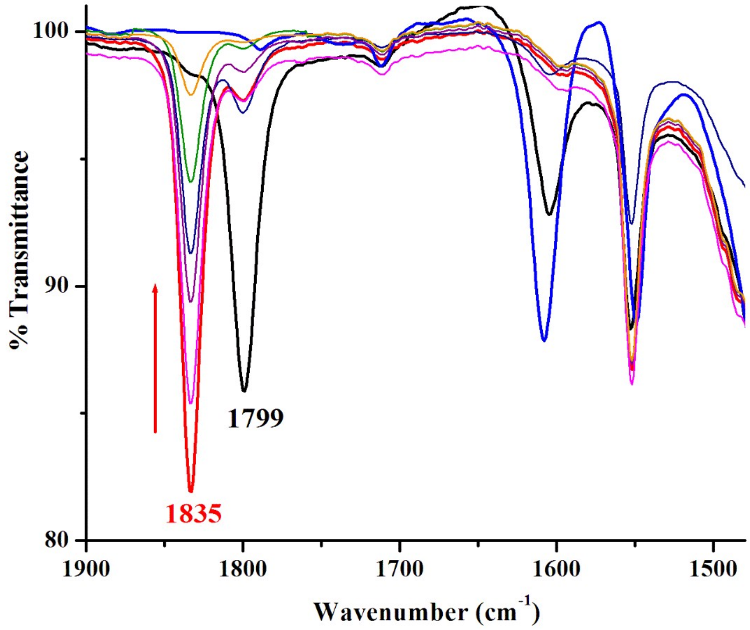

Figure A1.42: FT-IR decomposition spectra of $\{Fe(NO)\}^6$ intermediate in acetonitrile medium.

Table A1.1: Crystallographic data for complexes **2.1, 2.2, L′** and **$(\mathbf{tmpH_2^+})(\mathbf{NO_3^-})$**

	2.1	**2.2**	**L′**	**$(\mathbf{tmpH_2^+})(\mathbf{NO_3^-})$**
Formulae	$C_{20}H_{34}Cl_2N_8O_{10}Fe$	$C_{20}H_{30}Cl_2N_9O_9Fe$	$C_{15}H_{23}Cl_2N_7O_{10}$	$C_9H_{20}N_2O_3$
Mol. wt.	673.30	667.28	532.30	204.27
Crystal system	Triclinic	Monoclinic	Monoclinic	Orthorhombic
Space group	P -1	P 21/n	P 21	Pca21
Temperature /K	296(2)	101(2)	293(2)	293(2)
Wavelength /Å	0.71073	0.71073	0.71073	0.71073
a /Å	11.9018(6)	10.4501(6)	8.3825(5)	15.56(4)
b /Å	11.9774(6)	19.7521(12)	9.5056(5)	9.90(2)
c /Å	12.2326(6)	15.8247(9)	15.3798(8)	15.75(4)
α/°	84.555(3)	90	90	90
β/°	74.331(3)	91.422(4)	94.911(5)	90
γ/°	68.652(2)	90	90	90
V/ $Å^3$	1563.78(14)	3265.4(3)	1220.97(12)	2426(10)
Z	2	4	2	8
Density/Mgm^{-3}	1.430	1.357	1.448	1.118
Abs. Coeff. /mm^{-1}	0.714	0.682	0.328	0.083
Abs. correction	none	none	multi-scan	none
F(000)	700	1380	552	896
Total no. of reflections	5502	5764	3475	4258
Reflections, $I > 2\sigma(I)$	4355	3822	2853	2392
Max. 2θ/°	25.000	24.999	24.993	24.990
Ranges (h, k, l)	$-14 \leq h \leq 14$ $-14 \leq k \leq 14$ $-14 \leq l \leq 14$	$-12 \leq h \leq 12$ $-23 \leq k \leq 23$ $-18 \leq l \leq 18$	$-9 \leq h \leq 7$ $-10 \leq k \leq 11$ $-17 \leq l \leq 18$	$-18 \leq h \leq 18$ $-11 \leq k \leq 11$ $-18 \leq l \leq 18$
Complete to 2θ (%)	1.000	1.000	1.000	0.999
Refinement method	Full-matrix least-squares on F^2	Full-matrix least-squares on F^2	Full-matrix least-squares on F^2	Full-matrix least-squares on F^2
Goof (F^2)	1.012	1.024	1.026	1.023

R indices [$I > 2\sigma(I)$]	0.0564	0.0770	0.0641	0.0725
R indices (all data)	0.0723	0.1158	0.0780	0.1360

Table A1.2: Selected bond lengths (Å) of complexes **2.1, 2.2, L′** and **(tmpH$_2^+$)(NO$_3^-$)**

Atoms	**2.1**	**2.2**	**L′**	**(tmpH$_2^+$)(NO$_3^-$)**
Fe1-N1	2.161(4)	2.101(5)		
N1-N2	1.365(6)	1.354(6)	1.370(8)	
Fe1-N3	2.293(4)	2.330(4)		
Fe1-N8	2.118(5)	1.732(6)		
N8-O1		1.13(1)		
Fe1-N9		2.195(5)		
Fe1-O1	2.100(3)			
C1-C2	1.48(1)	1.476(9)	1.49(1)	1.549(1)
C2-C3	1.40(1)	1.395(9)	1.36(1)	
C3-C4	1.358(9)	1.379(9)	1.36(1)	
N1-C2	1.332(6)	1.343(8)		
N2-C2			1.357(9)	
Cl1-O3	1.417(7)	1.424(9)	1.36(1)	
Cl2-O7	1.412(5)	1.378(8)	1.372(7)	
N2-O1			1.50(1)	1.226(8)
N3-O1			1.442(9)	
N1-C1				1.552(1)
C1-C2				1.549(1)
C4-C5				1.563(13)
C5-C6				1.533(14)
C6-C7				1.511(11)
N2-O2				1.250(9)

Table A1.3: Selected bond angles (˚) of complexes **2.1, 2.2, L′** and **(tmpH$_2^+$)(NO$_3^-$)**

Atoms	**2.1**	**2.2**	**L′**	**(tmpH$_2^+$)(NO$_3^-$)**
N1-Fe1-N3	76.8(1)	76.0(2)		
N3-Fe1-N5	76.4(1)	75.3(2)		
N3-Fe1-N7	77.6(1)	77.1(2)		
N1-Fe1-N8	103.9(2)	104.3(2)		
Fe1-N8-O1		174.2(6)		
N1-Fe1-N9		86.2(2)		
N1-Fe1-O1	87.4(1)			

O3-Cl1-O4	106.6(4)	96.6(6)	109.2(7)	
O7-Cl2-O8	112.6(4)	116.5(7)	112.2(5)	
O1-N3-O2			117.9(6)	
N3-C7-N6			113.9(6)	
C6-N6-C8			118.3(6)	
N1-C1-C4				107.8(7)
C1-C4-C5				112.8(8)
C4-C5-C6				109.9(8)
O1-N2-O2				124.0(9)
O1-N2-O3				119.0(9)

Appendix II

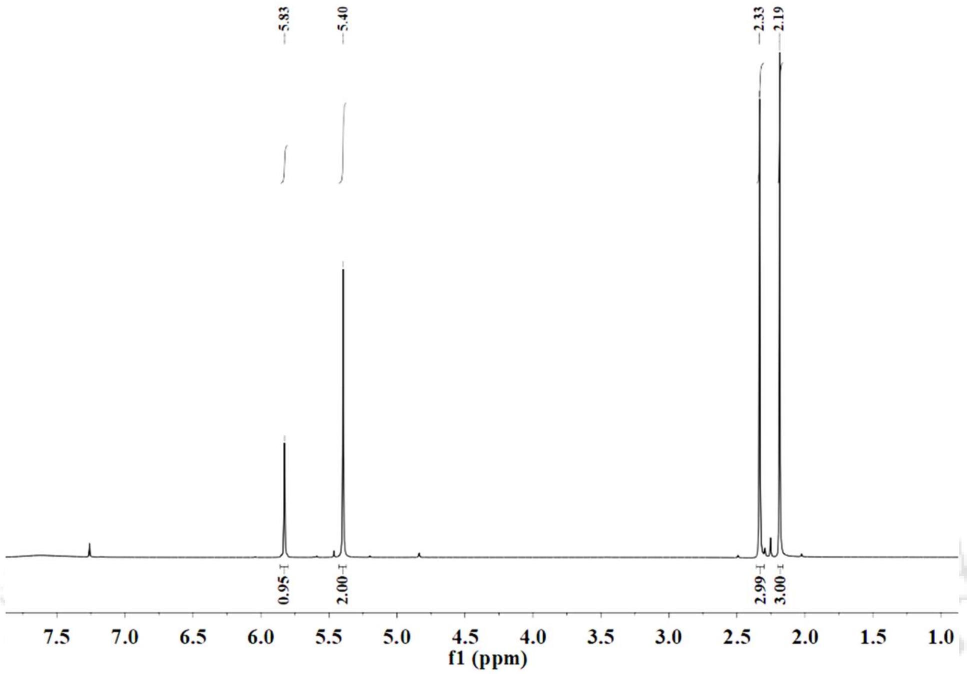

Figure A2.1: ^{1}H NMR spectrum of 1-(hydroxymethyl)-3,5-dimethyl-1-pyrazole in $CDCl_3$.

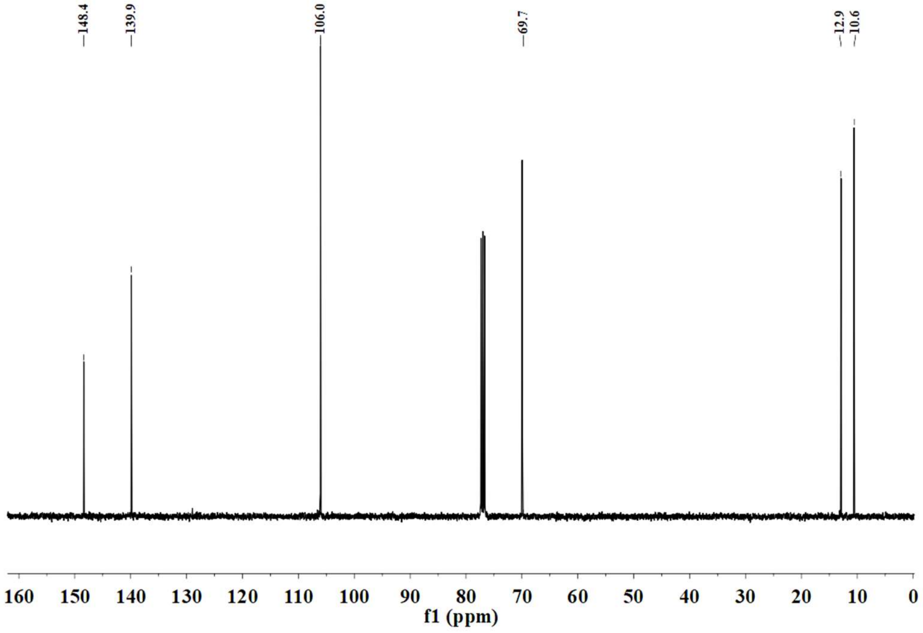

Figure A2.2: ^{13}C NMR spectrum of 1-(hydroxymethyl)-3,5-dimethyl-1-pyrazole in $CDCl_3$.

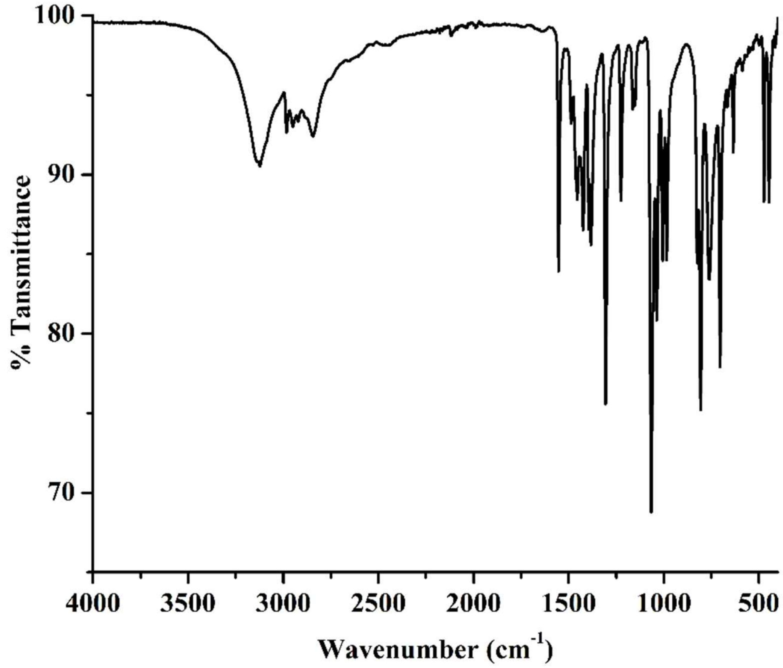

Figure A2.3: FT-IR spectrum of 1-(hydroxymethyl)-3,5-dimethyl-1-pyrazole in ATR probe.

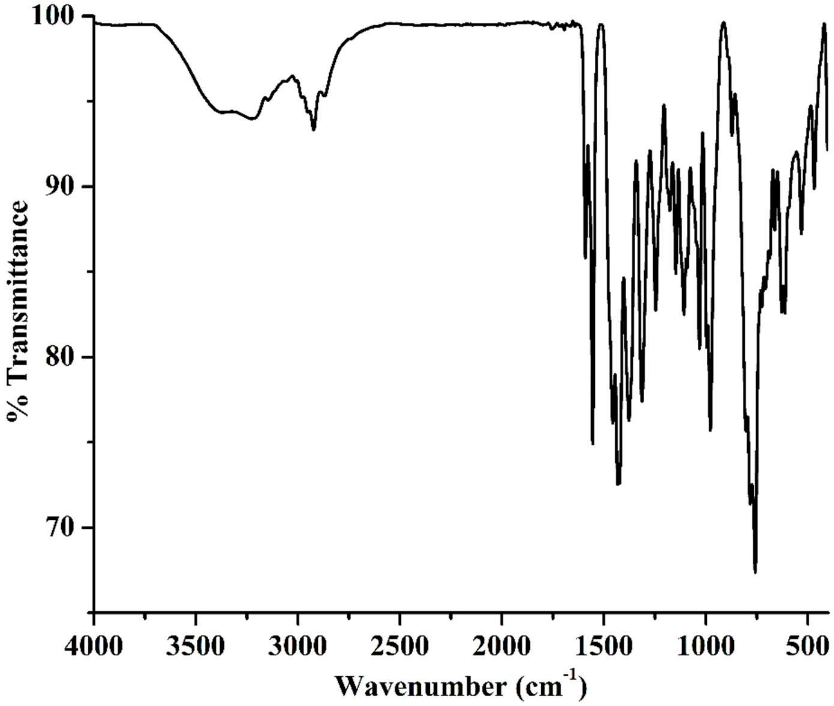

Figure A2.4: FT-IR spectrum of **Pz$_2$Py** in ATR probe.

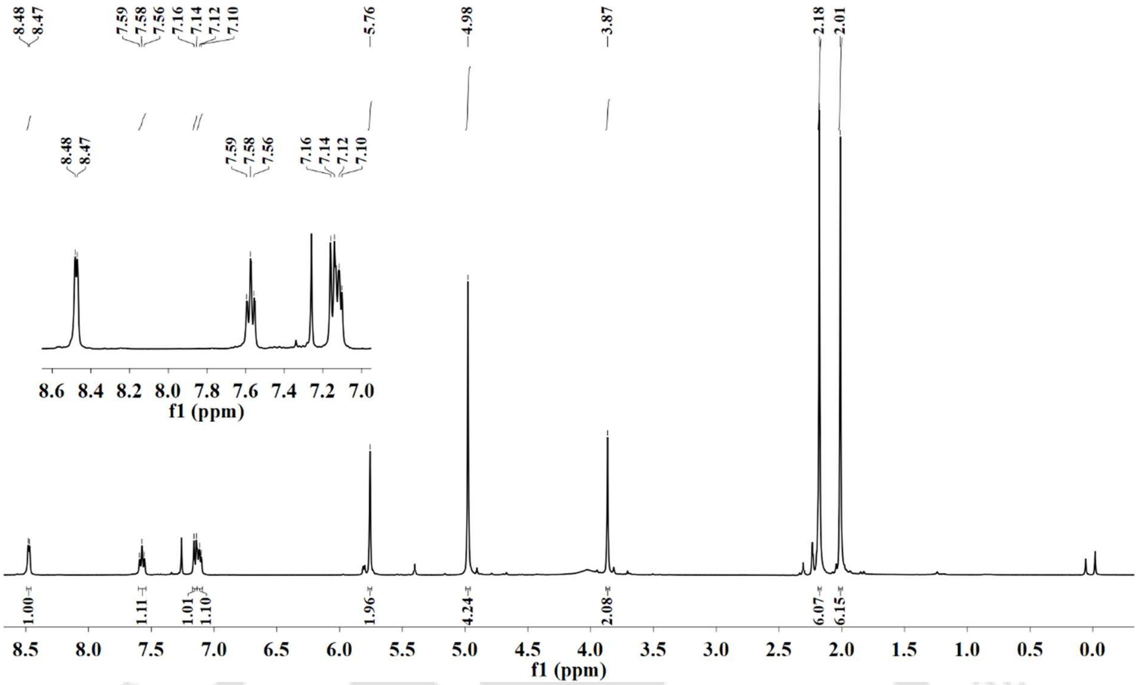

Figure A2.5: ^{1}H NMR spectrum of **Pz$_2$Py** in CDCl$_3$.

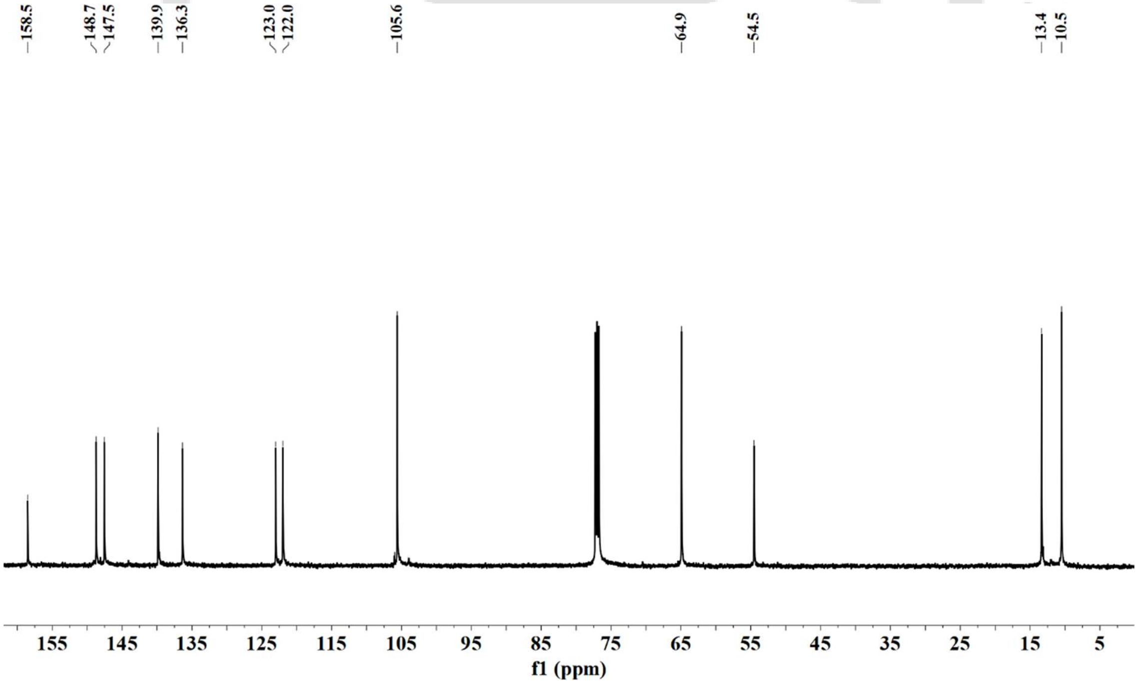

Figure A2.6: ^{13}C NMR spectrum of **Pz$_2$Py** in CDCl$_3$.

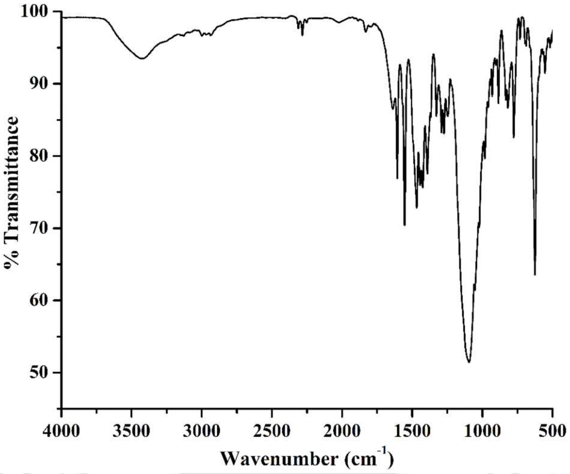

Figure A2.7: FT-IR spectrum of complex **3.1** in ATR probe.

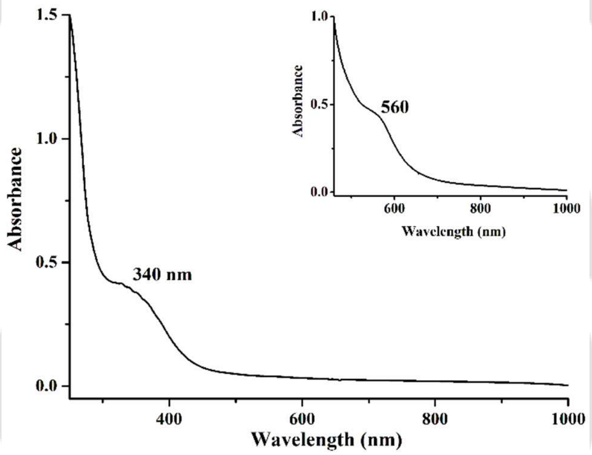

Figure A2.8: UV-visible spectrum of complex **3.1** in acetonitrile at room temperature.

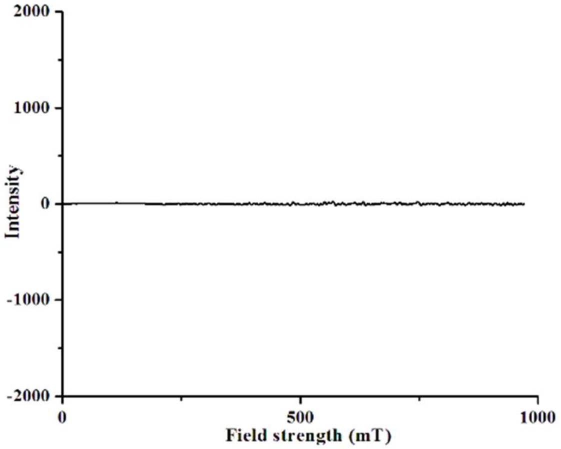

Figure A2.9: X-band EPR spectrum of complex **3.1** in acetonitrile at 77 K.

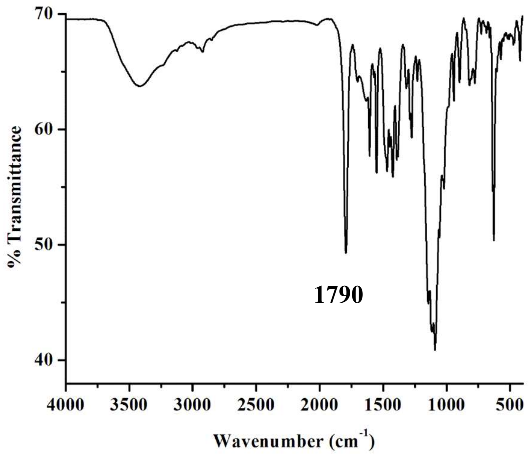

Figure A2.10: FT-IR spectrum of complex **3.2a** in KBr.

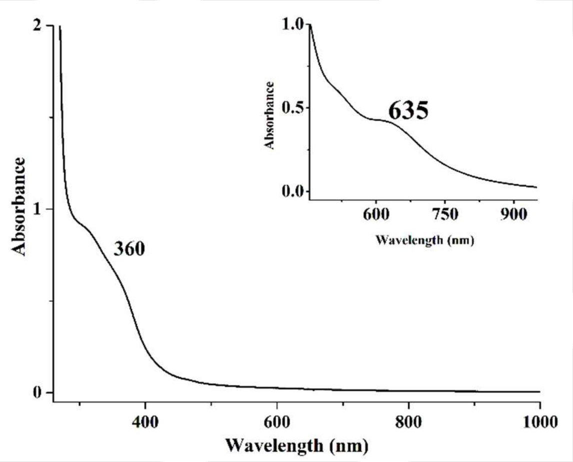

Figure A2.11: UV-visible spectrum of complex **3.2a** in acetonitrile at room temperature.

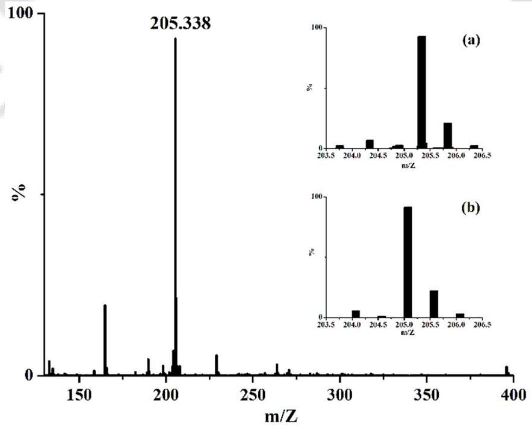

Calcd.: 205.069

Figure A2.12: ESI-mass spectrum of complex **3.2a** in acetonitrile. [Inset: (a) experimental and (b) simulated isotopic distribution pattern].

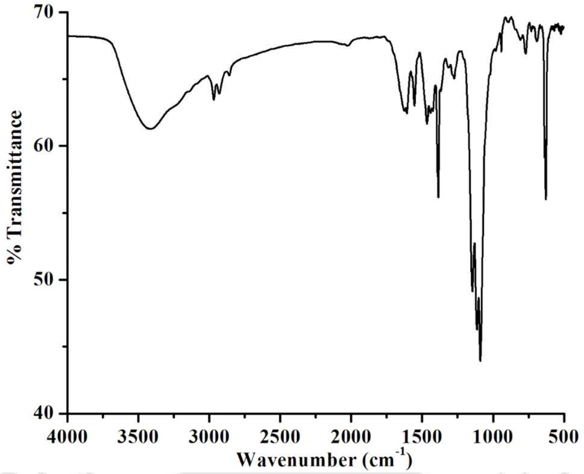

Figure A2.13: FT-IR spectrum of complex **3.3a** in KBr.

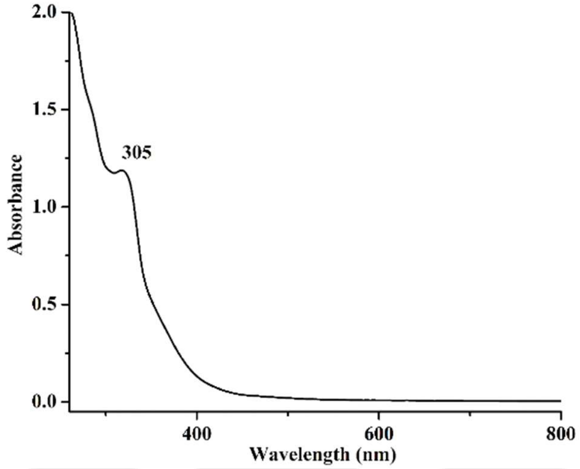

Figure A2.14: UV-visible spectrum of complex **3.3a** in acetonitrile at room temperature.

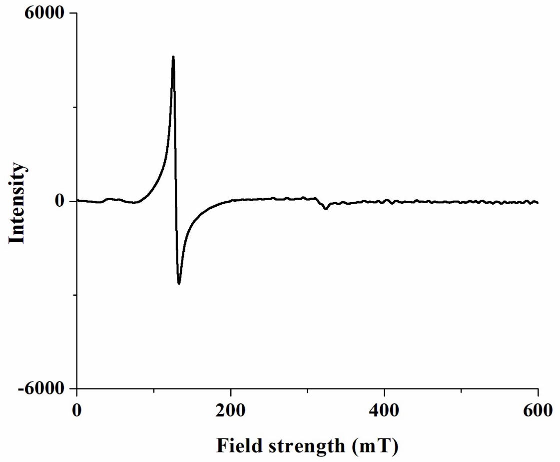

Figure A2.15: X-band EPR spectrum of complex **3.3a** in acetonitrile at 77 K (g ~ 5.19).

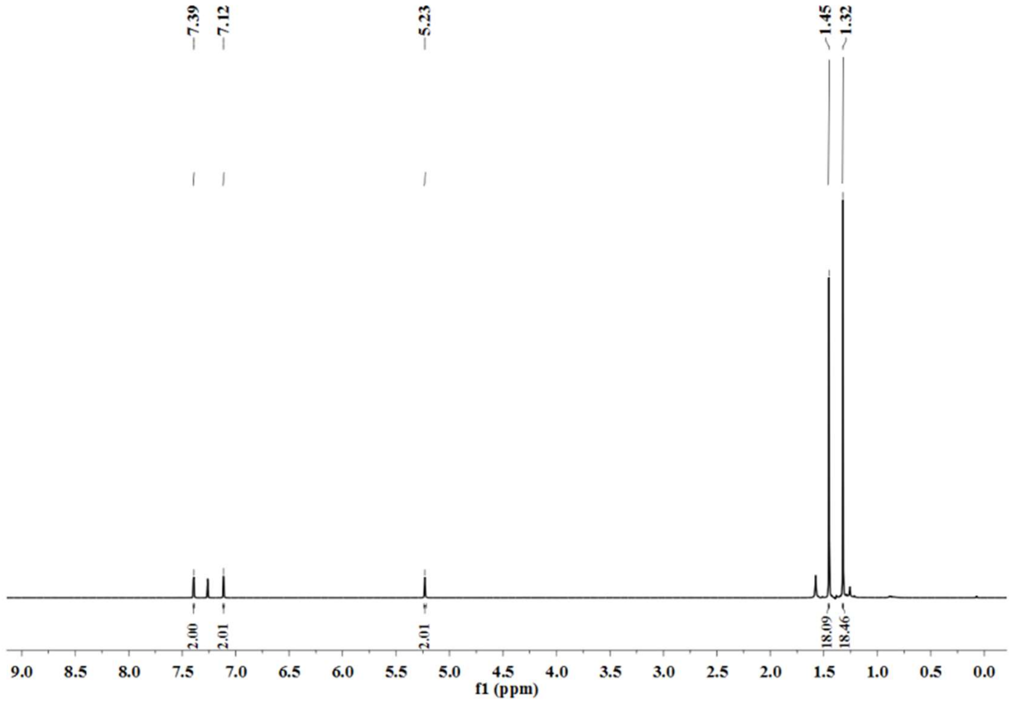

Figure A2.16: ^{1}H NMR spectrum of *bis*phenol in $CDCl_3$.

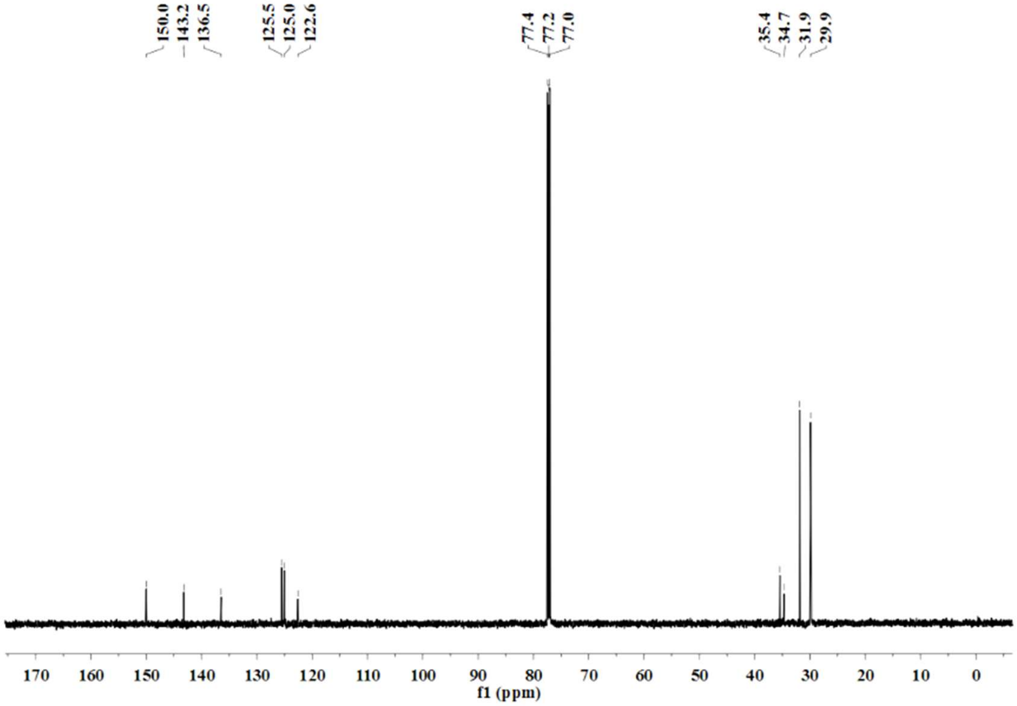

Figure A2.17: ^{13}C NMR spectrum of *bis*phenol in $CDCl_3$.

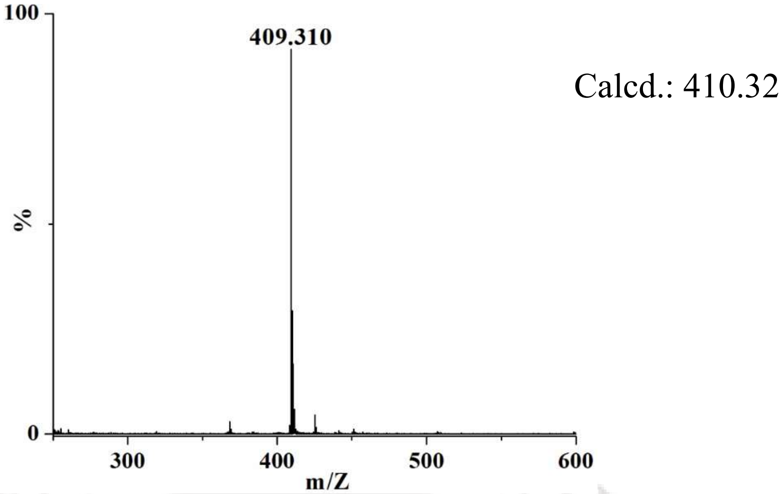

Figure A2.18: ESI-mass spectrum of *bis*phenol in acetonitrile.

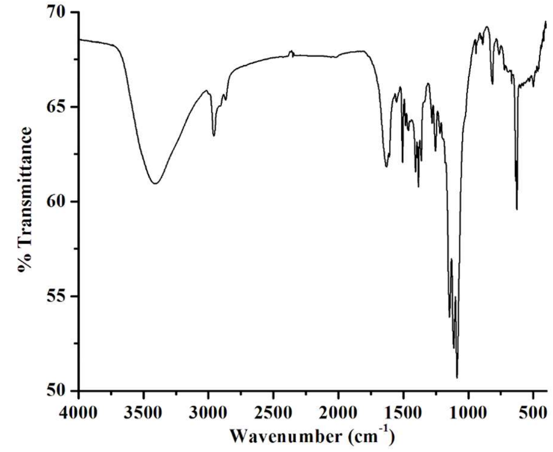

Figure A2.19: FT-IR spectrum of complex **3.4a** in KBr.

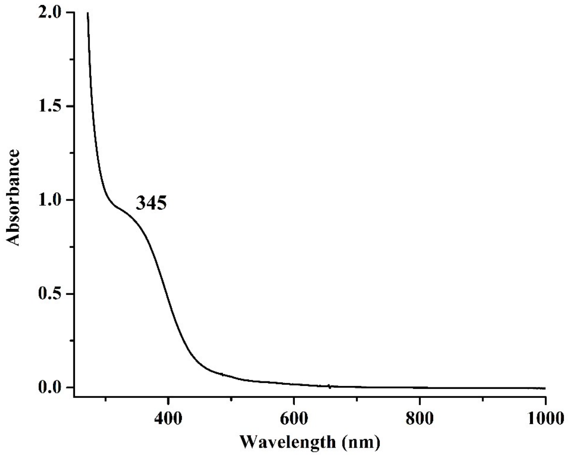

Figure A2.20: UV-visible spectrum of complex **3.4a** in acetonitrile at room temperature.

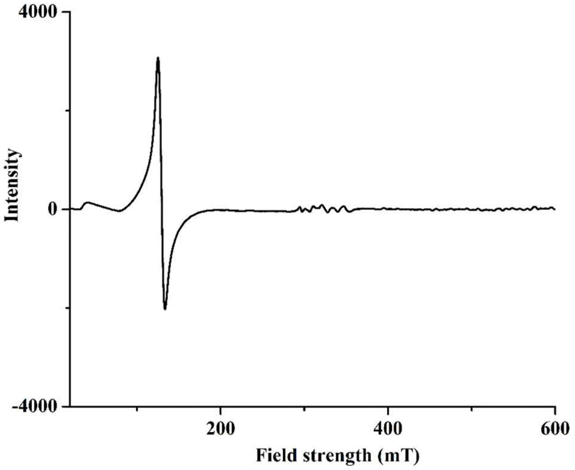

Figure A2.21: X-band EPR spectrum of complex **3.4a** in methanol at 77 K (g ~ 5.23).

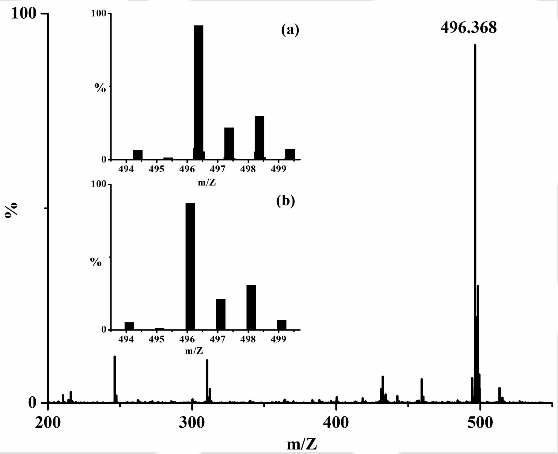

Calcd.: 496.092

Figure A2.22: ESI-mass spectrum of complex **3.4a** in methanol. [Inset: (a) experimental and (b) simulated isotopic distribution pattern].

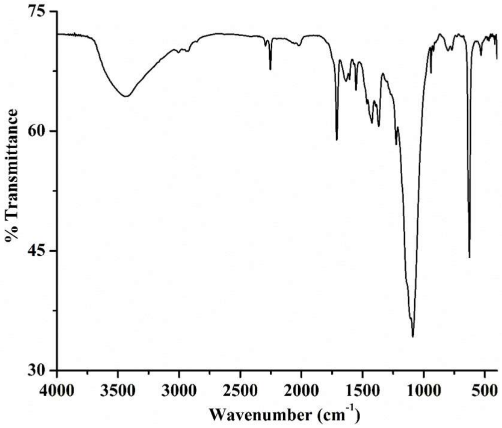

Figure A2.23: FT-IR spectrum of complex **3.2b** in KBr.

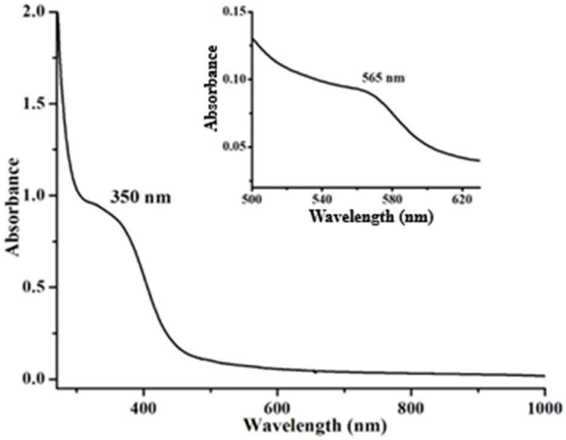

Figure A2.24: UV-visible spectrum of complex **3.2b** in acetonitrile at room temperature.

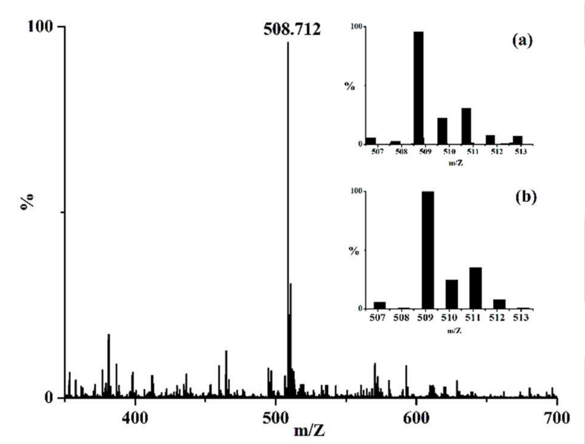

Calcd.: 509.092

Figure A2.25. ESI-mass spectrum of complex **3.2b** in acetonitrile. [Inset: (a) experimental and (b) simulated isotopic distribution pattern].

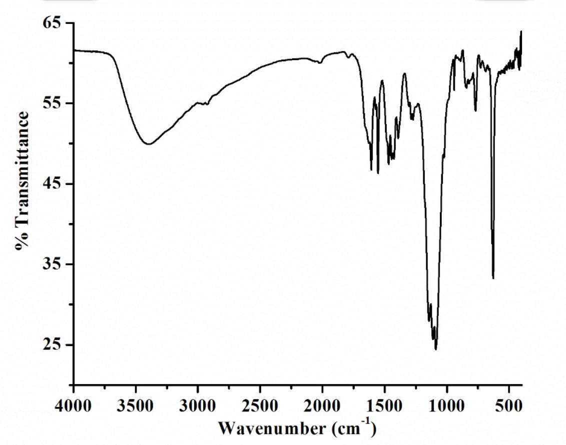

Figure A2.26: FT-IR spectrum of complex **3.3b** in KBr.

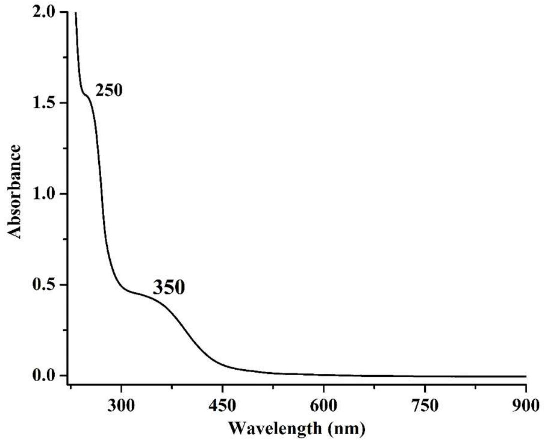

Figure A2.27: UV-visible spectrum of complex **3.3b** in acetonitrile at room temperature.

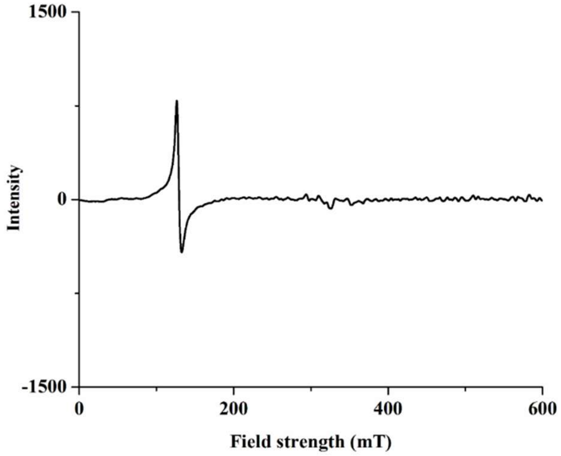

Figure A2.28: X-band EPR spectrum of complex **3.3b** in acetonitrile at 77 K (g ~ 5.21).

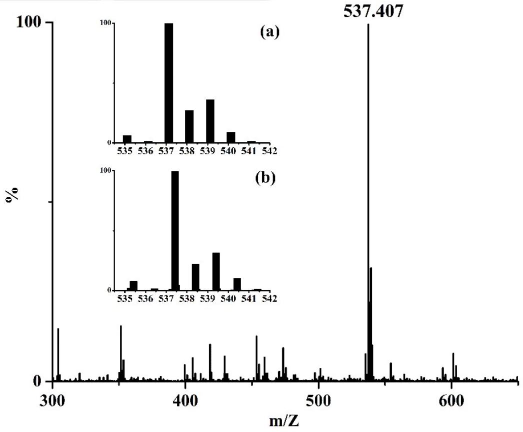

Calcd.: 537.119

Figure A2.29: ESI-mass spectrum of complex **3.3b** in acetonitrile [Inset: (a) experimental and (b) simulated isotopic distribution pattern].

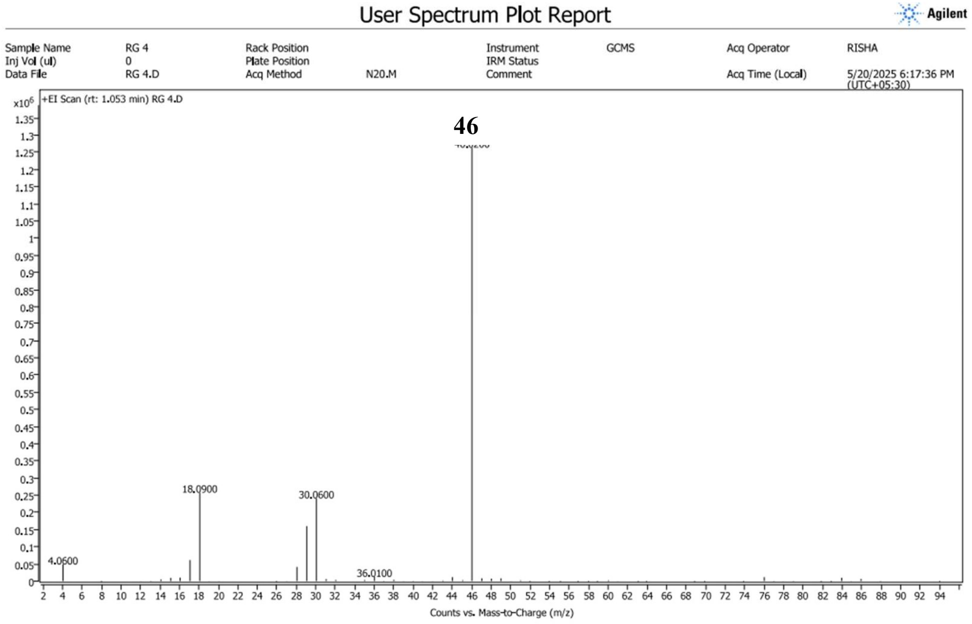

User Spectrum Plot Report

Sample Name	RG 4	Rack Position		Instrument	GCMS	Acq Operator	RISHA
Inj Vol (ul)	0	Plate Position		IRM Status			
Data File	RG 4.D	Acq Method	N20.M	Comment		Acq Time (Local)	5/20/2025 6:17:36 PM (UTC+05:30)

Figure A2.30: GC-Mass of the headspace gas obtained from the reaction of complex **3.2b** with O_2 in acetonitrile medium after 2 hr.

Table A2.1: Crystallographic data for complexes **3.1 and 3.2a**

Complex	**3.1**	**3.2a**
Formulae	$C_{20}H_{29}\ Cl_2N_7O_9Fe$	$C_{19}H_{28}FeN_7O_2$
Mol. Wt.	638.25	641.23
Crystal system	Monoclinic	Orthorhombic
Space group	P2(1)/n	Pca21
Temperature /K	107(2)	158.00
Wavelength /Å	0.71073	0.71073
a /Å	11.8219(15)	21.375(4)
b /Å	19.265(3)	8.7062(15)
c /Å	12.0754(16)	15.495(3)
α/°	90.00	90
β/°	95.723(3)	90
γ/°	90.00	90
V/ $Å^3$	2736.5(6)	2883.6(9)

Z	35	4
Density/Mgm^{-3}	4.287	1.477
Abs. Coeff. /mm^{-1}	6.961	0.769
Abs. correction	none	None
F(000)	3430	1324
Total no. of reflections	4772	4921
Reflections, $I > 2\sigma(I)$	4270	4258
Max. 2θ/°	24.99	24.827
Ranges (h, k, l)	$-14 \leq h \leq 14$ $-22 \leq k \leq 22$ $-14 \leq l \leq 14$	$-25 \leq h \leq 25$ $-10 \leq k \leq 10$ $-17 \leq l \leq 18$
Complete to 2θ (%)	1.000	99.4
Refinement method	Full-matrix least-squares on F^2	Full-matrix least-squares on F^2
Goof (F^2)	1.075	1.045
R indices [$I > 2\sigma(I)$]	0.0356	0.0523
R indices (all data)	0.0418	0.0663

Table A2.2: Selected bond lengths (Å) of complexes **3.1** and **3.2a**

Atoms	**3.1**	**3.2a**
Fe1-N1	2.161(2)	1.760(6)
Fe1-N2	2.265(19)	2.089(7)
Fe1-N4	2.143(2)	2.292(6)
Fe1-N6	2.116(2)	2.112(7)
Fe1-N7	2.091(2)	2.091(2)
Fe1-O1	2.195(2)	1.13(1)
Fe1 O2		2.132(7)
N1-O1		1.147(10)
N5-C9		1.351(10)
Cl2-O7	1.429(2)	1.436(15)
N3-C4		1.331(11)
C4-C3	1.380(4)	1.378(11)

C2-C1	1.383(4)	1.482(10)
N3-C4		1.331(11)
N4-C7		1.461(10)
N2-C2		1.345(10)

Table A2.3: Selected bond angles (˚) of complexes **3.1** and **3.2a**

Atoms	**3.1**	**3.2a**
N1-Fe1-N4	85.36(8)	175.6(4)
N4-Fe1-N2	79.22(7)	75.9(2)
N6-Fe1-N4		76.9(2)
N2-Fe1-N7		93.6(3)
N6-Fe1-N2	76.59(8)	152.1(2)
N7 Fe1 N1	100.38(8)	97.6(4)
O1-Fe1-N1		162.55(8)
O2-Fe1-N4		88.6(3)

Appendix III

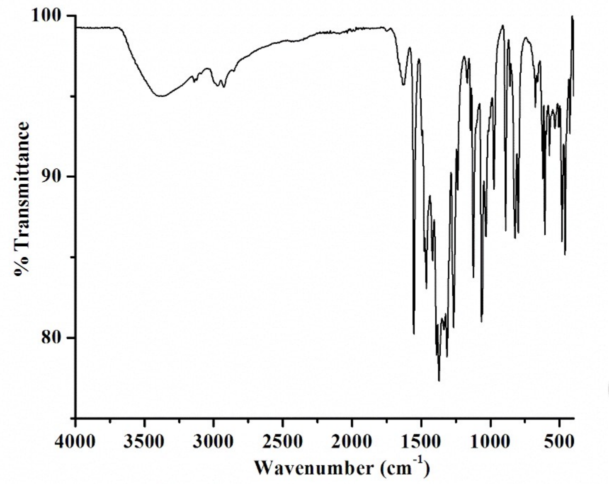

Figure A3.1: FT-IR spectrum of complex **4.1** in ATR probe.

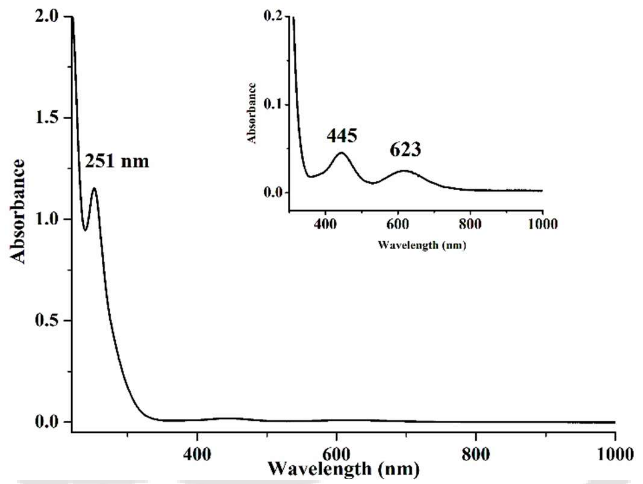

Figure A3.2: UV-visible spectrum of complex **4.1** in acetonitrile at room temperature.

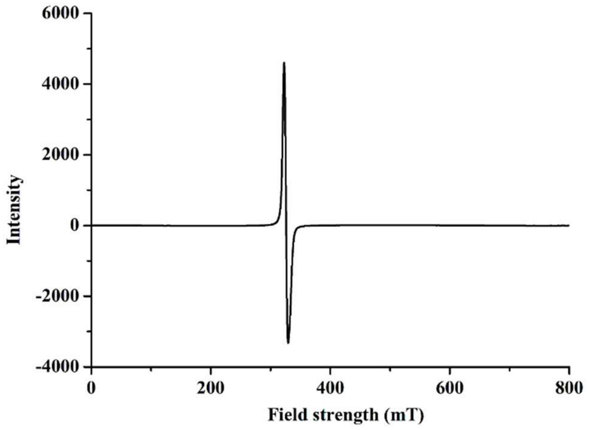

Figure A3.3: X-band EPR spectrum of complex **4.1** in acetonitrile at 77 K (g ~ 2.03).

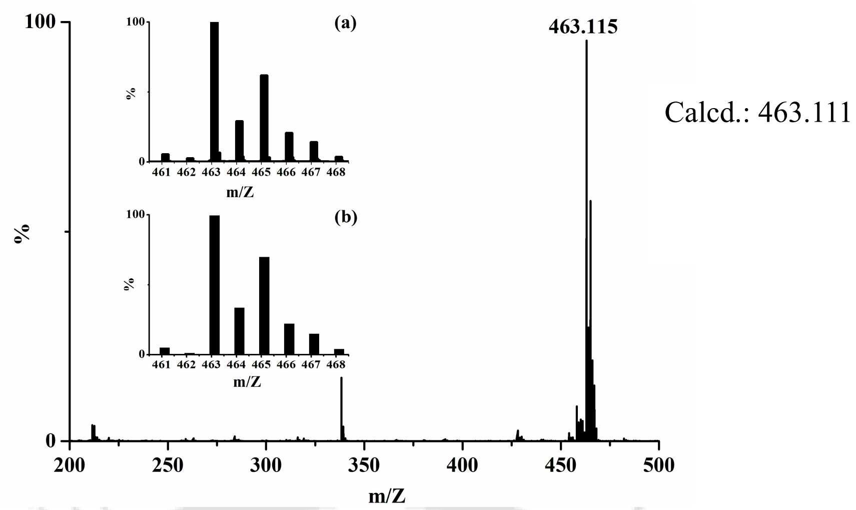

Figure A3.4: ESI-mass spectrum of complex **4.1** in acetonitrile. [Inset: (a) experimental and (b) simulated isotopic distribution pattern].

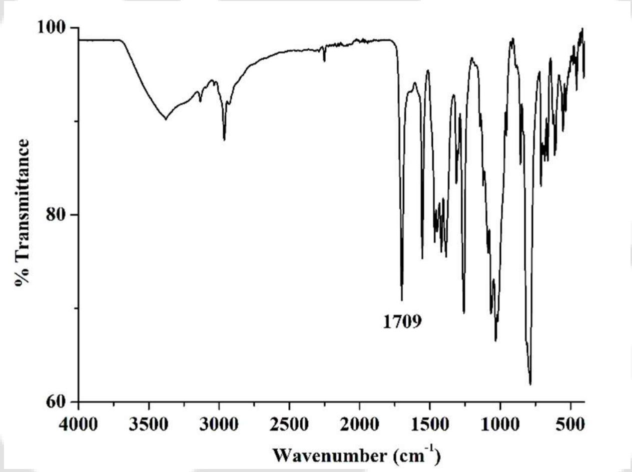

Figure A3.5: FT-IR spectrum of complex **4.2** using ATR probe.

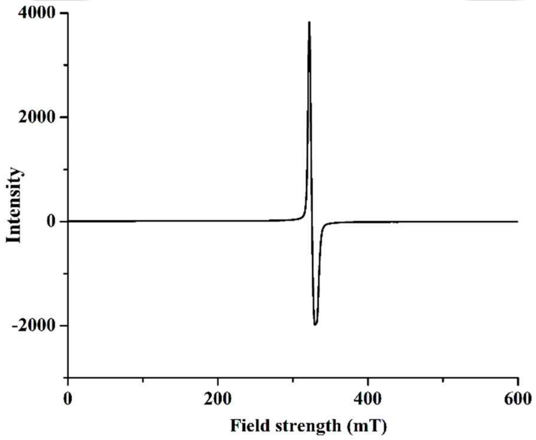

Figure A3.6: X-band EPR spectrum of complex **4.2** in acetonitrile at 77 K (g ~ 2.012).

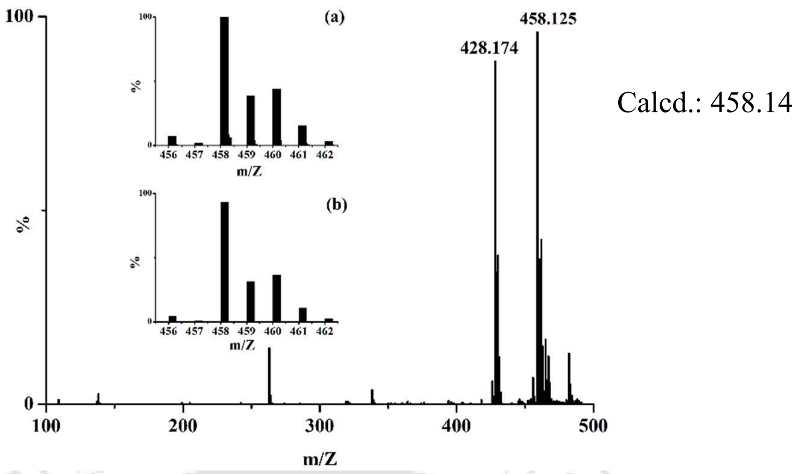

Figure A3.7: ESI-mass spectrum of complex **4.2** in methanol [Inset: (a) experimental and (b) simulated isotopic distribution pattern].

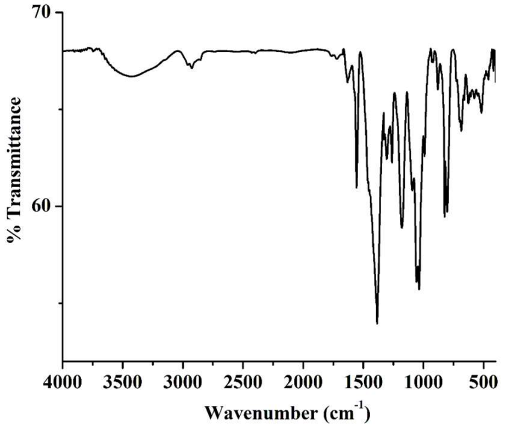

Figure A3.8. FT-IR spectrum of complexes **4.3** in ATR probe.

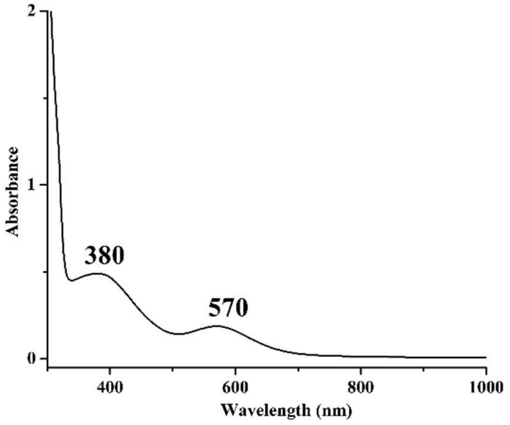

Figure A3.9: UV-visible spectrum of complex **4.3** in methanol at room temperature.

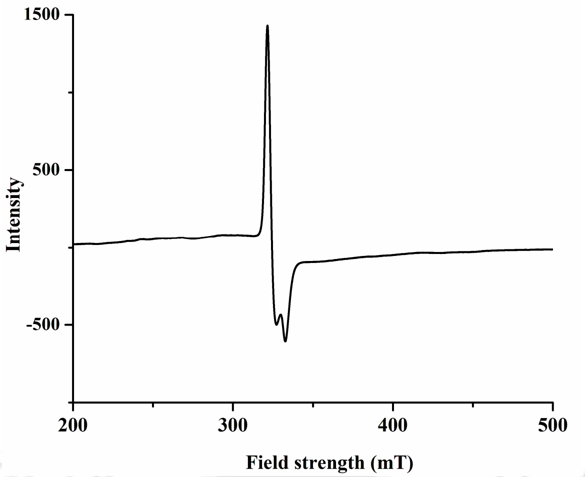

Figure A3.10: X-band EPR spectrum of complex **4.3** in methanol at 77 K (g ~ 2.04).

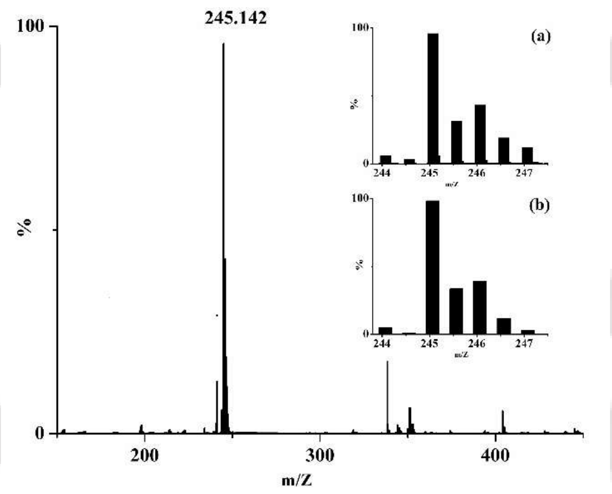

Calcd.: 245.065

Figure A3.11: ESI-mass spectrum of complex **4.3** in methanol [Inset: (a) experimental and (b) simulated isotopic distribution pattern].

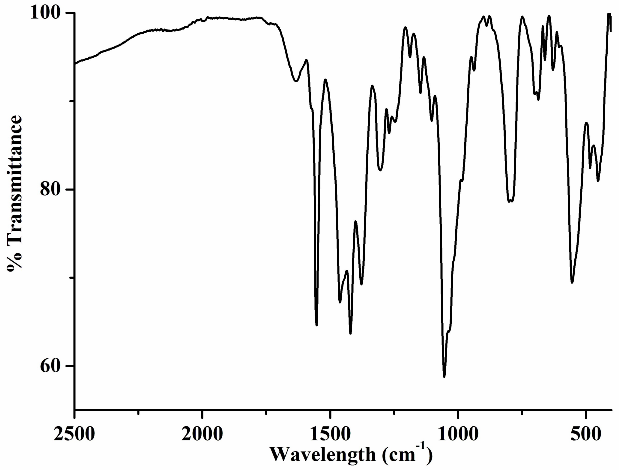

Figure A3.12: FT-IR spectrum of complex **4.4** in ATR probe.

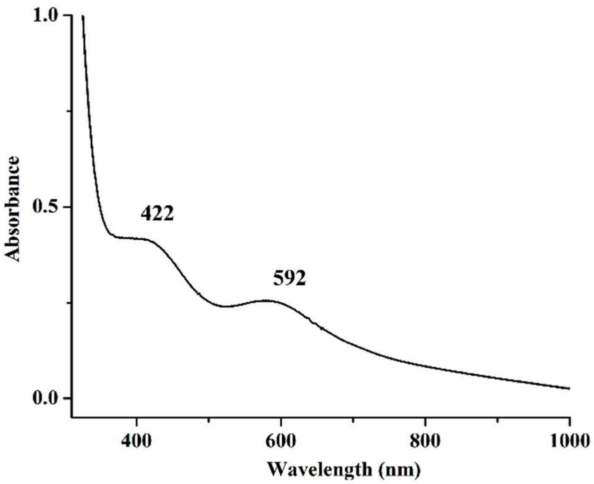

Figure A3.13: UV-visible spectrum of complex **4.4** in THF at room temperature.

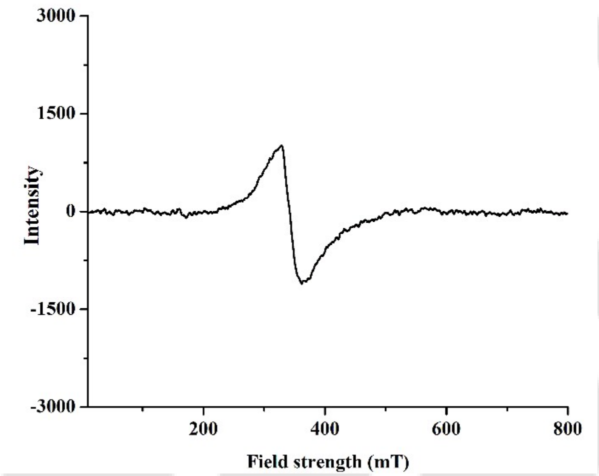

Figure A3.14: X-band EPR spectrum of complex **4.4** in THF at 77 K (g ~ 2.16).

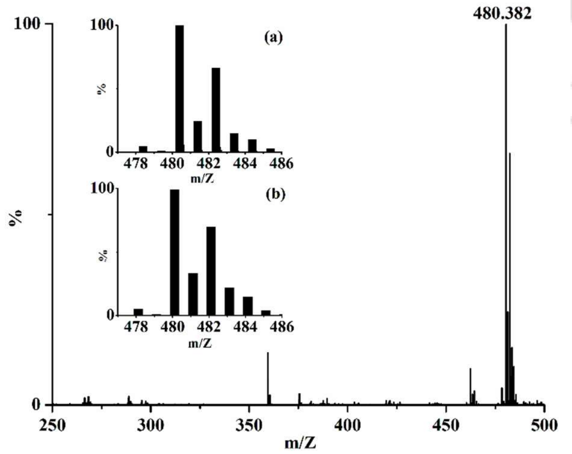

Calcd.: 480.113

Figure A3.15: ESI-mass spectrum of complex **4.4** in methanol [Inset: (a) experimental and (b) simulated isotopic distribution pattern].

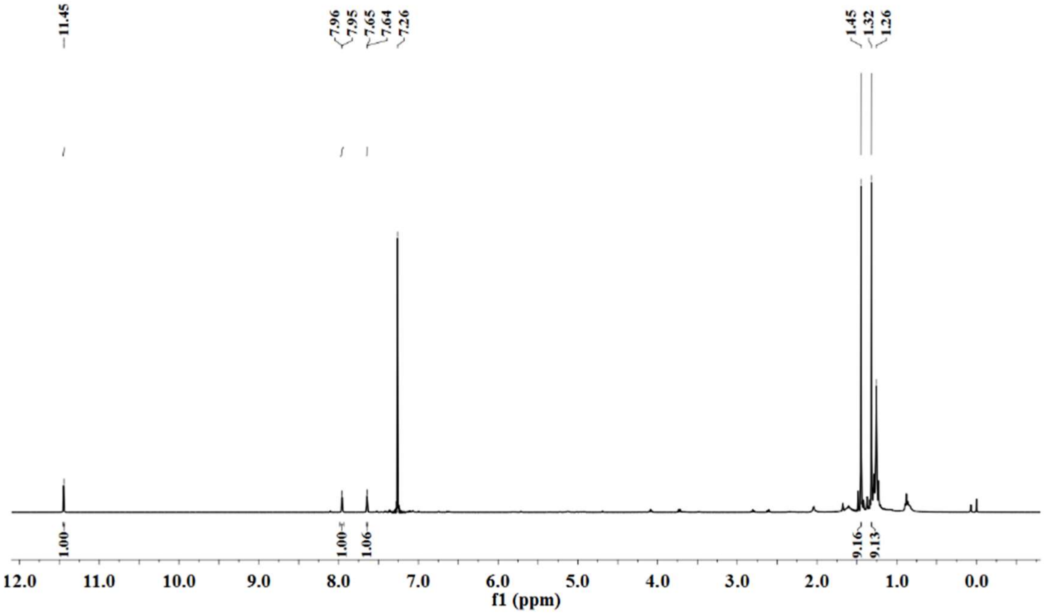

Figure A3.16: ^{1}H NMR spectrum of 2,4-di-*tert*-butyl-6-nitrophenol in $CDCl_3$.

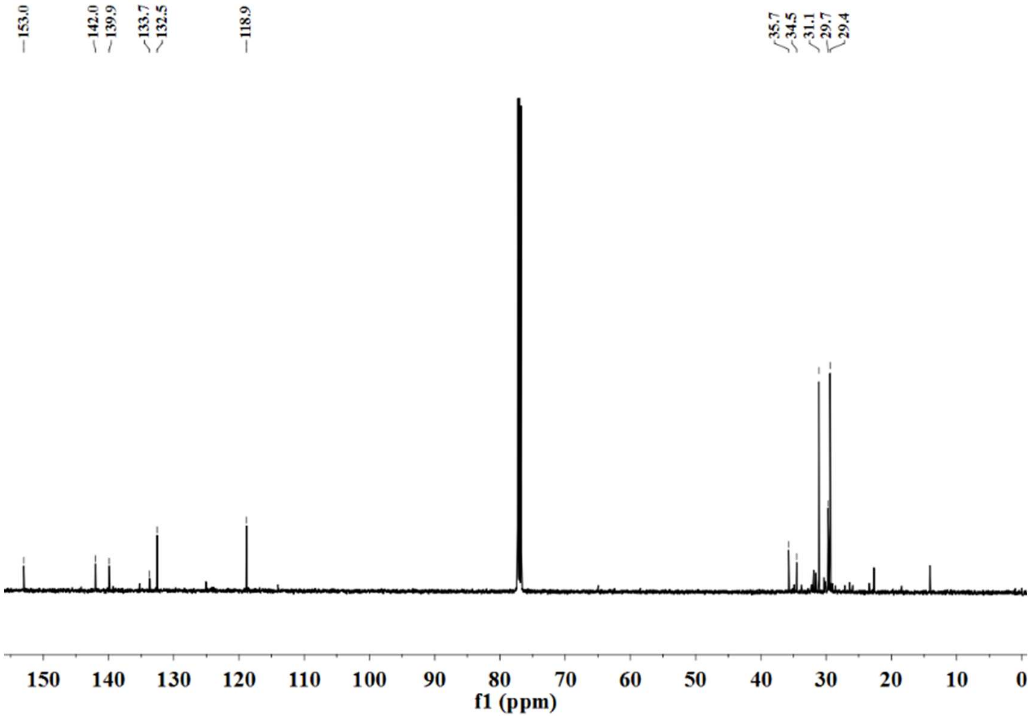

Figure A3.17: ^{13}C NMR spectrum of 2,4-di-*tert*-butyl-6-nitrophenol in $CDCl_3$.

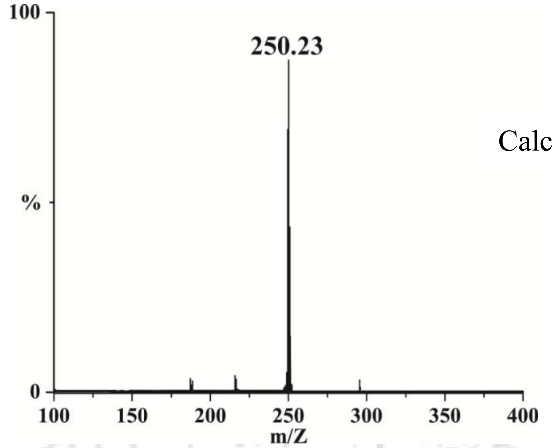

Calcd.: 251.15

Figure A3.18: ESI-mass spectrum of 2,4-di-*tert*-butyl-6-nitrophenol in methanol.

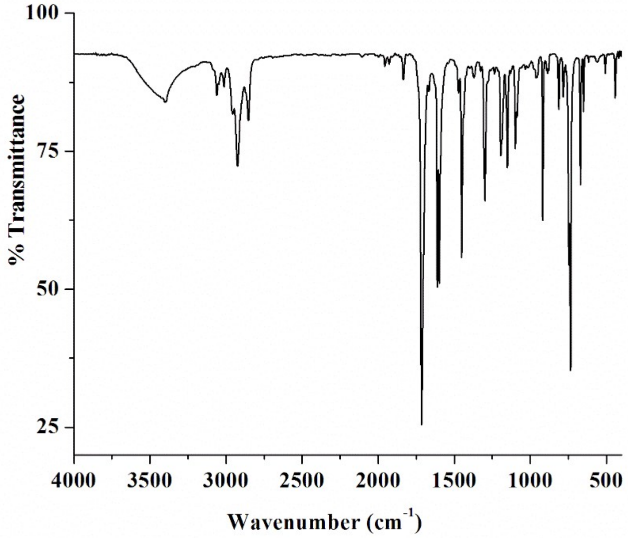

Figure A3.19: FT-IR spectrum of 9-fluorenone using ATR probe.

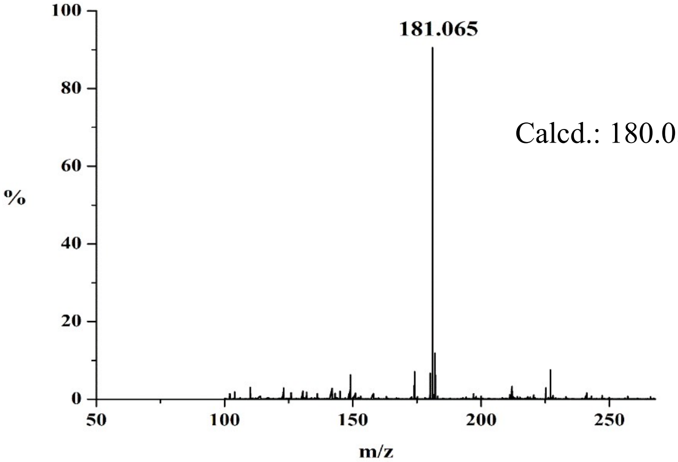

Calcd.: 180.057

Figure A3.20: ESI-Mass spectrum of 9-fluorenone in acetonitrile.

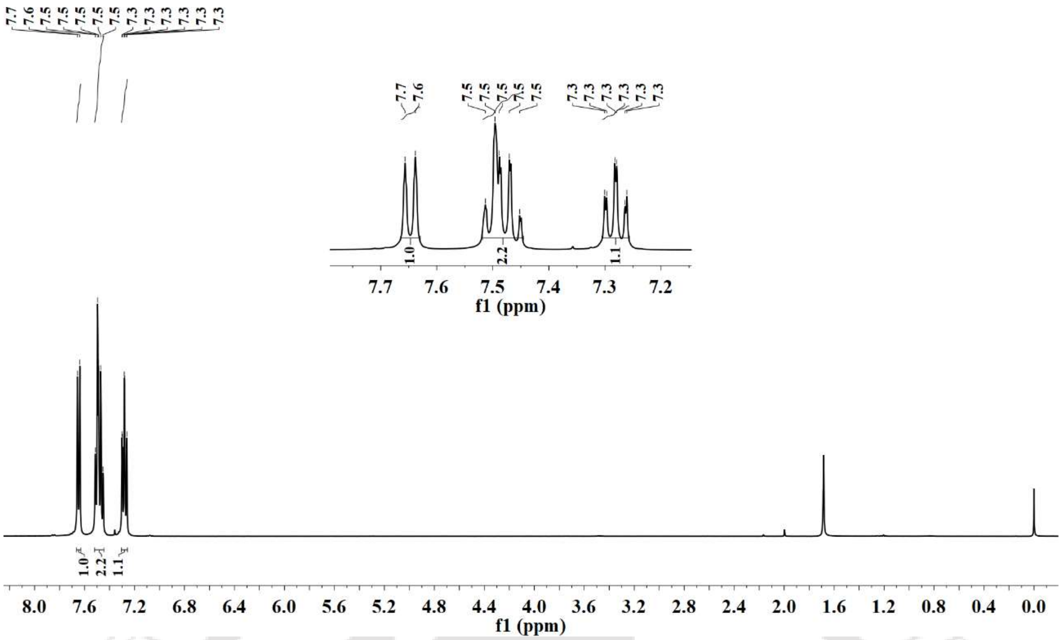

Figure A3.21: ^{1}H NMR spectrum of 9-fluorenone in CDCl$_3$.

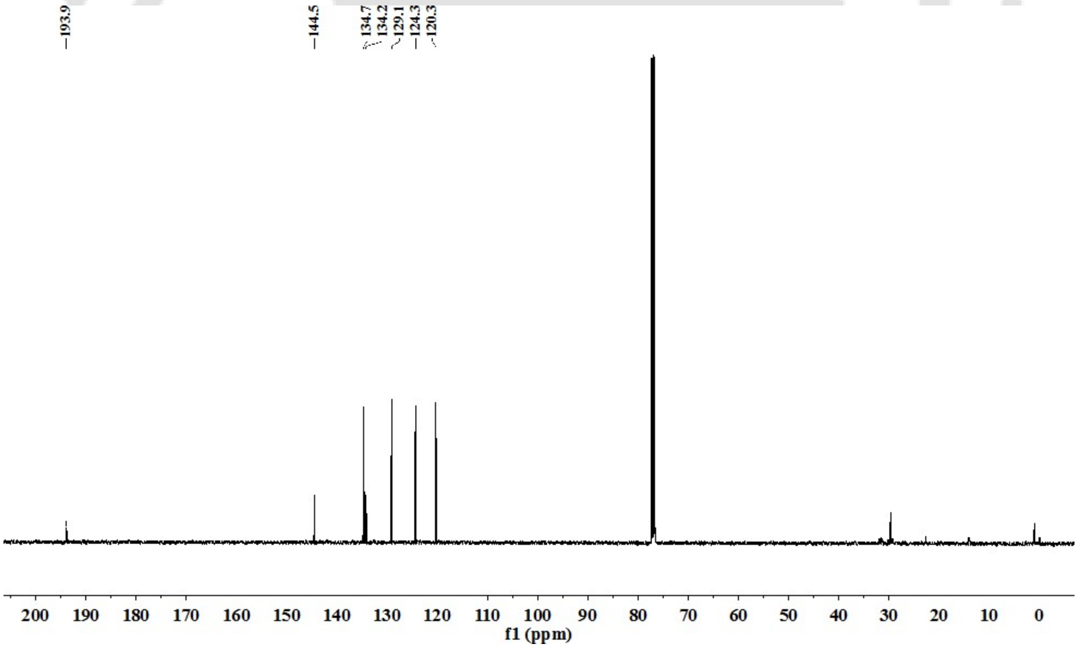

Figure A3.22: ^{13}C NMR spectrum of 9-fluorenone in CDCl$_3$.

Table A3.1: Crystallographic data for complexes **4.1** and **4.2**

	4.1	**4.2**
Formulae	$C_{18}H_{27}Cl_2CrN_7$	$C_{18}H_{33}Cl_2CrN_8O_4$
Mol. wt.	464.36	548.42
Crystal system	Triclinic	Triclinic
Space group	P -1	P -1
Temperature /K	293(2)	293(2)
Wavelength /Å	0.71073	0.71073
a /Å	8.7834(6)	8.7614(8)
b /Å	11.6945(9)	11.6683(10)
c /Å	13.4850(11)	13.5200(12)
α/°	80.812(7)	80.645(7)
β/°	73.265(7)	73.626(8)
γ/°	73.571(6)	74.039(8)
V/ $Å^3$	1267.70(18)	1269.6(2)
Z	2	2
Density/Mgm^{-3}	1.217	1.435
Abs. Coeff. /mm^{-1}	0.678	0.701
Abs. correction	multi-scan	multi-scan
F(000)	484	574
Total no. of reflections	4457	4457
Reflections, $I > 2\sigma(I)$	3465	3144
Max. 2θ/°	24.990	25.4270
Ranges (h, k, l)	$-10 \leq h \leq 9$ $-10 \leq k \leq 13$ $-16 \leq l \leq 14$	$-10 \leq h \leq 10$ $-13 \leq k \leq 13$ $-16 \leq l \leq 10$
Complete to 2θ (%)	0.999	0.998
Refinement method	Full-matrix least-squares on F^2	Full-matrix least-squares on F^2
Goof (F^2)	1.048	1.039
R indices [$I > 2\sigma(I)$]	0.0505	0.1018
R indices (all data)	0.0654	0.0754

Table A3.2: Selected bond lengths (Å) of complexes **4.1** and **4.2**

Atoms	**4.1**	**4.2**
Cr1-N1	2.067(3)	2.051(4)
Cr1-N3	2.138(3)	2.168(4)
Cr1-N7	2.067(3)	2.062(4)
Cr1-N5	2.074(3)	2.054(4)

Cr1-Cl1	2.3136(11)	2.3475(15)
Cr1-Cl2	2.2430(10)	
N1-N2	1.368(4)	1.365(5)
N1-C2	1.352(4)	1.356(6)
N2-C4	1.338(5)	1.342(6)
N2-C6	1.445(4)	1.437(6)
N3-C13	1.484(4)	1.481(6)
N3-C7	1.471(5)	1.476(6)
N4-C9	1.339(5)	1.362(7)
N4-C7	1.448(5)	1.444(7)
C1-C2	1.486(5)	1.476(7)
C4-C3	1.365(5)	1.379(8)
Cr1-N8		1.777(6)
N8 O1		0.974(6)

Table A3.3: Selected bond angles (˚) of complexes **4.1** and **4.2**

Atoms	**4.1**	**4.2**
N1-Cr1-N7	158.06(11)	156.59(16)
N3-Cr1-N7	79.67(10)	79.09(15)
N5-Cr1-N7	85.53(11)	86.06(16)
N8-Cr1-N7		102.08(19)
Cl1-Cr1-Cl2	91.46(4)	
N3-Cr1-Cl2	177.32(8)	
N3-Cr1-Cl1	90.49(8)	90.00(12)
N7-Cr1-Cl2	102.20(8)	
N7-Cr1-Cl1	88.92(9)	88.50(12)
N5-Cr1-Cl1	170.68(8)	169.61(12)
N5-Cr1-N3	81.16(11)	
C7-N3-C6	110.1(3)	109.3(4)
C17-N7-Cr1	141.5(2)	140.3(4)
Cl1-Cr1-N1	92.06(6)	91.95(12)
N1-Cr1-N5		89.54(16)
O1-N8-Cr1		176.0(6)

Appendix IV

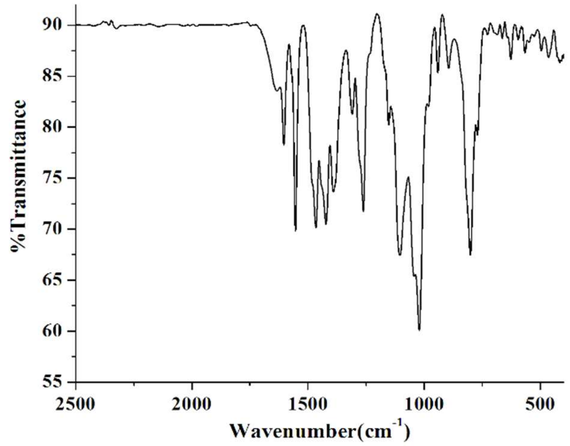

Figure A4.1: FT-IR spectrum of complex **5.1** in KBr.

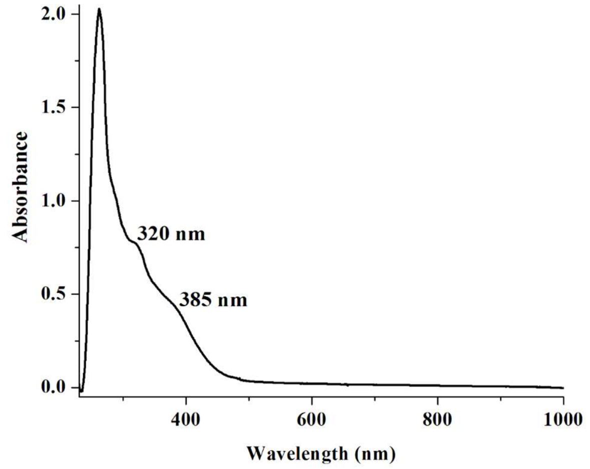

Figure A4.2: UV-visible spectrum of complex **5.1** in methanol at room temperature.

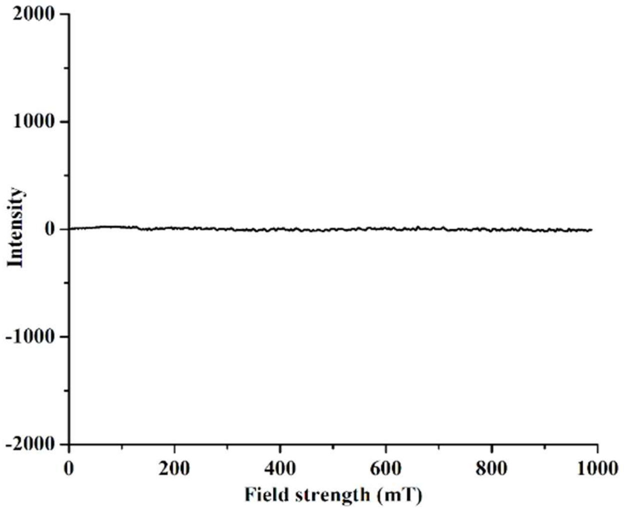

Figure A4.3: X-band EPR spectrum of complex **5.1** in methanol at 77 K.

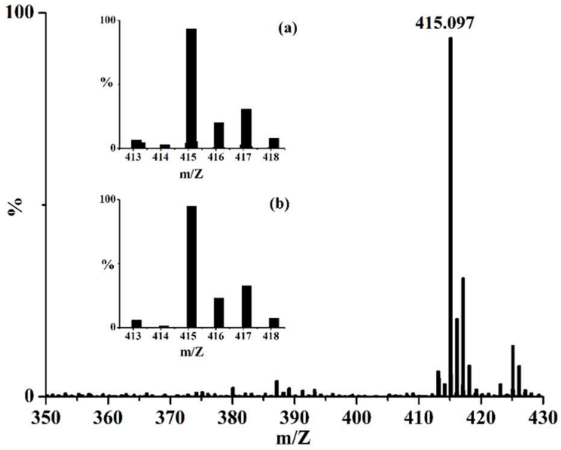

Figure A4.4: ESI-mass spectrum of complex **5.1** in methanol. [Inset: (a) experimental and (b) simulated isotopic distribution pattern].

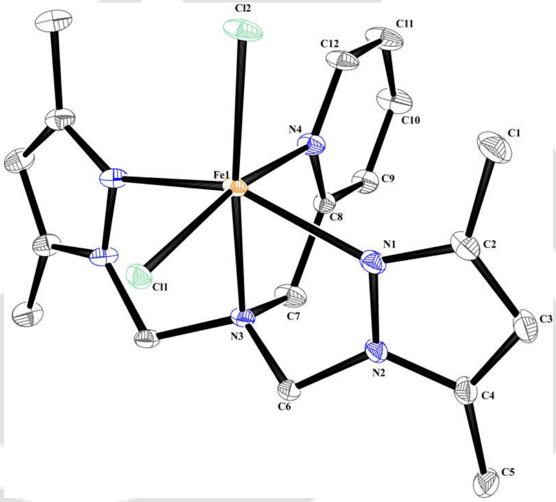

Figure A4.5: ORTEP diagram of complex **5.1** (30% thermal ellipsoid plot, H-atoms are omitted for clarity).

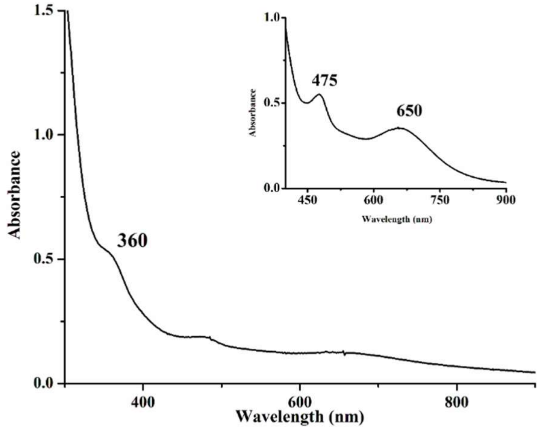

Figure A4.6: UV-visible spectrum of complex **5.2** in acetonitrile at room temperature.

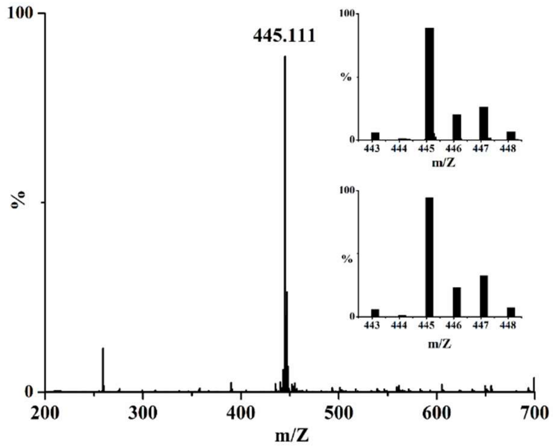

Figure A4.7: ESI-mass spectrum of complex **5.2** in methanol. [Inset:(a) experimental and (b) simulated isotopic distribution pattern].

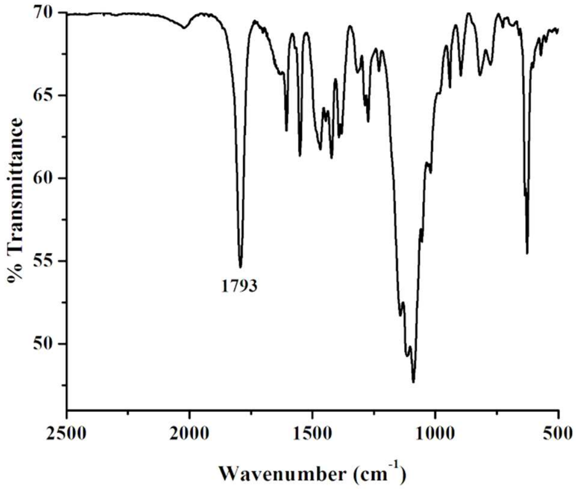

Figure A4.8: FT-IR spectrum of $[Fe(Pz_2Py)(NO)(MeOH)](ClO_4)_2$ complex (solid state) in KBr.

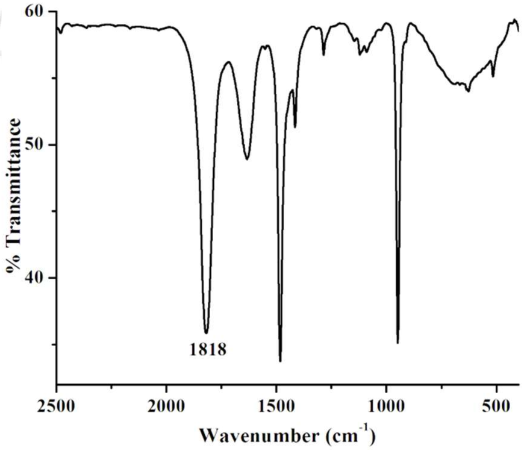

Figure A4.9: FT-IR spectrum of $[N(CH_3)_4][Fe(Cl)_3(NO)]$ complex (solid state) in KBr.

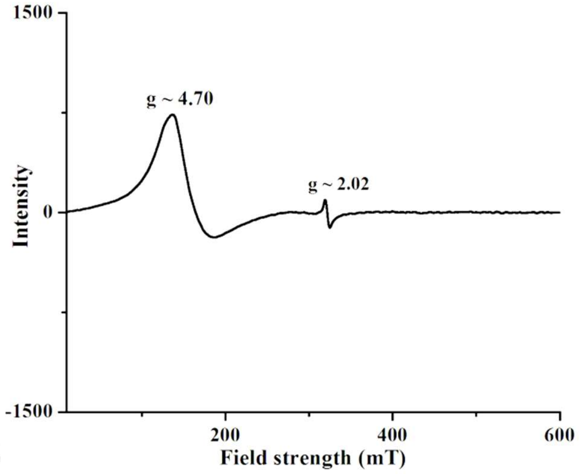

Figure A4.10: X-band EPR spectrum of [Fe(Pz$_2$Py)(NO)(MeOH)](ClO$_4$)$_2$ complex acetonitrile /toluene (2:1) mixture at 77 K.

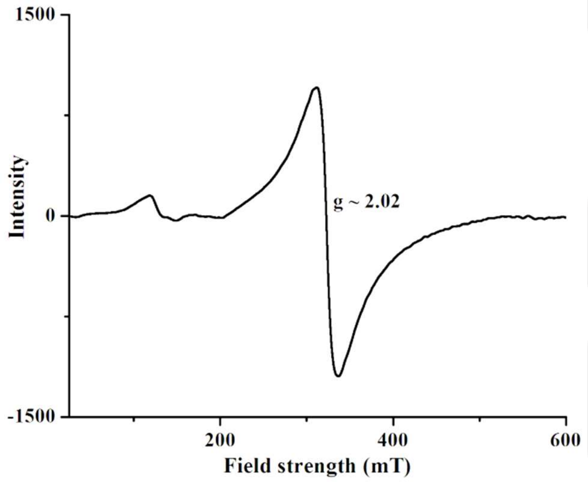

Figure A4.11: X-band EPR spectrum of [N(CH$_3$)$_4$][Fe(Cl)$_3$(NO)] complex acetonitrile/toluene (2:1) mixture at 77 K.

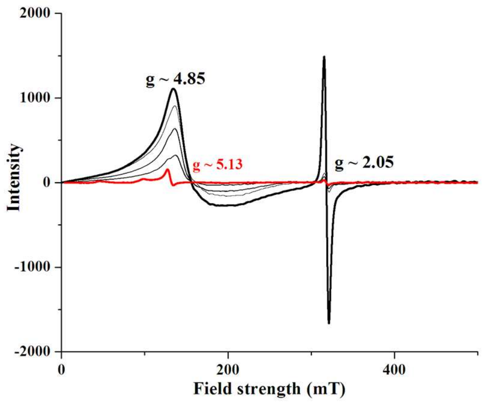

Figure A4.12: X-band EPR spectral monitoring decomposition of complex **5.2** to complex **5.3** in acetonitrile/toluene (2:1) mixture at 77 K.

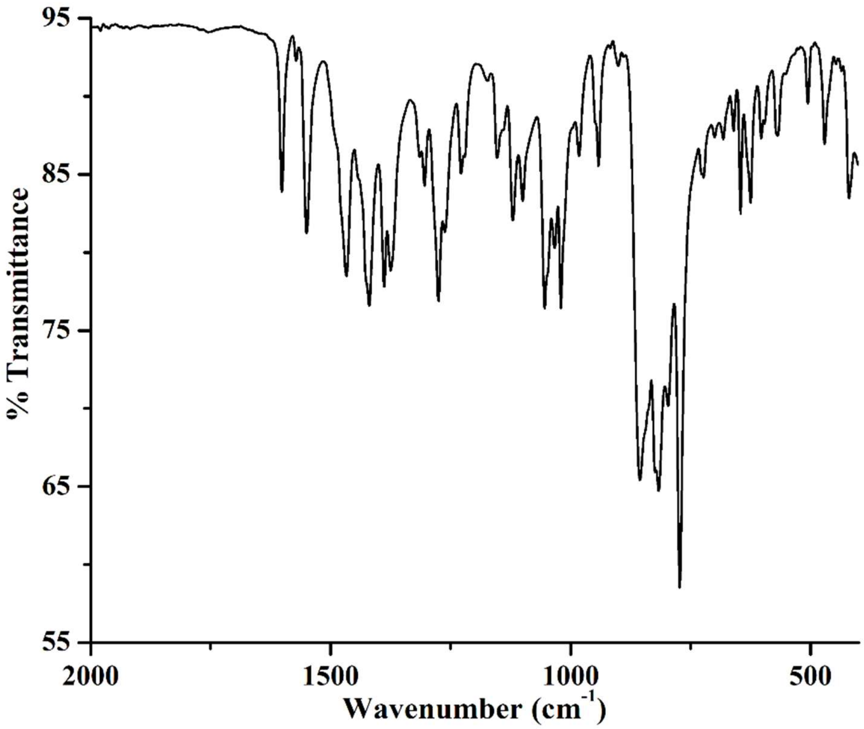

Figure A4.13: FT-IR spectrum of complex **5.3** using ATR probe.

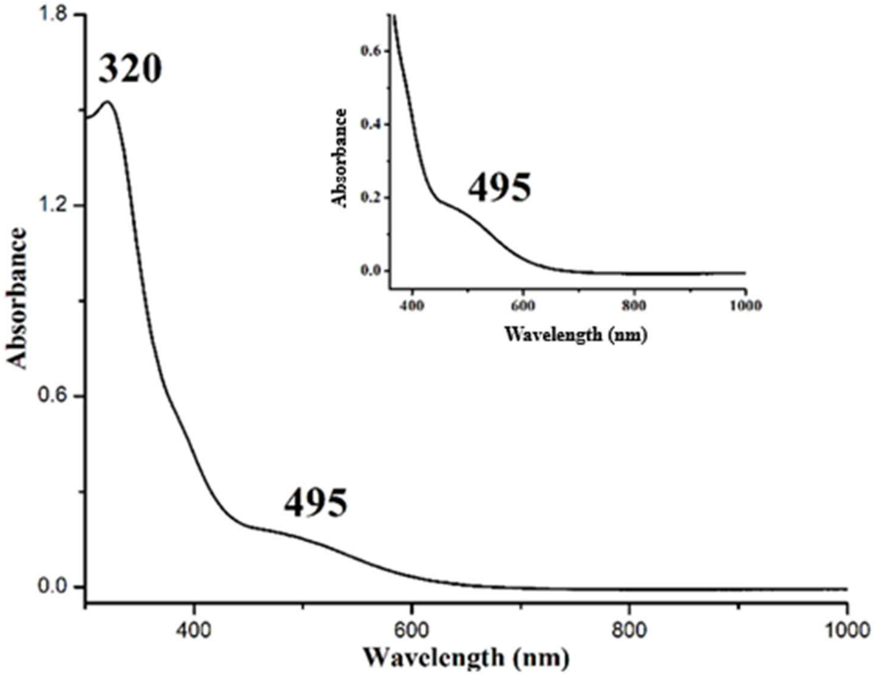

Figure A4.14: UV-visible spectrum of complex **5.3** in DMF at room temperature.

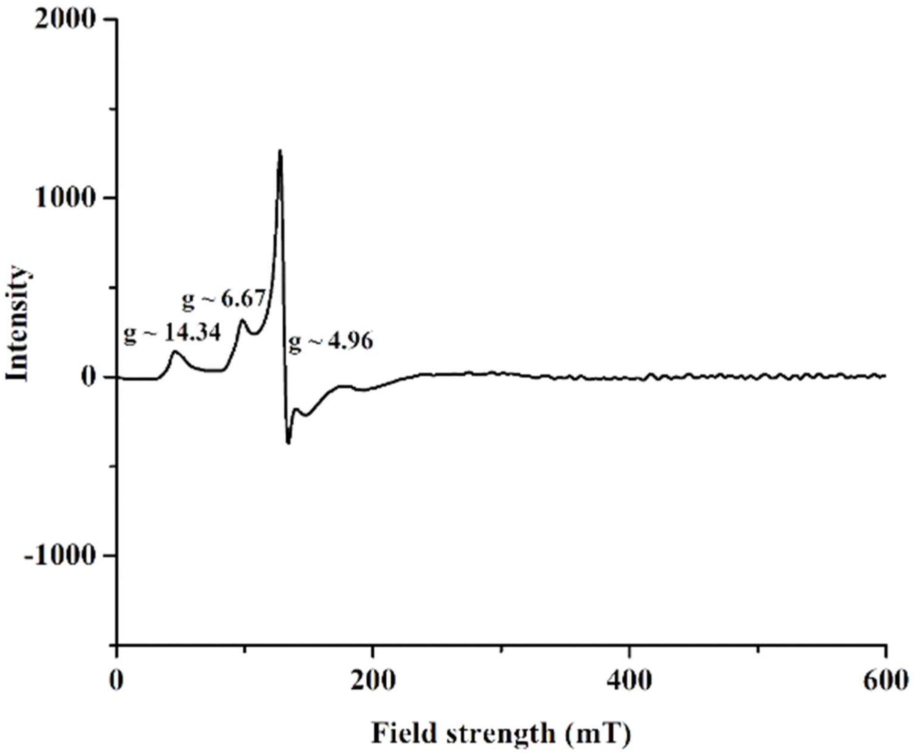

Figure A4.15: X-band EPR spectrum of complex **5.3** in DMF at 77 K**.**

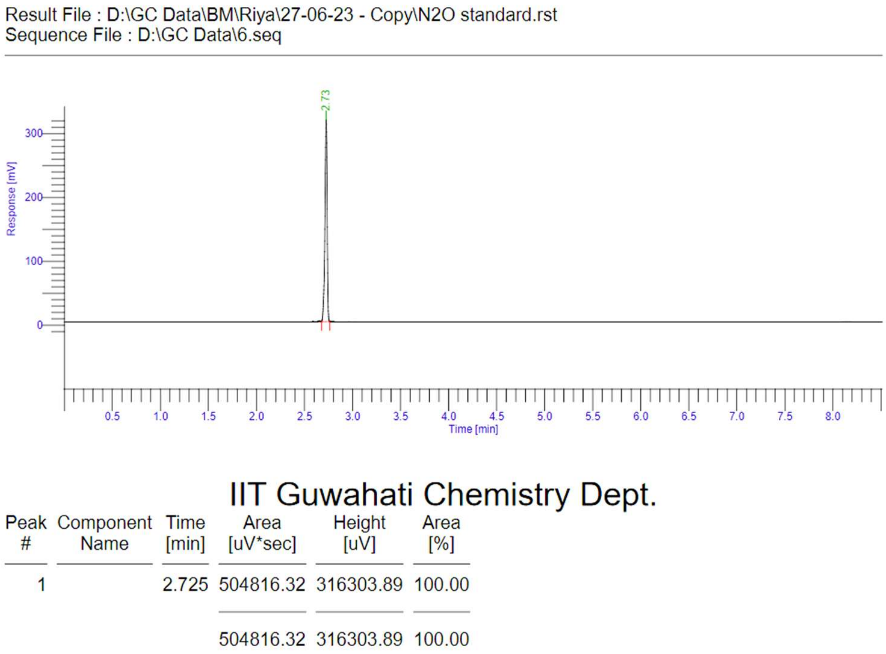
Result File : D:\GC Data\BM\Riya\27-06-23 - Copy\N2O standard.rst
Sequence File : D:\GC Data\6.seq

IIT Guwahati Chemistry Dept.

Peak #	Component Name	Time [min]	Area [uV*sec]	Height [uV]	Area [%]
1		2.725	504816.32	316303.89	100.00
			504816.32	316303.89	100.00

Figure A4.16: Gas chromatogram of standard N_2O (retention time = 2.73 min).

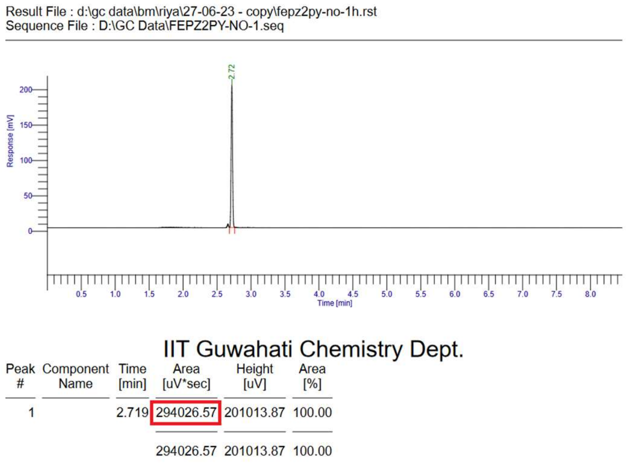

Result File : d:\gc data\bm\riya\27-06-23 - copy\fepz2py-no-1h.rst
Sequence File : D:\GC Data\FEPZ2PY-NO-1.seq

IIT Guwahati Chemistry Dept.

Peak #	Component Name	Time [min]	Area [uV*sec]	Height [uV]	Area [%]
1		2.719	294026.57	201013.87	100.00
			294026.57	201013.87	100.00

(A)

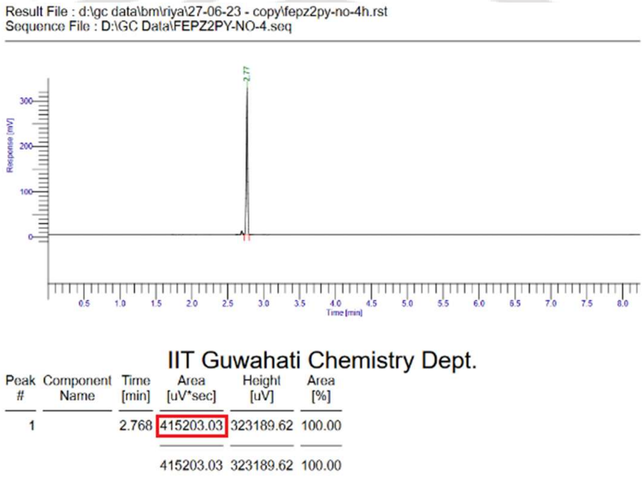

Result File : d:\gc data\bm\riya\27-06-23 - copy\fepz2py-no-4h.rst
Sequence File : D:\GC Data\FEPZ2PY-NO-4.seq

IIT Guwahati Chemistry Dept.

Peak #	Component Name	Time [min]	Area [uV*sec]	Height [uV]	Area [%]
1		2.768	415203.03	323189.62	100.00
			415203.03	323189.62	100.00

(B)

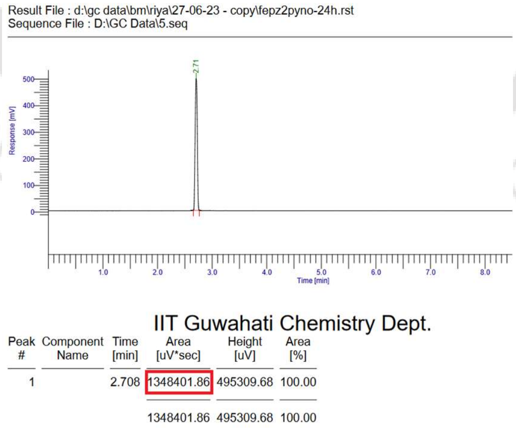

Result File : d:\gc data\bm\riya\27-06-23 - copy\fepz2pyno-24h.rst
Sequence File : D:\GC Data\5.seq

IIT Guwahati Chemistry Dept.

Peak #	Component Name	Time [min]	Area [uV*sec]	Height [uV]	Area [%]
1		2.708	1348401.86	495309.68	100.00
			1348401.86	495309.68	100.00

(C)

Figure A4.17: Gas chromatograms of headspace gas of the acetonitrile solution of complex **5.2** with respect to time. [after 1hr **(A)**, 4 hr **(B)** and 24 hr **(C)**]
(retention time for **(A)**, **(B)** and **(C)** are 2.72 min, 2.77 min and 2.71 min respectively)

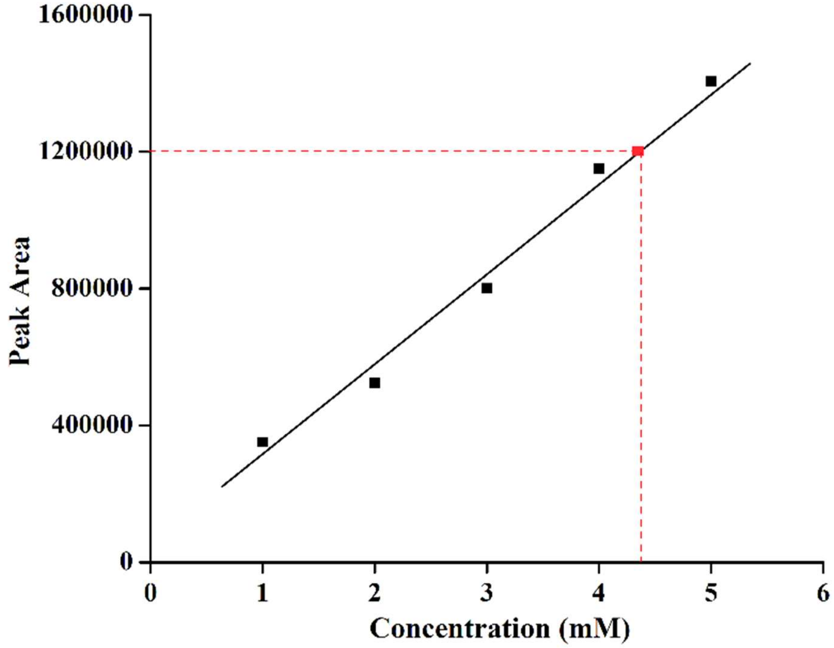

Figure A4.18: GC calibration curve for determination of amount of N_2O. [red dot corresponds to the acetonitrile solution (5 mL) of complex **5.2** (0.669 g, 0.437 mmol)]

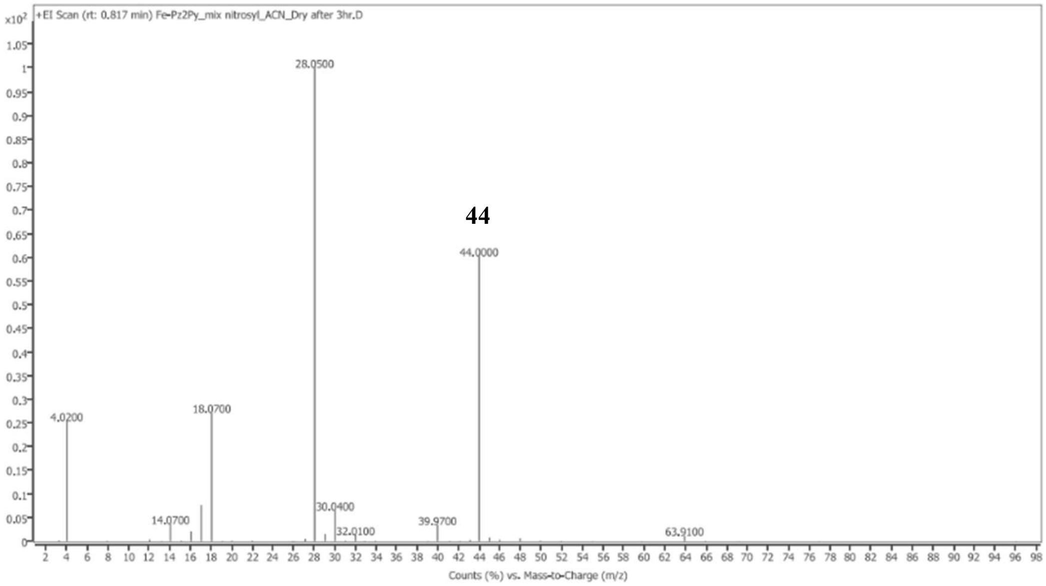

Figure A4.19: GC-mass spectrum of the headspace gas of the acetonitrile solution of complex **5.2** (after 24 hr).

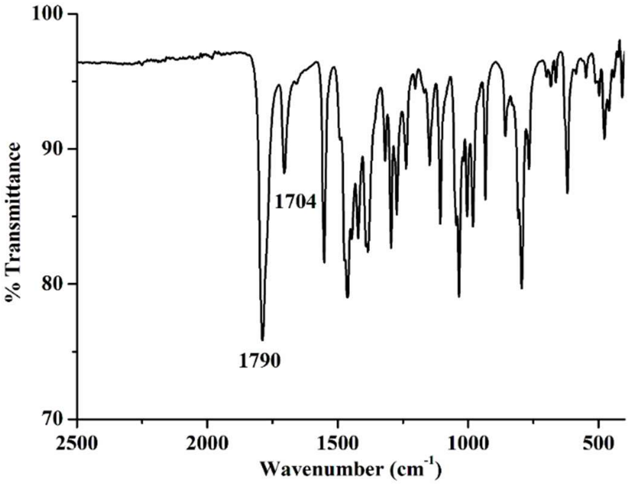

Figure A4.20: FT-IR spectrum of complex **5.2** after immidiately dissolving in acetonitrile solution.

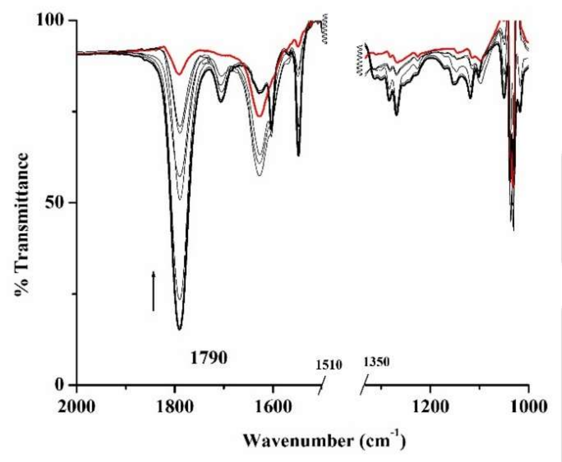

Figure A4.21: FT-IR spectral monitoring decomposition of complex **5.2** (black) to complex **5.3** (red) in acetonitrile medium under Ar atmosphere.

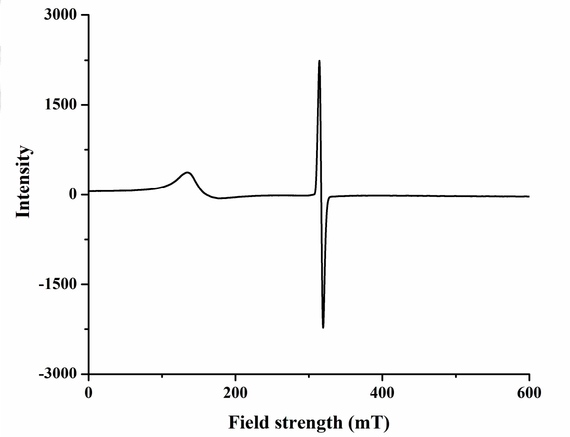

Figure A4.22: X-band EPR spectrum of complex **5.2** immediately after dissolving in acetonitrile at 77 K (g ~ 2.00).

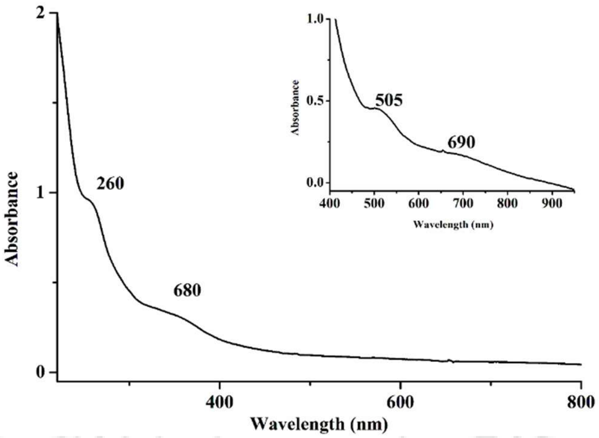

Figure A4.23: UV-visible spectrum of complex **5.2** immediately after dissolving in acetonitrile at room temperature.

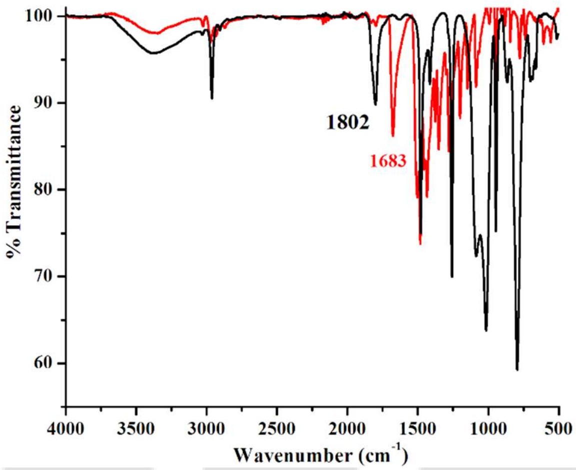

Figure A4.24: FT-IR spectra of [N(CH$_3$)$_4$][FeCl$_3$NO] complex (black), reaction mixture of [N(CH$_3$)$_4$][FeCl$_3$NO] complex + Fe(dtc)$_3$ in acetonitrile (red) in ATR Probe.

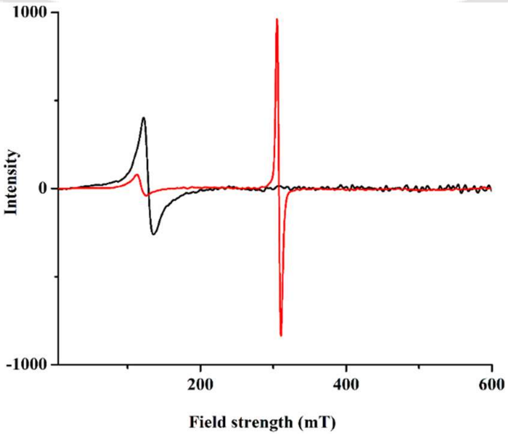

Figure A4.25: X-band EPR spectra of [N(CH$_3$)$_4$][FeCl$_3$(NO)] complex (black), reaction mixture of [N(CH$_3$)$_4$][FeCl$_3$NO] complex + Fe(dtc)$_3$ in acetonitrile (red) at 77 K (g ~ 2.02).

Table A4.1. Crystallographic data for complexes **5.1, 5.2** and **5.3.**

	5.1	**5.2**	**5.3**
Formulae	$C_{18}H_{24}FeN_6Cl_2$	$C_{18}H_{24}Cl_4N_8O_2Fe_2$	$C_{20}H_{27}Cl_4N_7O_1Fe_2$
Mol. wt.	451.18	637.95	634.98
Crystal system	Triclinic	Triclinic	Monoclinic
Space group	Cmc2(1)	P -1	P 2(1)/n
Temperature /K	120	293(2)	298(2)
Wavelength /Å	0.71073	0.71073	0.71073
a /Å	14.9471(11)	9.0385(7)	10.602(8)
b /Å	9.0306(7)	13.4837(12)	17.299(13)
c /Å	15.2638(11)	13.7543(14)	15.541(12)
α/°	90.00	111.275(9)	90
β/°	90.00	93.259(7)	90.28(3)
γ/°	90.00	99.813(7)	90
V/ $Å^3$	2060.3(3)	1526.3(3)	2850(4)
Z	4	2	4
Density/Mgm^{-3}	1.455	1.388	1.480
Abs. Coeff. /mm^{-1}	1.007	1.328	1.419
Abs. correction	none	multi-scan	none
F(000)	936.0	648	1296
Total no. of reflections	2362	5349	6665
Reflections, $I > 2\sigma(I)$	2313	3376	4464
Max. 2θ/°	27.129	24.995	24.993
Ranges (h, k, l)	$-19 \leq h \leq 19$ $-11 \leq k \leq 11$ $-19 \leq l \leq 19$	$-10 \leq h \leq 10$ $-14 \leq k \leq 16$ $-16 \leq l \leq 16$	$-12 \leq h \leq 12$ $-20 \leq k \leq 20$ $-18 \leq l \leq 18$
Complete to 2θ (%)	0.995	0.997	0.997
Refinement method	Full-matrix least-squares on F^2	Full-matrix least-squares on F^2	Full-matrix least-squares on F^2
Goof (F^2)	1.116	0.996	1.043

R indices [*I*>2σ(*I*)]	0.0225	0.0570	0.0346
R indices (all data)	0.0235	0.0870	0.0399

Table A4.2. Selected bond lengths (Å) of complexes **5.1, 5.2** and **5.3.**

Atoms	**5.1**	**5.2**	**5.3**
Fe1-N1	2.222(2)	2.145(4)	2.132(3)
Fe1-N3	2.342(3)	2.303(3)	2.327(3)
Fe1-N4	2.205(3)	2.190(4)	2.196(3)
Fe1-N6		2.129(3)	
Fe1-N5			2.141(2)
Fe1-Cl1	2.4138(10)	2.3378(13)	2.3252(18)
Fe1-O1			1.766(2)
Fe2-O1			1.745(2)
Fe2-Cl2		2.2410(17)	2.2245(15)
Fe2-Cl3		2.2295(16)	2.2222(14)
Fe2-Cl4		2.1952(19)	2.2108(19)
Fe1-Cl2	2.3514(10)		
N1-N2	1.372(3)	1.372(5)	1.360(3)
N1-C2	1.333(3)	1.342(5)	1.328(4)
N2-C4	1.357(3)	1.361(6)	1.348(4)
N2-C6	1.446(3)	1.462(5)	1.435(4)
N3-C6	1.463(3)	1.465(5)	1.468(3)
N3-C7	1.477(5)	1.463(5)	1.494(4)
N4-C8	1.342(5)	1.334(6)	1.333(3)
N4-C12	1.347(5)	1.323(6)	1.332(4)
C1-C2	1.499(4)	1.495(8)	1.461(5)
C7-C8	1.520(5)	1.515(6)	1.484(4)
N7-O1		1.143(6)	
N8-O2		1.109(6)	
Fe1-N7		1.737(5)	
Fe2-N8		1.724(6)	

Table A4.3. Selected bond angles (°) of complexes **5.1, 5.2** and **5.3.**

Atoms	**5.1**	**5.2**	**5.3**
N1-Fe1-N3	74.65(5)	74.87(13)	74.43(8)
N3-Fe1-N5			73.54(7)
N1-Fe1-N4	84.63(6)	84.81(14)	82.91(9)
N6-Fe1-N4		84.12(13)	
N4-Fe1-N5			85.68(9)
N3-Fe1-O1			168.57(9)
N1-Fe1-N9			
N1-Fe1-O1			104.46(9)
C6-N3-C7	112.96(18)	112.3(3)	112.8(2)
Fe1-O1-Fe2			166.04(13)
Cl1-Fe1-N1	92.06(6)	90.25(11)	93.71(8)
N1-Fe1-N5			147.80(9)
Cl1-Fe1-O1			101.33(8)
Cl2-Fe2-O1			112.27(7)
Fe1-N7-O1		161.6(5)	
Fe2-N8-O2		171.4(7)	

List of Publications

1. "Reaction of a nitrosyl complex of Mn(II)–porphyrinate with superoxide: NOD activity is favoured over SOD activity"

   Mazumdar, R.; Saha, S.; Samanta, B.; **Ghosh, R**.; Maity, S.; Mondal, B. *Dalton Trans.* **2023**, *52*, 7917 – 7925.

2. "Reaction of a Co(III)-peroxo complex with nitric oxide: putative formation of a peroxynitrite intermediate"

   Samanta, B.; **Ghosh, R**.; Mazumdar, R.; Saha, S.; Maity, S.; Mondal, B. *Dalton Trans.* **2023**, *52, 15815*-15821.

3. "Sixth Ligand Induced HNO/NO^- Release by a Five-Coordinated Cobalt(II) Nitrosyl Complex Having a $\{CoNO\}^8$ Configuration"

   Saha, S.; Maity, S.; Mazumdar, R.; Samanta, B.; **Ghosh, R**.; Guha, A .; Mondal, B. *Inorg. Chem.* **2023**, *62,* 17074 – 17082.

4. "Reaction of a Nitrosyl Complex of Co(II)-porphyrin with hydrogen peroxide: Formation of a Porphyrin Radical Cation"

   Samanta, B.; Saha, S.; **Ghosh, R.;** Maity, S.; Mondal, B. *Chem Asian J.* **2025***, 20,* e202401082.

5. "Photo-induced nitroxyl anion/HNO release from a nitrosyl complex of Mn(II)-porphyrinate"

   Saha, S.; Maity, S.; Samanta, B.; **Ghosh, R**.; Mondal, B. *Chem. Commun*. **2025**, *61*, 2353 – 2356.

6. "Reaction of a non-heme iron-nitrosyl with dioxygen: decomposition of the ligand through NOD-like activity''

Ghosh, R.; Samanta, B.; Mazumdar, R.; Saha, S.; Mondal, B. *Dalton Trans.* **2025**, *54*, 7793 – 7800.

7. "Spin state dependent reactivity of iron-nitrosyls with dioxygen"

   Ghosh, R.; Mondal, B.

   (Communicated)

8. "Nitric oxide reductase activity of a diiron-dinitrosyl complex through the formation of $\{Fe(NO)_2\}^9$ intermediate"

   Ghosh, R.; Mondal, B.

   (Communicated)